Intensification of Textile Treatments: Sonoprocess Engineering

Dissertation committee

Promotor:
prof.dr.ir. M.M.C.G. Warmoeskerken, University of Twente, the Netherlands

Co-promotor:
prof.dr. A. Prosperetti, University of Twente, the Netherlands

Members:
prof.dr. A.B. Pandit, University Department of Chemical Technology, University of Mumbai, India
prof.dr.ir. A.B. de Haan, University of Twente, the Netherlands
prof.dr.ir. J.A.M. Kuipers, University of Twente, the Netherlands
prof.dr. P. Kiekens, University of Ghent, Belgium
dr.ir. J.W. Gerritsen, Photon Tech, the Netherlands

This work has been financially supported by Stork Brabant B.V.

Twente University **Press**

Publisher:
Twente University Press,
P.O. Box 217, 7500 AE Enschede, the Netherlands,
www.tup.utwente.nl

Cover design: Jo Molenaar, [deel 4] ontwerpers, Enschede
Print: Océ Facility Services, Enschede

ISBN 9036517516

INTENSIFICATION OF TEXTILE TREATMENTS: SONOPROCESS ENGINEERING

PROEFSCHRIFT

ter verkrijging van
de graad van doctor aan de Universiteit Twente,
op gezag van de rector magnificus,
prof.dr. F.A. van Vught,
volgens besluit van het College voor Promoties
in het openbaar te verdedigen
op donderdag 20 juni 2002 te 15.00 uur

door

Vijayanand Suryakant Moholkar
geboren op 1 september 1972
te Mumbai (Bombay, India)

Dit proefschrift is goedgekeurd door de promotor
prof.dr.ir. M.M.C.G. Warmoeskerken

en de co-promotor
prof.dr. A. Prosperetti

To my parents

Contents

SUMMARY

Current wet textile processes such as washing, dyeing, rinsing etc. suffer from three major drawbacks – low energy and water efficiency and long process times. Mass transfer by diffusion and convection in the textile materials is one of the important mechanisms of the wet textile processes. Ultrasound offers a viable tool for the improvement of the wet textile processes. Over past several years the subject of ultrasound enhanced wet textile processing has been investigated extensively. However, ultrasound based wet textile technology has not served the interests of the textile industry yet. The causes behind this effect are: 1. lack of knowledge of the basic physical mechanism of ultrasound enhanced wet textile processes; and 2. inherent drawbacks of the ultrasonic processors such as non-uniform energy dissipation, erosion of the sonicator surface and the directional sensitivity of cavitation effects. In this thesis, attempts are made for the fulfillment of the above discrepancies that could facilitate the industrial application of this novel technology. The principal aims of this thesis were: 1. Determination of the physical mechanism of the ultrasound enhanced mass transfer in textile materials; and 2. Modeling and optimization of the ultrasonic processors and ultrasonic wet textile processes. To begin with, some basic concepts of acoustic wave phenomena have been discussed using theoretical analysis. The equations for radial motion of the bubble have been presented with and without accounting for the compressibility of the fluid. Numerical simulations of the radial bubble motion have been presented for different operating parameters. It has been found that the radial motion of the bubble and resulting acoustic emission is influenced by several parameters, such as acoustic pressure amplitude, static pressure in the medium, frequency of acoustic wave, and initial bubble radius. The magnitude of the shock wave emitted by the bubble can be taken as a measure of the cavitation intensity in the medium. Next, the studies in deducing the acoustical characteristics of textile materials are presented using precision-woven Polyamide monofilament screening fabrics as the model textiles. The change in the power consumption of the ultrasound horn after introduction of the textile in the acoustic field and the attenuation of the acoustic waves by the textile sample have been taken as the monitoring parameters. A simple mathematical model involving the structural (mass per unit area) and the hydrodynamic (specific flow resistance) characteristics of the textiles has been proposed to determine the acoustical impedance of the textile. It has been found that the textile material forms an almost transparent boundary for the acoustic waves with practically no transmission loss. Further, an attempt is made to characterize an ultrasonic system for the determination of the spatial distribution of cavitation intensity. The method uses wavelet transform analysis of the acoustic emission profiles. The periodic modulation of the acoustic pressure field causes unsteady radial motion of the bubbles, resulting in non-stationary acoustic emission profiles that cannot be analyzed by conventional Fourier Transform. Experimental quantification of relative cavitation intensity at different locations in the ultrasound bath was made using a *Cavitation Noise Coefficient* defined as the sum of the energies of different scales in the wavelet transform of the measured signal. The numerical method involved the simulation of the radial motion of a bubble using experimentally measured acoustic pressure signals as the driving function for radial bubble motion. The numerically predicted spatial variation of the cavitation intensity was in agreement with

the experimental measurements. In an ultrasonic processor, the input electrical energy undergoes many transformations before getting dissipated in the medium as the cavitation energy. Therefore, simultaneous optimization of the discrete steps in the energy transformation chain forms the basis of the optimization of an ultrasonic processor. A new methodology has been proposed for the optimization of an ultrasonic processor that uses the gas content of the system (free and dissolved gas) as the manipulation parameter. The results of the experiments reveal that the power consumption of the ultrasound horn and the cavitation intensity produced in the medium vary significantly with the gas content of the system. The results of the experiments have been explained using a unified physical model that combines the theory of the equivalent circuit of a piezoelectric transducer, the theory of impedance tube, the theory of acoustic wave propagation in bubbly liquid, and the theory of rectified diffusion. An attempt has been made to interpret the experimental and theoretical results for discerning the mechanism of discrete steps in the energy transformation chain, and establishing the inter-relations between the physical parameters involved in the transformation process. Thus this study reveals not only the energetics of an ultrasonic processor but also puts forth an "*integrated approach*" for the optimization of such a processor for any ultrasonic physical or chemical process. Investigations in the physical mechanism of the ultrasonic wet textile processes have been carried out by studying a model wet textile process (washing of EMPA 101 model fabric). Distinction between several possible mechanisms for the ultrasonic enhancement of wet textile processing is made by manipulation of those process parameters that manifest their effect on the process through their effect on the ultrasound wave phenomena and bubble dynamics. These parameters are: 1. gas content of the fabric and medium; 2. position of the fabric in standing wave field; 3. nucleation in the medium; and 4. static pressure of the system. The model process has been carried out using both commercial ultrasonic system as well as specially built ultrasonic equipment, which offers precise control over operating parameters. In addition, more advanced techniques such as microscopic analyses of the surface of the treated fabric and its cross-section and the high-speed photography of the washing process have also been used to elucidate the physical mechanism of the ultrasonic wet textile process. The conclusion of all the experiments and analyses presented in this study is that transient cavitation in the medium, in the close vicinity of the textile surface, is the principal physical mechanism of the ultrasonic wet textile processes. Finally, studies in the modeling and optimization of the ultrasonic wet textile processing are presented. In the absence of precise quantification of the convection created due to the transient bubble motion near the textile surface, a *convective diffusion coefficient* has been defined, which is representative of the mass transfer enhancement. The soil removal from the textile shows two distinct regimes with two different convective diffusion coefficients. This result is explained in terms of the non-uniform initial distribution of the soil over the textile surface with different fractions of total soil distributed in the inter-yarn and intra-yarn pores. The order of magnitude of the mass transfer enhancement is in the range 1000 - 2000. The second aspect of the optimization of an ultrasonic wet textile process is the prevention of erosion of the textile surface, which is responsible for reduction in the durability of the textile. S.E.M. analyses of the

surfaces of two textile samples treated at different acoustic pressure amplitudes reveal that a reduction in the acoustic pressure amplitude (while maintaining its value above the transient cavitation threshold) could be a possible way of reducing the textile erosion after ultrasonic treatment. Thirdly, simulations of a dual frequency acoustic processor, which has been employed by many researchers successfully for the intensification of wet textile treatments are presented. It is evident from the simulations results that the spatial distribution of the cavitation events can be controlled by the application of a dual frequency acoustic field, and manipulation of the characteristic parameters of such a field. This means that the major disadvantages of the sonic reactor mentioned earlier could be overcome by application of a dual frequency acoustic field. To put in a nutshell, two distinct contributions made by this thesis are: 1. Establishment of the physical mechanism of the ultrasonic enhancement of wet textile processes; 2. Proposition of principles of *Sonoprocess Engineering* by unification of the principles of physical acoustics (ultrasound wave phenomena and bubble dynamics) and the principles of process engineering.

SAMENVATTING

De huidige processen in de textielveredelingsindistrie (zoals wassen, verven, spoelen etc.) lijden aan drie grote tekortkomingen – een inefficient gebruik van water en energie en lange procestijden. Eén van de belangrijkste mechanismen in de natte textielveredeling is de stofoverdracht door diffusie en convectie. De toepassing van ultrasoon geluid zou een levensvatbare techniek kunnen zijn voor de verbetering van de natte textielveredelingsprocessen. Het afgelopen aantal jaren is de toepassing van ultrasoon geluid in de natte textielveredeling onderwerp geweest van een groot aantal studies. Toch wordt ultrasoon geluid nog niet in de praktijk toegepast. Hiervoor kunnen een tweetal oorzaken genoemd worden: 1. een gebrek aan fundamentele kennis van de toepassing van ultrasoon geluid in textiele veredelingsprocessen; en 2. de technische problemen van de toegepaste ultrasone systemen, zoals een niet-uniforme energiedissipatie, erosie van het transduceroppervlak en anisotropie van de cavitatie. In dit proefschrift zal geprobeerd worden om de toepassing van deze nieuwe technologie in de textielindustrie mogelijk te maken door het oplossen van de bovenstaande problemen. De hoofddoelstellingen van dit proefschrift zijn: 1. het bepalen van het mechanisme van de, door het toepassen van ultrasoon geluid, versnelde stofoverdracht in de natte textielveredelingsprocessen; en 2. het modelleren en optimaliseren van ultrasone systemen en ultrasone textielveredelingsprocessen. Er is gestart met een theoretische analyse van de basisconcepten van acoustische golfverschijnselen. De vergelijkingen voor de radiale trilling van een gasbel zijn besproken, al dan niet met verwaarlozing van de compressibiliteit van de vloeistof. Deze radiale trilling is vervolgens numeriek gesimuleerd. De trilling blijkt door een aantal grootheden bepaald te worden, zoals de amplitude van de akoestische druk, de statische druk in het medium, de frequentie van de geluidsgolf, de initiele beldiameter en de temperatuur van het medium. De kracht van de schokgolf die door de gasbel wordt uitgezonden is gebruikt als maat voor de *intensiteit van de cavitatie*. Vervolgens zijn de acoustische eigenschappen van textiele materialen onderzocht. Zeer precies gewoven polyamide filterdoeken werden hiervoor als modelmateriaal gebruikt. De invloed van de aanwezigheid van een textiel materiaal in het geluidsveld op het opgenomen vermogen van de ultrasone hoorn en op de verzwakking van de geluidsgolf werd bepaald. Er is vervolgens een eenvoudig mathematisch model opgesteld voor het bepalen van de akoestische impedantie van een textiel materiaal. Hierin zijn zowel de structurele (massa per eenheid van oppervlak) als de hydrodynamische (stromingsweerstand) eigenschappen van het textiele materiaal verwerkt. Textiele materialen blijken, akoestisch gezien, zo goed als transparant te zijn. Wavelet transformatie van het geluidsdrukspectrum is gebruikt om de ruimtelijke verdeling van de intensiteit van de cavitatie in een ultrasoon systeem te bepalen. Conventionele Fourier transformatie kan in een ultrasoon systeem niet gebruikt worden, omdat de periodieke modulatie van de geluidsdruk leidt tot een instabiele radiale trilling van de gasbellen, wat uiteindelijk resulteert in niet-stationaire geluidsdrukprofielen. De *Cavitation Noise Coefficient* werd gebruikt voor de experimentele bepaling van de ruimtelijke verdeling van de relatieve intensiteit van de cavitatie. Deze *Cavitation Noise Coefficient* is gedefinieerd als de som van de energieën in de verschillende schalen van de wavelet transformatie. De radiale trilling van een gasbel werd numeriek gesimuleerd, waarbij de experimenteel gemeten geluidsdrukken werden gebruikt als de drijvende

kracht voor deze radiale trillingen. De ruimtelijke verdeling van de cavitatieïntensiteit, zoals bepaald met de numerieke simulaties, kwam goed overeen met de experimenteel bepaalde. In een ultrasoon systeem ondergaat de elektrische energie een aantal transformaties voordat zij in het medium gedissipeerd kan worden als cavitatieënergie. Een gelijktijdige optimalisatie van de afzonderlijke stappen in deze transformatieketen vormt dan ook de basis voor een optimalisatie van het ultrasone systeem. Voor een dergelijke optimalisatie is een nieuwe methode ontwikkeld, met het gasgehalte van het systeem (zowel gedispergeerd als opgelost) als stuurparameter. Uit de experimentele resultaten blijkt dat zowel het opgenomen vermogen van de ultrasone hoorn, als de intensiteit van de cavitatie sterk worden beïnvloed door het gasgehalte van het systeem. De experimentele resultaten werden verklaard door een fysische model, waarin het equivalente elektrische circuit van een piëzo-electrische transducer, de theorie van de impedantiebuis, de voortbeweging van een geluidsgolf in een vloeistofsysteem met gasbellen en de 'rectified' diffusie zijn verwerkt. Met behulp van de theoretische en experimentele resultaten, is geprobeerd om het mechanisme van de afzonderlijke stappen in de energietransformatieketen te onderscheiden en om relaties op te stellen voor de fysische grootheden in dit transformatieproces. Dit proefschrift bespreekt niet alleen de energiehuishouding van een ultrasoon systeem, maar stelt ook een geïntegreerde aanpak voor om een dergelijk systeem te optimaliseren, onafhankelijk van de uiteindelijke applicatie. Het wassen van een EMPA 101 doek is gekozen als modelproces voor het onderzoek naar het fysisch mechanisme van ultrasone textielverdelingsprocessen. Een aantal parameters is gevarieerd om het juiste mechanisme van de intensivering van textiele veredelingsprocessen door middel van de toepassing van ultrasoon geluid vast te kunnen stellen. Deze parameters zijn: 1. het gasgehalte van het systeem; 2. de positie van het textiele materiaal in het het veld van de staande geluidsgolf; 3. de nucleatie in het medium; en 4. de statische druk in het systeem. Voor de experimenten is zowel gebruik gemaakt van een commercieel verkrijgbaar ultrasoon bad, als van een speciaal ontworpen en gebouwd ultrasoon bad, dat een exacte controle van de procesparameters mogelijk maakt. Verder is gebruik gemaakt van geavanceerde technieken als microscopische analyse van het weefseloppervlak en dwarsdoorsneden daarvan en high-speed fotografische opnamen van het wasproces, om het fysische mechanisme van het ultrasone textielveredelingsproces te kunnen bepalen. Uit de experimenten en analyses, zoals gepresenteerd in dit proefschrift, blijkt dat 'transient' cavitatie in de nabijheid van het textiele oppervlak het fysische mechanisme is van ultrasoon geïntensiveerde textielveredelingsprocessen. Ook is een studie uitgevoerd naar het modelleren en optimaliseren van ultrasone textielveredelingsprocessen. Omdat het niet mogelijk bleek om de convectie, gecreëerd door de transient cavitatie, exact te kwantificeren, is een convectieve diffusiecoëfficient gedefinieerd die representatief is voor de versnelling van de stofoverdracht. Bij de vuilverwijdering blijkt onderscheid gemaakt te kunnen worden in een tweetal afzonderlijke regimes in de tijd, met twee verschillende convectieve diffusiecoëfficienten. Dit wordt verklaard door de niet-uniforme verdeling van het vuil over het textiel, waarbij verschillende fracties verdeeld zijn over poriën tussen de garens en de poriën in het garen. De stofoverdracht blijkt een faktor 1000-10000 versneld te worden door de toepassing van ultrasoon geluid. Een tweede belangrijk aspect bij de

optimalisatie van een ultrasoon textielveredelingsproces is het voorkomen van beschadiging van het textiele oppervlak, waardoor de mechanische sterkte van het textiele materiaal af zou kunnen nemen. Analyse van het textieloppervlak met behulp van de SEM, laat zien dat een verlaging van de amplitude van de acoustische druk (uiteraard moet deze wel boven de cavitatie threshold blijven) een mogelijkheid is om de beschadiging van het textiel te verminderen. Als laatste is het dual-frequency acoustisch systeem gesimuleerd, dat al door een groot aantal onderzoekers succesvol is toegepast voor het intensificeren van textiele veredelingsprocessen. Uit deze simulaties is duidelijk naar voren gekomen dat de ruimtelijke verdeling van de cavitatie door de toepassing van een dergelijk systeem en manipulatie van de procesparameters geregeld kan worden. Dit betekent dat de eerder genoemde belangrijke problemen van de ultrasone reactor opgelost kunnen worden door de toepassing van een dergelijk dual-frequency acoustisch systeem. Nog eens kort samengevat, in dit proefschrift worden de volgende twee zaken behandeld: 1. het vaststellen van het fysische mechanisme van de intensivering van textielverdelingsprocessen met behulp van ultrasoon geluid; 2. het opstellen van algemene principes voor *'Sonoprocess Engineering'*, door het combineren van de fysica van ultrasoon geluid (acoustische golfverschijnselen en de dynamica van trillende gasbellen) met de principes van de procestechnologie.

GENERAL INTRODUCTION

Wet textile finishing is defined as the treatment of textile materials with chemicals in order to manipulate the properties of the textiles such as color, design, hydrophobicity etc. Wet textile finishing basically involves addition or removal of solid / liquid substances to or from the textiles. More precisely *mass transfer* in textiles is the basic phenomenon in the wet textile finishing. Wet textile finishing forms the most important stage in the textile processing chain shown in figure 1. Wet textile processes are called *wet* because they employ water as the medium for the transport of mass and heat across textile materials. Wet textile process technology involves know-how of several diverse scientific disciplines such as color chemistry, fiber science, polymer technology, enzyme technology, biochemistry, mechanical engineering, chemical engineering and applied physics. Thus, wet textile processing is the most *knowledge-intensive* area of the entire textile processing chain.

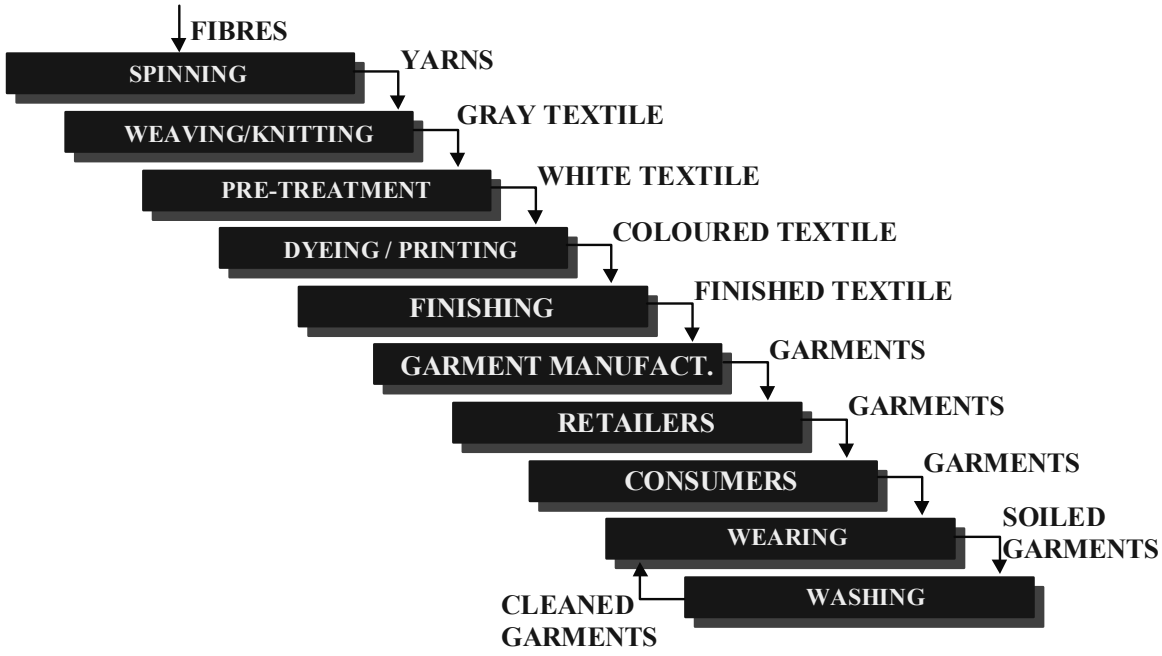

Figure 1: Textile processing chain.

The general structure of the textile is shown in figure 2. A textile can be characterized as a visco-elastic (bi)-porous solid surface made up of yarns of natural (e.g. cotton) or synthetic (e.g. polyester) material. Depending on the material of construction, the textiles can have either a single porosity between the yarns (inter-yarn), or dual porosity between and inside the yarns (inter and intra-yarn). Cotton textiles have dual porosity, while synthetic textiles can have either single or dual porosity depending on the type of the yarn, whether monofilament or multifilament. Monofilament textiles have yarns made up of a single endless filament. The multifilament fabrics are made up of a cluster of filaments. The difference between multifilament fabrics and cotton fabrics (although both are bi-porous) is that in case of multi-filament fabrics the length of filament is same as that of the yarn, while in case of cotton fabrics the filament (or staple fiber) is much shorter than the yarn.

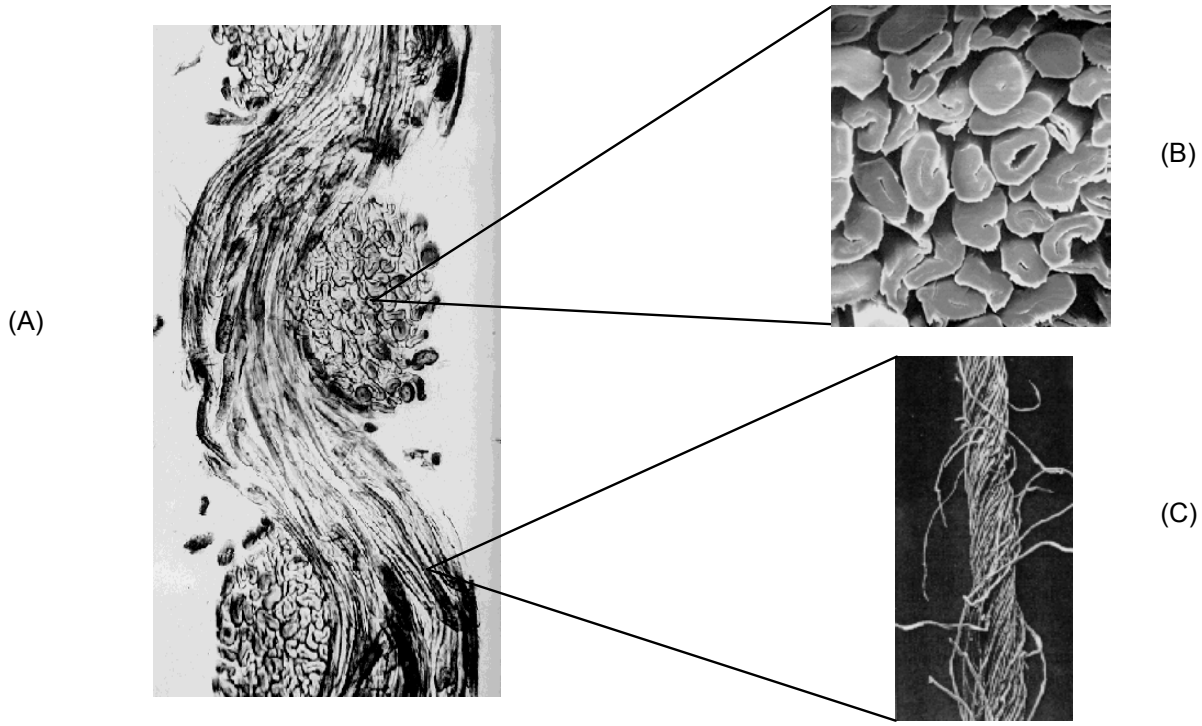

Figure 2: General structure of textile materials. (A) Cross-section of a cotton textile. (B) Fibers; (C) Yarn.

Till mid-1930s the textile industry in Europe was product oriented, very much like the contemporary chemical industry. This attitude started changing towards beginning of 1940s, with the introduction of the concepts of "*unit operations*" and "*transport phenomena*" to convert the product-oriented know-how into the language of "*process technology*". The need of the textile industry was two fold: basic understanding of the physics, chemistry and engineering principles of the wet textile processes and, secondly, the constructional skill in the design of textile machinery. It was proposed by Parish (1962, 1965) and Meier-Windhorst (1969) that chemical engineering principles of transport phenomena and unit operations could be used for the mathematical modeling of the wet textile processes. As such, the theory of transport phenomena in chemical engineering (a term used for combined description of mass, heat and momentum transfer) has been applied quite successfully for the design and optimization of the wet textile processes and the machinery for it. Due to extensive research in this area over past several decades, diverse sub-disciplines of process technology form an integral part of the present wet textile process technology as described in figure 3.

Textile Technology Group at University of Twente

In 1960s, in order to fulfil the needs for scientific know-how of Dutch textile industry, a working group called *Transport Phenomena in Textile Finishing* was founded under the leadership of Professor Groot Wassink with participation of representatives from the textile industry, TNO-Fiber Institute and the process technology group of University of Twente. A significant amount of work on the application of the theory of

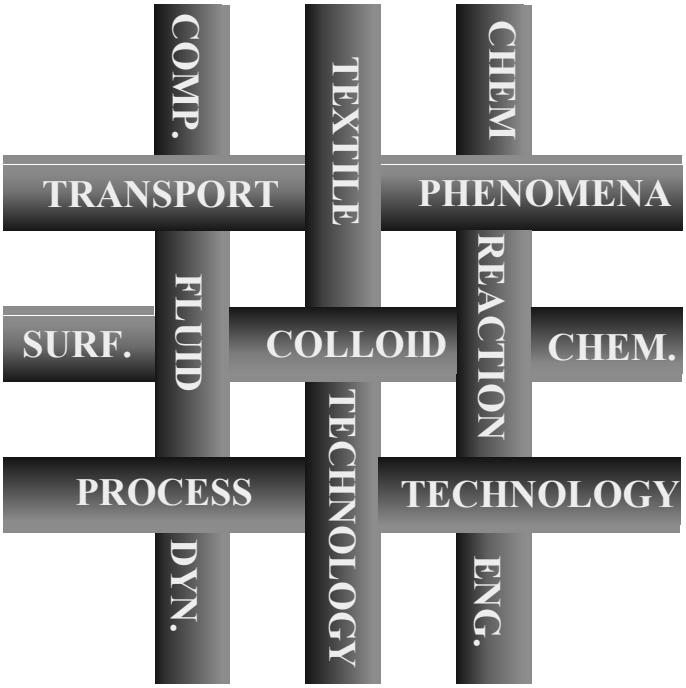

Figure 3: The weave between process technology and textile technology.

unit operations for modeling and optimization of different textile processes, such as washing, rinsing, and drying, was done at the University of Twente during 1980s by Groot Wassink and co-workers. An excellent compilation of the work of Groot Wassink is given in the thesis of van der Linden (1984). On the basis of the mathematical models for mass, heat and momentum transfer in textile materials, Groot Wassink and co-workers also outlined several useful design and optimization criteria for the machinery for wet textile processing. In 1991, the textile process technology group got an independent identity as *T.G.M.* (*Technology of structured materials*) group that was completely sponsored by the Dutch Textile Industry. The principal aim of this new group was to develop more efficient wet textile processes with application of the principles of physics, chemistry and engineering.

So far, the research in the T.G.M. group (now renamed as Textile Technology Group) has focussed on transport and surface phenomena in wet textile processing. An extensive research in foam finishing of textile materials was carried out, which resulted in three theses: Kroezen (1988), Lemmen (1991), and Engelsen (1996). Liquid flow through the textile materials during wet textile processes is an aspect that has critical influence on the efficiency of these processes. A thorough study of flow resistances of different types of textile materials was conducted by Gooijer (1998).

Aim and scope of the present thesis

Harnessing ultrasound for the process improvement is a highly active area of research. Several homogeneous and heterogeneous chemical reactions have been

demonstrated to benefit from the application of ultrasound. In the last 10 years, significant research has also been conducted to investigate the engineering aspects of ultrasound-enhanced chemical processes (for a detailed discussion on this subject refer to Shah *et al*., 1999). Ultrasound has been employed quite successfully for the improvement of wet textile processes over past several decades. But, the exact physical mechanism of the enhancement in wet textile processing due to ultrasound is not known yet, although several researchers have proposed different hypotheses for it. Secondly, all of the studies in the ultrasound-enhanced wet textile processes have been restricted to laboratory scale only with no application on industrial or even pilot scale. The major reason that has led to this effect is that most of the research in this area is of a *black box* type, where the primary focus is only on the results with very little or no effort directed at elucidating the basic physical mechanism of these processes. In addition, very limited attempt was devoted to establish a link between the process parameters and the actual physical or chemical effect. The second reason that has hampered the implementation of ultrasound-based technology on an industrial scale is the inherent drawbacks of the sonic processor themselves. These are: directional sensitivity of the ultrasonic effect, non-uniform energy dissipation pattern in the sonic processor, and erosion of the sonicator surface itself.

The present thesis is aimed at two objectives: (1) to establish the exact physical mechanism for the enhancement of wet textile processes with ultrasound, and (2) to provide design and optimization strategies for ultrasonic wet textile processes that will help realize their application on industrial scale. The aim of this thesis can also be described as the development of the *sonoprocess engineering* (a newly coined term for process engineering with application of ultrasound) principles for wet textile processes. The outline of the thesis is as follows:

- In chapter 1 we present the chemical engineering perspectives of wet textile processing. The salient features of flow through and the mass transfer in the textile materials are demonstrated using a simple analysis. Later, a brief review of the literature in the area of transport phenomena in the textile materials is presented, followed by a literature review in the area of ultrasound assisted wet textile processes.
- Some basic principles and equations of the ultrasound wave phenomena and bubble dynamics are presented in chapter 2. With the help of numerical simulations of the bubble dynamics, some salient features of cavitation phenomena are explained, which form useful basis for the explanation of the results of subsequent chapters.
- In chapter 3, the acoustical characteristics of textile materials are described. The change in the power consumption of the ultrasound horn with the presence of the textile at different locations in a standing wave field, and the attenuation of the acoustic wave by the textile are analyzed to deduce the specific acoustic impedance of the textile materials. The experimental results are explained with help of a theoretical model that involves both structural and hydrodynamic properties of the textiles.
- Chapter 4 presents a new methodology for the characterization of large-scale ultrasonic processors, using the wavelet transform of the acoustic emission to determine the spatial distribution of cavitation events, and hence, the energy

dissipation patterns.

- Chapter 5 depicts the energetics (or the energy mechanism) of an ultrasonic processor. In an ultrasonic processor, the input electrical energy undergoes many transformations before getting dissipated in the medium as cavitation energy. In this chapter we describe, with experiments and numerical simulations, the mechanism of discrete steps in the energy transformation chain by identifying the involved physical parameters and the inter-relations among them.
- Chapter 6 describes the investigations of the mechanism of the ultrasound-enhanced mass transfer in textile materials. Washing of EMPA 101 fabric (a cotton textile soiled with carbon soot and olive oil) is used as a model process in these investigations.
- In chapter 7, an attempt is made to model and optimize the ultrasound-enhanced wet textile processes. The quantification of the mass transfer enhancement in textiles with ultrasound is done with the help of a *convective diffusion coefficient*. Some additional aspects of the optimization ultrasonic wet textile processes, such as prevention of the fabric erosion and advantages of dual frequency ultrasonic processors, are also presented in this chapter.

References

- Engelsen, C.W. den, *Structure, properties and behavior of three phase foam*, Ph.D. thesis, University of Twente, 1996.
- Gooijer, H., *Flow resistance of textile materials*, Ph.D. thesis, University of Twente, 1998.
- Kroezen, A.B.J., *Flow properties of foam in rotor-stator mixers and distribution equipment*, Ph.D. thesis, University of Twente, 1988.
- Lemmen, J.T.E., *Foam finishing technology*: *The interaction of foam with stagnant and moving substrates*, Ph.D. thesis, University of Twente, 1991.
- Linden, H.J.L.J. van der, *Transport phenomena in textile finishing equipment*, Ph.D. thesis, University of Twente, 1984.
- Meier-Windhorst, C.A., *Melliand Textielberichte*, **50**, 832 (1969).
- Parish, G.J., "Continuous rinsing of impurities from textile fabrics", *American Dyestuff Reporter*, 402-408 (May 1965).
- Parish, G.J., "Some fundamental aspects of the washing process", *Journal of Society of Dyers and Colorists*, **78**(3), 109-114 (1962).
- Shah, Y.T., A.B. Pandit, and V.S. Moholkar, *Cavitation Reaction Engineering*, Kluwer academic/Plenum publishers, New York, 1999.

1

CHEMICAL ENGINEERING ASPECTS OF WET TEXTILE PROCESSESING: A LITERATURE REVIEW

1.1 Transport phenomena in textile materials

1.1.1 Fluid flow through the fabric

The nature of fluid flow through fabric is an important aspect of wet textile processes. This subject has been extensively studied by numerous researchers for both gaseous and liquid flows through textile. In accordance with the theme of the present thesis, we give herewith an analysis of the liquid flow through the fabric. Van den Brekel (1988), and van den Brekel & de Jong (1989) have studied the hydrodynamics of packed textile beds using several existing correlations for the flow of fluid through porous materials. They conclude that most reported theories on the fluid flow through porous materials are not suitable for predicting the overall permeability coefficients of cotton fabrics due to the dual porosity of the fabric itself and the structural changes in the fabrics (such as swelling of fibers) that take place after contact with a liquid. For synthetic fabrics (with better defined structure and smoother, cylindrical yarns) a better match between the observed and predicted permeability coefficients has been found. A more detailed and extensive study of the flow resistances of the textile materials is given by Gooijer (1998). Gooijer assesses the three existing models in the literature, viz. Kozeny-Carman model, drag model, and pore model for possible application to the three kinds of textiles, viz. monofilaments, multifilaments and nonwovens. In order to have a better insight into the flow resistances of the fabrics, Gooijer also takes into account the characterization of the fabrics by determining the pore size distributions, and the constructional details of the textile surface (such as the nature of the inter-yarn cells for different weaves) with new models for the description of the inter-yarn pores.

For a fluid flowing through the textile, the inter-yarn and intra-yarn regions form two parallel paths. The relative contribution of the flows in these two regions can be judged by the ratio of the permeabilities of these regions. The permeabilities of the inter-yarn and intra-yarn regions are (Gooijer, 1998):

$$K_{\text{intra-yarn}} = \frac{1}{16\,K_o}\,\frac{\varepsilon_f^3}{(1-\varepsilon_f)^2}\,d_f^2 \tag{1}$$

$$K_{\text{inter-yarn}} = \frac{1}{16\,K_o}\,\frac{\varepsilon_y^3}{(1-\varepsilon_y)^2}\,d_y^2 \tag{2}$$

We make an assumption of constant K_o for the inter-yarn and intra-yarn pores on basis of similar porosities of an individual yarn and the overall textile (Gooijer, 1998). The ratio of equations 7a and 7b with representative values of the parameters: $\varepsilon_f = 0.35 - 0.45$; $\varepsilon_y = 0.4 - 0.5$; $d_y = 250$ μm.; $d_f = 15$ μm. gives:

$$\frac{K_{\text{intra-yarn}}}{K_{\text{inter-yarn}}} = \frac{1}{200} \text{ to } \frac{1}{2000} \tag{3}$$

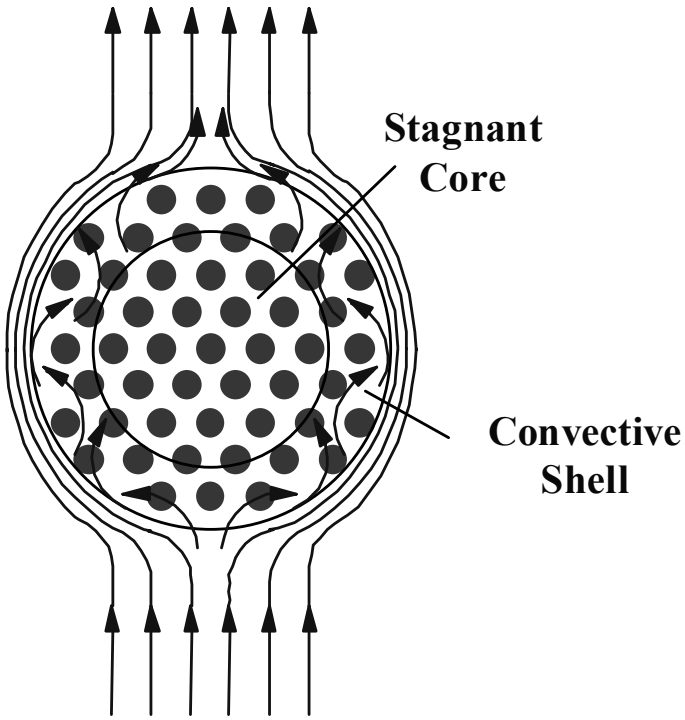

Figure 1: Top view of a yarn held in the fluid flow perpendicular to it. It can be seen that most of the flow takes place through the larger inter-yarn pores, which is the least-resistant path for the flow. The flow in the inter-yarn region may penetrate to a small extent inside the yarn, thus giving rise to a convective shell near its periphery. However, the central core of the yarns remains a stagnant zones where the mass transfer occurs by diffusion alone.

The ratio of $K_{intra\text{-}yarn}$ and $K_{inter\text{-}yarn}$ indicates that the permeability between the yarns is far higher than the permeability in the yarns. Therefore, most of the flow will follow the path of least resistance (between the yarns), and practically no flow will occur through the yarns. The flow through the inter-yarn region may, however, penetrate an individual yarn to a small extent. This can create a thin convective shell near the periphery of the yarn, as shown in figure 1. Nonetheless, the central core of the yarn still remains a stagnant core zone with no flow inside. Therefore, the mass transfer in this region occurs only by the slow process of diffusion.

1.1.2 Mass transfer in the fabric

Mass transfer in the inter-yarn and intra-yarn pores of the fabric forms one of the basic physical mechanisms of the wet textile processes such as washing, dyeing, bleaching, mercerization and rinsing. Like in other porous materials, such as catalysts, mass transfer in the textiles also occurs by the convection and diffusion in the pores of the textiles. We consider here the case of textiles with dual porosity: inter-yarn and intra-yarn porosity. For washing, the mass transfer in these textile materials can be divided into three distinct steps:

1. Mass transfer from the stagnant intra-yarn region to the inter-yarn region through the

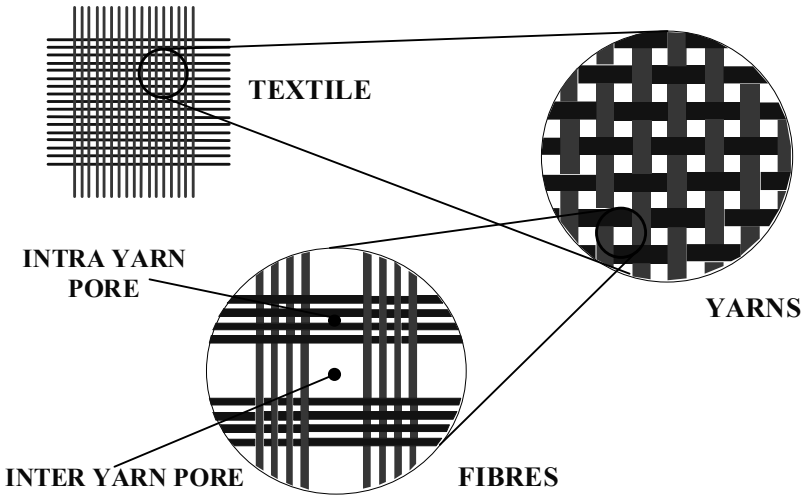

(A)

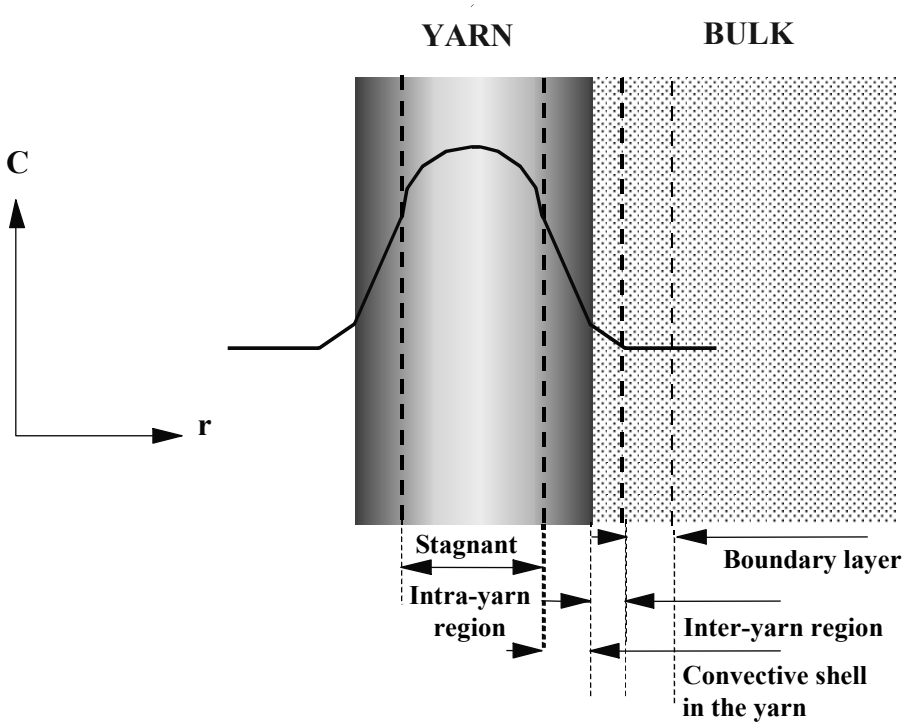

(B)

Figure 2: The mass transfer mechanism in the textiles. (A) Schematic diagram indicating the general structure and dual porosity of the textiles; (B) The three stages of mass transfer in textile materials and the typical concentration profiles of the diffusing substance.

convective shell on the periphery of the yarn.

2. Mass transfer from the inter-yarn region to the boundary layer between the bulk liquid and the textile surface.
3. Mass transfer from the boundary layer to the bulk liquid.

Typical concentration profiles of the substance being transported through the textile are shown in figure 2, along with a schematic diagram of the structure of the woven textile. As can be inferred from figure 2, the mass transfer steps occur in series. In order to assess the relative contribution of each of these steps to the overall mass transfer process, one needs to have an insight into the nature of fluid flow through the textiles. In order to find the overall mass transfer coefficient (K_T) in the textile, we specify k_1, k_2 and k_3 as the individual mass transfer coefficients for the first, second, and third step of mass transfer mentioned above. K_T can be determined using familiar relationship in the mass transfer theory:

$$\frac{1}{K_T} = \frac{1}{k_1} + \frac{1}{k_2} + \frac{1}{k_3} \tag{4}$$

We make a simplifying assumption that the mass transfer in the third step (from the boundary layer to the bulk) is very fast compared to the other steps. Now, to estimate the relative magnitudes of k_1 & k_2, we use the mass transfer correlations developed for a packed bed. Several correlations for the mass transfer coefficients are listed by Janssen and Warmoeskerken (1997). A single yarn can approximately be described as a cylinder. To estimate the inter-yarn mass transfer coefficient, we choose the following correlation for the flow past long cylinders perpendicular to the flow:

$$\langle Sh \rangle = 0.42\, Sc^{1/5} + 0.57\, Re^{1/2}\, Sc^{1/3} \quad 1 < Re < 10^4;\ Sc > 0.7;\ Pe >> 1. \tag{5}$$

The non-dimensional numbers are defined as:

$$Re = \frac{\rho_L \bar{v} d_y}{\mu}; \qquad Sh = \frac{k d_y}{D}; \qquad Pe = \frac{\bar{v} d_y}{D} \tag{6}$$

To estimate the inter-yarn mass transfer coefficient, we substitute the following representative values in the above correlation: $\bar{v}$ = 2 cm s^{-1}; d_y = 250 μm; ρ_L = 1000 kg m^{-3}; D = 1 × 10^{-5} cm^2 s^{-1}; ε = 0.5 and Sc ≈ 1000. Substituting the above values, we find that Sh ≈ 25, and from the definition of the Sherwood number it follows that $k_2 \approx 1.4 \times 10^{-2}$ cm s^{-1}. To estimate the mass transfer coefficient inside the yarn, we make use of the analysis given by Masui *et al*. (1978), who have shown that for longer contact times [Dt/d_y^2 >> 1] the Sherwood number ~ 5.8. Due to the porous structure of the yarns, the effective diffusion coefficient inside the yarn is smaller than the actual diffusion coefficient. Therefore, we use the correction given by Rietema (1976) to estimate the effective diffusion coefficient in a porous medium:

$$D_e = \frac{\varepsilon_y}{\alpha^2} D \tag{7}$$

Substituting representative values of ε_y and α (tortuosity factor) as 0.4 and 2 respectively, gives $D_e \approx 2 \times 10^{-6}$ cm^2 s^{-1}. The mass transfer coefficient inside the yarn

(k_1) is then calculated from the Sherwood number as $\approx 4 \times 10^{-4}$ cm s^{-1}. The ratio of k_1 and k_2 gives us an idea of the mass transfer process in the textiles: 97% of the mass transfer resistance is determined by the diffusion process inside the yarns. As such, the diffusional mass transfer in the yarn is the rate-controlling step in the overall mass transfer in the textile. This also implies that enhancement of the mass transfer in the textile would necessitate reduction of the stagnant zone in the yarns or in other words conversion of the intra-yarn diffusion process into the faster convection.

1.2 Mass transfer in textile materials: A literature review

The subject of mass transport in textile materials has been investigated for over past five decades both experimentally and theoretically. In 1960s it was first proposed by Parish (1962) and Meier-Windhorst (1969) that the chemical engineering principles of transport phenomena can be applied for the mathematical modeling and optimization of the wet textile processes. Thereafter, several papers have appeared that have tried to mathematically describe and optimize the wet textile processes, such as dyeing and washing, using chemical engineering principles. We present a brief review of the literature in this area. We would like to specifically mention that both academic institutions and the textile machinery manufacturers have contributed to the literature in this area. We have included, in this review, only the literature contributed by the academic institutions, since it presents a more scientific and fundamental approach to the problem of modeling mass transfer in the wet textile processes. The literature on the mass transfer in the wet textile processes treats two types of processes: the mass transfer in textile finishing process, and the mass transfer in laundry processes.

Tuzcon and Short (1960) have studied the mass transfer in a laundry washing machine. Using a simple mass transfer model for batch processes, they gave the following expression for the variation of the concentration of an impurity in the washing bath as a function of time:

$$\frac{C_\infty - C}{C_\infty - C_{b0}} = \exp\left[-\frac{kAt}{V_c}\right] \tag{8}$$

Tuzcon and Short have also investigated the relation between the mass transfer coefficient and the hydrodynamics of the bath using correlations for the Sherwood number. The major conclusions of their study can be summarized as: (1) variation in the concentrations of the impurity in the bath is exponential in time; (2) the relation between the transfer coefficient and the angular velocity of the fluid is a direct proportionality, when the washing load is introduced uniformly in the machine; (3) the amount of water in the bath has practically no influence on the rate of impurity removal; (4) the transfer coefficient (kA/V_c) is independent of the size of the washer, provided that all the other parameters remain unaltered. The conclusions of this study hinted that increasing the flow through the textile could be a solution for the enhancement of the mass transfer.

A more general treatment of the washing process in the textile finishing using the

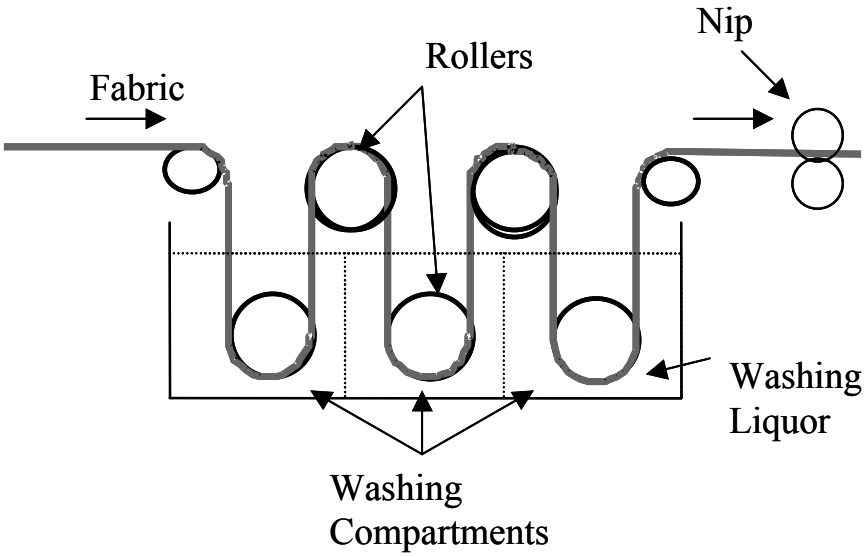

Figure 3: A conventional open-width washing unit (with three compartments).

principles of the extraction process has been given by Parish (1962, 1965). For a simple washing unit operated in counter-current fashion (shown in figure 3), Parish has defined the washing performance as the ratio of the impurity concentration on the incoming fabric ($C_{F,0}$) and the impurity concentration on the washed fabric ($C_{F,1}$):

$$\frac{C_{F,1}}{C_{F,0}} = \frac{1}{1+F} \tag{9}$$

where F is the liquor flow ratio defined as:

$$F = \frac{\text{Weight of wash water passing across the washing unit in given time}}{\text{Weight of water carried by fabric}} \tag{10}$$

For an imperfect washing unit, where the equilibrium concentrations in the fabric and the washing liquor are not equal, Parish has defined a "washing parameter" as:

$$K' = \frac{C_{F,1} - C_{eq}}{C_{F,0} - C_{eq}} \tag{11}$$

where C_{eq} is the equilibrium impurity concentration on the fabric for imperfect washing. The washing performance relation for a single unit is:

$$\frac{C_{F,1}}{C_{F,0}} = \frac{1 - K' + FK'}{1 - K' + F} \tag{12}$$

For the case of preferential retention of the impurity by the fabric, the equilibrium relation is modified as: $(C_{eq})_1 = A' C_{L,1}$; with $C_{L,1}$ being the impurity concentration in the liquid. The modified expression for the washing parameter is:

$$\frac{C_{F,1}}{C_{F,0}} = \frac{A'(1 - K') + FK'}{A'(1 - K') + F} \tag{13}$$

An additional correction to the washing theory of Parish has been provided by Ratna Prabhu *et al.* (1970, 1971), who have presented the effect of *squeezing dilution*. When the fabric with a certain impurity concentration and moisture content enters the washing unit, it is squeezed at the nip, and some of the moisture is removed. Thus, the moisture content of the fabric is reduced below saturation, but the impurity concentration remains the same. When the fabric enters the washing unit, some of the washing liquor is adsorbed by the fabric, thus causing a reduction in the concentration of the impurity. Ratna Prabhu *et al.* have proved that the washing parameter is the same as the squeeze factor, defined as the ratio of moisture content of the fabric to the saturation moisture content of the fabric.

Another perspective on the problem of mass transfer in textiles during the dyeing process has been presented by McGregor and co-workers (1965). In the first part of their analysis of the effect of the liquid flow rate on the rate of dyeing, they have given a description of the "rate limiting step" of the dyeing process. The dyeing process occurs in three steps:

1. Transport of the dye from the bath to the fiber surface.
2. Adsorption of the dye on the fiber surface.
3. Diffusion of the dye into the fiber.

McGregor and Peters have used Fick's diffusion theory to conclude that the major concentration changes, as a consequence of the absorption of the dye by a porous solid such as textile, are located in a thin layer of liquid close to the surface of the solid. This layer is called *diffusional boundary layer*, and is usually much thinner than the hydrodynamic boundary layer. Figure 4 shows the two boundary layers and their relative thicknesses. McGregor and Peters have attributed dyeing rate enhancement of the fabric with stirring to the reduction in the diffusional boundary layer thickness.

In a second paper on the effect of the flow rate on the rate of dyeing, McGregor (1965) have examined the structure of the fluid flow through the textile, and its effect on the diffusional boundary layer. Using an analysis similar to the one given in section 1.1.1, he concluded that most part of the total flow through the textile will occur through the least resistant path of inter-yarn region, while very little or no flow in the intra-yarn region. This is true for both situations: a single isolated yarn and the complete textile, which is an assembly of woven yarns. Therefore, the penetration of the dye in the intra-yarn pores will be a diffusion process. Apart from this, McGregor has also given a theoretical analysis of the flow through the porous solids and its adoption for the analysis of the flow through the textile. With the combination of the capillary theory and the drag

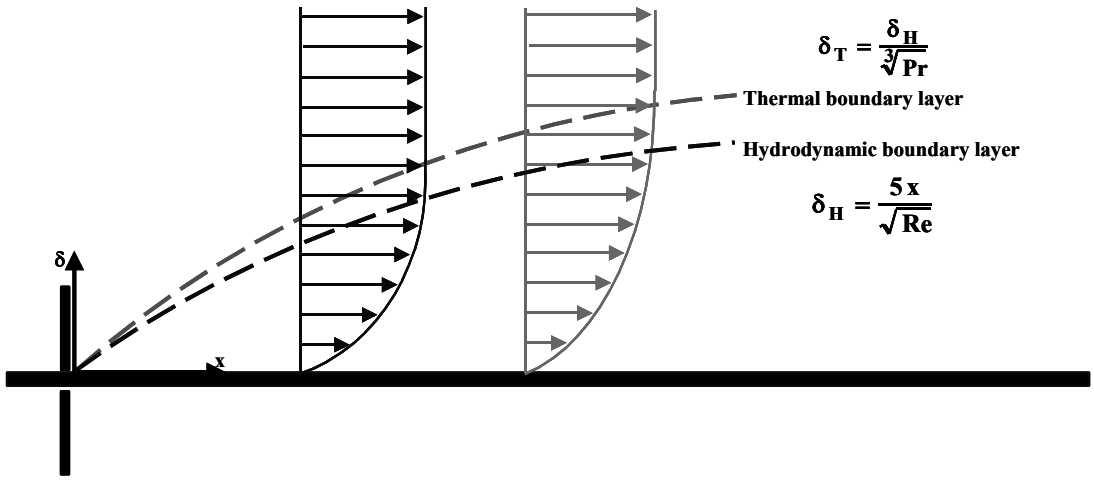

Figure 4: Formation of boundary layers over a solid surface. The diffusion boundary layer is almost 10 times thinner than the hydrodynamic boundary layer, whose thickness is a function of the Reynolds number for the flow.

theory, McGregor has given the following expression for Kozeny's constant for the textiles:

$$K_o \approx 5.5 + 0.48 \frac{\varepsilon^2}{1 - \varepsilon} \tag{14}$$

McGregor has also made a further distinction for the special effects arising in case of a high Reynolds number flow. At these flow conditions, the relation between the pressure drop across the textile and the mean fluid velocity through the textile is not linear. McGregor has proposed that at these flow conditions there is a formation of wakes in the flow behind the yarns (where flow separation occurs) and, hence, the absorption of the dye does not rise with the fluid velocity. In the case of multi-layer textiles, the fluid velocity in the inter-yarn region takes some time to develop a parabolic profile after the fluid enters textile matrix. In this case, the process of dye transport occurs by diffusion in the region where the velocity profile is not fully developed.

Groot Wassink and co-workers at the University of Twente have applied the principles of extraction theory for modeling, design and optimization of textile finishing equipments. An excellent compilation of several papers from Groot Wassink group can be found in the thesis of van der Linden (1984).

Using mass balances across a counter-current extractor, Groot Wassink and van der Linden (1983) have given a theoretical expression for the washing (or extraction) efficiency (E) of a single washing unit as a function of extraction factor (ε′) and NTU (number of transfer units) as:

$$E = \frac{\varepsilon' \left(1 - e^{-NTU\,(1 - 1/\varepsilon')}\right)}{\varepsilon' - e^{-NTU\,(1 - 1/\varepsilon')}} \tag{15}$$

The above analysis can be easily extended for multiple washing units by adding the NTUs of the individual washing units. Equation 15 needs to be corrected for two practical circumstances where the underlying assumptions in the derivation of the extraction factor may not hold true. In the first case, the effect of the difference in the inter-yarn and intra-yarn mass transport needs to be taken into account. As a result of faster inter-yarn mass transport (that occurs due to convection), the impurity in the inter-yarn region is removed in the first two or three compartments. This gives higher mass transfer rates in these compartments compared to the subsequent compartments. This effect is approximated by assuming that the removal of the inter-yarn impurity occurs in the first two compartments, and is evenly distributed over these compartments. The second deviation from the theoretical washing efficiency occurs due to the entrainment of the liquor from one compartment to the next with the moving fabric. This non-ideality is compensated by replacing the extraction factor ε' by the separation factor, S (defined as a function of the extraction factor and the entrainment factor), in the expression for the extraction efficiency. Groot Wassink and van der Linden further present an application of the above-mentioned theoretical analysis for the design and optimization of a wet textile process. In another paper, van der Linden *et al.* (1984) analyzed the non-stationary mass transfer in open-width washing machine, treating the washing machine as a plug flow reactor. The expression for the variation in the impurity concentration over the textile (in space and time), are rather cumbersome. Van der Linden *et al.* have, therefore, proposed use of a nomogram, which is a set of three plots representing the mutual relationship between several operating and process parameters, such as initial and final impurity concentration in the fabric and the washing liquor, process time, NTU, residence time of the fabric, and the extraction factor.

In a paper in 1985, Groot Wassink has reviewed his earlier theories of transport phenomena in textile materials, along with an analysis of the momentum transfer in a beam rotating washing machine. In this paper, Groot Wassink has also demonstrated that the theory of transport phenomena could easily be extended to the drying process on porous rollers. Kroezen *et al.* (1986) have extended the theory of extraction (E-NTU model) to the rinsing process using a simulator of an open-width washing machine. Kroezen *et al*. have proposed that the use of E-NTU model can help determine the actual rinsing ratio (as an extrapolation of the infinite rinsing ratio), and could be of critical help in the design of open-width washing machines and optimization of process variables.

The other major contributions to the study of mass transfer in textile materials include the work of Nils Gralén (1980) who studied the step-wise counter-current rinsing process using the theoretical model developed by Parish (and its subsequent modifications described earlier) as basis. Gralén defined a ‘leveling factor’ for the impurity concentration in the internal solution in the textile, as well as for the external solution (or liquor). The results of Gralén state that the process of intra-yarn diffusion (which is the rate controlling step as mentioned earlier) can be transformed into faster convection process by stirring the external liquid, which can cause higher liquid flows through the textile. Drawing an idea from the work of McGregor (mentioned earlier), Gralén concluded that rate enhancement in a rinsing process can be caused due to reduction in the thickness of the diffusional boundary layer.

A theoretical and experimental study of the mass transfer during the textile washing process in laundry machines has been given by Ganguli and Eendenburg (1980), using KCl as a model substance for diffusion. They have proposed that the mass transfer in the textile is a combination of convection (between larger inter-yarn pores) and diffusion (between smaller intra-yarn pores) processes. Assuming that the rate-controlling step in the overall mass transfer in textile is the intra-yarn diffusion process, they have used Fick's diffusion equation to obtain time-averaged rate of KCl removal for longer diffusion times. Ganguli and Eendenburg (1980) have concluded that the overall mass transfer in the textiles is mainly determined by the thickness of the boundary layer between the textile and the bulk. At high Reynolds number (fast agitation of the liquid), the boundary layer vanishes, and the transport is mainly determined by convection. This effect is even more pronounced for the textiles with a higher porosity.

Similar results in washing of textiles, using caustic soda as a mass transfer monitor have been given by Matsui *et al*. (1978). Their conclusions are summarized as: (1) the rate of washing is inversely proportional to the fabric or yarn thickness, (2) stirring the water in the bath has a large effect on washing rate, and (3) the rate of washing is high in the initial stages of the consecutive washing cycles. Matsui *et al*. have also argued that diffusion in the intra-yarn pores becomes the rate-limiting step in the overall mass transfer in the textiles as a result of different diffusivities of the monitor in the inter-yarn and intra-yarn pores. Some of the results of Matsui *et al*. can be explained on basis of the theoretical models of Groot Wassink and Ganguli and Eendenburg.

Van der Donck (1997, 1998, 1999) has presented several different perspectives of the mass transfer problem of in textiles. Mass transport during laundering processes occurs by mechanical action as the plugs of the textiles are compressed, and water is squeezed out. During this process, the applied stress acts simultaneously on water and the textile. Van der Donck (1997) has proposed a new model to describe the stress acting on water, using the model of van Wyk (1946) as basis. This model describes the stress acting on the textiles. During the compression of the textiles, the capillary diameter stays constant, while the cavities are compressed resulting in a generation of new capillaries. The new model was verified by experiments for the compression of textiles at a constant rate. The theoretically calculated stress-strain curves using the experimental parameters (such as capillary diameter, fraction of mobile water and fraction of capillaries) matched the stress-strain curves observed experimentally. In another paper, van der Donck *et al.* (1998) has assessed the effect of yarn stretching on the mass transfer enhancement using magnesium sulfate salt as a monitor substance. The yarn diameter decreased by 7% per 1% elongation of the yarn. The salt release from the yarn increased with stretching, which implies that liquid flow exists inside the yarn. Later, van der Donck (1999) published results on the influence of flow through textile layers on the soil removal from the textiles. It was found that pulsating flow enhanced the soil removal considerably. This effect was attributed to stretching of the yarns, due to frequent stretching of the textile layer as a result of pulsating nature of flow.

Charette *et al.* (2001) have presented a theoretical and experimental study on the mass transfer in cotton fabrics. In their model, Charette *et al*. (2001) used Fick's diffusion equation to calculate the concentration profiles in the yarn. The mass transfer

model is presented in two parts: 1. The first bath, in which the initial concentration in the yarn is uniform; and 2. The second and subsequent baths, in which the concentrations in the yarns have a pre-established profile. Nonetheless, Charrette *et al*. ignore the effect of inter-yarn convection that gives a higher mass transfer rate in the first few compartments of the washing unit due to the faster convection process that removes inter-yarn impurity.

The literature reviewed above treats the case of mass transfer in the textile materials during both laundry processes and textile finishing processes. The primary conclusion of these studies is that the intra-yarn diffusion is the rate-controlling step in the overall mass transfer in the textiles during wet textile treatments. As such, enhancement of the mass transfer in the textile materials by converting the slow process of intra-yarn diffusion into the faster convection process is the keystone to the improvement of the efficiency of wet textile processes.

1.3 Ultrasound in wet textile processing

The need for improved methods of introducing energy into the system during wet textile processing arises from various drawbacks of current wet textile processes. These drawbacks are: (1) requirement of large quantities of water and energy, and (2) long process times. As concluded from the literature study presented in the previous section, enhancement of mass transfer in textile materials is the basis of the improvement of the efficiency of the wet textile processes. The conventional solutions for mass transfer enhancement, such as operation at elevated temperatures, are offset by undesired side effects such as damage to the textile. Increasing flow through the textile does not deliver the desired rate enhancement due to the complex geometry of the textiles. Use of ultrasound for the improvement of wet textile processes has been investigated for the past 5 decades. In this section we review the literature in the area of ultrasound assisted wet textile processing. Although most of the research done is in the area of ultrasonic dyeing, recently ultrasound has also been applied in novel processes, such as enzymatic wet textile processing.

One of the earliest studies on the effect of (audible) sound (9.5 kHz.) on the dyeing of cellulose by substantive dyes has been done by Sokolov and Tumansky (1941). They reported a 2-3 fold rise in the dyeing rate with application of sound waves. Subsequently, Brauer (1951) has reported about 25% reduction in dyeing time of cellulose with vat dyes by application of ultrasound. Wührmann et al. (1946) have reported “fibrillation” of cellulose fibers (such as cotton) after exposure to ultrasound. They found that the sizes of the fibrils were not uniform and that the dimensions of the fibrils were a function of the time of the ultrasound exposure and the ultrasound intensity. Extending this work, Morehead (1950) has reported that if the cellulose fibers are subjected to acid hydrolysis prior to the ultrasonic treatment, particles instead of fibrils are obtained. The sizes and shapes of the particles are a function of their origin: whether they originate from the native fibers or regenerated fibers. Particle dimensions were found to be related to the crystalline and amorphous structure of the original fiber. Schwenker and Whitwell (1953) have demonstrated the effect of ultrasonic irradiation on

the change in the viscosity of cellulose solutions. Rath and Merk (1952) have reported an effect of both audible sound and ultrasound on the dyeing of cotton, viscose, and wool, with both acid and direct dyes. They found that the effect of ultrasound frequencies was independent of the system, while the effect of audible sound was system specific. Alexander and Meek (1953) have studied the acceleration in the rate of dyeing of wool, acetate, and nylon with direct, acid, and disperse dyes respectively, and compared the results with the change in rate of dyeing achieved by simple stirring. The acceleration of the dyeing rates of cotton and wool achieved by ultrasound exposure was similar to that obtained with stirring. However, the rate enhancement in case of dyeing of acetate and nylon with ultrasound was higher than that achieved by stirring. Alexander and Meek have, therefore, concluded that ultrasound has a greater effect on the dyeing of hydrophobic textile than hydrophilic textiles. Significant improvements in the dye uptake of VAT dyes by cotton have also been reported by Chuz and Demoroslov (1962) using 22 kHz ultrasound. They also reported, along with 50% rise in the dyeing rate, a reduction (upto 10%) in the requirement of dye, water and steam. They attributed their results to better dispersion and rapid diffusion of the dye particles assisted by reduction in the boundary layer thickness, and improved dye-fiber contact due to degassing of the medium, as a result of cavitation. Ramaszeder (1965) has given an excellent review of the contemporary literature on the possible applications of ultrasonics for various processes in the textile industry. The structural changes in the cotton fibers treated with Karbomol TsEM, due to deeper penetration of a resin into the fiber, under the effect of ultrasound have been reported by Simkovich *et al.* (1976). An increase in the crease-resistance of the fibers to laundering observed on ultrasound treatment was related to a decrease in resin hydrolysis due to a strong intra-molecular interaction and hindered penetration of alkali into the fiber. The change in the degree of crystallinity and orientation of crystallites was attributed to the penetration of the resin molecules into the micro-voids between fibrils and fibers in presence of ultrasound. Safonov (1984) has investigated the effect of ultrasound on the bleaching of cotton fabrics. Ultrasound (at an intensity of 2.5 W cm^{-2}) accelerated peroxide bleaching and gave cotton fabrics increased whiteness. Kovaleva *et al.* (1985) have studied the scouring of printed fabrics in an ultrasound field. The rate of deposition of the unfixed dye after dyeing or printing increased by a factor of 2-3 with ultrasound treatment (frequency – 22 kHz, intensity – 0.5-2 W cm^{-2}).

Smith *et al*. (1988) have studied the dyeing kinetics of direct dyes on cotton with ultrasound in a beaker-scale experiment, with an ultrasound horn placed directly in the dye bath. They studied the kinetics of dyeing with as many as 10 different dyes, each yielding a different rate of dyeing. Smith *et al*. have proposed several possible reasons for the observed rate enhancement with ultrasound: (1) the disruption of the boundary layer between the textile and the dye liquor; (2) an increased segmental mobility in the amorphous regions of cellulose increasing the dye diffusion rate; (3) a decreased dye aggregation and dye solubility in the bath. Thakore (1988, 1988a) has published his study on the kinetics of dyeing of cotton fabrics with direct dyes using ultrasound waves of 40 kHz in two parts. In the first part of his work, Thakore (1988) has reported effects of several parameters such as fabric construction, temperature, intensity of ultrasound

waves, dye bath concentration, electrolyte concentration on the dyeing kinetics. He has concluded that the dyeing rate enhancement is more pronounced for thicker fabrics, which cannot be dyed evenly with conventional techniques. The other conclusions of his study are: (1) ultrasound permits a reduction in the dye bath concentration; (2) ultrasound also causes a reduction in the dyeing time and the operating temperature; (3) the effect of ultrasound increased with its intensity above a certain threshold. In the second part, Thakore (1988a) has presented the diffusion kinetics during the dyeing of cotton fabrics with direct dyes. In this study, Thakore has not only assessed the rise in diffusion coefficient with application of ultrasound, but has also given a SEM image analysis of the surface of the textile after ultrasonic treatment. These images did not reveal any damage to the primary wall of the fabric or any permanent change in the fiber structure. The rise in the diffusion coefficient is ascribed to a better dispersion of the dye and acoustic cavitation that decreases the thickness of the boundary layer between the textile and the bulk. Shimizu *et al*. (1989) have reported an effect of ultrasound on the dyeing of Nylon 6 with disperse, acid, acid mordant, and reactive dye at different temperatures using 27 kHz ultrasound. The ultrasound exposure increased the uptake of all four dyes and decreased the activation energy by different amount for each dye. Thakore *et al*. (1988) have studied the diffusion and permeability coefficient of direct dye on cellulose. In this study, in a slightly different approach than the usual, the substrate (cellophane film) was held parallel to the ultrasound horn tip. Both the diffusion coefficient and permeability coefficient (defined as the quantity of the dye diffusing through the cellophane film per unit time per unit area) showed a substantial rise with the application of ultrasound. Smith and Thakore (1991) have also studied the fiber reactive dye hydrolysis under the influence of ultrasound. The reaction takes place in two steps: first, the conversion of the β-sulfatoethyl group to a vinyl group and, secondly, the conversion of the vinyl group to a β-hydroxyethyl group. The first reaction rate was accelerated by 50%, while the second reaction rate was boosted by over 500% with the application of ultrasound. Saligram *et al*. (1993) have studied the dyeing of polyester fibers (PET and PBT) with disperse dyes using 26 kHz ultrasound. Their results showed that the dye uptake of PBT fibers at lower temperatures (45^{o}C) rose almost 4-fold with the application of ultrasound. A combination of ultrasound and dye carrier (Dilatin TCI) gave a further rise of 184% in the dye uptake, although the dye uptake obtained with ultrasound technique was only 75% of that obtained with the conventional techniques (i.e., dyeing at higher temperatures). Similar results were also obtained for the dyeing of PET fibers. Ahmed and Lomas (1996) have also studied the low-temperature ultrasonic dyeing of polyester fabrics with disperse dyes with similar conclusions. Reactive dyeing of cellulosic fibers has also been studied by Oner *et al*. (1995) using two reactive dyes. The results of this study indicated an improvement in dye fixation and the percentage dye-exhaustion during ultrasound exposure. Shukla and Mathur (1995) have reported low temperature dyeing of silk with five different dyes (cationic, acid and metal complex dyes). The dye uptake in all cases increased by different amounts. Mock *et al*. (1995) have studied the dyeing of cotton textiles with direct dyes and the results showed that the application of ultrasound reduces both salt and energy consumption by about 50% compared to a conventional process. Birla *et al*. (1996) have studied the continuous

dyeing of cotton textiles with four different vat dyes with the NEARFIELD acoustic processor, which uses a dual frequency acoustic field, viz. 16 kHz and 20 kHz. The depth of the shade increased in all four cases, although by different amounts. Another factor affecting the depth of the shade was the dye bath concentration. Application of ultrasound in open-width washing of mercerized cotton has been studied by Rathi *et al*. (1997) using two different ultrasound modules: a tank with a single frequency (18.6 kHz) source, and a dual frequency NEARFIELD acoustic processor. The washing efficiency was found to decrease with increasing fabric speed. The washing efficiency obtained with the dual frequency processor was higher than that obtained with a single frequency washing box. In addition, the washing efficiency at 50^{o}C in presence of ultrasound was equal to that at 87^{o}C without ultrasound, which shows that the ultrasound also offers prospects for energy saving in open-width processes. The application of ultrasound in the dry cleaning laundry process has been successfully attempted by McCall *et al*. (1998) using the NEARFIELD dual frequency processor. Any conventional dry cleaning solvent was able to remove the hydrophobic soil with as much as 90% aqueous dilution under influence of ultrasound. From this result McCall *et al*. have proposed that "ultrasonic wet cleaning" could be an alternative to the conventional dry cleaning processes. Lee and co-workers (2001, 2001a) have investigated the change in the dye particle size distribution after exposure to ultrasound using the turbidity concept. Specific breakage rates of dye particles were found to be a function of the crystalline properties of the dye: a higher breakage rate was observed for a well-crystallized dye. Continuous dyeing of cotton fabrics with vat dyes has been studied by McCall *et al*. (1998) using the NEARFIELD acoustic processor. In order to precisely estimate the dye uptake, McCall *et al*. have used the dye extraction method in addition to the conventional method of fabric reflectance measurements. The major conclusion of this study is that the ultrasound assisted dyeing process saves upto 17% dye giving similar results for lower dye bath concentrations. David Klutz has investigated some fundamental interactions between ultrasound and cotton fabrics and VAT dyes in his Ph.D. thesis (1997). Klutz has assessed two principal hypotheses proposed to explain the enhancement in dye uptake during ultrasound treatment: (1) swelling of the fibers, which increases their dye uptake capacity and facilitates easier penetration of dye into them; (2) reduction of the dye particle size, which increases their diffusion coefficient. Experimental results of Klutz corroborated the above two hypotheses. The swelling of fibers in presence of ultrasound was found to be higher than swelling in water alone. The dye particle sizes were also found to reduce leading to a higher diffusivity.

A more recent application of ultrasound in wet textile processing is in the area of enzymatic treatment of the fabrics. Enzyme based wet textile processing is becoming increasingly popular due to milder processing conditions, and the replacement of harsh chemicals, resulting in more environmentally friendly processes. Yachmenev group at the South Regional Research Center (USDA, New Orleans) has extensively studied the ultrasonic enhancement of enzymatic wet textile processes. Several research papers published by Yachmenev group (Yachmenev *et al.* 1998, 1999, 2001) have demonstrated that combination of ultrasound with conventional enzymatic textile treatments offers significant advantages such as a reduction in the consumption of enzymes (thus reducing

the cost of operation), shorter process times, less fiber damage and greater uniformity of the enzyme treatment. The effect of ultrasound has been found to be more pronounced at lower enzyme concentrations. The tensile strength of cotton has been found to remain unaffected after ultrasound treatment. Studies conducted on the cotton preparation with pectinase bioscouring in presence of ultrasound reveal that the results are not only comparable to those with conventional alkaline scouring, but also shortened the process times of the conventional techniques significantly. Thus, ultrasound irradiation is a promising tool for the improvement of novel enzymatic wet textile processes as well. The improvements in the enzymatic wet textile processes observed by the application of ultrasound are attributed to several effects: 1. desorption of the enzyme molecules from the surface of the cellulose fiber, thus, increasing the number of free sites for the enzyme reaction; 2. deagglomeration of the enzyme molecules; 3. faster transport of the enzyme molecules towards the textile surface; 4. acceleration of the overall reaction rate due to removal of the products of enzymatic hydrolysis from the reaction zone.

It is quite clear from the literature survey presented above that although research on ultrasound enhanced wet textile processing is being conducted for past several decades, most of this research is of *black box* type where the emphasis is mainly on the results. No attempt is devoted to investigate the basic physical mechanism of these processes, although different hypotheses have been proposed. In addition, most of the research has been conducted on laboratory scale with no application on industrial scale. Therefore, the principal aims of this project are to discern the physical mechanism of the ultrasound enhanced wet textile processes, and provide suitable scale-up and optimization strategies for a large-scale application of this novel technology.

Notation

A	–	area for mass transfer, m^2
A'	-	impurity retention ratio in the fabric, dimensionless.
C	–	concentration in bath at time t, kg m^{-3}.
C_∞	-	equilibrium concentration, kg m^{-3}.
$C_{F,1}$	–	impurity concentration in the exit fabric in washing unit, kg m^{-3}.
C_{b0}	–	initial concentration in the bath, kg m^{-3}.
C_{eq}	–	equilibrium impurity concentration on the fabric for imperfect washing, kg m^{-3}.
$C_{F,0}$	–	impurity concentration in the entering fabric in washing unit, kg m^{-3}.
$C_{L,1}$	-	equivalent impurity concentration in the liquid, kg m^{-3}.
D	–	diffusion coefficient, m^2 s^{-1}.
D_e	–	effective diffusivity in the textile, m^2 s^{-1}.
d_f	–	diameter of the fibers, m.
d_y	–	diameter of the yarns, m.
E	–	efficiency of a single washing unit, dimensionless
F	–	liquor flow ratio, dimensionless.
k	–	mass transfer coefficient, m s^{-1}.

K' - washing parameter, dimensionless.
k_1 – mass transfer coefficient for intra-yarn region, m s^{-1}.
k_2 - mass transfer coefficient for inter-yarn region, m s^{-1}.
k_3 - mass transfer coefficient for the boundary layer, m s^{-1}.
$K_{intra\text{-}yarn}$ – permeability between the fibers, m^2.
K_T – overall mass transfer coefficient in the textile, m s^{-1}
$K_{inter\text{-}yarn}$ – permeability between the yarns, m^2.
K_o - Kozeny's constant, dimensionless.
t – time, s.
$\bar{v}$ – mean velocity, m s^{-1}.
V_c – water content of the cloth load, m^3.

Greek letters

α - tortuosity factor, dimensionless.
ε - porosity, dimensionless.
ρ_L – density of liquid, kg m^{-3}.
ε' - extraction factor ($\phi_b/k_e\phi_d$), dimensionless.
μ - viscosity, Pa-s.
ε_f – porosity between the fibers, dimensionless.
ε_y – porosity between the yarns, dimensionless.

References

- Ahmad, M.Y.W, and M. Lomas, "The low-temperature dyeing of polyester fabric using ultrasound", *Journal of Society of Dyers and Colorists*, **112**(9), 245-248 (1996).
- Alexander, P., and G.A. Meek, "Application of acoustic waves to dyeing", *Melliand Textilberichte*, **34**, 57-59 & 214-216 (1953).
- Birla, A.M., M.J. Cato, and G.N. Mock, "Continuous dyeing of cotton using ultrasound", *AATCC International Conference & Exhibition 1996 - Book of Papers*, 309-322 (1996).
- Bräuer, M., "Some experiments with sonic and ultrasonic waves in dyeing", *Melliand Textilberichte*, **32**, 701-707 (1951).
- Charrette, H., J.L. Houzelot, and V. Ventenat, "Modeling and experimental studies of mass transfer in cotton fabrics", *Textile Research Journal*, **71**(11), 954-959 (2001).
- Chuz, E.I., and S.P. Demoroslov, *Tekstil'na Promyslennost*, **22**(2), 54 (1962).
- Ganguli, K.L., and J. van Eendenburg, "Mass transfer in a laboratory washing machine", *Textile Research Journal*, **50**(7), 428-432 (1980).
- Gooijer, H., *Flow resistance of textile materials*, PhD Thesis, University of Twente, 1998 (ISBN: 90 365 1124 0).
- Gralen, N., "Rinsing of textiles", *Journal of Society of Dyers and Colorists*, **96**(2), 52-64 (1980).
- Groot Wassink, J., and H.J.L.J. van der Linden, "E-NTU method as a mass transfer model in design and operation of textile finishing equipment", *Textile Research*

Journal, **53**(12), 751-757 (1983).
- Groot Wassink, J., "Transport phenomena in textile finishing equipment", *Journal of Society of Dyers and Colorists*, **101**, 212-220 (1985).
- Janssen, L.P.B.M., and M.M.C.G. Warmoeskerken, *Transport Phenomena Data Companion*, Delft University Press, Delft, 1997. (ISBN: 90 407 1302 2)
- Klutz, D.S., *Fundamental interactions of ultrasound with cotton fibers and vat dyes*, PhD Thesis, North Carolina State University, 1997.
- Kovaleva, L.F., I.V. Popikov, R.G. Sarukhanov, G.E. Krichevskii, and N.N. Khavskii, "Accelerating the washing-off of printed fabrics in a field of elastic vibrations", *Technol. Tekstil'na Promyslennost*, **163**(1), 66-69 (1985).
- Kroezen, A.B.J., H.J.L.J. van der Linden, and J. Groot Wassink, "Rinsing process in open-width washing machines", *Journal of Society of Dyers and Colorists***, 102**, 54-58 (1986).
- Lee, K.W., and J.P. Kim, "Effect of ultrasound on disperse dye particle size", *Textile Research Journal*, **71**(5), 395-398 (2001).
- Lee, K.W., Y.S. Chung, and J.P. Kim, "Effect of ultrasound treatment and dye crystalline properties on particle size distribution", *Textile Research Journal*, **71**(11), 976-980 (2001a).
- Matsui, H., M. Kobayashi, and K. Koji, "Washing of fabrics Part 1: Washing of cotton fabrics and its theoretical analysis", *Journal of the Textile Machinery Society of Japan*, **24**(2), 41-49 (1978).
- McCall, R.E., E.R. Lee, G.N. Mock, and P.L. Grady, "Improving dye yields of vats on cotton fabric using ultrasound", *AATCC International Conference & Exhibition 1998 - Book of Papers*, 188-194 (1998).
- McCall, R.E., F.M.A. Patel, G.N. Mock, and P.L.Grady, "Solvent and ultrasonic alternatives to perchloroethylene drycleaning of textiles", *Textile Chemist and Colorist*, **30**(11), 11-18 (1998).
- McGregor, R., "The effect of rate of flow on rate of dyeing II – The mechanism of fluid flow through textiles and its significance in dyeing", *Journal of Society of Dyers and Colorists*, **81**(10), 429-438 (1965).
- McGregor, R., and R.H. Peters, "The effect of rate of flow on rate of dyeing I – The diffusional boundary layer in dyeing", *Journal of Society of Dyers and Colorists*, **81**(9), 393-400 (1965).
- Meier-Windhorst, C.A., *Melliand Textielberichte*, **50**, 832 (1969).
- Mock, G.N., D.S. Klutz, C.B. Smith, P.L. Grady, R.E. McCall, and M.J. Cato, "Reducing salt and energy needs in direct dyeing of cotton through use of ultrasound", *AATCC International Conference & Exhibition 1995 - Book of Papers*, 55-64 (1995).
- Morehead, F.F., "Ultrasonic disintegration of cellulose fibers before and after acid hydrolysis", *Textile Research Journal*, **20**, 549-553 (1950).
- Oner, E., I. Baser, and K. Acar, "Use of ultrasonic energy in reactive dyeing of cellulosic fabrics", *Journal of the Society of Dyers and Colorists*, **111**, 279-281 (1995).
- Parish, G.J., "Continuous rinsing of impurities from textile fabrics", *American*

Dyestuff Reporter, 402-408 (May 1965).
- Parish, G.J., "Some fundamental aspects of the washing process", *Journal of Society of Dyers and Colorists*, **78**(3), 109-114 (1962).
- Ramaszeder, K., "Application of ultrasonics in the textile industry", *Textil Praxis*, **20**, 840-848 (1965).
- Rath, H., and H. Merk, "Influencing dyeing with sonic vibrations", *Melliand Textilberichte*, **34**, 24-26 & 311-314 (1952).
- Rathi, N.H., G.N. Mock, R.E. McCall, and P.L. Grady, "Ultrasound aided open width washing of mercerized 100% cotton twill fabric", *AATCC International Conference & Exhibition 1997 - Book of Papers*, 254 – 262 (1997).
- Ratna Prabhu, M., P.B. Jhala, and K. Subrahmanyam, "Extension of the theory of washing", *Journal of Society of Dyers and Colorists*, **86**, 368-369 (1970).
- Ratna Prabhu, M., P.B. Jhala, and K. Subrahmanyam, "Washing by diffusion", *Journal of Society of Dyers and Colorists*, **87**, 349-350 (1971).
- Rietema, K., *Fysische Transport –en Overdrachtsverschijnselen*, Het Spectrum, Utrecht, 1976.
- Safonov, V.V., "Effect of ultrasonics on the bleaching of cotton fabrics", *Tekstil'na Promyslennost***, 44**(1), 60-61 (1984).
- Saligram, A.N., S.R. Shukla, and M. Mathur, "Dyeing of polyester fiber using ultrasound", *Journal of the Society of Dyers and Colorists*, **109**, 263-266 (1993).
- Schwenker Jr., R.F., and J.C. Whitwell, "Effect of ultrasonic radiation on viscosity of cellulose solutions", *Textile Research Journal*, **23**, 436-437 (1953).
- Shimizu, Y., R. Yamamoto, and H. Shimizu, "Effect of ultrasound on dyeing of Nylon-6", *Textile Research Journal*, **59**(11), 684-687 (1989).
- Shukla, S.R., and M.R. Mathur, "Low-temperature ultrasonic dyeing of silk", *Journal of the Society of Dyers and Colorists*, **111**, 343-345 (1995).
- Simkovich, N.N., and A.A. Yastrebinskii, "Effect of acoustic waves on structural changes in cotton fibers treated with Karbomol TsEM", *Technol. Tekstil'na Promyslennost*, **106**(3), 15-19 (1975).
- Smith, C.B., and K.A. Thakore, "The effect of ultrasound on fiber reactive dye hydrolysis", *Textile Chemist and Colorist*, **23**(10), 23-25 (1991).
- Smith, C.B., G. Mcintosh, and S. Shanping, "Ultrasound – A novel dyeing accelerant", *American Dyestuff Reporter,* **77**(10), 15-18 (1988).
- Sokolov, A.I., and S.S. Tumansky, "Influence of ultrasonic field on dyeing process of cotton goods", *Zurnal Prikladnoj Chimii (Journal of Applied Chemistry)*, **14**, 843-848 (1941).
- Thakore, K.A., "Application of ultrasonics in dyeing of cotton fabrics with direct dyes: Part I – Kinetics of dyeing", *Indian Journal of Textile Research*, **13**, 133-139 (1988).
- Thakore, K.A., "Application of ultrasonics in dyeing of cotton fabrics with direct dyes: Part II –Diffusion kinetics", *Indian Journal of Textile Research*, **13**, 208-212 (1988a).
- Thakore, K.A., C.B. Smith, D. Hite, and M. Carlough, "The effects of ultrasound and the diffusion coefficient of C.I. Direct Red 81 in cellulose", *American Dyestuff*

Reporter, **77**(10), 15-16 (1988).
- Tuzson, J., and B.A. Short, "Mass transfer and the washing process", *Textile Research Journal*, **30**, 983-989 (1960).
- van den Brekel, L.D.M., *Hydrodynamics and mass transfer in domestic drum-type fabric washing machines*, PhD Thesis, Technical University of Delft, 1988.
- van den Brekel, L.D.M., and E.J. de Jong, "Hydrodynamic in packed textile beds", *Textile Research Journal*, **59**(8), 433-440 (1989).
- van der Donck, J.C.J., "Compression of wet textile", *Tenside Surfactants and Detergents*, **34**(5), 322-326 (1997).
- van der Donck, J.C.J., A. So, and G. Frens, "The influence of stretching on salt release from porous yarns", *Tenside Surfactants and Detergents*, **35** (2), 119-122 (1998).
- van der Donck, J.C.J., "The influence of flow through textile layers on soil removal", *Tenside Surfactants and Detergents*, **36** (4), 222-224 (1999).
- van der Linden, H.J.L.J., *Transport phenomena in textile finishing equipment*, PhD Thesis, University of Twente, 1984.
- van der Linden, H.J.L.J., J. Groot Wassink, and H.J. Vos, "Non-stationary mass transfer in open-width washing machine", *Textile Research Journal*, **54**(2), 77-82 (1984).
- van Wyk, C.M., "Note on the compressibility of wool", *Journal of Textile Institute,* **37**, T285-292 (1946).
- Yachmenev, V.G., E.J. Blanchard, and A.H. Lambert, "Study of the influence of ultrasound on enzymatic treatment of cotton fabric", *Textile Chemist & Colorist and American Dyestuff Reporter,* **1**(1), 47-51 (1999).
- Yachmenev, V.G., E.J. Blanchard, and A.H. Lambert, "Use of ultrasound energy in the enzymatic treatment of cotton fabric", *Industrial & Engineering Chemistry Research*, **37**(10), 3919-3923 (1998).
- Yachmenev, V.G., N.R. Bertoniere, and E.J. Blanchard, "Effect of sonication on cotton preparation with alkaline pectinase", *Textile Research Journal*, **71**(6), 527-533 (2001).
- Yachmenev, V.G., E.J. Blanchard, and A.H. Lambert, "Study of the influence of ultrasound on enzymatic treatment of cotton fabric", *AATCC International Conference & Exhibition 1998 - Book of Papers*, 472 – 481 (1998).
- Wührmann, K., A. Heuberger, and K. Muhlethaler, "Electron microscopic investigations of cellulose fibers after supersonic treatment", *Experimentia*, **2**, 105-107 (1946).

2

ULTRASOUND WAVE PHENOMENA AND BUBBLE DYNAMICS: BASIC PRINCIPLES AND GOVERNING EQUATIONS

2.1 Introduction

The use of ultrasound in enhancing the rates of homogeneous and heterogeneous chemical reactions is well known. A more recent application of ultrasound is in wet textile processes. Processes such as washing, dyeing, rinsing, bleaching, desizing, and mercerization can be improved with the application of ultrasound. Although several papers have appeared, which report improvement of the water and energy efficiency of the wet textile processes with the application of ultrasound, the exact physical mechanism underlying this improvement is not known yet. The principal aims of this thesis are: first, to elucidate the basic physical mechanism of the ultrasound enhanced mass transfer in textiles and, secondly, to provide an optimization strategy for ultrasound assisted wet textile processing.

Before we proceed, it is necessary to have a general introduction to ultrasound wave phenomena and its secondary effect, acoustic cavitation. In this chapter we provide the basic principles and the governing equations of ultrasound wave and acoustic cavitation (or bubble dynamics) that are relevant for chemical engineering purposes.

2.2 Basic concepts of the ultrasound wave phenomena

2.2.1 Wave theory of sound

In sound waves, the density of the medium undergoes periodic alterations with regions of alternating compression and rarefaction (refer to figure 1). It can be seen from this figure that the particle displacement and the pressure are out of phase. The regions of minimum displacement correspond to pressure maxima, while those of maximum displacement correspond to pressure minima.

One of the most basic properties of sound is its frequency. On the basis of the frequency, sound is subdivided in three categories: infrasonic, sonic, and ultrasonic. The human hearing frequency range is 20 Hz to 20 kHz, and this range is termed the sonic range. Frequencies below 20 Hz fall in the category infrasound, and frequencies greater than 20 kHz are called *ultrasonic* waves.

The mathematical theory of sound propagation is based on three basic equations:

1. The equation of conservation of mass:

$$\frac{\partial \rho}{\partial \mathrm{t}} + \nabla \cdot (\rho\, \mathrm{v}) = 0 . \tag{1}$$

2. The Euler equation of motion:

$$\rho \left[\frac{\partial \mathrm{v}}{\partial \mathrm{t}} + \left(\mathrm{v} \cdot \nabla \mathrm{v} \right) \right] = - \nabla \mathrm{p} . \tag{2}$$

3. The pressure-density relationship of the medium:

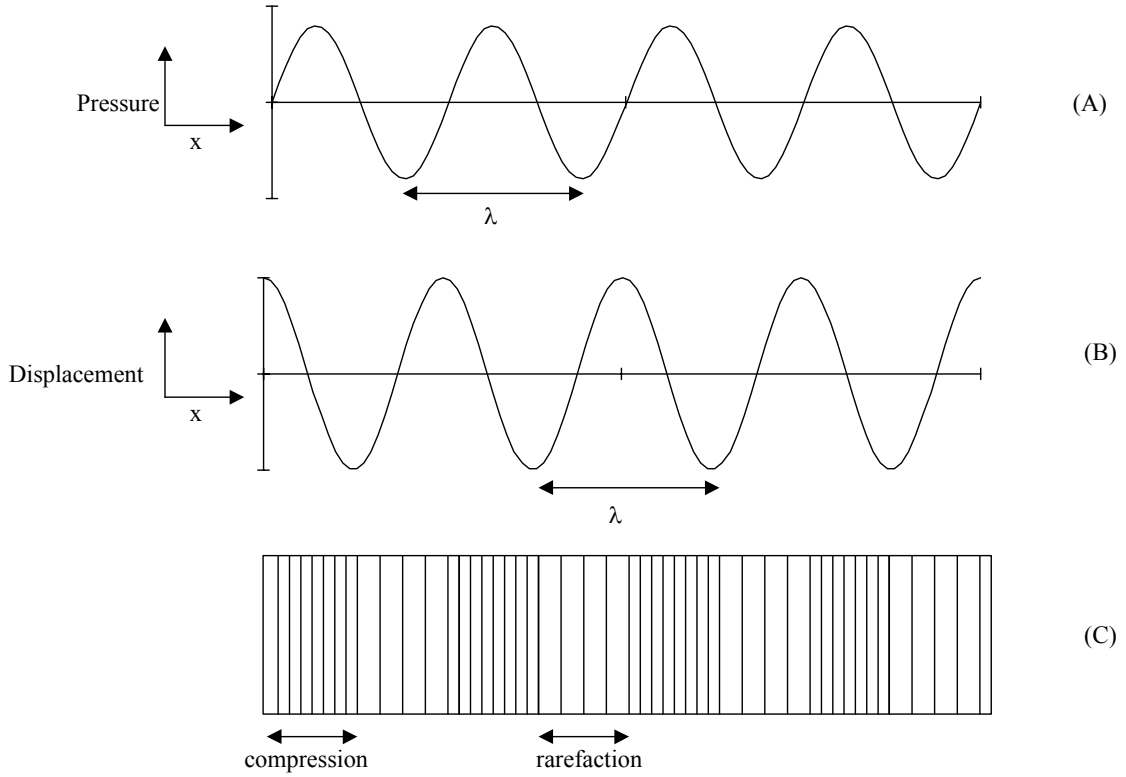

Figure 1: The acoustic wave phenomena in a compressible medium. **(A)** Propagation of the pressure in time; **(B)** The displacement of particles in time; **(C)** Compression and rarefaction modes.

$$c^2 = \left(\frac{\partial p}{\partial \rho} \right)_{s = \text{constant}} \tag{3}$$

The propagation of the acoustic wave in the medium causes small amplitude variations in the pressure, velocity, and density of the medium. The mathematical expression that describes the variation in these properties due to acoustic wave propagation is called *wave equation.* The equation for the pressure field in a sound wave is (Pierce, 1989):

$$\nabla^2 p - \frac{1}{c^2} \frac{\partial^2 p}{\partial t^2} = 0 . \tag{4}$$

The wave equation can also be expressed in the terms of the velocity potential as:

$$\nabla^2 \Phi - \frac{1}{c^2} \frac{\partial^2 \Phi}{\partial t^2} = 0 \tag{5}$$

where $v = \nabla\Phi$, and $p = -\rho\, \partial\Phi/\partial t$. A simple solution to the above equation can be found, when the pressure depends only on spatial variable, x, and thus, $p = p(x, t)$. This implies that the velocity v and acceleration ($\partial v/\partial t$) of the fluid particles or elements also depend

on one variable. With this simplification the general solution of equation 4 is:

$$p = f\left(t - \frac{x}{c}\right) + g\left(t + \frac{x}{c}\right). \tag{6}$$

The relation between pressure and velocity in the medium of wave propagation can also be derived from the set of equations 1-3 as (Pierce, 1989):

$$v = \frac{1}{\rho c}\left[f\left(t - \frac{x}{c}\right) - g\left(t + \frac{x}{c}\right)\right]. \tag{7}$$

In the expressions for the pressure and velocity the functions f and g represent two waves moving in +x and –x directions with speed c. However, for a uni-directional progressive wave in the positive x direction, the function g vanishes. The proportionality between the pressure and velocity (ρc) is called as the characteristic impedance of the medium. For air, the value of characteristic impedance is (ρ = 1.2 kg m^{-3}; c = 341 m s^{-1}) ~ 400 kg m^{-2} s^{-1}, while for water it is (ρ = 1000 kg m^{-3}; c = 1500 m s^{-1}) ~ 1.5 × 10^6 kg m^{-2} s^{-1}.

For plane traveling wave of constant frequency (f), the expression for the pressure variation in the medium at any position in the direction of the wave is:

$$p(x, t) = P_A \cos(\omega t - kx) \tag{8}$$

ω is the angular frequency (2πf) and P_A is the amplitude of the acoustic disturbance. Comparing this with the earlier general expression for the pressure (equation 6), we find:

$$p = P_A \cos\left[\omega\left(t - \frac{x}{c}\right)\right] = P_A \cos(\omega t - kx) = P_A\, e^{ikx}\, e^{-i\omega t} \tag{9}$$

where k = ω/c. The expression for the acoustic disturbance indicates that it is not only repetitive in time but also in space. The repetition length is λ = 2π/k. The speed of the wave is: wavelength (λ) × frequency (f). The speed of sound is a function of the density and the compressibility of the medium. For air, as mentioned earlier, the speed of sound is 341 m s^{-1}, while for water it is 1500 m s^{-1}. The speed of sound varies with the static pressure and the temperature of the medium and an approximate expression for variation in the speed of sound in water with temperature and pressure is (Pierce, 1989):

$$c = 1447 + 4.0\,\Delta T + \left(1.6 \times 10^6\right)p \tag{10}$$

with ΔT = (T – 283.16) basis temperature being 10^oC. p is the absolute pressure in Pascal. Nonetheless, for all practical calculations a value of c = 1500 m s^{-1} is sufficient.

2.2.2 Specific acoustic impedance

The word *impedance* basically refers to resistance. The scientific usage of this word has its origin in electrical engineering, where it is used to describe the ratio of driving force (i.e. voltage) and the resulting velocity or motion (i.e. current). In acoustics, the concept of impedance or more specifically *acoustic impedance* is the ratio of acoustic pressure and velocity of the particle of the medium. The acoustic impedance is the ratio of the acoustic pressure and the velocity in the medium:

$$Z = \frac{p}{v} \tag{11}$$

Substituting the expressions for the acoustic pressure and corresponding velocity as given in equations 6 & 7, we get:

$$Z = \rho\, c \tag{12}$$

Since the pressure is a quantity per unit area, the ratio p/v is called *specific acoustic impedance*, which means the acoustic impedance per unit area.

2.2.3 Acoustic energy and intensity

The acoustic intensity is defined as the rate at which energy in the wave crosses a unit area perpendicular to the direction of propagation. The particles of the medium undergo oscillatory motion as the wave propagates. A detailed derivation of the acoustic energy passing through the medium due to propagation of a sinusoidal acoustic wave with amplitude P_A per unit time per unit area (I) is given by Leighton (1994). We give herewith only the final form of the equation:

$$I = \frac{1}{2} Z \left(\frac{P_A}{Z} \right)^2 = \frac{1}{2} \frac{P_A^2}{Z}. \tag{13}$$

where Z is the acoustic impedance of the medium given by equation 12.

2.2.4 Plane wave reflection at a surface

If a wave strikes a surface or a boundary between two media during its propagation in a medium, a reflected wave is produced. The physical characteristics of the reflected wave depend on the characteristics of the surface as well as that of the medium or on the characteristics of the two media. We treat the general case, of a plane wave reflection at a boundary between two media with specific acoustic impedances Z_I ($\rho_I\ c_I$) and Z_{II} ($\rho_{II}\ c_{II}$). The incident wave is now split into two parts: first, a reflected wave back in the first medium and, secondly, a transmitted wave as shown in figure 2. We assume that the boundary is massless, and there is no loss of energy due to absorption or dissipation.

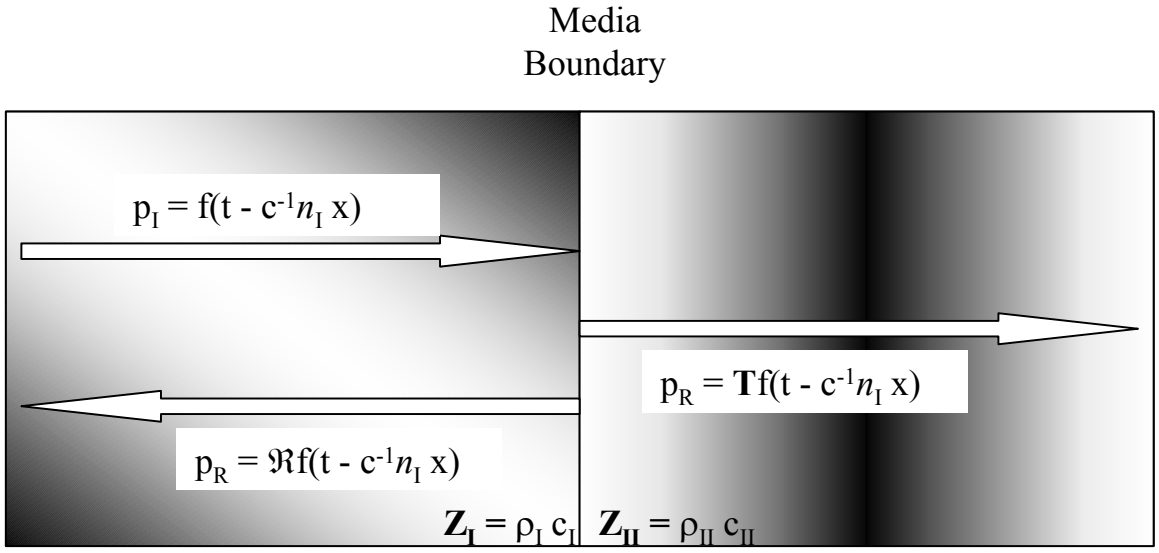

Figure 2: Reflection and transmission of a plane wave after incidence on a boundary between two media.

Let p_I, p_R and p_T denote the pressure amplitudes of the incident, reflected and transmitted acoustic waves respectively. The ratio p_R/p_I is termed the reflection coefficient of the wave ($\Re$), while the ratio p_T/p_I is termed the transmission coefficient of the wave (**T**). At the boundary, there cannot be discontinuity of pressure nor of the velocities. Using this argument we can write:

$$p_I = p_R + p_T \text{ or } 1 - \Re = \mathbf{T}. \tag{14}$$

$$\frac{1}{(\rho_I c_I)}(1 - \Re) = \frac{1}{(\rho_{II} c_{II})}\mathbf{T} \tag{15}$$

Solving for $\Re$ and **T** we have:

$$\mathbf{T} = \frac{2 Z_{II}}{Z_I + Z_{II}} \;\&\; \Re = \frac{Z_{II} - Z_I}{Z_I + Z_{II}}. \tag{16a \& b}$$

Various combinations of relative values of Z_I and Z_{II} help defining different kinds of boundaries with specific characteristics.

1. When $Z_I = Z_{II}$, **T** = 1, and $\Re$ = 0. This means that the entire incident wave is transmitted to the other medium, and there is no reflection. This situation is called *impedance matching* between the two media.
2. For $Z_{II} >> Z_I$, $\Re \approx 1$. This kind of boundary is called a *rigid boundary*. In this case, the entire wave is reflected back into the first medium, and practically no transmission occurs.
3. In case $Z_I >> Z_{II}$, $\Re \approx -1$. This type of boundary is called a *pressure release boundary*. In this case as well there is practically no transmission, and the entire wave

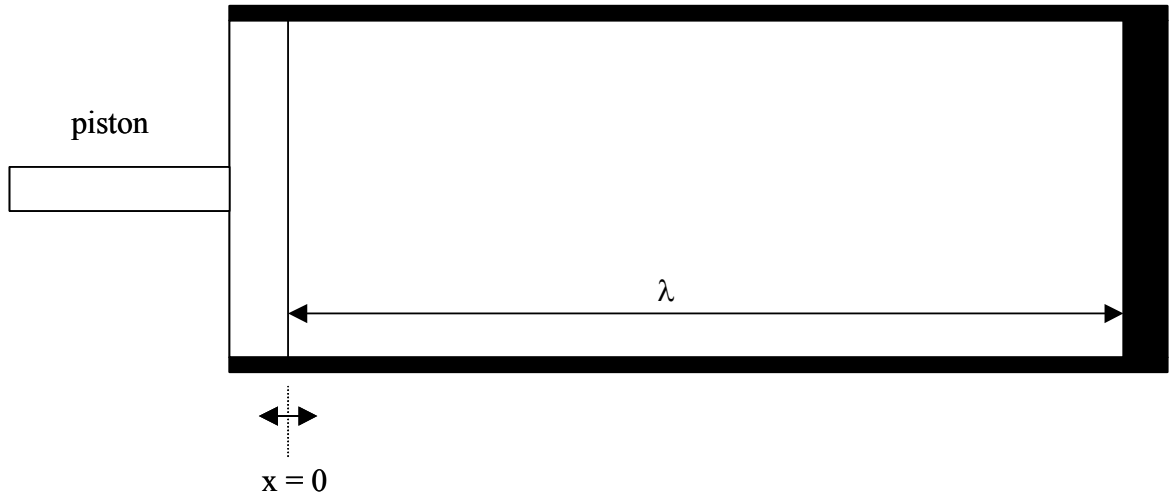

Figure 3: Oscillations of a piston in a snugly fitting tube with the other end as a rigid reflector.

is reflected back into the first medium. However, an interesting feature of this kind of boundary is that the incident wave is inverted after reflection, i.e. it is out of phase by 180^o.

2.2.5 Standing waves

When a progressive or traveling wave is incident on a boundary, it is reflected as discussed in the preceding section. The interference between the incident and the reflected wave can give rise to *standing wave*, where there is no net flow of energy in any direction. A detailed discussion on the formation and properties of standing waves, using a simple model of a piston oscillating inside a snuggly fitting rigid tube of area A, and length L is given by Pierce (1989). The piston on one side of the tube is driven back and forth by some external source making sound waves that propagate inside the tube (figure 3). The other end of the tube (at x = L) is a rigid boundary, which reflects the waves incident on it. We give herewith the steady state asymptotic expressions for the acoustic field variables, pressure and velocity, in the tube:

$$\frac{p}{\rho c} = V_o \frac{\sin(\omega t)\,\cos[k(L-x)]}{\sin(kL)} \;\&\; v_x = V_o \frac{\cos(\omega t)\,\sin[k(L-x)]}{\sin(kL)} \qquad (17a \;\&\; b)$$

The pressure at the piston (or at x = 0) is:

$$p_{x=0} = \rho c\,[1 + N(t)]\,v_{x=0} \qquad (17c)$$

where N(t) is the largest integer less than (ct/2L) or in other words N is the number of echoes returned to the piston from the rigid reflector at x = L in time t. The boundary conditions for these expressions are:

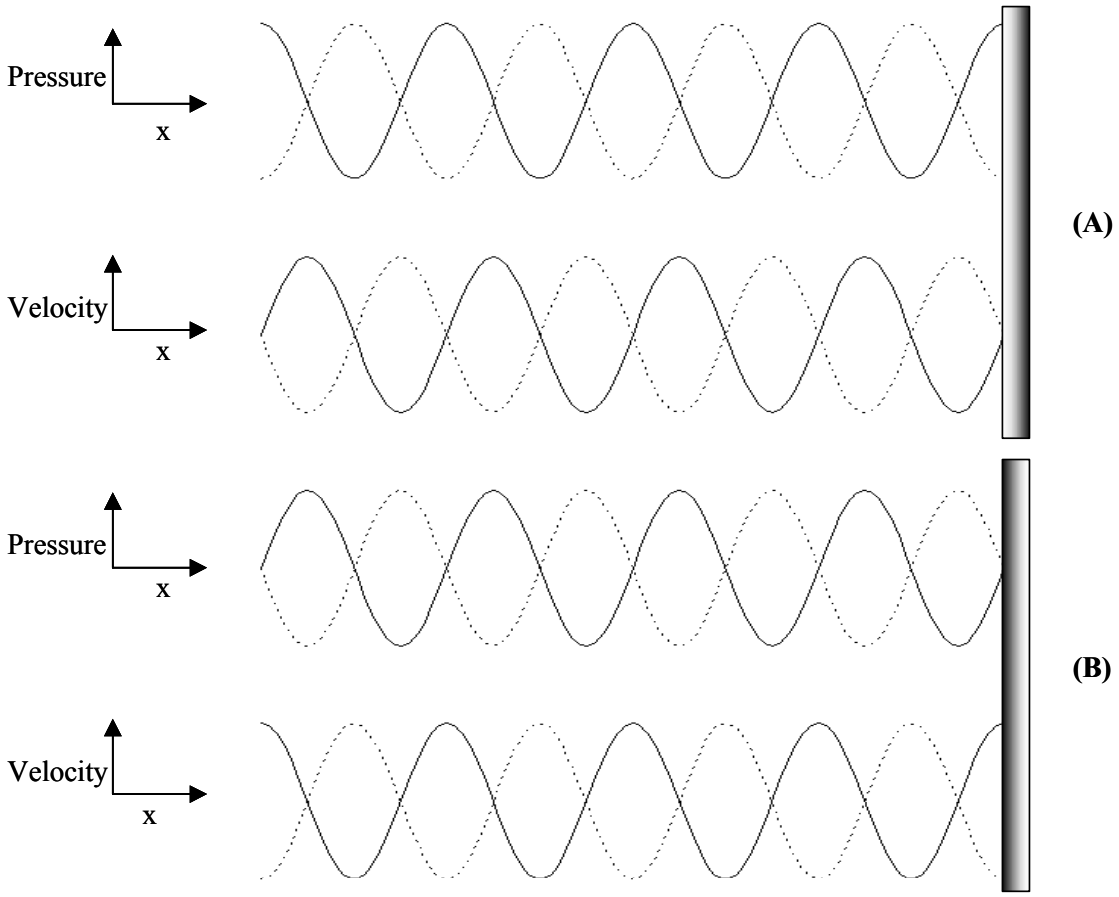

Figure 4: Spatial variation of the pressure and velocity in a standing wave field formed by reflection of a plane traveling wave at: (A) rigid boundary and (B) pressure-release boundary. It can be seen that the pressure and velocity are out of phase by 90^o everywhere in the standing wave field. In case of a rigid boundary there is a pressure-maximum at the boundary while for a pressure-release boundary there is a velocity maximum at the boundary.

$$\text{For } x = 0,\ v_x = V_o \cos(\omega t) \text{ and for } x = L,\ v_x = 0 \tag{18}$$

It can be perceived from above expressions that the pressure and velocity are out of phase by 90^o everywhere in the tube. In addition, the pressure amplitude becomes singular when $\sin(kL) = 0$. Another interesting result indicated by equation 17c is that for periodic motion of the piston the pressure at the piston is always *in phase* with the velocity of the piston, and ever increases with $t \rightarrow \infty$. Nonetheless, due to viscous dissipation and friction losses in the medium, the pressure amplitudes remain large yet finite.

A similar analysis can be given for the case where the other end of the tube (at $x = L$) is a pressure release boundary, with the boundary conditions: for $x = L$, $p = 0$. The boundary condition at $x = 0$ in this case is same as in case of a rigid boundary (equation 18). Figure 4 shows the variation of pressure and velocity in space for the acoustic wave reflections at a rigid and a pressure-release boundary. It can be deduced from figure 4 that for a standing wave caused by a plane wave reflection at a rigid boundary the successive pressure maxima (antinodes) occur at distances $n\lambda/2$ from the sound source,

while the successive pressure minima (node) occur at distances $(2n - 1)\lambda/4$ (where n is an integer ≥ 1). In case of plane wave reflection at a pressure release boundary, the successive pressure maxima (antinodes) occur at a distance $(2n + 1)\lambda/4$, while the successive pressure minima (nodes) occur at a distance $n\lambda/2$ from the sound source. The resultant velocity in the standing wave field created by the two kinds of boundaries exhibits an opposite phase with respect to the pressure.

2.3 Cavitation and Bubble Dynamics

The word *cavitation* basically refers to the formation, growth and collapse of gas or vapor bubbles under the influence of a pressure variation in the medium. The word formation also refers to the excitation of the cavities or small micro-bubbles that are already present in the medium under the influence of the pressure variation. These cavities or micro-bubbles may be suspended in the liquid or may be trapped inside crevices of the liquid-solid interface. Cavitation was first reported in 1895 by Sir John Thornycroft and Sidney Barnaby during their study of erosion of the propeller blades of navy ships. The cause of the pressure variation can be taken as a criterion for distinguishing between different kinds of cavitations:

1. **Hydrodynamic Cavitation** is caused by the pressure variation in the flow of a liquid, due to variation in the velocity of flow as a result of a change in the geometry of the conduit.
2. **Acoustic Cavitation** is a result of pressure variation in the liquid, due to passage of an acoustic wave.
3. **Optic Cavitation** is a result of the rupture of the liquid, due to high-intensity light such as laser.
4. **Particle Cavitation** is produced by any type of elementary particle (for example proton) rupturing the liquid as in a bubble chamber.

Lauterborn (1980) has stated that the hydrodynamic and acoustic cavitation are the results of tensions prevailing in the liquid, while the optic and particle cavitation are the consequence of local deposition of energy. The typical frequency range for acoustic or ultrasonic cavitation is 20 kHz to 1 MHz. Optical and particle cavitation require intense energy source, such as a ruby laser. These kinds of methods of producing cavitation offer a precise control over the cavitation parameters, such as size of the bubble, and the bubble location in the medium. These methods are basically useful for the fundamental research in cavitation but not suitable for large-scale applications, such as intensification of various physical and chemical processes, due to high cost of operation. Among the four types of cavitation stated above, only the hydrodynamic cavitation and acoustic (or ultrasonic) cavitation have potential towards large-scale application, mainly due to the simplicity of the method of creating them.

Since all effects of cavitation have their origin in the characteristic radial motion of a bubble, a detailed knowledge of the bubble dynamics is of paramount importance for the study of any cavitation-based process.

2.3.1 Cavitation inception

The theoretical pressure amplitude to cause cavitation in water can be approximated by ~ $2\sigma/R_e$, (where σ is the surface tension of water ~ 0.072 N-m, and R_e is the van der Waal's distance between molecules ~ 4×10^{-10} m.), resulting in 1500 atm. But, in practice cavitation occurs at a far lesser pressure amplitude (< 5 atm or so). This is probably due to the presence of weak spots in the liquid in the form of tiny micro-bubbles, which lower the tensile strength of the liquid. Thus, the word *acoustic cavitation* can more generally be defined as *creation of new bubbles or growth or collapse of pre-existing bubbles driven by an acoustic wave.* Free-floating bubbles may not always form suitable nuclei for two reasons: first, these bubbles may rise due to buoyancy and escape out of the liquid and, secondly, if the surrounding liquid is under-saturated, they dissolve completely [Epstein & Plesset (1950)]. According to Flynn (1964), bubbles with a radius of only 5 μm or less should remain in water that is left standing for a few hours. Nonetheless, the bubbles may be stabilized against buoyancy if they are adhering to a surface. Such bubbles may form suitable nuclei for cavitation. Another potential candidate for cavitation nuclei are gas pockets trapped in the crevices of a solid surface (figure 5). It is well known that for any gas bubble to be stable, the pressure inside the bubble should be higher than the pressure in the bulk by an amount equal to $2\sigma/R$, which is the surface tension pressure that acts towards the center of the bubble. In the case a gas pocket is trapped in the crevice, it may be possible that the radius of the curvature of the bubble is concave as seen from the liquid side, which causes the surface tension pressure act towards the liquid thus reducing the gas pressure inside the bubble. In this case, gas may enter the bubble thus stabilizing it. When the static pressure is lowered, as is the case in the rarefaction half period of an acoustic wave, the gas pocket changes its volume starting with the change in shape of its meniscus. Nonetheless, as long as the meniscus remains concave, as seen from the liquid, the surface tension force still acts in the liquid. If the liquid pressure is reduced further, the meniscus can become convex. If the gas-liquid imbalance can overcome the surface tension, nucleation will take place in liquid due to release of the gas pocket as it reaches the top of the crevice. The minimum reduction in pressure for growing the bubble to visible size is called cavitation threshold.

Strasberg (1959) attempted to predict the effect of imperfectly wetted conical crevices on the cavitation threshold considering the dissolved gas, and the degree of pre-pressurization of the liquid. The work of Strasberg was extended by Apfel (1970), who included the effect of several other parameters such as the effect of vapor pressure, temperature and size of the crevice to predict the cavitation threshold. Apfel found that the cavitation threshold for smaller crevices was a strong function of surface tension but was independent of the dissolved gas content. On the contrary, the cavitation threshold for larger crevices was independent of the surface tension, but depended on the dissolved gas content and also the pre-treatment of the liquid. Crum (1979) has presented a more rigorous model for the cavitation threshold that treats the dependence on the surface tension in greater detail. The discrepancies of the crevice model were pointed out by Atchley and Prosperetti (1989). They proposed that as the meniscus of the gas pocket

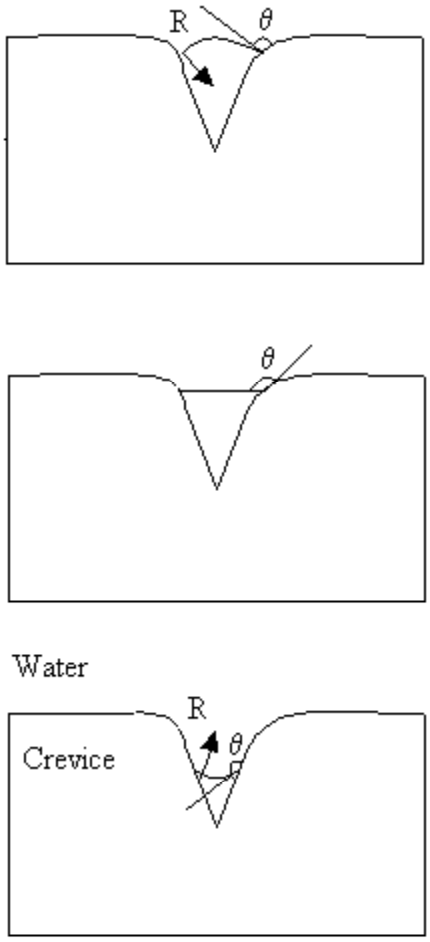

Figure 5: Nucleation of a liquid due to a gas pocket trapped inside a crevice. As the static pressure in the medium is reduced, the concave radius of curvature can become convex due to imbalance between the static pressure and Laplace pressure and the a bubble is grown from the crevice surface.

trapped in the crevice recedes, it causes simultaneous reduction in the Laplace pressure, and partial pressure of gas. If the reduction in the partial pressure of gas is faster than the reduction in the Laplace pressure, the bubble grows slowly. However, in the case of a reversed situation (i.e. faster reduction of the Laplace pressure) the gas pocket grows rapidly and nucleation takes place. The rate of reduction in gas pressure is determined by the rate of diffusion of dissolved gas in the liquid into the gas pocket. If the process of diffusion is more rapid than the rate of reduction in the Laplace pressure, the treatments given by Apfel and Strasberg hold true. In case it is slower, a greater pressure drop is required to cause nucleation.

2.3.2 Radial motion of the bubble

The dynamic behavior of an empty cavity was first studied by Lord Rayleigh in 1917. Rayleigh's analysis of the collapse of empty cavity was along the definition of cavity given by Besant (1889): "a spherical portion of liquid suddenly annihilated". Using a simple energy-balance argument Rayleigh (1917) obtained the equation for

collapse of an empty cavity under constant static pressure as:

$$R\frac{d^2R}{dt^2}+\frac{3}{2}\left(\frac{dR}{dt}\right)^2=\frac{P(R)-P_\infty}{\rho} \tag{19}$$

In the above equation, the pressure at infinity is assumed to be constant (= P_o, i.e. the ambient pressure in the liquid), while the pressure inside the bubble [P(R)] is assumed to be zero since it is an "empty" cavity. Rayleigh also did not take into account viscous and surface tension effects in his analysis. Later, Plesset (1949), while presenting the theoretical work on hydrodynamically generated cavities included the surface tension effects. Rayleigh's analysis needs modifications, if the void is in the form of a gas or vapor bubble. In case of a gas bubble, the gas pressure inside the bubble (to a first approximation) would vary as:

$$P_g=P_{go}\left(\frac{R_o}{R}\right)^{3k}=\left(P_o+\frac{2\sigma}{R_o}\right)\left(\frac{R_o}{R}\right)^{3k}. \tag{20}$$

k is the polytropic index of the bubble contents. k = 1 indicates isothermal behavior of bubble contents, and $k = C_p/C_v$ (ratio of specific heats of the bubble contents) indicates adiabatic behavior. During the radial pulsation of the bubble, the liquid at the bubble wall (gas-liquid interface) undergoes evaporation and condensation. This process is assumed to be very fast (compared to the period of radial pulsation) and, hence, the bubble interior is always saturated with vapor. With this, the pressure on the liquid side of the bubble surface can be written as:

$$P(R)=\left(P_o+\frac{2\sigma}{R_o}-P_v\right)\left(\frac{R_o}{R}\right)^{3k}+P_v-\frac{2\sigma}{R} \tag{21}$$

The viscosity effects were included in the radial motion of cavities by Poritsky (1952). If the bubble is acted upon by an acoustic wave, the pressure far from the bubble is:

$$P_\infty = P_o - P_A \sin(\omega t) \tag{22}$$

P_A being the pressure amplitude of the acoustic wave. Substituting for P(R) and P_∞ in equation 19 gives an equation for the radial motion of the bubble driven by an ultrasound wave:

$$R\frac{d^2R}{dt^2}+\frac{3}{2}\left(\frac{dR}{dt}\right)^2=\frac{1}{\rho_o}\left\{\left(P_o+\frac{2\sigma}{R_o}-P_v\right)\left(\frac{R_o}{R}\right)^{3k}-\frac{2\sigma}{R}+P_v-\left[P_o-P_A\sin(\omega t)\right]\right\} \tag{23}$$

This equation is known as the Rayleigh-Plesset equation for bubble dynamics. Although this equation is very useful in studying the radial motion of the bubble under different

conditions of the acoustic wave field (pressure amplitude and frequency), it has several simplifying assumptions that make its application limited:

1. It assumes the bubble to be in an infinite medium, thus, ignoring wall effects.
2. The bubble is assumed to remain spherical at all time during the radial motion.
3. The bubble interior is uniform; i.e. there are no temperature and pressure gradients inside the bubble.
4. The bubble radius is assumed to be much smaller than the wavelength of ultrasound.
5. No body forces (such as gravity) act on the bubble.
6. The liquid is assumed to be incompressible.
7. There is no heat or mass transfer across the bubble wall during radial motion.
8. The vapor pressure remains constant during oscillations.

Assumption no. 6, the compressibility of the liquid, is one of the major assumptions in bubble dynamics formulation. This assumption limits the applicability of Rayleigh-Plesset equation for large-amplitude radial motions of the bubble, where the bubble wall velocity during collapse phase can exceed the sonic velocity. There are two approximations that take into account the compressibility of the liquid are: 1. The acoustic [or Herring (1941)] approximation, and 2. The Kirkwood-Bethe (1942) approximation.

Acoustic approximation: In this approximation, the speed of sound is taken as a finite constant that implies a constant stiffness for the liquid. The equation of state for the liquid is then: p/ρ = constant or $\partial p/\partial \rho = c^2$. This approximation holds valid only for cases $U/c << 1$. When the bubble wall velocity approaches sonic velocity, the acoustic approximations can provide only a qualitative picture of the collapse of the bubble.

Kirkwood-Bethe approximation: This approximation states that, for spherical waves with finite amplitude, the quantity $r\varphi$ (r – radial coordinate, φ - velocity potential) propagates with a velocity equal to the sum of the velocity of the liquid (u) and sonic velocity (c). The local velocity of sound is expressed as a function of the free enthalpy on the surface of the bubble. Thus, the Kirwood-Bethe approximation provides a better picture of the radial motion of the bubble overcoming the demerits of the acoustic approximation.

Gilmore (1952) has given the equation for radial bubble motion based on Kirkwood-Bethe hypothesis as:

$$R\left(1-\frac{U}{c}\right)\frac{d^2R}{dt^2}+\frac{3}{2}\left(1-\frac{U}{3c}\right)\left(\frac{dR}{dt}\right)^2=\left(1+\frac{U}{c}\right)H+\frac{U}{c}\left(1-\frac{U}{c}\right)R\frac{dH}{dR} \tag{24}$$

H is the free enthalpy on the bubble and is written as:

$$H = \int_{P_\infty}^{P(R)} \frac{dp}{\rho} \tag{25a}$$

The values of P(R) and P_∞ can be substituted from equations 21 and 22. The pressure p can be expressed, using Tait's equation of state, as:

$$p = A\left(\frac{\rho}{\rho_o}\right)^n - B \tag{25b}$$

A, B and n are the constants and are given as: A = 3001 atm, B = 3000 atm, n = 7 for water. With these substitutions, the evaluation of the integral for H gives:

$$H = \frac{n}{(n-1)}\frac{A^{1/n}}{\rho_o}\left\{\left[\left(P_o + \frac{2\sigma}{R_o}\right)\left(\frac{R_o}{R}\right)^{3k} - \frac{2\sigma}{R} + B\right]^{\left(\frac{n-1}{n}\right)} - \left[P_o - P_A \sin(\omega t) + B\right]^{\left(\frac{n-1}{n}\right)}\right\} \tag{26}$$

2.3.3 Determination of local sound velocity

Using the expression $c = (\partial p/\partial \rho)_s^{1/2}$, and equation of state for water we get:

$$c^2 = c_o^2 \left(\rho/\rho_o\right)^{n-1} \tag{27}$$

An alternative evaluation of the free enthalpy gives:

$$H = \int_{\rho_o}^{\rho} \frac{dp}{\rho} = \frac{c_o^2}{(n-1)}\left[\left(\frac{\rho}{\rho_o}\right)^{n-1} - 1\right] \text{ where } c_o = \sqrt{\frac{A\,n}{\rho_o}} \tag{28}$$

Elimination of term $(\rho/\rho_o)^{n-1}$ from above equation using equation 27 gives an expression for velocity of sound in terms the free enthalpy as:

$$c = \left[c_o^2 + (n-1)H\right]^{1/2} \tag{29}$$

In order to simulate the radial motion of a bubble under the given conditions of acoustic field, one needs to solve equation 24 together with equations 26 and 29.

2.3.4 Thermal behavior of bubble contents

The thermal behavior of the bubble contents (whether gas, vapor, or mixture of both) is an important aspect of the radial bubble motion. This subject has been investigated by several researchers. Flynn (1964) hypothesized that the bubble motion is a combination of isothermal (k = 1) and adiabatic behavior ($k = C_p/C_v$). The transition

from the isothermal to the adiabatic phase is assumed to occur in the collapse phase, when the partial pressure of the gas in the bubble equals the vapor pressure of the liquid during compression phase. Plesset and Prosperetti (1977) have shown that the thermal behavior of the bubble depends on the (thermal) Péclet number $Pe = R_0^2 \omega/\kappa$, and thermal diffusion length $\sqrt{\kappa/\omega}$, where κ is the thermal diffusivity of the bubble contents, and ω is the angular frequency of the ultrasound wave. Hilgenfeldt *et al.* (1996) proposed that, since the bubble dynamics equation contains time scales much smaller than ω^{-1}, the frequency ω in the calculation of Pe should be replaced by $|U|/R$. This replacement leads to a value of Pe to be as large as 10^4 at the instants of rapid bubble wall movement, which implies that the bubble motion is adiabatic. However, the condition for which Pe >> 1 lasts only for very small time intervals ≈ 1 nsec. Therefore, Hilgenfeldt *et al.* (1996) proposed that the global dynamics of the bubble are not affected by setting the polytropic exponent k equal to 1 uniformly in time, thus parametrizing the isothermal conditions at the bubble wall, induced by the large heat capacity of water.

2.3.5 Pressure radiation by pulsating bubble

The amplitude of the acoustic waves radiated by the bubbles at a distance r >> R (far field) can be calculated from (Grossman *et al.*, 1997):

$$P_{AR}(r, t) = \frac{\rho}{4\pi r}\frac{d^2 V_b}{dt^2} = \rho\frac{R}{r}\left[2\left(\frac{dR}{dt}\right)^2 + R\frac{d^2 R}{dt^2}\right] \tag{30}$$

The amplitude of the shock wave emitted by the bubble during radial motion can be calculated using an approximation made by Akulichev (1971) as:

$$P_s(r, t) = A\left\{\frac{2}{(n+1)} + \frac{(n-1)}{(n+1)}\left[1 + \frac{G(n+1)}{r C_o^2}\right]^{1/2}\right\}^{2n/(n-1)} - B \tag{31}$$

G is a function of space and time given by:

$$G(R, t) = R\left(H + \frac{U^2}{2}\right) \tag{32}$$

It should be noted that the function G(R, t) also propagates with a velocity equal to sum of the velocity of sound and the fluid velocity (Akulichev, 1971). The pressure amplitude of the shock wave as well as acoustic wave generated from the bubble dissipates rapidly in water. Equation 29 and 30 do not take into account this dissipation. However, for an approximate estimation of the shock wave or acoustic waves at different cavitation conditions, these expressions are useful. The higher the intensity of the collapse of the bubble, the higher is the magnitude of the shock wave or acoustic wave radiated by the bubble. Thus, the magnitudes of either P_{AR} or P_s are a measure of the cavitation intensity resulting out of the bubble motion.

2.3.6 Stable and transient cavitation

Based on the radial motion of a bubble under the influence of an acoustic wave, the cavitation is categorized in two types: *stable* cavitation and *transient* cavitation. In stable cavitation, the bubble undergoes relatively small-amplitude oscillations around a mean radius for several acoustic cycles. In transient cavitation, the bubble undergoes an explosive growth to several times its original size followed by an extremely rapid collapse. The type of motion that the bubble undergoes (stable or transient) is a function of four parameters: the pressure amplitude of the acoustic wave (P_A), the frequency of the acoustic wave (f), the initial bubble radius (R_o), and the static pressure in the medium (P_o). Using the bubble dynamics equation, Flynn (1964) has proven that the bubble motion for a given parameter set of R_o, P_o, and f exhibits transient behavior only for a certain range of P_A. For a very low P_A, the bubble motion is stable, and of oscillatory nature. The amplitude of the bubble oscillations and the intensity of the collapse (indicated by the temperature and pressure pulses produced out of collapse) increase with rising pressure amplitude.

Generally the *transient cavitation threshold* means the lower value of P_A at which the bubble motion switches from stable to transient.

2.3.7 Determination of cavitation thresholds

As mentioned earlier, Flynn (1964) tried to distinguish between the stable and transient bubble motion using the bubble dynamics equation. He assumed that the initial bubble size is below the resonance size, but large enough to make the surface tension force insignificant and simulated the radial motion for rising pressure amplitudes. Flynn found that an increasing pressure amplitude accelerates the growth of the bubble accompanied by a sharp rise in the collapse velocity as the transient threshold is approached. When the acoustic pressure amplitude equals the static pressure ($P_A \approx P_o$), the bubble motion becomes transient. At this threshold the expansion ratio of the bubble (R_{max}/R_o) is greater than 2, and the collapse velocity is almost equal to the sonic velocity in the medium. Akulichev (1967) and Rosenberg (1971) have proposed the use of a phase-plane, which is a plot of dR/dt vs. R calculated from the bubble dynamics equation, to determine the transition from stable to transient bubble motion. For stable bubble motion, the phase-plane shows closed curves, while for transient behavior, the phase-plane shows discontinuities.

2.3.8 Analytical expressions for the transient cavitation threshold

The work of Flynn (1964), Rozenberg (1971) and Akulichev (1967) does not provide an analytical estimate for the transient cavitation threshold pressure. However, Neppiras (1980) has given a simple relation between the parameters P_A, R_o, and P_o as follows:

The liquid pressure just outside the bubble boundary is given by equation 21. For liquids such as water, the contribution made by vapor pressure, for low to moderate temperatures (20-25^{o}C), is always small. P(R) reaches a minimum during the bubble

motion when dP(R)/dR = 0. The bubble radius for which P(R) is a minimum is:

$$R = \left[\frac{3R_o^3}{2\sigma} \left(P_o + \frac{2\sigma}{R_o} \right) \right]^{1/2} \tag{33}$$

The natural oscillation frequency of the bubble is:

$$f_r = \frac{1}{2\pi R_o} \sqrt{\frac{3\gamma P_o \left(1 + 2\sigma/P_o R_o\right) - 2\sigma/R_o}{\rho}} \tag{34}$$

For a quasi-static regime, which means that $f_r >> f$, the pressure in the liquid far from the bubble (P_∞) should be equal to the pressure just outside the bubble boundary [P(R)]. From equation 22 we can calculate the maximum negative value of P(R) as $P_A - P_o$: Equating P(R) with P_∞ we find that the bubble becomes transient if:

$$P_A > P_o + \left(P_o + \frac{2\sigma}{R_o} \right) \left(\frac{R_o}{R} \right)^{3k} - \frac{2\sigma}{R} \tag{35}$$

Substituting for R from equation (33) we get the expression for transient cavitation threshold (P_T):

$$P_T > P_o + \frac{4}{3} \left[\frac{2\sigma^3}{3R_o^3 \left(P_o + 2\sigma/R_o\right)} \right]^{1/2} \tag{36}$$

There are three special cases for which the above expression can be reduced:

(i) For the case of very small bubbles, where $2\sigma/R_o >> P_o$:

$$P_T \approx P_o + \left(4\sigma/3\sqrt{3}\, R_o\right) \tag{37a}$$

(ii) For the case that $P_o > 2\sigma/R_o$ but the bubble size still much smaller than the resonance size corresponding to drive frequency:

$$P_T \approx P_o + \sqrt{\frac{32\sigma^3}{27\, P_o\, R_o^3}} \tag{37b}$$

(iii) For the case that $P_o >> 2\sigma/R_o$:

$$P_T \approx P_o \tag{37c}$$

2.3.9 Apfel's analysis

A limitation of the above formulation is that it applies only for the bubbles driven

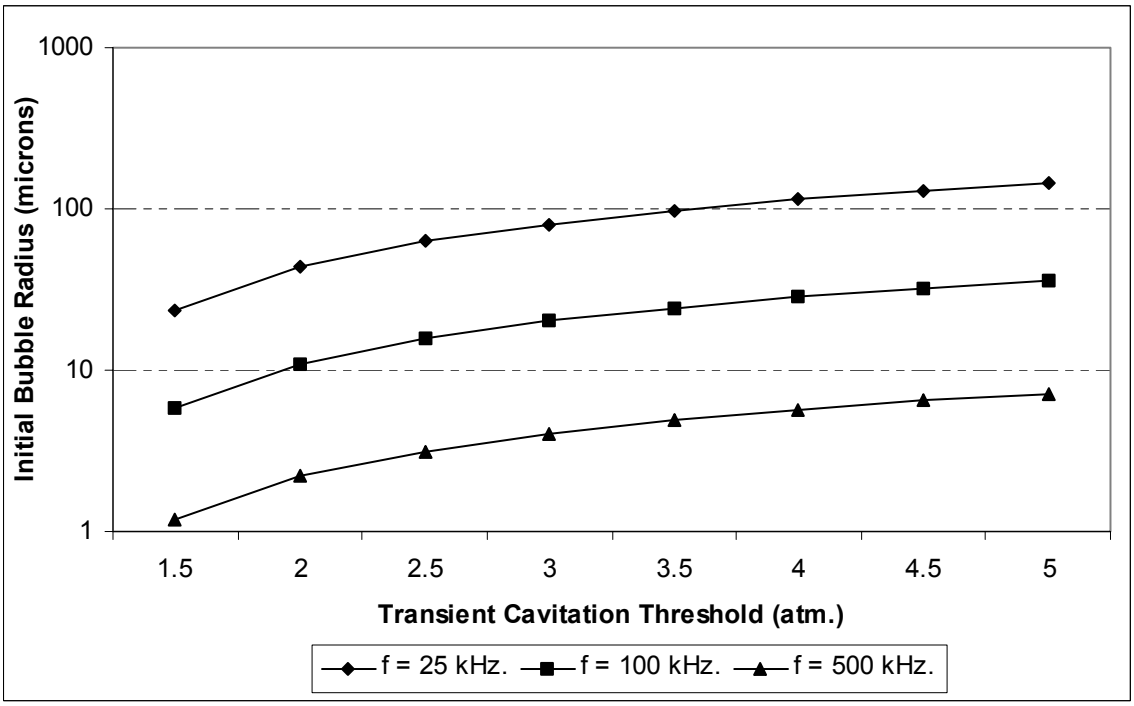

Figure 6: Variation in the transient cavitation threshold with initial bubble radius or different frequencies using Apfel's formula.

well below the resonance frequency, thus it neglects the inertial terms. Apfel (1981) has given a more general treatment of this problem. His analysis is valid for bubbles whose radial velocity reaches a maximum value in less than one quarter of the period of the acoustic wave. For this to happen, the bubble radius should be less than an inertial radius defined as:

$$R_I = \frac{\pi}{2\omega}\sqrt{\frac{P_A - P_o}{\rho}} \tag{38}$$

Apfel estimated the maximum radius that a bubble would reach during expansion as:

$$R_{max} = \frac{4}{3\omega}\left(P_A - P_o\right)\sqrt{\frac{2}{\rho P_A}}\left(1 + \frac{3}{2P_o}\left(P_A - P_o\right)\right)^{1/3} \tag{39}$$

Coupling of Apfel's analysis with that of Flynn, gives the general expression for transient cavitation threshold as follows:

As stated earlier, Flynn predicted that the bubble motion would be transient if the expansion ratio exceeds 2; as above this expansion ratio the collapse of the bubble is dominated by the inertial forces with spherical convergence of the surrounding liquid supplying an ever increasing amount of energy to the collapsing bubble. This ratio was corrected by Apfel as ~ 2.3. Substituting $R_{max}/R_o = 2.3$ in equation 39, and simplifying we get the general expression for the transient cavitation threshold that relates P_T, R_o, and f as:

$$R_o = \frac{0.82}{\omega} \frac{1}{\sqrt{P_T / P_o}} (P_T - P_o) \left[1 + \frac{2}{3} \frac{(P_T - P_o)}{P_o} \right]^{1/3} \quad (40)$$

Figure 6 depicts the variation in R_o as a function of P_T for three different ultrasound frequencies.

2.4 The acoustic emission

During the radial oscillations under the influence of an ultrasound field, the bubbles act as a secondary source of sound emitting spherical acoustic waves of various frequencies. The analysis of acoustic emission provides a tool for distinguishing between stable and transient cavitation.

At low intensities (or alternatively at low acoustic pressure amplitudes), bubbles execute small-amplitude oscillations at the frequency of the driving sound. As the sound intensity is increased, harmonics of the fundamental frequency set in, with the second harmonic being the most prominent. Non-linearity of the medium can also contribute to the harmonics, but the gassier the liquid the higher is the dominance of the acoustic emission from the bubbles.

The inception of transient cavitation causes drastic changes in the acoustic emission spectrum. The intensities of all subharmonics, ultraharmonics, and harmonics gradually rises as transient cavitation is approached. The intensity of the white noise also increases very rapidly with increasing pressure amplitude, once the transient cavitation threshold is passed. One of the important characteristics of the acoustic emission spectrum in transient cavitation is the prominent presence of the subharmonic signal (well above the white noise).

***Period-doubling route to chaos*:** Cramer and Lauterborn (1980) and Lauterborn and Cramer (1981) have observed experimentally the dynamics of the cavitation noise spectrum with rising pressure acoustic pressure amplitude. The acoustic emission progressed to broadband noise through *period-doubling*, a phenomenon in which the period of oscillations of a bubble becomes multiple of the period of the wave driving bubble motion. Period-doubling has also been predicted using numerical simulations of the bubble motion by Lauterborn and Parlitz (1988) and Ilyichev *et al.* (1989). The radial motion of the bubble shows interesting features variation in the sound pressure amplitude at constant frequency or variation in the frequency at constant pressure amplitude. Despite the periodic nature of sound field driving the bubble motion, chaotic bubble oscillations are encountered for some parameter values. These values at which significant changes occur to the radial bubble motion are known as "*bifurcations*". The bifurcations were found to be closely related to the resonances of the bubble (Parlitz *et al.*, 1990). Simulations of bubble dynamics presented by Ilyichev *et al.* (1989), for a bubble driven far below resonance ($f_r >> f$), have shown that the bubble motion transforms from periodic to non-periodic through a series of period-doubling bifurcations with rising

pressure amplitude. The subharmonic component appears in the emission spectrum at large pressure amplitudes close to transient cavitation thresholds.

2.5 Acoustic streaming

During the propagation through a medium, the acoustic wave loses its momentum due to several mechanisms, such as viscous losses. The momentum absorbed by the medium can result in the formation of bulk flow in the direction of propagation of the sound. This phenomenon is known as acoustic streaming. For plane acoustic waves traveling in an infinite medium, the energy (instead of momentum) of the wave is a more relevant parameter. Therefore, the definition of acoustic streaming for the plane waves can be given as the formation of energy gradient in the direction of the propagation of the wave from which energy will be absorbed by the attenuating medium. The pressure gradient that accelerates the liquid and is:

$$\nabla p = \frac{F}{V} = \frac{2Ib}{c} \tag{41}$$

I is the intensity of the acoustic wave, F/V is the force per unit volume of the fluid element, and b is the attenuation coefficient. It can be seen that increasing either the intensity or the attenuation coefficient will increase acoustic streaming.

Another type of acoustic streaming occurs, when the acoustic wave encounters a solid wall or a boundary. This is a result of the friction between the boundary and the medium that carries the acoustic wave. For this kind of acoustic streaming to occur, the size of the obstacle in the flow region should be much less than the wavelength of the acoustic wave, but should be greater than the penetration depth of the wave $\approx \sqrt{2\mu/\rho\omega}$. This kind of streaming, which exists in the form of small circulating currents in a confined region near the solid obstacle, is often called *micro-streaming*.

2.6 The effect of several parameters on cavitation

The radial motion of the bubble is affected by several parameters, and so are the magnitudes of the pressure and temperature maxima resulting from the radial motion of the bubble. The most prominent parameters that affect the radial bubble motion are:

- The acoustic pressure amplitude.
- The frequency of the acoustic wave.
- The initial bubble radius.
- The static pressure in the medium.

We give herewith a brief description of the variation in the bubble behavior with these parameters using numerical simulations of the bubble dynamics equation (equation 24) for air-water system. We have used the magnitude of the pressure radiated by the bubble

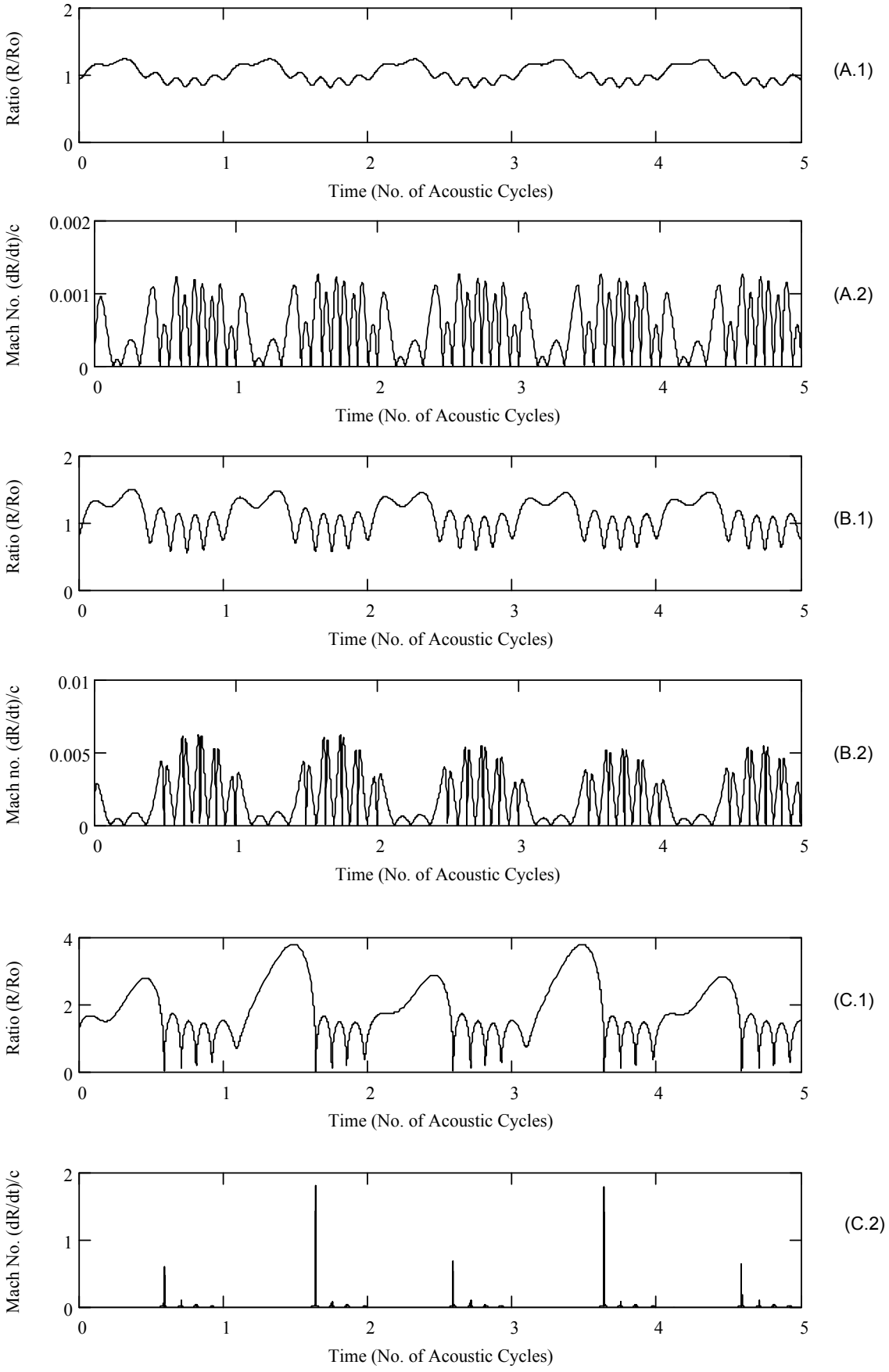

Figure 7: The characteristics of the radial motion of the bubble (the radius history and the bubble wall velocity) with increasing pressure amplitude of the acoustic wave driving the motion. Parameters for simulation: (A) P_A = 0.5 bar; (B) = P_A = 0.75 bar; (C) P_A = 1.25 bar. Other parameters: R_o = 5 μm.; f = 25 kHz.; ρ = 1000 kg m^{-3}; σ = 0.072 N-m; T = 25°C.

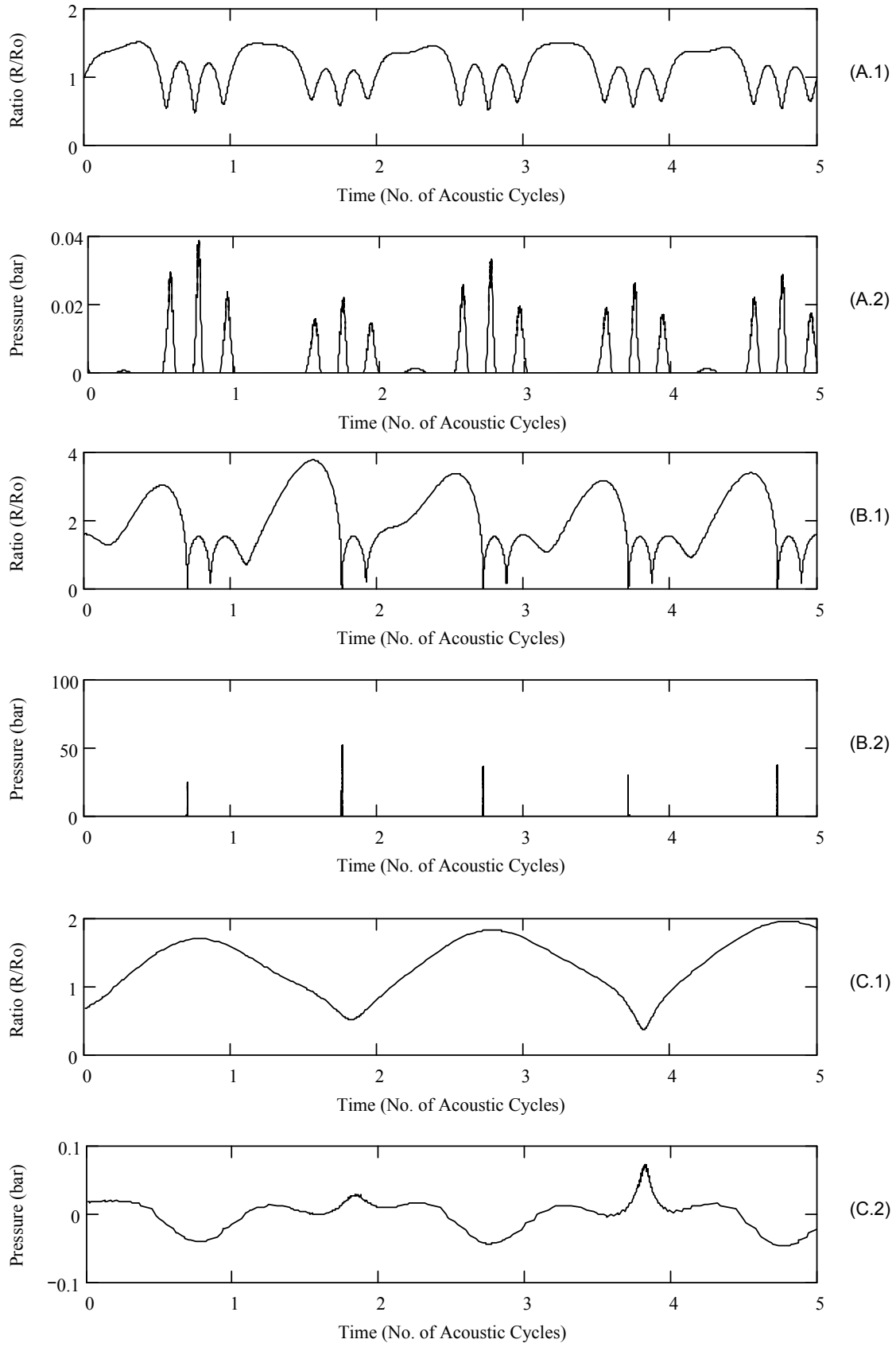

Figure 8: The behavior (radius history and amplitude of radiated pressure by the bubble) of a bubble with R_o = 10 μm. (f_r = 346 kHz.) under stable and transient cavitation conditions. Parameters for simulation: (A) f = 20 kHz., P_A = 0.75 bar; (B) f = 20 kHz., P_A = 1.5 bar; (C) f = 125 kHz., P_A = 1.5 bar.

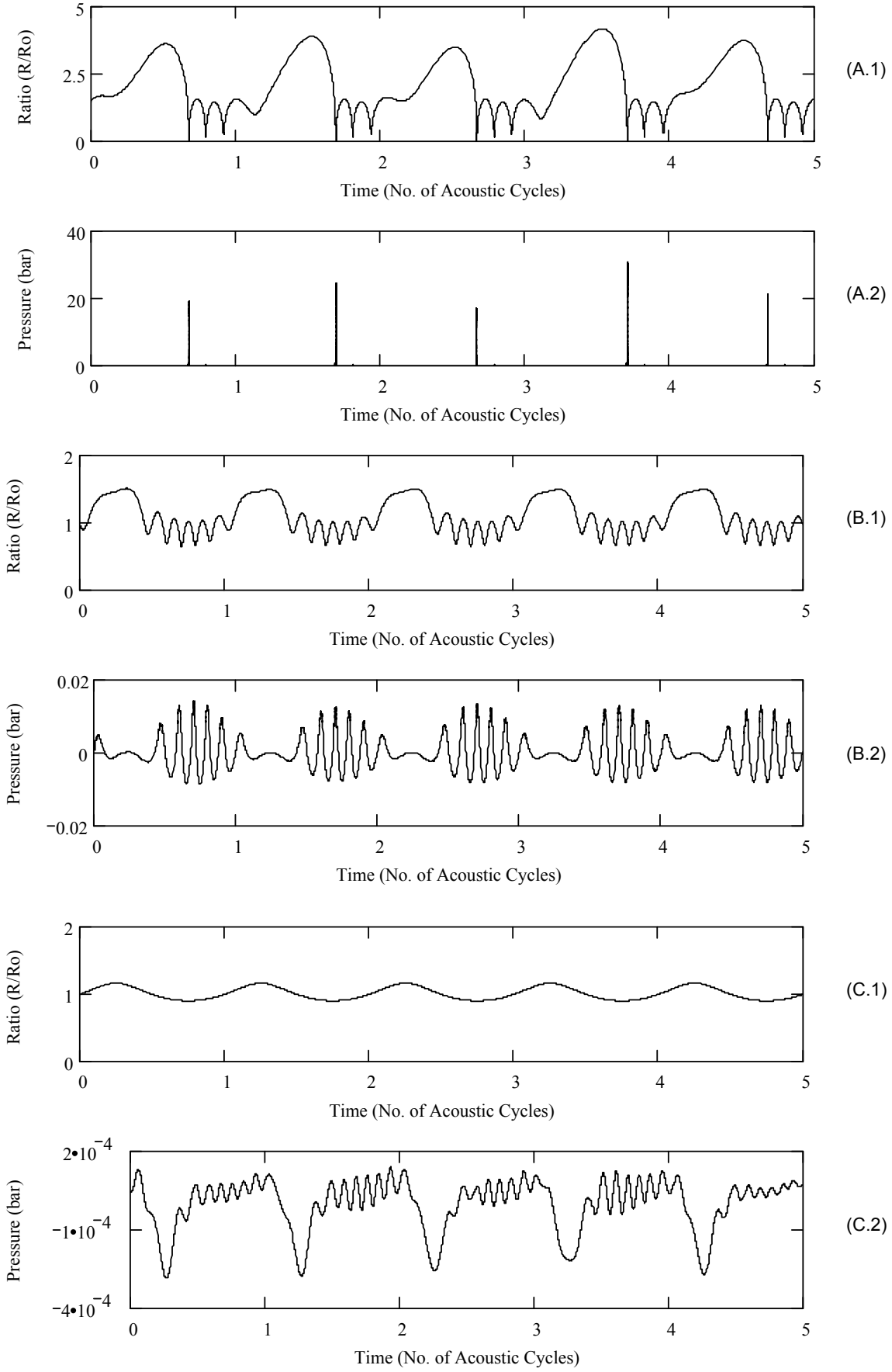

Figure 9: Effect of the static pressure in the medium on the radial motion of a bubble (radius history and amplitude of radiated pressure by the bubble). Parameters for simulation: (A) P_o = 1 bar; (B) P_o = 2 bar; (C) P_o = 4 bar. Other parameters: R_o = 5 μm.; f = 30 kHz.; P_A = 1.5 bar, ρ = 1000 kg m^{-3}; σ = 0.072 N-m; T = 25°C.

calculated using equation 30 as an indicator of the intensity of the bubble collapse. Value of r in equation 30 is taken as 1 mm in these calculations.

2.6.1 Acoustic pressure amplitude, frequency and initial bubble radius

The effect of P_A, f, and R_o are coupled and, therefore, need to be jointly assessed. Equation 40 relates the transient cavitation threshold to these three parameters together. It is quite clear that for the bubbles with a natural oscillation frequency far higher than the driving frequency, the intensity of the collapse will increase with a rising acoustic pressure amplitude, with the bubble motion becoming transient when $P_A > P_T$. However, for a given P_A and R_o, the bubble behavior is a function of the frequency. When the frequency of the acoustic wave approaches the natural oscillation frequency of the bubble (or exceeds it), the transient bubble behavior can become stable again, as is the case for conditions: $f_r >> f$ and $P_A < P_T$. These trends are shown in figures 7 and 8, using representative values for the parameters for the simulations of the radial motion of the bubble.

2.6.2 Static pressure

The rise in the static pressure with a fixed acoustic pressure amplitude and frequency reduces the intensity of the bubble collapse. The rise in the static pressure increases the transient cavitation threshold. Therefore, if the ratio $P_A/P_o < P_A/P_T$ the bubble motion becomes stable oscillatory, thus, reducing the temperature and pressure pulses produced out of it. These trends are depicted in figure 9 using simulations of radial motion of the bubble.

Notation

A - area, m^2.
b - attenuation coefficient of the acoustic wave, Neper m^{-1}.
c - velocity of sound, m s^{-1}
c_I - sound velocity in the first medium, m s^{-1}.
c_{II} - sound velocity in the second medium, m s^{-1}.
c_o - sound velocity in undisturbed medium, m s^{-1}.
C_p - specific heat capacity at constant pressure, J kg^{-1} $^oK^{-1}$.
C_v - specific heat capacity at constant volume, J kg^{-1} $^oK^{-1}$.
F - force in the liquid due to acoustic wave, N.
f - frequency of the acoustic wave, Hz.
f_r - resonance frequency of the bubble, Hz.
H - enthalpy on the bubble surface, J kg^{-1}.
I - acoustic wave intensity, W m^{-2}.
k - wave number, m^{-1}
k - polytropic constant of bubble contents, dimensionless.
L - length of the tube, m.
p - pressure, Pa

P_∞ - pressure in the liquid far from the bubble, Pa.
P(R) - pressure at the bubble surface, Pa.
P_A - acoustic pressure amplitude, Pa.
P_{AR} - amplitude of the acoustic wave emitted by the bubble, Pa
P_g - gas pressure in the bubble, Pa
P_{go} - initial gas pressure in the bubble (at t = 0), Pa.
p_I - pressure amplitude of the incident wave, Pa.
P_o - ambient pressure in the liquid, Pa.
p_R - pressure amplitude of the reflected wave, Pa.
P_s - pressure amplitude of the shock wave emitted by the bubble, Pa.
P_t - acoustic pressure amplitude threshold for subharmonic emission, Pa.
p_T - pressure amplitude of the transmitted wave, Pa.
P_T - transient cavitation threshold pressure, Pa.
P_v - vapor pressure of the liquid, Pa.
r - radial coordinate, m.
R - radius of the bubble, m.
R_e - van der Waal's distance, m.
R_I - inertial radius of the bubble, m.
R_{max} - maximum radius of the bubble during radial motion, m.
R_o - initial radius of the bubble, m.
R_r - resonance radius of the bubble, m.
s - entropy of the medium, J $^oK^{-1}$.
T - acoustic pressure transmission coefficient, dimensionless
T - temperature, ^oC.
t - time, s.
U - bubble wall velocity, m s^{-1}.
v - velocity of the acoustic wave, m s^{-1}.
V - volume, m^3.
V_b - volume of the bubble, m^3.
V_o - velocity amplitude of the piston, m s^{-1}.
v_o - velocity in undisturbed state (in absence of acoustic wave), m s^{-1}
v_x - velocity in x-direction, m s^{-1}.
x - distance coordinate, m.
Z - specific acoustic impedance, N-s m^{-1}.
Z_I - specific acoustic impedance of first medium, N-s m^{-1}.
Z_{II} - specific acoustic impedance of second medium, N-s m^{-1}.

Greek letters

ρ - density of the medium, kg m^{-3}.
ρ_o - density of the medium in undisturbed state, kg m^{-3}.
ρ_I - density of the first medium, kg m^{-3}
ρ_{II} - density of the second medium, kg m^{-3}.
σ - surface tension , N m^{-1}.
μ - viscosity of the medium, Pa-s.

λ - wavelength of sound wave, m.
γ - ratio of specific heats, dimensionless.
Φ - velocity potential, $m^2 s^{-1}$.
ϕ - phase of the acoustic wave, rad.
δ - damping constant of the bubble, dimensionless.
δ_μ - viscous damping coefficient, dimensionless.
ω_r - angular resonance frequency of the bubble ($=2\pi f_r$), rad.
ω - angular frequency of the acoustic wave., Hz.
κ - thermal diffusivity of the bubble contents, $m^2 s^{-1}$.
$\Re$ - acoustic pressure amplitude reflection coefficient, dimensionless.

References

- Akulichev, V.A., "Pulsations of cavitation voids" in *High Intensity Ultrasonic Fields* (Ed. L.D. Rosenberg), Plenum Press (1971) p. 205.
- Akulichev, V.A., "The structure of solutions of equations describing pulsations of cavitation bubbles", *Akusticeskij Zurnal*, **13**, 533-537 (1967).
- Apfel, R.E., "Methods in experimental physics", Vol. 19, (Edmonds, P.D. Ed.), Academic Press, New York (1981).
- Apfel, R.E., "The role of impurities in cavitation-threshold determination", *Journal of the Acoustical Society of America*, **48**, 1179-1186 (1970).
- Atchley, A.A., and A. Prosperetti, "The crevice model of bubble nucleation", *Journal of the Acoustical Society of America*, **86**, 1065-1084 (1989).
- Besant, W., *Hydrostatics and Hydrodynamics*, Deighton-Bell, Cambridge (1889).
- Cramer, E., and W. Lauterborn, "Acoustic cavitation noise spectra", in *Cavitation and Inhomogeneities in Underwater Acoustics*, (W. Lauterborn, Ed.), Springer-Verlag, New York (1980) pp. 209-214.
- Crum, L.A., "The tensile strength of water", *Nature*, **278**, 148-149 (1979).
- Epstein, P.S., and M.S. Plesset, "On the stability of gas bubbles in liquid-gas solutions," *Journal of Chemical Physics*, **18**(11), 1505-1509 (1950).
- Flynn, H.G., "Physics of Acoustic Cavitation in Liquids," *Physical Acoustics*, Vol. IB, W. P. Mason, ed., Academic Press, New York (1964).
- Gilmore, F.R., *Hydrodynamic Laboratory Report*, California Institute of Technology, **26-4** (1954).
- Grossmann, S., S. Hilgenfeldt, M. Zomack, and D. Lohse, "Sound radiation of 3 MHz driven gas bubbles", *Journal of the Acoustical Society of America*, **102**, 1223-1227 (1997).
- Herring, C., *Office of Naval Research and Development*, Washington, USA, Report No. 236 (1941).
- Hilgenfeldt, S., D. Lohse, and M.P. Brenner, "Phase diagrams for sonoluminescing bubbles", *Physics of Fluids*, **8(11)**, 2808-2826 (1996).
- Ilyichev, V.I., V.L. Koretz, and N.P. Melnikov, "Spectral characteristics of acoustic cavitation", *Ultrasonics*, **27**, 357-361 (1989).

- Kirkwood, J.B., and H.A. Bethe, *Office of Science Research and Development*, Report 558, USA (1942).
- Lauterborn, W., "Cavitation and coherent optics", in *Cavitation and Inhomogeneities in Underwater Acoustics*, (W. Lauterborn, Ed.), Springer-Verlag, New York (1980) pp. 3-12.
- Lauterborn, W., and E. Cramer, "Subharmonic route to chaos observed in acoustics", *Physical Review Letters*, **47**, 1445-1448 (1981).
- Lauterborn, W., and U. Parlitz, "Methods of chaos physics and their application to acoustics", *Journal of the Acoustical Society of America*, **84**, 1975-1993 (1988).
- Neppiras, E.A., "Acoustic Cavitation", *Physics Reports*, **61**, 159-251 (1980).
- Parlitz, U., V. Englisch, C. Scheffczyk, and W. Lauterborn, "Bifurcation structures of bubble oscillators", *Journal of the Acoustical Society of America*, **88**, 1061-1077 (1990).
- Pierce, A.D., *Acoustics: An introduction to its physical principals and applications*, Acoustical Society of America, New York (1989).
- Plesset, M.S., "Dynamics of Cavitating Bubbles," *Journal of Applied Mechanics: Transactions of the ASME*, **16**, 277-282 (1949).
- Plessset, M.S., and A. Prosperetti, "Bubble dynamics and cavitation", *Annual Review of Fluid Mechanics*, **9**, 145-185 (1977).
- Poritsky, H., "The collapse or growth of a spherical bubble or cavity in a viscous fluid", in *Proc. 1st U.S. National Congress on Applied Mechanics* (E. Sternberg, Ed.) pp. 813-821 (1952).
- Rayleigh, Lord, "On the pressure developed in a liquid during the collapse of spherical cavity," *Philosophical Magazine*, **34**, 94-98 (1917).
- Strasberg, M., "Onset of ultrasonics cavitation in tap water", *Journal of the Acoustical Society of America*, **31**, 163-176 (1959).

3

ACOUSTICAL CHARACTERISTICS OF TEXTILE MATERIALS

3.1 Introduction

Ultrasound is known to improve the efficiency of several wet textile processes, such as washing, dyeing, bleaching, desizing, mercerization etc. Despite a significant research on ultrasound enhanced wet textile processes, and encouraging results, no large-scale (or even pilot-scale) application of this novel technology is reported yet. One principal reason behind this is the lack of knowledge of the exact physical mechanism of the ultrasonic enhancement of the wet textile processes. In addition, the secondary aspects of this technology need to be taken into consideration, in order to realize implementation of this novel technology on an industrial scale. One such aspect is the acoustical characteristics of the textile materials.

As mentioned in previous chapters, the structural properties of the textile materials are quite complex, and are a function of their material of construction. A textile is basically a (bi)-porous visco-elastic material made of either natural fibers (such as cotton) or synthetic fibers (such as polyester). Textiles can have either a single (inter-yarn) porosity or a dual (inter-yarn and intra-yarn) porosity. However, due to high flow resistance of the intra-yarn pores, most of the flow occurs in the inter-yarn region, with little or no flow in the intra-yarn pores, as explained in chapter 1.

Acoustically the porous materials are categorized as: (i) sheet materials, and (ii) bulk materials on the basis of their thickness compared to the wavelength of sound. Sheet materials are those materials, whose thickness is much smaller than the wavelength of sound, while the thickness of the bulk materials is much larger than the wavelength of sound. The acoustic behavior of the sheet materials is controlled by the viscous effects and the area density (mass per unit area), while viscous and thermal effects and the solid-material density control the acoustic behavior of bulk materials.

In this chapter, we make an attempt to discern the acoustical characteristics of different textile materials. The parameters that form the basis of the acoustical characterization of the textile materials in this study are: (1) attenuation of the acoustic wave by the textile materials, and (2) the acoustic impedance of the textile materials. These two parameters, however, are related to each other, as will be discussed in detail subsequently in this chapter. Since the study is a part of our attempt to investigate the physical mechanism of the ultrasonic enhancement of the wet textile processes, we have used water as the medium for ultrasound.

3.2 Previous work

The acoustical properties of porous sheet materials have been investigated for past several decades. The principal contributions in this area were made by Beranek (1947, 1949), Nichols (1947), Zwikker and Kosten (1949), Bies (1971), and Vér and Holmer (1971). A large amount of literature has been accumulated over past decades on this subject.

Attempts to determine the acoustical characteristics of the textile materials, however, are few. Datar *et al.* (1996a, b) have studied the attenuation of ultrasound

through textile materials for low and high intensity ultrasound. Datar *et al*. (1996a, b) have reported the effect of several parameters, such as fabric weight, ultrasound frequency, fiber type, and wetting of the textile surface, on the attenuation of ultrasound as it passes through the fabric. The study of Datar *et al*. (1996a, b), despite being thorough, has several questionable conclusions.

The acoustic wave, during its passage through water, can also be attenuated by the bubbles in water, in case the water is not completely degassed. The extent of attenuation of the wave by the bubbles is determined by two factors: the bubble population, and the size of the bubbles. During the radial oscillations of the bubbles driven by the acoustic wave, the bubble size distribution can change as a result of rectified diffusion, which is a process of gas transport in and out of the bubbles. Whether the bubble will grow or shrink as a result of rectified diffusion, is determined by the dissolved gas content of the medium, the pressure amplitude and frequency of the acoustic wave, and the size of the bubble. The topic of rectified diffusion and acoustic wave propagation through bubbly liquid will be treated in greater detail in chapter 5. However, we would like to specifically state that while studying the attenuation of the acoustic wave by textile materials, it is necessary to isolate the above-mentioned effect of gas bubbles.

In their experiments Datar *et al*. (1996a, b) have used water, which was not completely degassed, as the medium. In addition, they have conducted experiments at acoustic pressure amplitudes higher than the transient cavitation threshold. Under the conditions of their experiments, it is very difficult to distinguish the effect of cavitation and the effect of the fabric properties on the attenuation of the ultrasound. Therefore, these results are questionable as far as the acoustical properties of the textiles alone are concerned.

In the present study, we have made an attempt to deduce the acoustical characteristics of the textile materials, while excluding the secondary effects due to cavitation bubbles. For this purpose, we have used two methodologies: (1) raising the static pressure of the experimental system well above the pressure amplitude of the ultrasound wave, which results in suppression of cavitation and, (2) using of precision-woven mono-filament textiles in which the intra-yarn pores (which can entrap gas-pockets that can provide nuclei for cavitation in the vicinity of the textiles) are absent.

3.3 The physical model

3.3.1 Transmission loss through porous sheet materials

When an acoustic wave is incident on a sheet material, such as a thin slab or a plate, a fraction of the wave energy is reflected and the rest is transmitted. In this situation, the sound-power transmission coefficient is defined as the ratio of the transmitted sound power to the incident sound power. If the incident wave is a plane wave, and if the structural properties of the slab do not change in the direction of the propagation of the wave, the transmitted wave will also be a plane wave traveling in the same direction as incident wave (Pierce, 1989). The transmission loss coefficient is

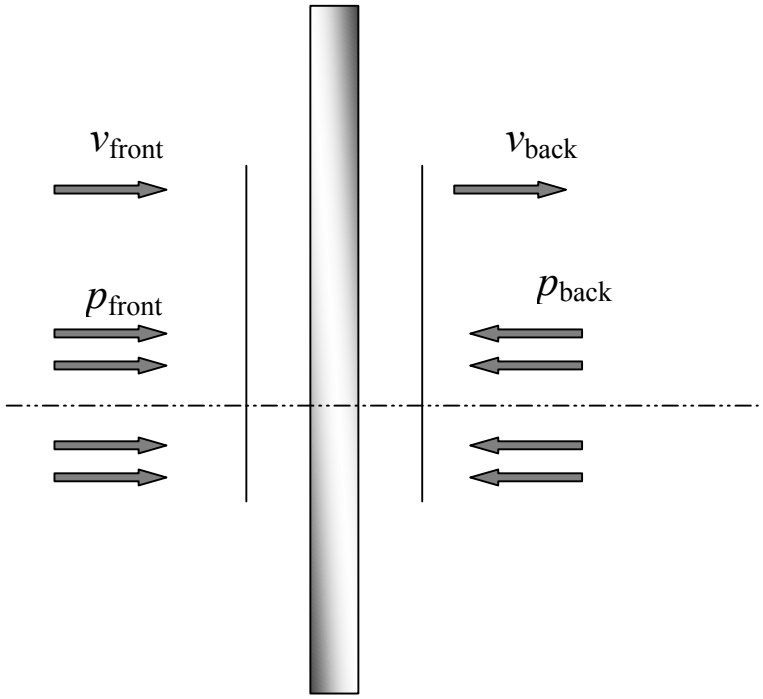

Figure 1: The interaction of an acoustic wave with a thin porous sheet.

defined as:

$$R_{TL} = 10 \log (1/\tau) \quad (1)$$

where τ is the ratio of mean squares of the pressure amplitudes of the transmitted wave (P_T) and the incident wave (P_I) (Vér & Holmer, 1971). In other words, τ is equal to the square of the transmission coefficient of the acoustic wave, as described in chapter 2.

If the properties of the sheet are such that the oscillatory velocities of the fluid elements on the two sides of the sheet v_f and v_b are equal, then the analysis of acoustic wave transmission can be simplified (Pierce, 1989). In the case of a porous sheet, the above condition holds true if the pore volume per unit area of the sheet is substantially less than a quarter of the wavelength of the acoustic wave. This hypothesis is based on two assumptions:

1. Density variation in the pores of the sheet is not much different from the density variation in the bulk fluid on both sides of the sheet.
2. Although the velocity of the fluid in individual pores is different from the inlet or outlet velocity, these variations are smoothed out, if the velocities of the fluid elements are averaged over a large area of the sample.

Consider an acoustic wave incident on a porous sheet, as shown in figure 1. Using the basic definition of the acoustic impedance (Z) in terms of the acoustic pressure (p) and velocity (v) given in chapter 2 (Z = p/v), we can write:

$$P_f - P_b = Z_s\, v_f = Z_s\, v_b \tag{2}$$

P_f and P_b are the pressures at the front and the back side of the slab, and v_f and v_b are the corresponding fluid velocities. Z_s is the specific acoustic impedance of the porous sheet. Dividing equation 2 by $v_f = v_b = v$, we obtain:

$$Z_f = Z_b + Z_s \tag{3}$$

This is analogous to an electric circuit, in which the combined or resultant impedance of two elements in series is the summation of their individual impedances. The pressure-amplitude transmission coefficient can now be calculated.

The pressure-amplitude reflection coefficient for a sound wave incident on an interface between two media, as given in chapter 2, is:

$$R = \frac{Z_2 - Z_1}{Z_2 + Z_1} \tag{4}$$

The velocity on the front side of the sheet is:

$$v_f = \frac{P_I}{Z_I}(1 - R) \tag{5}$$

Setting $Z_2 = (Z_s + Z_I)$ and $Z_1 = Z_I$ we get:

$$v_f = \frac{2\,P_I}{2\,Z_I + Z_s} \tag{6}$$

At the rear side of the slab, since the phase or media is homogeneous, we have:

$$P_T = Z_I\, v_b \tag{7}$$

Since $v_f = v_b$, the pressure-amplitude transmission coefficient is:

$$R = \frac{2\,Z_I}{2\,Z_I + Z_s} \tag{8}$$

The transmission loss coefficient is now calculated using equation 1 as:

$$R_{TL} = 10 \log\left(\left|1 + \frac{Z_s}{2\,Z_I}\right|^2\right) \tag{9}$$

It can be seen that in order to calculate the transmission loss coefficient, one needs to determine the specific acoustic impedance of the porous sheet, Z_s. In the next section we

present a simple model for this purpose.

3.3.2 Specific acoustic impedance of a porous sheet

Consider a porous sheet on which an acoustic wave is incident, as shown in figure 1. For a steady oscillatory flow, the transverse velocity in the bulk on either side of the sheet (relative to the velocity of the sheet itself) is (Pierce, 1989):

$$v_f - v_s = v_b - v_s = \frac{1}{R_f}\left(P_f - P_b\right) \tag{10}$$

This relation is analogous to an electric circuit, where the velocity and pressure difference are the counterpart of the current and voltage respectively. The flow resistance of the porous sheet (R_f) can be determined by holding the sheet fixed and forcing the liquid through it at a known rate, and measuring the pressure drop across the textile.

If the porous sheet is moving freely, one can write on the basis of Newton's law (rate of change of momentum is directly proportional to the applied force):

$$m_s \frac{\partial v_s}{\partial t} = \left(P_f - P_b\right) \tag{11}$$

Substitution for v_s gives:

$$m_s \frac{\partial}{\partial t}\left(v_f - \frac{1}{R_f}\left(P_f - P_b\right)\right) = \left(P_f - P_b\right) \tag{12}$$

Setting $\partial/\partial t \sim -i\omega$ and dividing by $(P_f - P_b)$ we have:

$$-i\omega m_s \frac{v_f}{\left(P_f - P_b\right)} + \frac{1}{R_f} i\omega m_s = 1 \tag{13}$$

Substituting $\frac{v_f}{\left(P_f - P_b\right)} = Z_s$ gives:

$$\frac{1}{Z_s} = \frac{-1}{i\omega m_s} + \frac{1}{R_f} \tag{14}$$

A simplification of the above expression gives:

$$Z_s = \frac{R_f \left(\omega m_s\right)^2 - iR_f^2 \left(\omega m_s\right)}{R_f^2 + \left(\omega m_s\right)^2} \tag{15}$$

For two limit cases, depending on the relative magnitudes of R_f and ωm_s, the expression

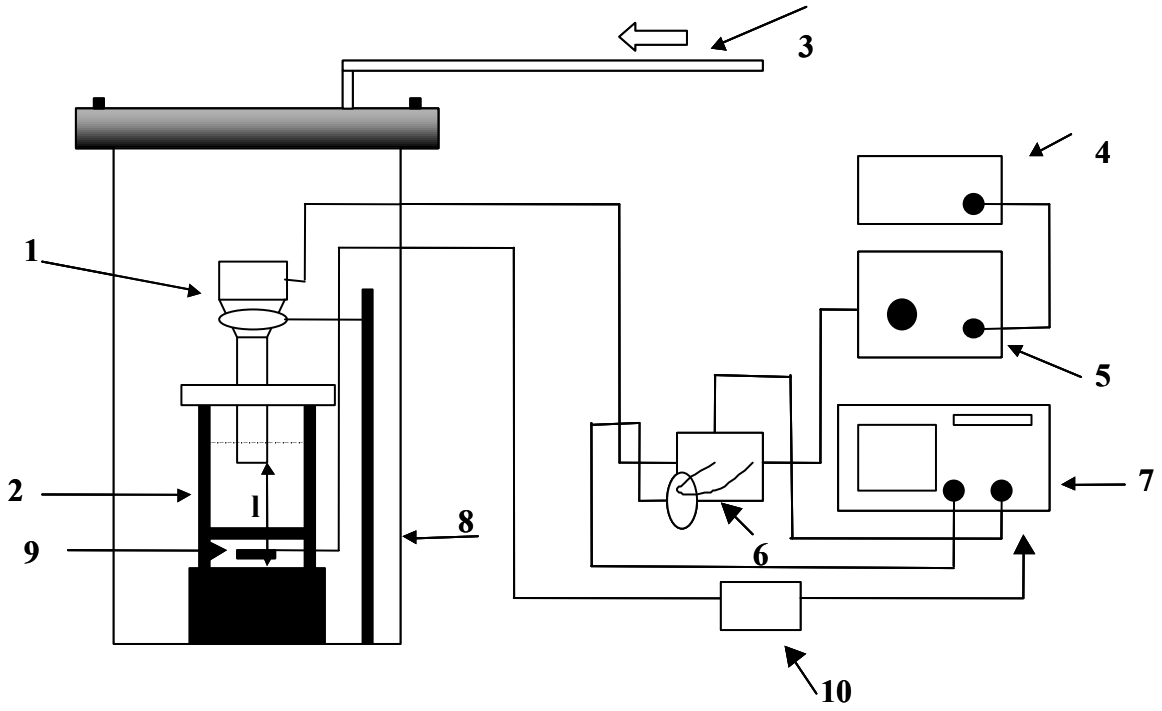

Figure 2: Schematic diagram of the experimental set-up in the ultrasound unit. Legends: 1. Ultrasound horn; 2. Experimental cell with textile sample; 3. Compressed air (7 bar); 4. Signal generator; 5. RF amplifier; 6. Voltage and current monitoring unit; 7. Digital oscilloscope; 8. High-pressure vessel; 9. Hydrophone; 10. Charge amplifier.

for Z_s can be reduced to:

$$Z_s = -i\omega m_s \quad \text{for } \omega << R_f/m_s. \qquad (16a)$$

$$= R_f \quad \text{for } \omega >> R_f/m_s. \qquad (16b)$$

The transmission loss coefficient (in dB) for a porous sheet can be calculated by substituting equation 16 in equation 9 for the two limit cases mentioned above.

3.4 Experimental

The experimental system in this study comprised of two sections: The ultrasound system, and the flow resistance measurement unit. The description of each unit and the operational procedure are given below:

3.4.1 Ultrasound system

The ultrasound system had three main components: an experimental cell, a high-pressure vessel, and an ultrasound horn, along with a signal generator and amplifier. A schematic diagram of the set-up is shown in figure 2.

The experimental cell: The experimental cell was made of 3 detachable glass rings and a lid made of Teflon. The height of the two rings was 15 mm, which corresponds to one-

quarter of the wavelength of 25 kHz ultrasound (6 cm) in water, while the height of the third ring was 60 mm. The cell was mounted on a 51 mm thick stainless steel bottom, with four vertical bars that act as support for the glass rings placed above each other. The stainless steel bottom of the experimental cell acts as a rigid reflector for the ultrasound waves. The cell had calibrated distance marks on it to measure the distance between the ultrasound horn tip and the rigid bottom. The textile sample could be placed in-between the glass rings at a certain distance from the bottom, and the glass rings could be pressed together with the lid on the top of the third ring. Rubber gaskets were placed between the textile and glass rings in order to avoid leakage. At the bottom of the cell, a special arrangement was made to place the hydrophone (Bruel & Kaejer Ltd., Type 8103) for the measurement of the acoustic pressure amplitude. The output of the hydrophone was transformed into proportional voltage by a charge amplifier (Nexus Range, Model 2690). This voltage was monitored on a digital oscilloscope (Tektronics Ltd., Model 430A). When the hydrophone was not needed, the connections (in the cell and in the pressure vessel) for the hydrophone could be closed with plugs.

The ultrasound unit: The ultrasound unit comprised of a special made ultrasound horn, with a central resonance frequency of 25 kHz when vibrating in air. The horn had a facility of cooling the piezoelectric element during operation in order to keep its temperature constant. The horn was driven by a signal generator (Hewlett-Packard Inc., Model 3324A) and a radio frequency amplifier (ENI Inc., Model 2100L). The amplifier could supply a maximum of 200W of electrical power for a large frequency range (10 kHz to 1 MHz) for an input-impedance of 50 ohms. The output power of the amplifier could be controlled by adjusting the input signal voltage to the amplifier (maximum allowed input signal voltage: 1 $V_{p\text{-}p}$). The signal generator could supply signals in the frequency range of 1 mHz to 21 MHz, with voltage upto 3.5 V_{rms} (at an output impedance of 50 ohm). The voltage and frequency of the signal generated by the signal generator could be varied in the steps of 1 mV and 1 mHz respectively. Thus, both the voltage and the frequency of the input signal to the amplifier and, hence, the electrical power consumption of the ultrasound horn could be precisely controlled for different sets of experiments with varying process parameters. The voltage and current supplied to the ultrasound horn were monitored using a voltage probe (Tektronics Ltd., Model 6138A) and a current clamp (Farnell Inc., Model PR-20). The peak-to-peak voltage ($V_{p\text{-}p}$), peak-to-peak current ($I_{p\text{-}p}$) and the phase angle (ϕ) between them were measured using a digital oscilloscope. The power consumed by the ultrasound horn could be calculated from these measurements as:

$$\text{Power} = \frac{V_{p\text{-}p} \times I_{p\text{-}p} \times \cos\phi}{4} \tag{17}$$

The ultrasound horn was mounted onto the shaft of a laboratory jack and the experimental cell was placed on its base. The base of the jack could be raised or lowered to adjust the distance between the bottom of the cell and the tip of the horn.

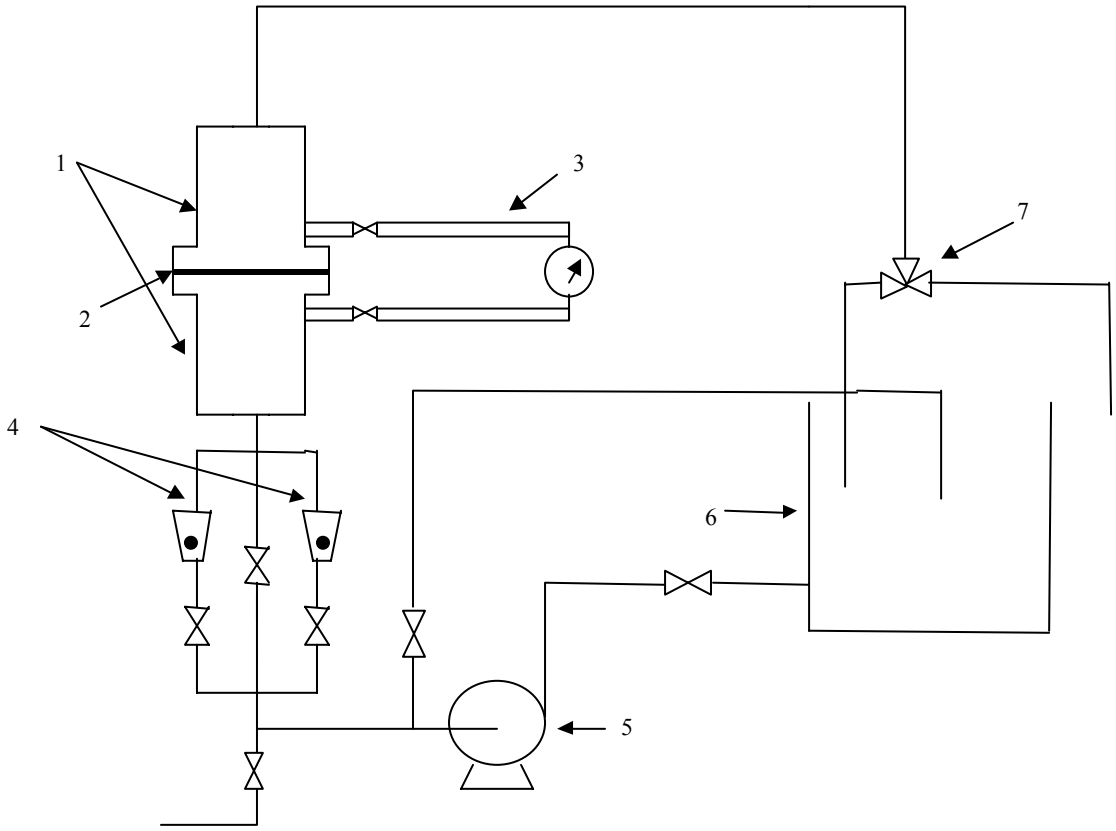

Figure 3: Schematic diagram of the experimental set-up for the flow resistance measurement. Legends: 1. Detachable columns to hold the textile; 2. Textile sample; 3. Pressure transmitter with air locks; 4. Rotameters; 5. Pump; 6. Water reservoir; 7. 3-way valve for collecting samples for the analysis.

The pressure vessel*:* In order to conduct the experiments under raised static pressure, a high-pressure vessel (volume: 40 lit; max. working pressure: 10 bar) was constructed that could accommodate the jack (with the ultrasound horn mounted on the shaft and the experimental cell placed on the base). The pressure vessel was equipped with electrical connections for the ultrasound horn, the hydrophone connections, and a safety release valve.

It must be specifically mentioned that, since the diameter of the cell was 60 mm, with the diameter of the ultrasound horn tip being 30 mm, the standing wave field generated in the cell does not have exact planar characteristics: small residual pressure amplitude exists at the velocity antinode, while small residual velocity amplitude exists at the pressure antinode. This non-ideality needs to be considered while interpreting the results of the experiments, which use position of the fabric in the standing wave field as a parameter.

3.4.2 Flow resistance measurement unit

The schematic diagram of the set-up for the flow resistance measurement of the textile materials is shown in figure 3. The set-up comprised of two circular columns of 50 mm diameter and approximately 50 cm length (made of acrylic material), between

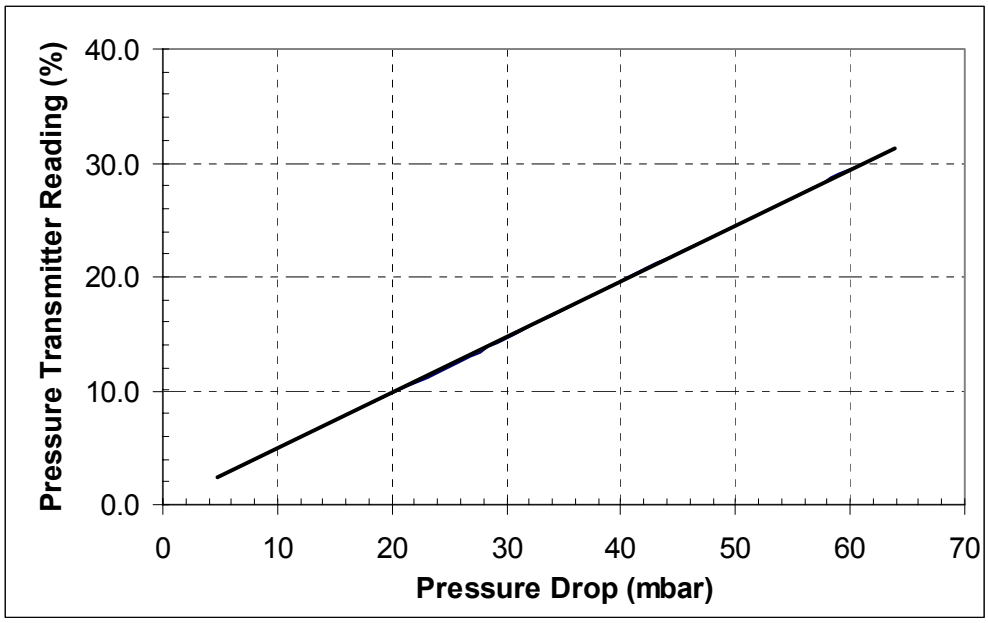

Figure 4: Calibration of the pressure indicator. The X-axis represents the absolute pressure drop while Y-axis indicates the pressure indicator reading.

which the textile sample was fixed during experiments. A thin rubber gasket was placed on the textile to avoid leakage. A 50-liter plastic tank was used as water reservoir. A IWAKI-MD6 pump (max. output: 38 lit/min) was used for the circulation of water in the flow loop. The flow through the column (and hence the textile) was measured with help of two GF rotameters (each with range 5-50 lit/hr and 30-300 lit/hr). The pressure difference across the textile sample was measured with a Honeywell STD-120 differential pressure indicator. Air locks were provided on the tubes connecting the acrylic columns to the pressure indicator, in order to isolate the flow loop to the pressure indicator from the main flow loop during the replacement of the textile samples. This prevents admittance of any air bubble in the pressure indicator flow loop, which can hinder the accurate measurement of the pressure drop across the textile. The pressure indicator was calibrated against a water manometer. The calibration chart is shown in figure 4. The maximum pressure drop range of the pressure indicator is 200 mbar, with a resolution of 0.2 mbar.

3.4.3 Model textiles

As written earlier, monofilament precision woven screening fabrics (made of Polyamide) were used as model textiles. These types of monofilament textiles have only a single porosity, i.e. the inter-yarn porosity. These samples were obtained from Sefar Inc. (Filtration Division), Switzerland. A total of 7 samples with different specifications were selected. Detailed specifications of these model textiles are given in table 1.

Table 1: Specifications of Sefar model textiles

Sample	Mesh Opening (μm.)	Open Area (%)	Mesh Count Warp/Weft (n/cm.)	Wire Dia. (μm.) Warp	Wire Dia. (μm.) Weft	Weight (g/m^2)	Thickness (μm.)
03-20/14	20	14	188/188	34	34	35	55
03-30/20	30	20	150/150	40	40	35	70
03-48/26	48	25.5	106/106	47	47	35	75
03-41/31	41	31	136/136	33	33	25	50
03-63/30	63	30	78/94	43	43	35	95
03-53/30	53	30	144/104	43	43	43	100
03-35/16	35	16	100/128	43	43	49	97

3.4.4 Experimental procedure

Ultrasound experiments: The amplitude of the acoustic wave generated by the ultrasound horn was measured with only water in the experimental cell (without textile) as 1.2 bar. This value was regarded as the *reference* or (un-attenuated) incident acoustic pressure amplitude (it must be noted that due to the formation of standing waves in the cell the acoustic pressure amplitude is doubled. So the reference acoustic pressure amplitude of 1.2 bar corresponds to traveling acoustic waves with amplitude of 0.6 bar). The power consumption of the ultrasound horn was determined for these conditions, using the voltage and current measurements on the digital oscilloscope. This power consumption value was regarded as the *reference* power value. In the subsequent experiments, the textile sample was placed between the rings of the experimental cell (at either the pressure antinode or the pressure node) inside a water bath to avoid entrapment of air below the textile surface. The quantity of de-mineralized water in the cell was fixed as 250 ml. The distance between the ultrasound horn tip and the bottom of the experimental cell was fixed as 6 cm (which is the wavelength of ultrasound wave of 25 kHz frequency in water). This apparatus was placed inside the high-pressure vessel, with the pressure inside the vessel being raised to 6.5 bar. The apparatus was then pressurized for approximately 1 hour to minimize the effect of ultrasound wave attenuation due to the gas bubbles present in the medium. Later, the ultrasound was turned on (with a signal input of 50 mV_{rms} to the amplifier), with the experimental apparatus still kept pressurized at 6.5 bar (conducting the experiments under high static pressure helps completely remove the effect of attenuation due to the bubbles). The voltage and current supplied to the ultrasound horn were monitored on the digital oscilloscope, and the frequency of the ultrasound was tuned slightly to remove the phase angle between the voltage and current. In order to measure the attenuation of the acoustic wave by the textile, the power consumption of the ultrasound horn was re-adjusted to the *reference* value (by slightly changing the signal input to amplifier), and the amplitude of the acoustic wave sensed by the hydrophone was noted.

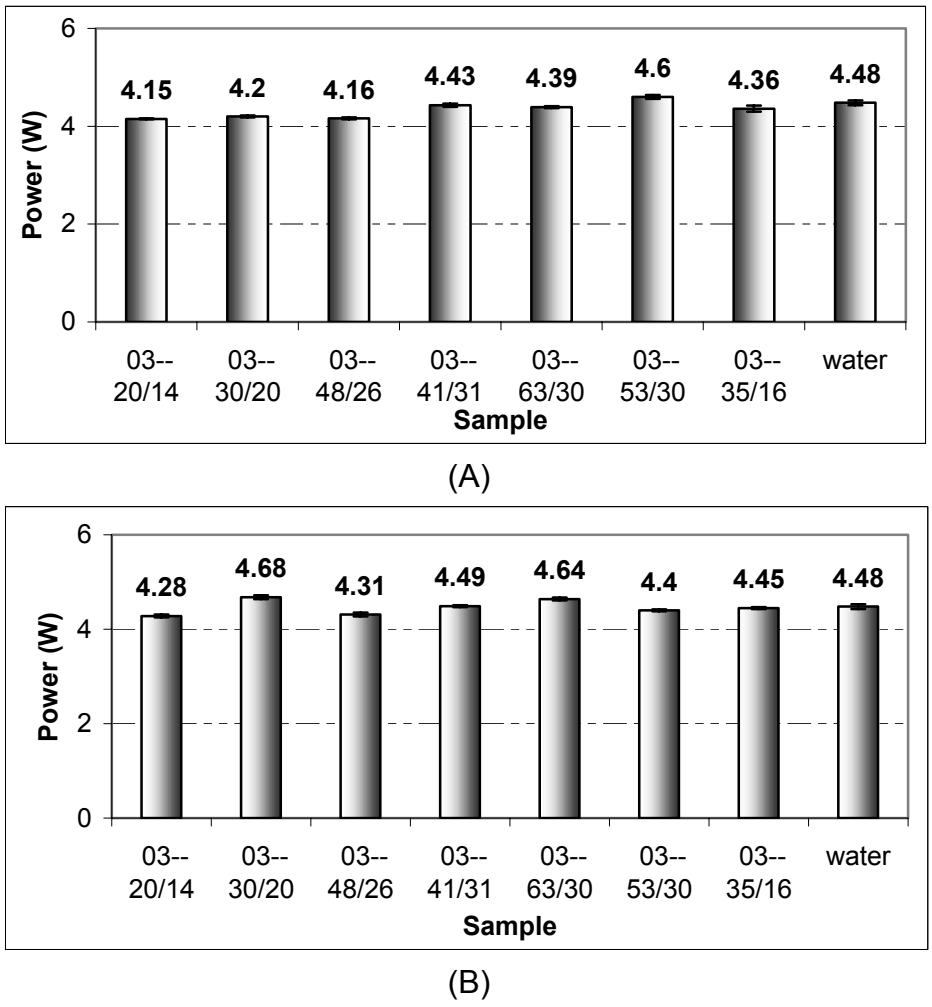

Figure 5: The power consumption of the ultrasound horn with the placement of different textile samples in the standing wave field. (A) Textile samples at pressure antinode, (B) Textile samples at pressure node.

Flow resistance measurement: The acrylic columns were fixed together without the textile, and water was circulated in the flow loop for about half an hour (with all the valves opened except the bypass valve and the holdup-removal valve) to completely remove the air trapped in the loop. Once no air bubbles were visible in the water flow in the columns, the flow in the columns was allowed only through one rotameter (30-300 lit/hr), with all the other valves closed. The air locks in the flow loop of the pressure indicator were closed before the columns were opened for removing or replacing the textile sample. The textile samples were thoroughly wetted before they were placed between the columns, so as to remove the air trapped in the inter-yarn pores of the textile. Special attention was paid to avoid any entrapment of air bubbles beneath the textile surface, which could hamper the accurate measurement of the pressure drop. A small amount of chlorine bleaching agent was added to avoid any bacterial growth in the water reservoir during storage of water.

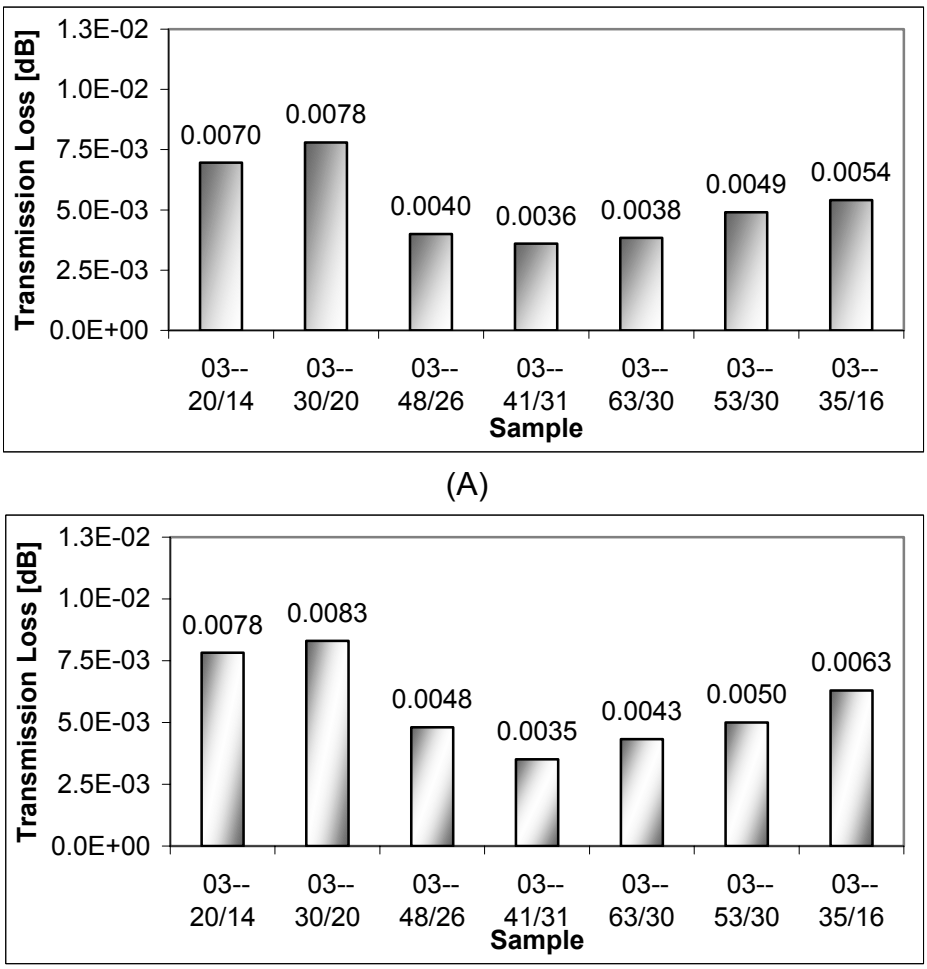

Figure 6: Experimental sound-power loss coefficients (R_{TL}) for different textile samples. (A) Textile samples at pressure antinode; (B) Textile samples at pressure node.

3.5 Results and discussion

The theory of the equivalent circuit of piezoelectric transducer states that the electrical power consumed by the transducer is a function of the specific acoustic impedance of the medium in which it is oscillating (Ensminger, 1988). In the present case, the impedance that a piezoelectric transducer encounters for the oscillatory motion is the sum of the acoustic impedance of the medium (water) and the acoustic impedance of the textile sample given by equation 2.

The power consumption of the ultrasound horn with the textile positioned at the pressure node and the pressure antinode in the standing wave field are shown in figures 5A and 5B respectively. The reference power value, which is the power consumption of the ultrasound horn with only water as the medium, is also shown in these figures. The sound-power transmission loss calculated using experimentally measured values of incident and transmitted acoustic pressure amplitudes for textile positioned at the pressure node and the pressure antinode are shown in figures 6A and 6B respectively. The results of the flow resistance measurement of the model textiles are shown in figures

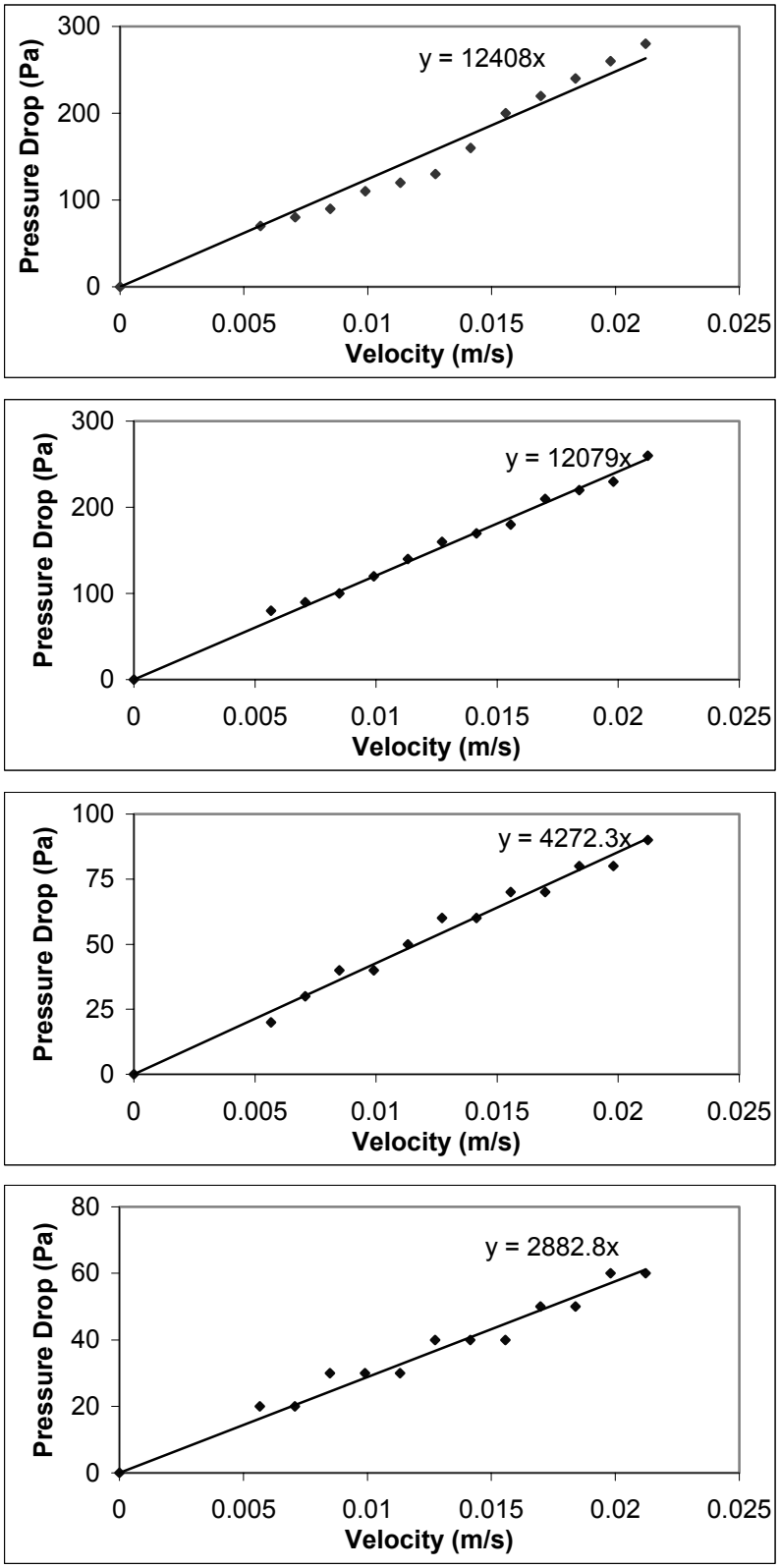

Figure 7: The flow resistance measurement for different textile samples. The slope of the plot of pressure drop vs. velocity is the specific flow resistance of the sample. (A) Sample 03-20/14, (B) Sample 03-30/20, (C) Sample 03-48/26, (D) Sample 03-41/31, (E) Sample 03-63/30, (F) Sample 03-53/30, (G) Sample 03-35/16.

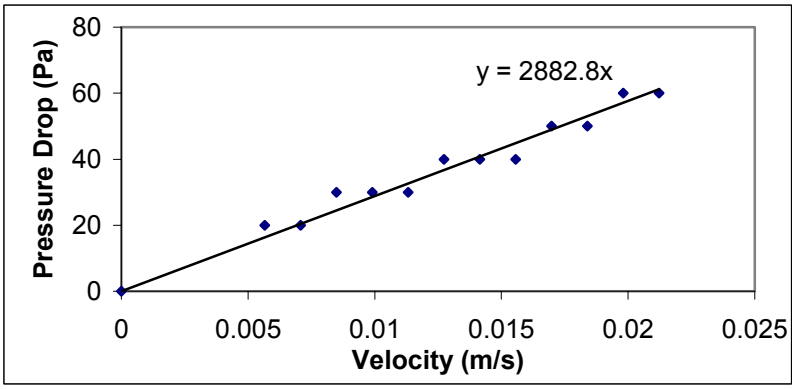

(E)

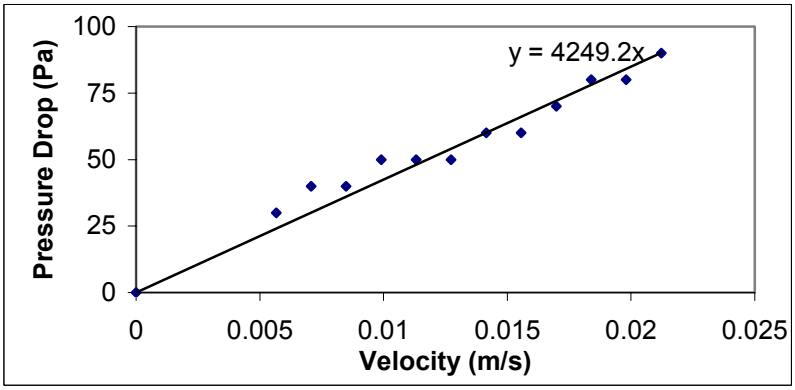

(F)

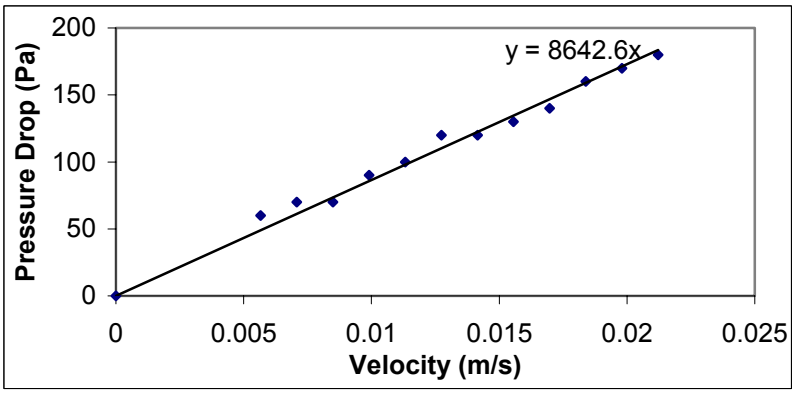

(G)

Figure 7 (*continued*….)

7A-7G for different samples. The flow resistance of the textile samples can be found from the slope of the plot of the pressure drop vs. the liquid velocity, which is linear in the laminar flow regime (Gooijer, 1998). It could be inferred from figure 6 that the presence of the textile in the standing wave causes a negligible change to the power consumption of the ultrasound horn. This is indicative of the fact that the total acoustic impedance of the system remains practically constant after placing the textile in the standing wave field generated in the experimental cell. Explanations for these results can be given on the basis of the physical model for the acoustic impedance of the textile materials presented earlier in this section.

The two components of the acoustic impedance of the textile are:

1. The flow resistance (real part, independent of the frequency of the acoustic wave).
2. Mass reactance (imaginary part, which is a function of the frequency of the

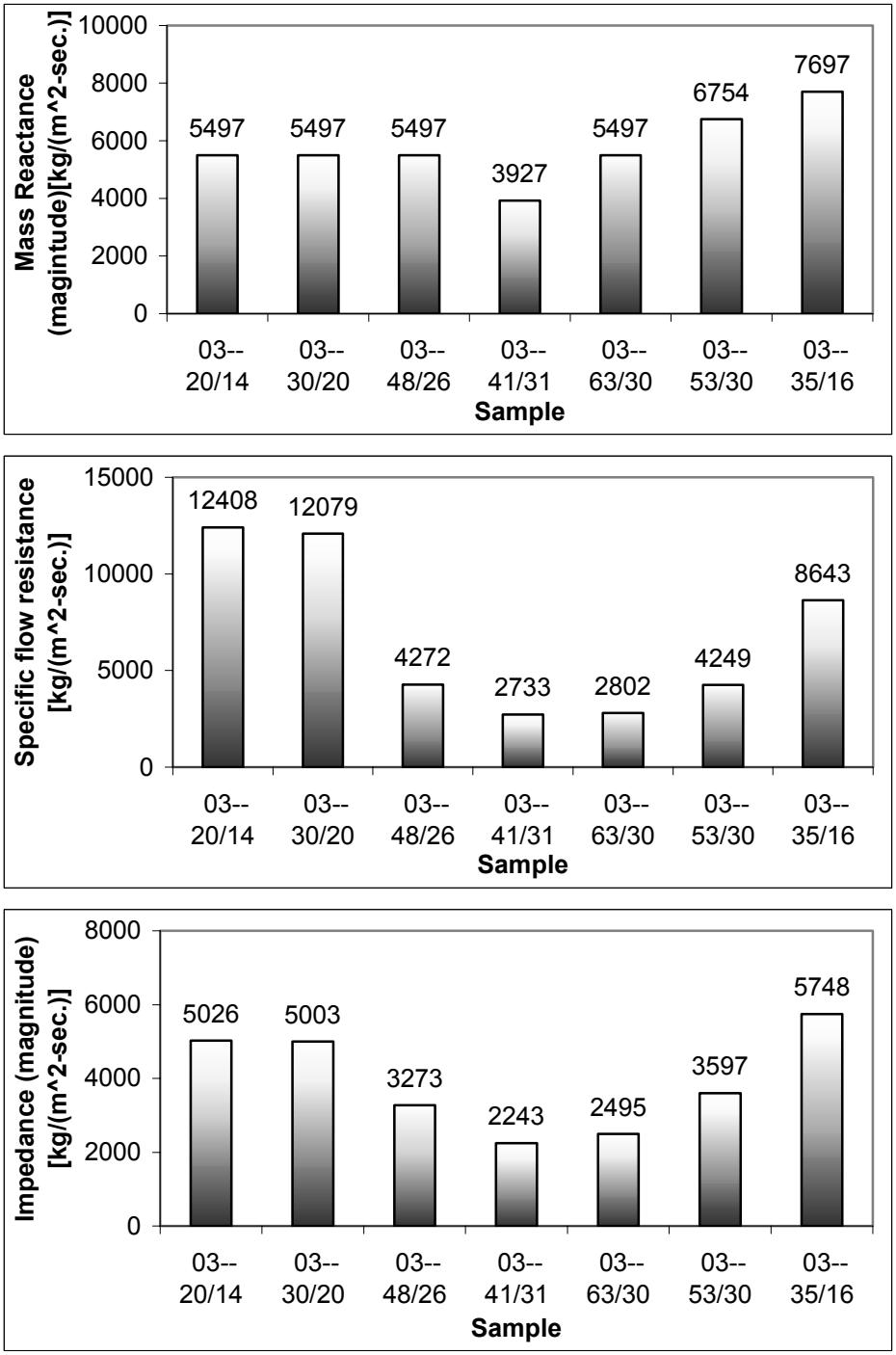

Figure 8: The acoustic impedance of the textile samples. (A) The mass reactance (imaginary) component; (B) The flow resistance (real) component; (C) The resultant acoustic impedance of the textile samples.

acoustic wave).

The individual magnitudes of these two components, along with the resultant acoustic impedance for different textile samples, are shown in figures 8A-8C. The medium for ultrasound, used in the present experiments, was water whose acoustic impedance is 1.5 $\times 10^6$ kg m^{-2} s^{-1} (ρ = 1000 kg m^{-3}, c = 1500 m s^{-1}). The specific acoustic impedance of all

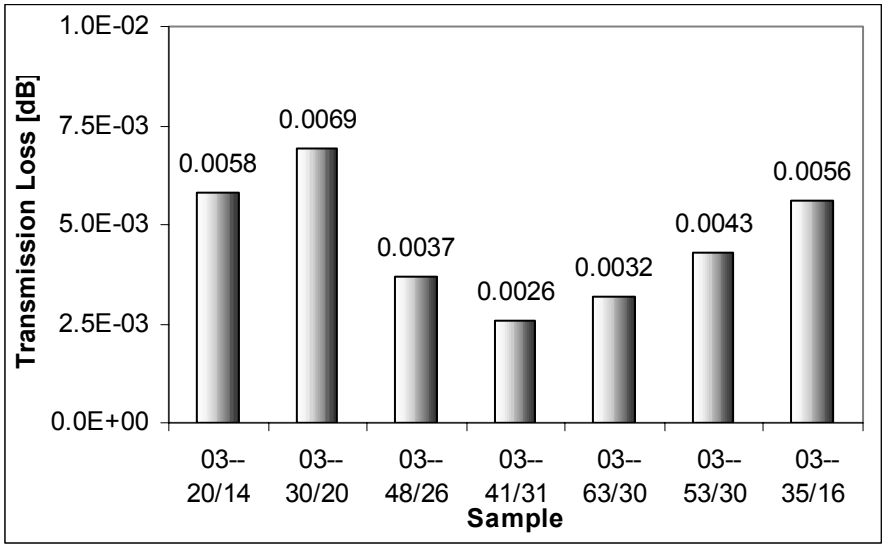

Figure 9: The theoretical sound-power transmission loss for different textile samples.

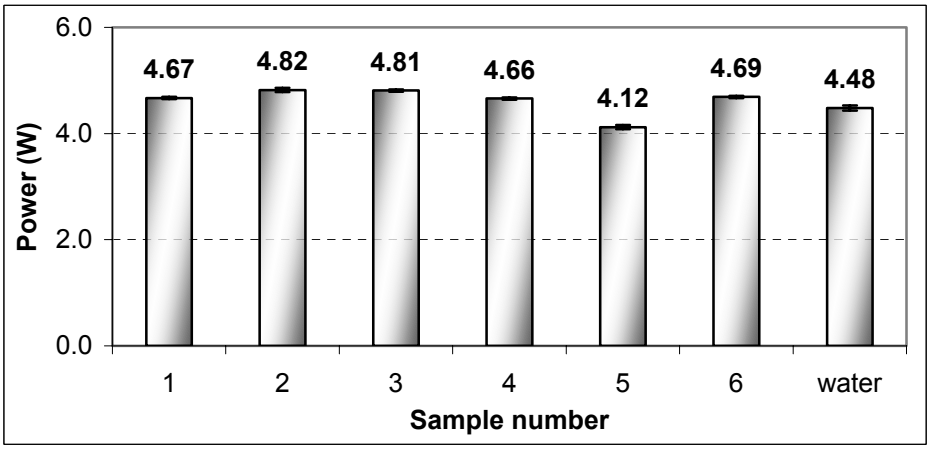

(A)

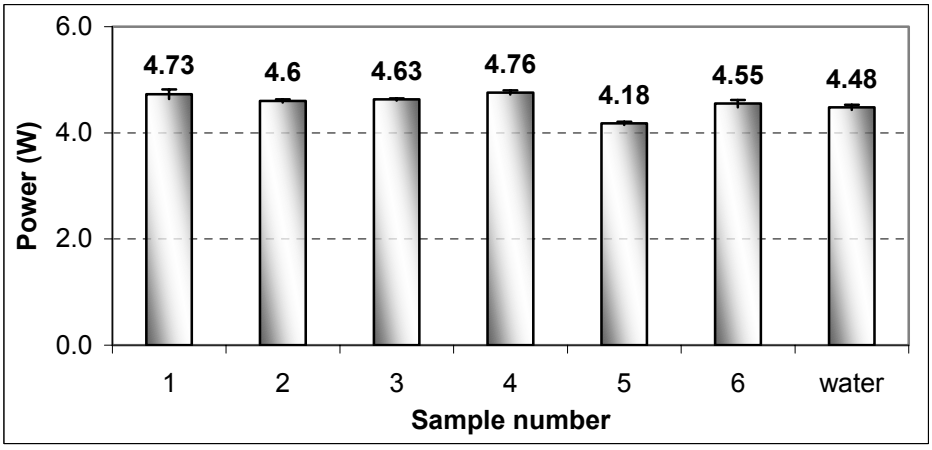

(B)

Figure 10: Variation in the power consumption of the ultrasound horn with presence of commercial textile in the standing wave field. Description of the samples with samples numbers: 1. Ten Cate sample B (cotton, 207g/m^2), 2. Ten Cate sample C (cotton, 196g/m^2), 3. Ten Cate sample D (cotton, 185g/m^2), 4. Vlisco 4212 (cotton, 112g/m^2), 5. Vlisco 4350 (cotton, 118g/m^2), 6. Ten Cate Cotton Polyester (cotton 60% - polyester 40%, 580g/m^2).

the samples shown in figure 8 is much smaller than the acoustic impedance of the medium itself. Therefore, the impedance of the experimental cell remains practically constant after introduction of the textile sample, thus, causing no change in the power consumption of the ultrasound horn.

The results shown in figure 8 along with equation 16 also help determine the theoretical sound-power transmission loss coefficient for the acoustic wave (figure 9). Since $(Z_s/\rho c) \sim 10^{-3}$ or so, the textile transmits practically all the energy of the acoustic wave incident on it.

3.6 Conclusion

This study proposes a simple methodology for determining the acoustical characteristics of the textile materials. The theoretical model for the acoustic impedance of the textile reveals that the acoustic impedance of the textile is determined by both structural (area density), and hydrodynamic (flow resistance) properties of the textile materials. The mass per unit area and the flow resistance act as two resistances in parallel. The presence of the textile material causes practically no change in the acoustic impedance of the system and, hence, in the power consumption of the ultrasound horn. The results of this study reveal that the textile materials form a practically transparent boundary for the acoustic wave, transmitting most of the acoustic power incident on them. In order to verify the validity of this conclusion in case of practical textiles, experiments were carried out using several commercial textiles of different properties. In these experiments, only the change in the power consumption of the ultrasound horn after placement of the textile at the pressure node and the pressure antinode in the standing wave field has been measured. The results of the experiments are shown in figure 10, along with the reference power value. It can be inferred from figure 10 that the presence of the textile in the standing wave field does not cause any significant change in the power consumption of the ultrasound horn. This result confirms the validity of the conclusion of this study in case of commercial textiles.

Notation

c - velocity of sound, m s^{-1}.
m_s - mass per unit area of the porous sheet, kg m^{-2}.
P_b - acoustic pressure on the back side of the slab, Pa.
P_f - acoustic pressure on the front side of the slab, Pa.
P_I - acoustic pressure amplitude of the incident wave, Pa.
P_T - acoustic pressure amplitude of the transmitted wave, Pa.
R - pressure-amplitude reflection coefficient, dimensionless.
R_f - specific flow resistance of the porous slab, Pa-s m^{-1}.
R_{TL} - sound-power transmission loss, dB
v_b - fluid velocity on the back side of the slab, m s^{-1}.

v_f - fluid velocity on the front side of the slab, m s^{-1}.
v_s - velocity of the porous sheet , m s^{-1}.
Z_1 - acoustic impedance of the first media, Pa-s m^{-1}.
Z_2 - acoustic impedance of the second media, Pa-s m^{-1}.
Z_b - acoustic impedance at the back side of the slab, Pa-s m^{-1}.
Z_f - acoustic impedance at the front side of the slab, Pa-s m^{-1}.
Z_I - acoustic impedance of the medium, Pa-s m^{-1}.
Z_s - acoustic impedance, Pa-s m^{-1}.

Greek letters

ρ - density of the medium, kg m^{-3}.
τ - sound-power transmission loss coefficient, dimensionless.
ω - angular frequency of the acoustic wave, rad s^{-1}.

References

- Beranek, L.L., "Acoustical properties of homogeneous, isotropic rigid tiles and flexible blankets", *Journal of the Acoustical Society of America*, **19 (4)**, 556-568 (1947).
- Beranek, L.L., *Acoustical Measurements*, Wiley, New York (1949).
- Bies, D.A., "Acoustical properties of porous materials", in *Noise and Vibrations Control* (Beranek, L.L., Ed.), McGraw Hill, New York (1971) pp. 245-269.
- Datar, G.V., P. Banks-Lee, and P.L. Grady, "Acoustical characteristics of fabrics in high intensity ultrasound", *Applied Acoustics*, **48(1)**, 33-45 (1996).
- Datar, G.V., P. Banks-Lee, and P.L. Grady, "Acoustical characteristics of fabrics in low intensity ultrasound", *Applied Acoustics*, **47(4)**, 345-350 (1996).
- Ensminger, D., *Ultrasonics: Fundamentals, Technology, Applications*, Marcel Dekker Inc., New York, (1988) pp. 139-175.
- Gooijer, H. *Flow resistance of textile materials*, Ph.D. Thesis (ISBN: 90 36511240), University of Twente, 1998.
- Niichols Jr., R.H., "Flow resistance characteristics of fibrous acoustical materials", *Journal of the Acoustical Society of America*, **19(5)**, 866-871 (1947).
- Pierce, A.D., *Acoustics: An Introduction to Its Physical Principals and Applications*, Acoustical Society of America, New York (1989). pp. 140-148.
- Vér, I.L., and C.I. Holmer, "Interaction of sound waves with solid structures", in *Noise and Vibrations Control* (Beranek, L.L., Ed.), McGraw Hill, New York (1971) pp. 270-361.
- Zwikker, C., and C.W. Kosten, *Sound absorbing materials*, Elsevier Science, London (1949).

4

CHARACTERIZATION OF AN ULTRASONIC SYSTEM USING WAVELET TRANSFORMS

4.1 Introduction

Power ultrasound as a means of improving the efficiency of both chemical as well as physical processes has been attempted for last several years (for details see Shah *et al.*, 1999; Suslick, 1988). Ultrasound makes available a range of energies on time scales that are not available from any other source. Despite its efficacy on the laboratory scale processes, the interests of the process industries are not served by the ultrasound technology. Three major factors have contributed to this. The first is that cavitation, which is paramount to all sonochemical and sonophysical effects, occurs only very near the surface of the sonicator and, thus, severely limits the volume of the *active* sonochemical reactor. The second problem is the inability to obtain the desirable and uniform volumetric energy density at optimum cavitation conditions in the bulk volume of the reactor. This is attributed to both the current state of transducer technology, and the attenuation of the acoustic field by cavitation at the sonicator surface. The third problem is the erosion of the sonicator surfaces at the high power intensities that are required for larger scale reactors suitable for industrial scale operations. In the present work, we have tried to address the second of the three problems stated above. Our aim is to develop a new technique to find the distribution of the cavitation intensity in an ultrasound bath.

The energy density at a particular location in an ultrasound processor is comprised of the energy due to the ultrasound waves, and energy due to cavitation activity. The second component of the total energy is responsible for all the observed "*sonochemical*" effects. Therefore, mapping of the energy dissipation pattern in an ultrasound processor is an important aspect of the effective design and scale up of the ultrasound processor for any physical or chemical process.

The aim of the present study is to provide a simple methodology for mapping the energy dissipation pattern in an ultrasound processor using a non-stationary signal analysis technique. This novel technique treats the bubbles as the secondary source of sound and wavelet transform of the acoustic emission resulting from them are applied to outline the spatial distribution of the energy intensity in the processor.

4.2 Previous work

In the past, many attempts have been made to map the energy dissipation pattern in an ultrasound bath. Ratoarinoro *et al*. (1995) have measured the bulk power dissipation in an ultrasound bath using calorimetric measurements. Contamine *et al*. (1994) have made attempts to distinguish between the physical and chemical effects of ultrasound using thermochemical and electrochemical probes. Romdhane *et al*. (1997) have measured the attenuation of ultrasound waves in a chemical reactor using a thermoelectric probe. Martin and Law (1980, 1983) have suggested the use of thermister probes for determining ultrasound intensity distributions in an ultrasound bath.

Dähnke and Keil (1998) and Dähnke *et al.* (1999) have reported simulations of 3-D pressure fields in ultrasonic reactors of different geometries using the Helmholtz and Kirchoff integral equation, with homogeneous and inhomogeneous distribution of the

cavitation bubbles. Dähnke and Keil (1998) use, in their model, the modified wave equation of Prosperetti and Commander (1989), which takes into account the effect of small amplitude oscillations of gas bubbles present in the liquid on the propagation of the pressure waves. Despite its mathematical rigor, the practical utility of the model of Dähnke and Keil (1998) in the design of ultrasound reactors is limited due to several reasons. The homogeneous density distribution of the bubbles, as assumed by Dähnke and Keil (1998), is difficult to achieve even in a well-stirred ultrasound bath. In addition, the bulk movement of the liquid in the bath due to stirring may disturb the pressure field due to scattering of the ultrasound waves. In the simulation of the pressure fields with an inhomogeneous distribution of the bubbles, Dähnke and Keil divided the space between the source of ultrasound and the opposite boundary in several planes with the assumption of a varying gas volume fraction in these planes. However, the gas volume fraction in one particular plane is assumed to be homogeneous in these simulations. This assumption is not valid in practical cases, since the local bubble volume fraction at any point in the bath changes continuously with the propagation of the ultrasound wave, and does not remain homogeneous even for all points in one plane as assumed by Dähnke and Keil. In addition, the assumption of a small amplitude radial motion of the bubble in the modified wave equation (Prosperetti and Commander, 1989) used by Dähnke and Keil loses validity in the case of pressure waves of high amplitudes (> 1 atm), where the bubble undergoes a large amplitude non-linear motion.

Another perspective of this problem was given by Moholkar *et al.* (2000), who tried to identify separately the two components of the energy intensity in an ultrasound bath, viz., the intensity due to the ultrasound waves and the intensity due to the cavitation activity treating the bubble as a secondary sound source. This technique employed two media for the propagation of ultrasound in the bath, one undergoing cavitation and the other non-cavitating under the conditions of the ultrasound field in the bath. The spectral characteristics of the acoustic emission in these two media were used to outline the spatial distribution of the cavitation intensity in the bath.

The technique of Moholkar *et al*. (2000), which makes use of Fourier Transform as a basis for the analysis of the acoustic emission, can only be applied to those ultrasound equipments, where the ultrasound source produces a constant amplitude signal. However, in most of the commercial ultrasound equipments the ultrasound source produces a modulated wave resulting in a periodic change of the amplitude of the wave. The cause of the modulation lies in the electrical design of the signal amplifier in the processor, and is beyond the scope of this study. When the bubbles are driven by ultrasound with constantly changing amplitude, their radial response does not reach the steady state and, hence, the acoustic emission in this case contains non-stationary frequency components. As such, the conventional Fourier transform cannot be used to characterize commercial ultrasound equipment.

Wavelet transform (WT) is a relatively new technique for the analysis of non-stationary signals that overcomes the resolution problem in the conventional non-stationary signal processing technique, Short Term Fourier Transform (STFT). This kind of analysis is most suitable when the signal consists of high frequency components of short duration and low frequency components of long duration (see appendix A for more

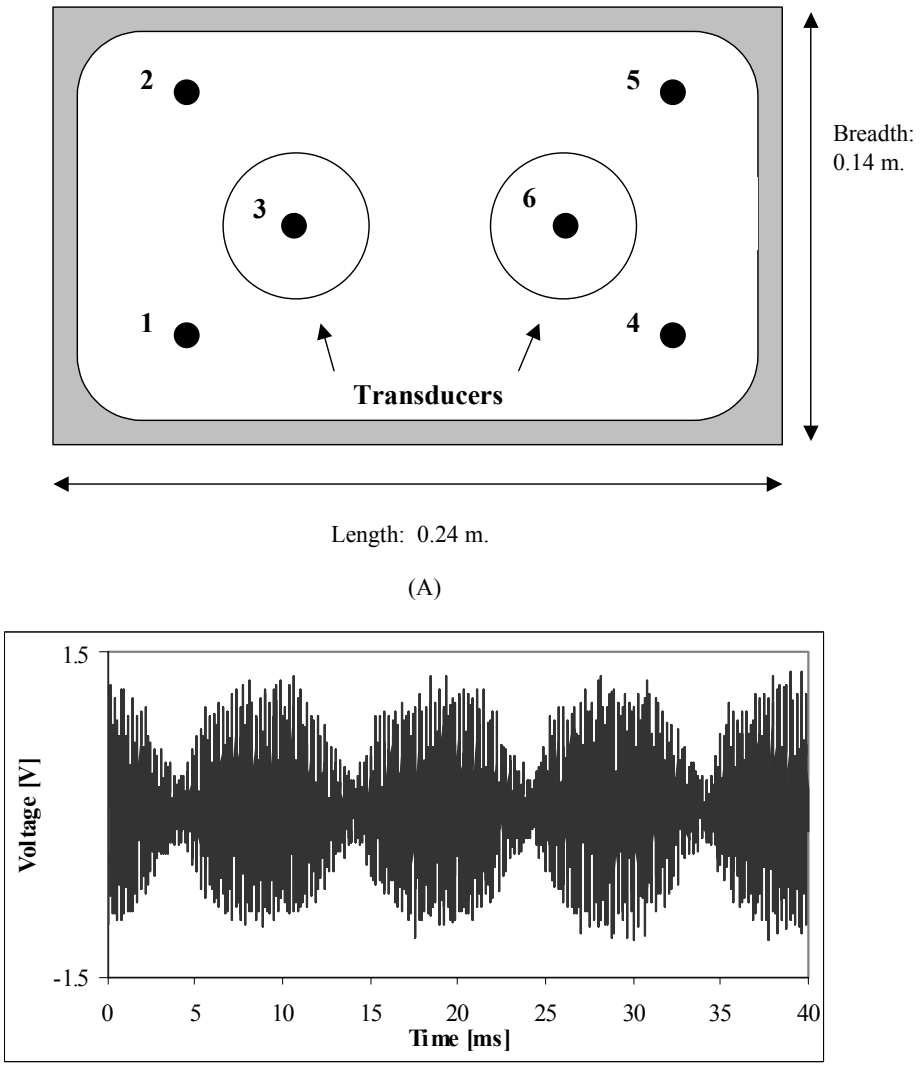

Figure 1: (A) Top view of the ultrasound bath showing the transducers and locations of cavitation intensity measurements. (B) Modulation of the ultrasound field in the bath.

discussion). This is exactly the case for the acoustic emission in an ultrasonic system, where the two components of the signal are the ultrasound itself and the pressure pulses of short duration due to cavitation activity superimposed over it. Therefore, we have chosen the wavelet transform as the basis of the analysis in the present study.

4.3 Experimental

4.3.1 Experimental system and procedure

The experiments were carried out in a stainless steel ultrasound bath (Elma Inc., Germany, Model T470/H, Freq: 35 kHz). The dimensions of the bath were: length = 0.24 m; width = 0.14 m; height = 0.095 m. Thus, the liquid in the bath had a surface area of

0.034 m^2. Two ultrasound transducers were attached at the bottom. The measurements were carried out with a small hydrophone (Bruel and Kaejer Ltd., Type 8103) connected to a charge amplifier (Nexus Amplifiers, Type 2690). The output of this amplifier was fed to a digital oscilloscope (Tektronics Ltd., Model 430A XL, Bandwidth 400 MHz.). The waveforms measured on the oscilloscope were transferred to a computer in the form of discrete data via a GPIB card. The bath was placed inside a x-y-z translation system, which was designed to hold the hydrophone at a particular position inside the bath. The distance between the hydrophone and the bottom of the bath was fixed at 10 mm. This value is based on the cavitation intensity measurements conducted by Chivate and Pandit (1995) and Moholkar *et al.* (2000) The measurements were conducted using 1.95 l of demineralised water in which the dissolved oxygen content was lowered to 1.67 p.p.m. The dissolved oxygen content of water was measured with an oxygen meter (Schott Handylab Inc., Model OX1).

Six measurement locations, assigned numbers 1 to 6, were chosen inside the bath. They are shown in figure 1A, along with the positions of the ultrasonic transducers. The temperature of water was 20^{o}C. To avoid any significant rise in temperature, the bath was operated intermittently with a short duration of the pulses. The record length of the oscilloscope (the total number of points within one measurement) was set at 60000 with a sampling frequency of 1 MHz. Since the phenomena of cavity oscillation and collapse have a random nature, 25 measurements were done at each location.

4.3.2 Method for degassing of water

One of the most important parameters in cavitation is the number density of the bubbles. This parameter cannot be measured accurately. The entrapped gas pockets in the crevices at the walls of the ultrasound bath can act as nuclei, i.e., cavitation generating spots. When the liquid is subjected to ultrasound, these nuclei respond differently depending on the initial sizes and the amplitude and frequency of the sonic field. In a gassy liquid, the bubble population is so large that the dynamics of a single bubble is affected not only by the ultrasound field but also by the interaction with adjacent bubbles. Simulations of the sound radiation from the bubble field have been reported by several researchers (Cramer and Lauterborn (1981), Ilychev *et al.* (1989), Grossman *et al.* (1997), and Hilgenfeldt *et al.* (1998)) but the bubble dynamics models introduced so far cannot handle bubble fields with millions of bubbles, with strong interaction between them. Even with this limitation, Ilychev *et al.* (1989) have proved that all characteristics feature of the acoustic emission spectra are explained by the dynamical behavior of a single bubble.

Reducing the dissolved gas content of the liquid can be an approximate method to reduce the number density of the bubbles, so that the bubble-bubble interactions are minimum, and the dynamics of a single bubble is influenced mainly by the ultrasound field. We have, therefore, conducted the experiment with partially degassed water. A chemical method was used for degassing the water (van der Vlist *et al.*, 1994). The air in 20-liter demineralised water was stripped out using CO_2, bubbling from four circular porous glass slabs mounted at the bottom of the water vessel. After 12 minutes of

bubbling the water was transferred to the ultrasound bath. Thereafter, the dissolved CO_2 was converted to carbonate by increasing the pH to a value between 9 and 10 by adding 6 to 7 g of NaOH. With this method, the gas content of water can be lowered below a value of 2 p.p.m.

4.3.3 Modulation of the bath

The transducers in the ultrasound bath used in this work do not produce an ultrasound wave with constant amplitude. Measurements with a hydrophone showed that the amplitude undergoes a periodic variation. Figure 1B shows the hydrophone signal collected with the oscilloscope, and it can be seen from this figure that the period of modulation of the ultrasound in the bath was 100 Hz. Therefore, the duration of one pressure signal measured with the hydrophone was fixed at 60 msec, thus averaging over six consecutive modulations.

4.3.4 Data analysis

The signal data from the experiments were comprised of 60000 points, collected with a sampling frequency of 1 MHz. Wavelet transform requires that the length of a data vector should be a power of 2. Therefore, the length of the data was adjusted to 65536 (= 2^{16}) by adding a sufficient number of zeros at the end of the signal. The wavelet transform was obtained using Mathcad (version 8.0). The algorithm for the wavelet transform is described in detail by Press *et al.* (1992). Herewith we give only the salient features of this algorithm:

1. The mother function or the wavelet used is *Daubechies four-coefficient wavelet*. The data vector is multiplied by the wavelet coefficient matrix, where the even and odd rows of this matrix perform two related but different convolutions, and decimate each of the convolution by half and interleave the remaining half.
2. While calculating the wavelet transform of the complete signal, the wavelet coefficient matrix is applied hierarchically: first to the full data vector of length 2^N, then to the *smooth* vector of length 2^{N-1}, and then to *smooth-smooth* vector of length 2^{N-2} until only 2 *smooth* components remain. Thus, the complete wavelet transform yields one *smooth* and N-1 *detail* levels for a signal of length 2^N.
3. The power or energy (E) of each particular scale or level is:

$$E = \sum_{0}^{N-1} |h_k|^2 \qquad (1)$$

The frequency band contained in each level (f_L – lowest frequency; f_H – highest frequency) is written in terms of the sampling frequency (f_s) according to the method suggested by Lorczak (1998):

$$f_L = \frac{f_s}{2^{N-L+1}} \qquad (2A)$$

$$f_H = \frac{f_s}{2^{N-L}} \tag{2B}$$

4.4 The physical model

4.4.1 Bubble dynamics

We have presented the simulations of the radial motion of the bubble on basis of the free field model, due to low gas content of the water, in which the mutual interaction between the adjacent bubbles is ignored, and the dynamics of the bubbles is assumed to be influenced by the ultrasound field only (Bailey *et al.*, 1999). For the simulation of the radial motion of the bubbles, we use the Gilmore (1952) equation based on Kirkwood-Bethe hypothesis (1942). This equation is discussed in chapter 2, however, we briefly reproduce it here:

$$R\left(1-\frac{U}{C}\right)\frac{d^2R}{dt^2}+\frac{3}{2}\left(1-\frac{U}{3C}\right)\left(\frac{dR}{dt}\right)^2-\left(1+\frac{U}{C}\right)H-\frac{U}{C}\left(1-\frac{U}{C}\right)R\frac{dH}{dR}=0 \tag{3}$$

H is the free enthalpy on the surface of the bubble:

$$H=\frac{n}{n-1}\frac{A^{1/n}}{\rho_o}\left\{\left[\left(P_o+\frac{2\sigma}{R_o}\right)\left(\frac{R_o}{R}\right)^{3\gamma}-\frac{2\sigma}{R}+B\right]^{\frac{n-1}{n}}-\left[P_o-P_A\sin\omega t+B\right]^{\frac{n-1}{n}}\right\} \tag{4}$$

A, B and n are the constants in the equation of state of water: $p=A\left(\frac{\rho}{\rho_o}\right)^n-B$.

C, the velocity of sound in liquid, is expressed as a function of H as:

$$C=\left[C_o^2+(n-1)H\right]^{1/2} \tag{5}$$

C_o is the velocity of sound in the liquid at standard temperature (298°K) and pressure (101.35 kPa) conditions and is written as $C_o=\sqrt{A\,n/\rho_o}$. The amplitude of the shock wave P_r (outside the bubble, measured at a distance r from the bubble center) radiated by the pulsating bubble is:

$$P_r=A\left\{\frac{2}{(n+1)}+\frac{(n-1)}{(n+1)}\left[1+\frac{G(n+1)}{r\,C_o^2}\right]^{1/2}\right\}^{2n/(n-1)}-B \tag{6}$$

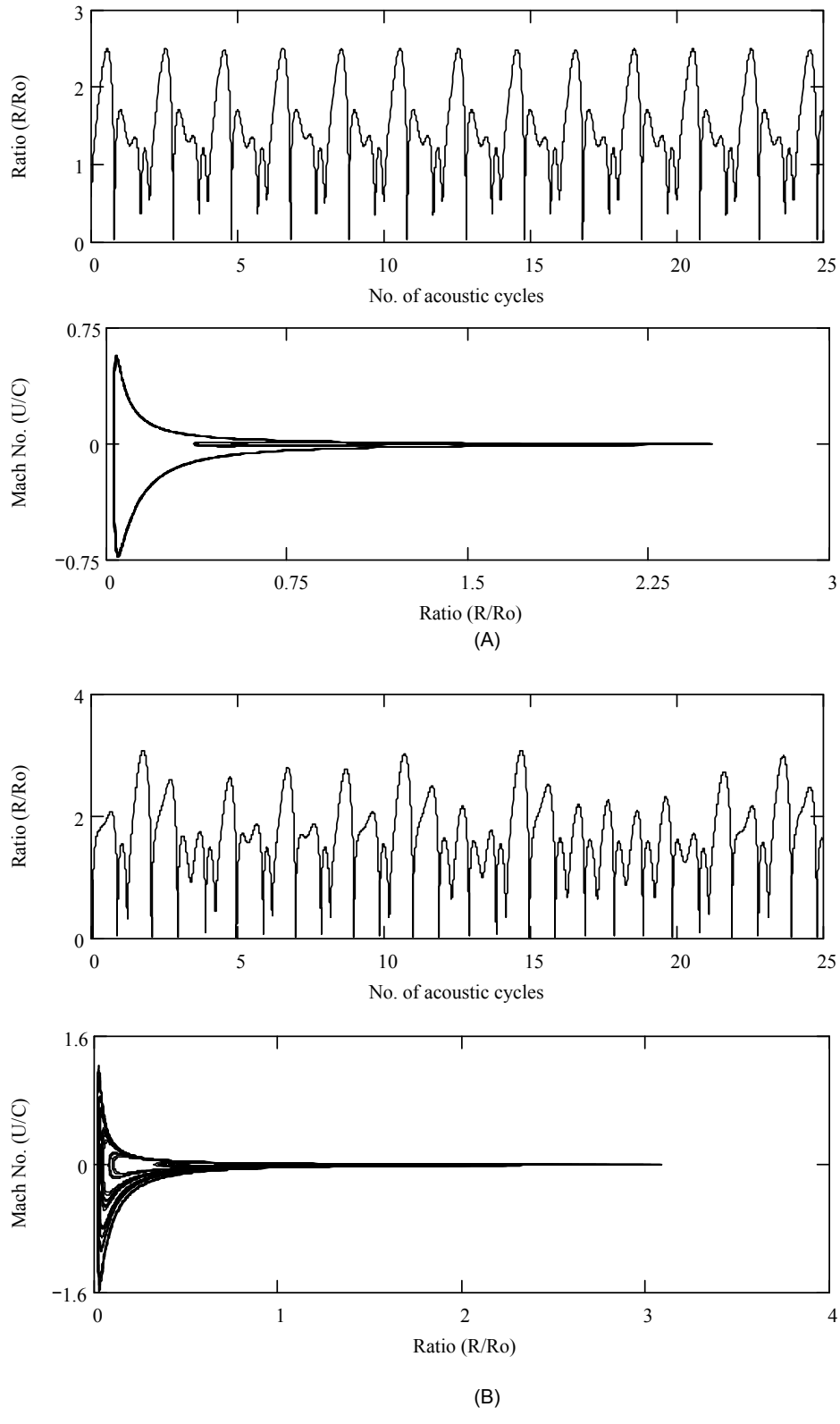

Figure 2: Characteristics of radial bubble motion driven by constant amplitude and modulated ultrasound wave: **(A)** Constant amplitude ultrasound. (2A.1) Radius history of the bubble; (2A.2) Basin of the attractor for radial motion of bubble. [Conditions for simulation: R_o = 10 μm., P_A = 1.1 atm., f = 35 kHz.]. **(B)** Modulated ultrasound. (2B.1) Radius history of the bubble; (2B.2) Basin of the attractor for radial motion of bubble. [Conditions for simulation: R_o = 10 μm., P_A (R.M.S. value) = 1.1 atm., f = 35 kHz., Modulation frequency = 100 Hz.].

G is a function of space and time:

$$G(R, t) = R\left(H + \frac{U^2}{2}\right) \tag{6a}$$

Since the dissipation of the shock waves from various mechanisms in the liquid is neglected, this model leads to errors in the calculations of amplitude of the shock wave. However, our aim in this work is not to predict the exact amplitude of the shock wave due to bubble activity, but to investigate the relative difference between the magnitudes of the shock waves at different locations in the bath.

4.4.2 Numerical program implementation

The numerical program for the bubble dynamics can also use, along with the analytical waveform for the ultrasound (generated using a sinusoidal function with acoustic pressure amplitude P_A), an experimentally measured ultrasound signal with hydrophone as forcing function, thus indicating the theoretical value of the pressure radiated by a single isolated bubble under the conditions of ultrasound field present in the bath. The sound waves originating from the bubble undergo attenuation due to their spherical divergence. Therefore, we fix the parameter r in equation 6 at 10 mm as a representative value.

The initial conditions for the solution of equation 3 using a Runge-Kutta fifth order-fourth order method with adaptive time step size control (Press *et al.*, 1992) are, t = 0, R = R_o and U = 0. For the experimentally measured ultrasound signal, a linear interpolation method was used to generate a continuous ultrasound signal. As stated earlier, the experimental signal had two components: signal of the ultrasound wave and the sound radiation from the bubbles superimposed over it. Therefore, the experimentally measured signal was de-noised to remove the bubble sound radiation component using the algorithm "*Soft thresholding*" (MatLab Version 5.2.1, The Mathworks Inc., MA, USA). In this algorithm the input signal of length 2^N is denoised by first setting to zero those elements whose absolute values are lower than a certain threshold (THR), and then shrinking the non-zero coefficients to zero. This threshold is given by Donoho (1995) as:

$$\sqrt{2\log\left(\frac{n\log n}{\log 2}\right)} \quad \text{where } n = 2^N.$$

Some physical constants used in the program are: A = 300.1 MPa, B = 300 MPa, n = 7, P_o = 101.3 kPa., ρ_o = 1000 kg/m^3, σ = 0.072 N/m. Due to the random nature of the cavitation events, the successive pulses vary in magnitude. Therefore, calculations were made using 25 experimentally measured pulses at a single location, and the values of $P_{r,\,max}$ (the peak radiated pressure by the bubble) were averaged.

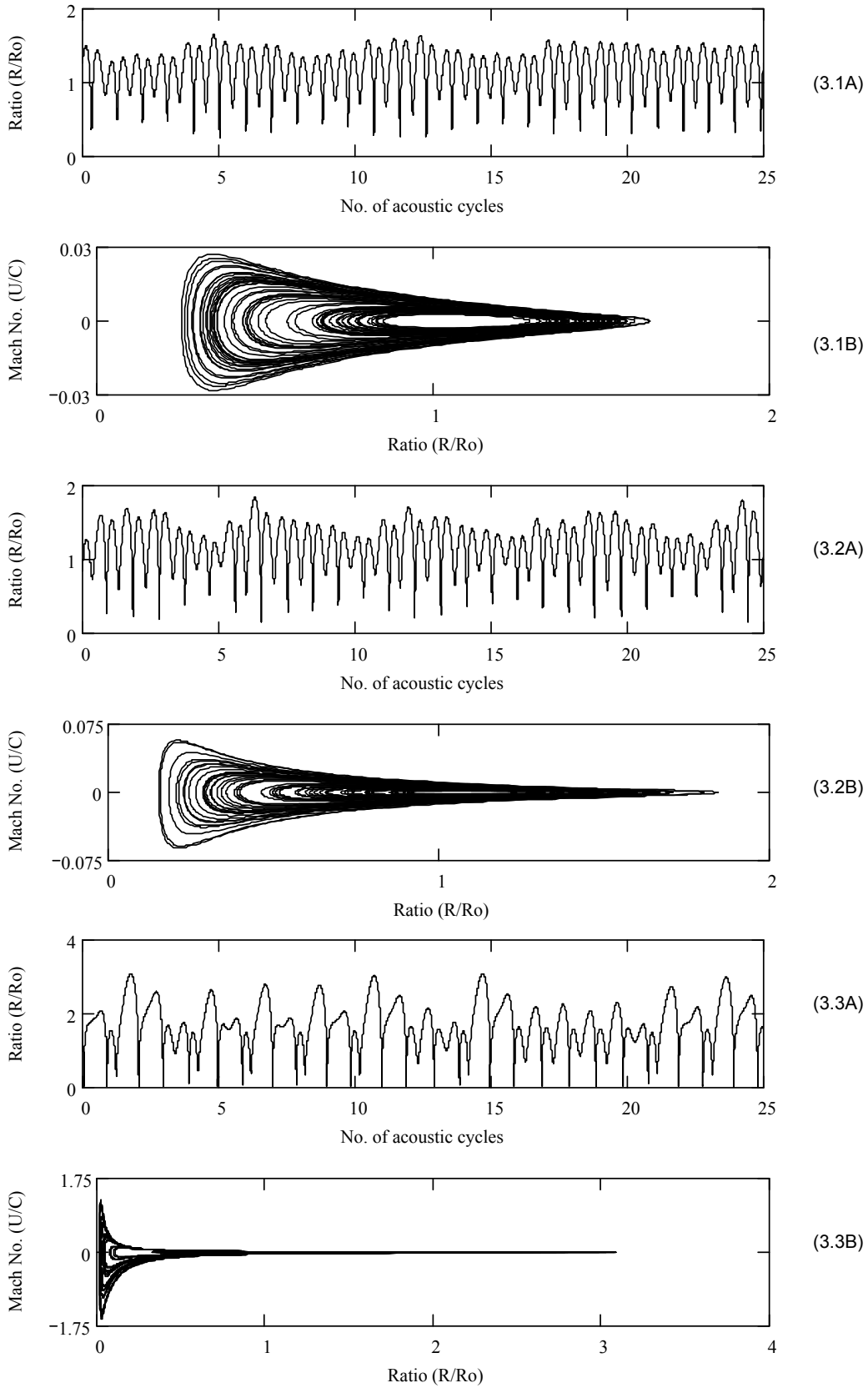

Figure 3: Characteristics of the bubble motion at different locations in the bath. (3.XA) Radius history of the bubble; (3.XB) Basin of attractor for the radial motion of the bubble. *X* is number corresponding to the location in the bath (refer to figure 1A for locations).

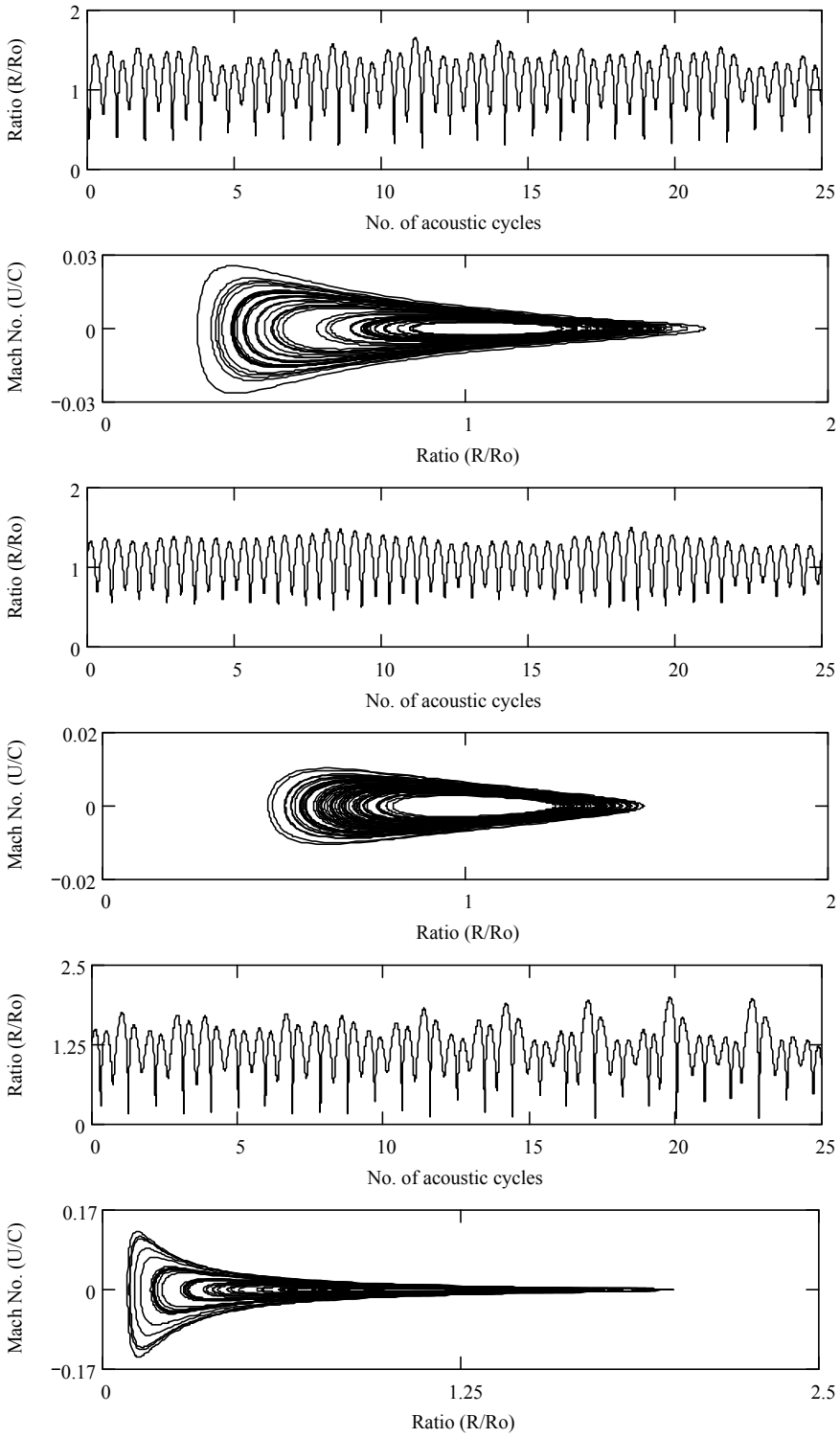

Figure 3: *continued…..*

4.5 Chaotic bubble oscillations

To demonstrate the difference between the radial bubble motions under the influence of modulated and non-modulated (constant amplitude) ultrasound field, we present here simulations of the radial motion of the bubble first with a constant amplitude ultrasound signal and, secondly, with an experimentally measured (i.e. undergoing

modulation) ultrasound signal with an average amplitude of the same magnitude. Figure 2A shows the first case and figure 2B shows the second case. Now to distinguish between figure 2A and 2B, we make use of the analysis of the bubble oscillators with the methods of chaos physics given by Lauterborn and Parlitz (1988). Figure 2A and 2B shows plots of the bubble wall velocities as a function of the bubble radius. Lauterborn and Parlitz (1988) showed that a bubble, as other non-linear oscillators, undergoes a period doubling route to chaos, as revealed by a plot of R vs. U (Figure 2). When a state of chaotic oscillations is reached, the bubble gives rise to a chaotic acoustic emission, which cannot be analyzed with Fourier transform. Figure 3 shows the simulation of the radial motion of the bubble at different locations of measurement in the bath. It can be seen that the bubble motion exhibits chaotic nature at all locations of the bath and, thus, needs to be analyzed using a non-stationary signal analysis technique like wavelet transform.

4.6 Detection of the cavitation intensity

A description of the acoustic emission by the cavitation bubbles under two distinct cavitation regimes, viz., stable and transient cavitation is given in chapter 2. We briefly reproduce it here for the convenience of the reader. It is generally known that the acoustic cavitation noise spectrum is comprised of various frequencies related to the fundamental or the driving frequency. These frequencies are subharmonics, ultraharmonics and harmonics of the fundamental frequency *f*. As transient cavitation is approached, the intensities of all subharmonics, ultraharmonics and harmonics rise sharply. The intensity of the white noise also increases very rapidly with increasing pressure amplitude once the transient cavitation threshold is passed. One of the important characteristics of the acoustic emission spectrum in transient cavitation is the prominent presence of the subharmonic signal (well above the white noise).

The relative cavitation intensity at different locations in the bath has been assessed experimentally, by the wavelet transform analysis of the pressure pulses collected at different locations in the bath, and numerically, by the pressure radiated by the bubble using the bubble dynamics model. In the numerical method, we use the values of $P_{r,max}$ at different locations as a numerical measure of the intensity of the collapse of an individual bubble, and hence the overall cavitation intensity resulting out of the oscillation and collapse of several bubbles. We use an alternative definition for the relative cavitation intensity, which is derived from the discussion on acoustic emission given in chapter 2.

We define the relative cavitation intensity as the ratio of sum of the energies of level 11, 13 and 14. It can be inferred from equation 2 that level 11 contains the components corresponding to the subharmonic of the driving frequency (17.5 kHz), level 13 contains components corresponding to the second and the third harmonics (70 and 105 kHz respectively) and the first and the second ultraharmonic (87 kHz and 123 kHz respectively) and the level 14 contains the fourth and the fifth harmonic (140 kHz and 175 kHz) and the third ultraharmonic (158 kHz). The frequencies above 200 kHz are ignored taking into consideration the frequency response of the hydrophone. The subharmonic, ultraharmonic and the harmonic components of the fundamental or the

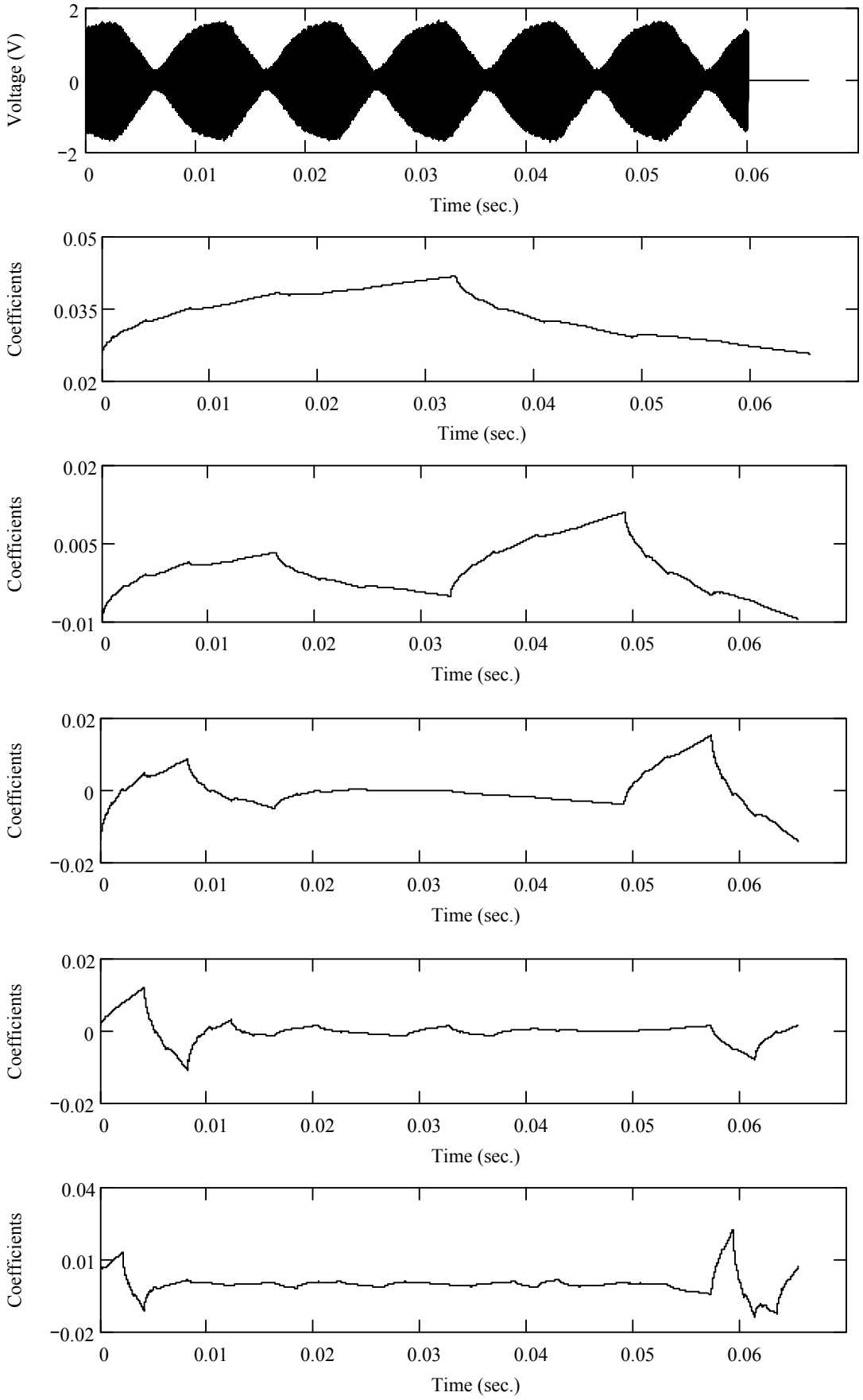

Figure 4: Wavelet transform decomposition of the hydrophone signal in "smooth" and "detail" information along with the energy content of different levels. **(A)** The original signal; **(B)** Smooth information, **(C.X)** Different levels of detailed information (the number **X** indicates the level), **(D)** Energy contents of different levels.

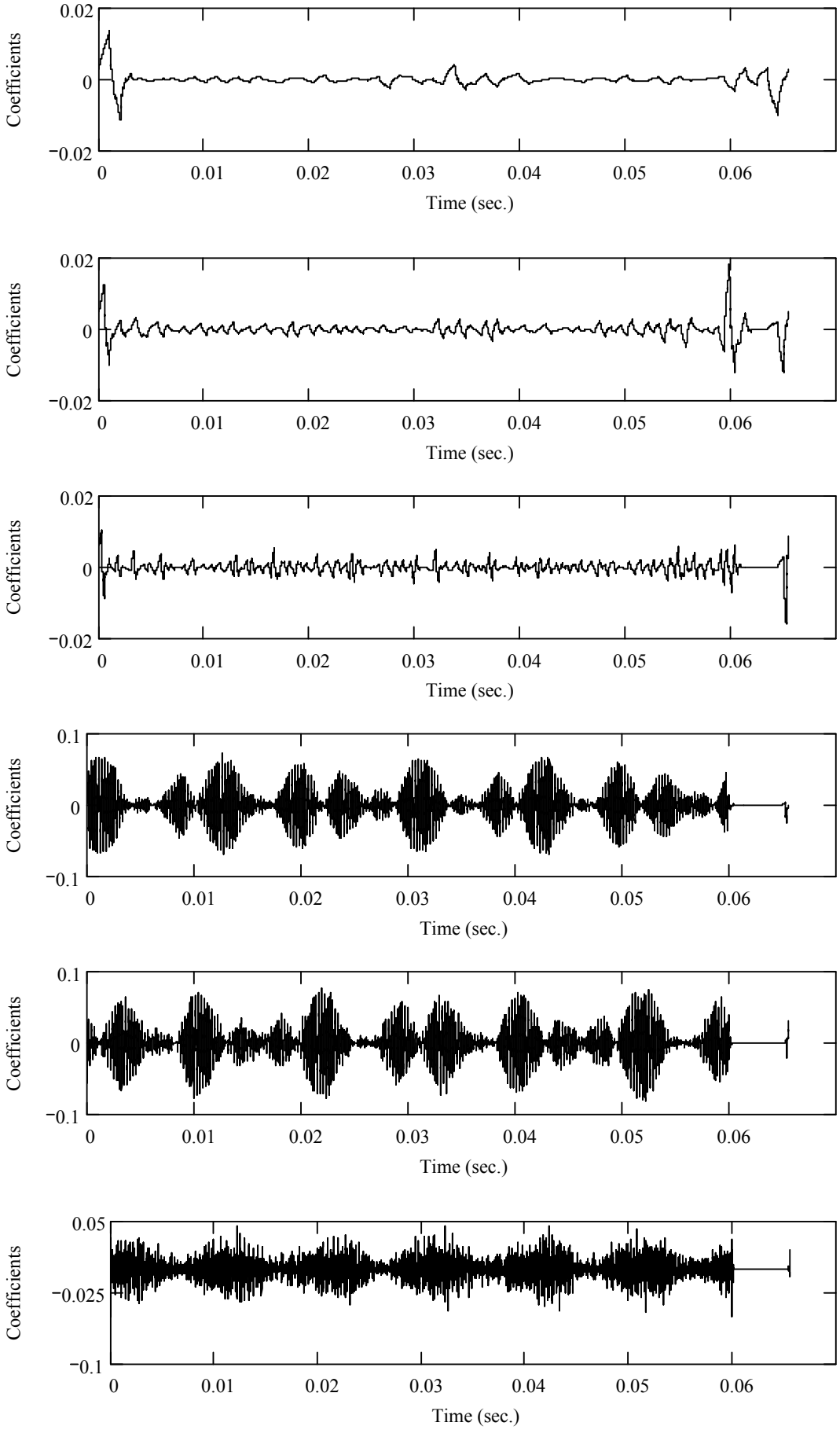

Figure 4: *continued…*

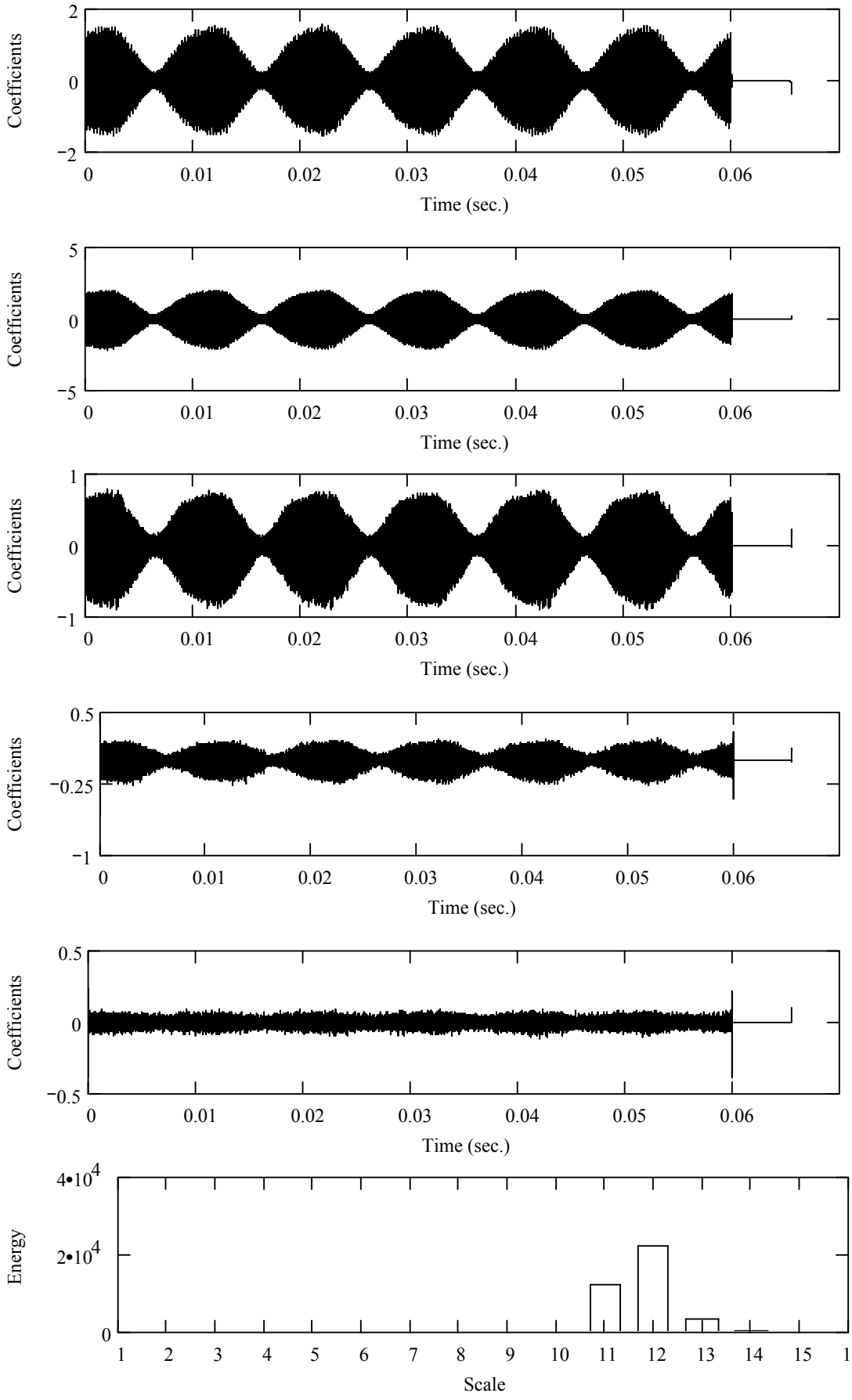

Figure 4: *continued…*

driving frequency are representatives of the cavitation activity at a particular location. Hence, the total energy of the levels 11, 13 and 14 is analogous to the "cavitation noise coefficient" (Akulichev, 1971), which is representative of the relative cavitation intensity at different locations. Therefore, we define the cavitation noise coefficient as follows:

$$K = E_{11} + E_{13} + E_{14} \tag{7}$$

where E is the power or energy of a level defined by equation 1 and the subscript indicates the level.

4.7 Results and discussion

4.7.1 Results of wavelet transform analysis

The variation of the cavitation intensity in the bath was determined using the wavelet transform of the signal measured with hydrophone at different locations. Figure 4 shows the complete wavelet transform decomposition of a hydrophone signal. The signal is decomposed into one "smooth level" and 15 different "detail levels". In the end (figure 4D), the relative energy distribution of these levels is given. It can be seen that most of the energy of the signal is concentrated in level 12, which corresponds to the driving or fundamental frequency of the bath. The results of the complete analysis are shown in figure 5, which depicts the distribution of the cavitation noise coefficients at various locations in the bath. It can be inferred from figure 5 that the cavitation noise coefficient, which is representative of the cavitation intensity, has the highest value for point 3, which is located above the left transducer in the bath (refer to figure 1A). The value of K decreases considerably towards the corners of the bath. This can be attributed to the conical divergence of the ultrasound waves originating from the transducers, due to which the corners of the bath remain outside the insonated zone, thus receiving very low ultrasound wave intensity. Another interesting observation is that for point 6, which is located above the right transducer, the value of K is unexpectedly lower than that for point 3, which is located above the left hand transducer. This difference can be attributed to the difference in the acoustical and electrical characteristics of the transducers, such as the natural oscillation frequency and internal impedance (Ensminger, 1988). Due to these differences, the two transducers driven by same electrical source consume different amount of power and hence emit ultrasound waves of different amplitude that results in different cavitation intensity.

4.7.2 Results of numerical simulations

The relative variation of the cavitation intensity was determined using numerical simulations of the bubble dynamics at different locations of the bath using denoised version of experimentally measured signal. Figure 5 shows the magnitude of the $P_{r,\,max}$ plotted at different locations in the bath along with K. It is evident from figure 5 that the cavitation noise coefficients at different locations in the bath calculated from the wavelet

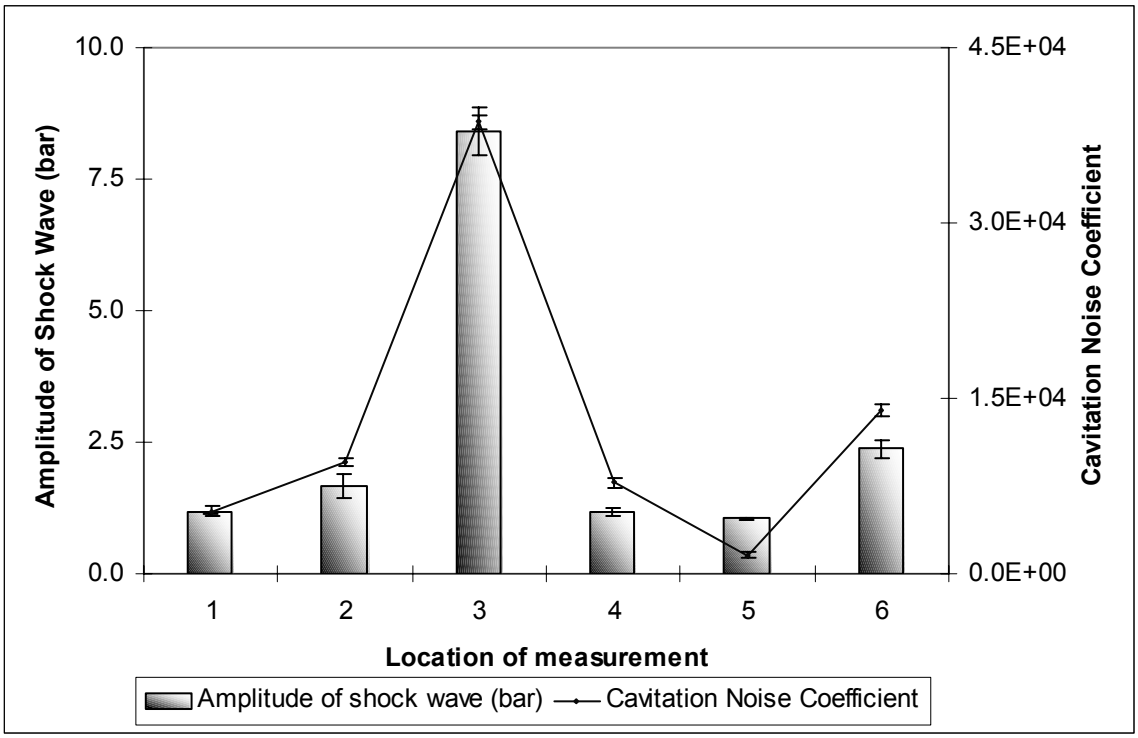

Figure 5: Spatial distribution of the cavitation noise coefficient and average amplitude of the shock wave radiated by the bubble (calculated using the numerical simulations of the bubble dynamics) in the bath.

transform of the acoustic emission are directly proportional to the magnitude of $P_{r,\,max}$ calculated from the bubble dynamics program. This supports the definition of the cavitation noise coefficient given by equation 7.

4.8 Conclusion

In the present chapter, we have proposed a method of using non-stationary signal analysis technique for the characterization of an ultrasound bath for the distribution of cavitation intensity in it. In the presence of cavitation, the noise is a non-stationary signal that cannot be analyzed by conventional Fourier transforms. The difference between the radial bubble motion under constant amplitude and modulated amplitude ultrasound field was demonstrated on the basis of the basins of the attractor of the bubble motion. It was shown that the radial bubble motion is chaotic irrespective of the location of the bubble in the bath. The cavitation noise coefficient at different locations in the bath calculated by WT analysis of the acoustic emission is directly proportional to the theoretically calculated amplitude of the shock wave radiated by an individual bubble indicative of the cavitation intensity. This confirms the definition of the cavitation noise coefficient made on the basis of the WT analysis of the acoustic emission.

For an effective scale up of the ultrasonic processor for intensification of either chemical or physical processes, such as wet textile processes, exact knowledge of the spatial distribution of the cavitation intensity and, hence, the energy dissipation pattern is of prime importance. The present study introduces the use of the wavelet transform to

achieve this goal. We expect this study to contribute towards the design and scale-up of the medium and high power ultrasonic processors for intensification of physical or chemical processes.

Notation

A, B	-	constants in equation of state for water, Pa
C	-	velocity of sound in water, m s^{-1}
C_o	-	velocity of sound in water in undisturbed state, m s^{-1}
E	-	power or energy of a scale in wavelet transform, dimensionless.
f	-	frequency of the ultrasound wave, Hz.
H	-	free enthalpy at the bubble surface, J kg^{-1}
K	-	cavitation noise coefficient, dimensionless
n	-	constant in equation of state for water, dimensionless
P	-	pressure (in the equation of state), Pa
P_∞	-	pressure in the bulk liquid away from the bubble, Pa
P_A	-	pressure amplitude of the ultrasound wave, Pa
P_o	-	ambient pressure in the bulk liquid, Pa
P_r	-	amplitude of the pressure radiated by the bubble during oscillation, Pa
$P_{r, max}$	-	maximum amplitude of the pressure radiated by the bubble, Pa
P_v	-	vapor pressure of the liquid, Pa
r	-	distance coordinate from the bubble center, m.
R	-	radius of the bubble at any time, m.
R_o	-	initial bubble radius, m.
t	-	time, s
U	-	velocity of the bubble wall (dR/dt), m s^{-1}

Greek letters

γ	-	polytropic constant of the contents of the bubble, dimensionless
σ	-	surface tension, N m^{-1}
ρ	-	density of the liquid, kg m^{-3}
ρ_o	-	density of the liquid in undisturbed state, kg m^{-3}
κ	-	thermal diffusivity of the bubble, m^2 s^{-1}
ω	-	angular frequency of the ultrasound wave, s^{-1}

References

- Akulichev, V.A., "Pulsations of cavitation voids", in *High Intensity Ultrasonic Fields* (Ed. L.D. Rosenberg), Plenum Press, New York (1971).
- Bailey, M.R., D.T. Blackstock, R.O. Cleveland, and L.A. Crum, "Comparison of electrohydraulic lithotripters with rigid and pressure-release reflectors. II. Cavitation fields", *Journal of the Acoustical Society of America*, **106**(2), 1149-1160 (1999).

- Chivate, M.M., and A.B. Pandit, "Quantification of the cavitation intensity in fluid bulk", *Ultrasonics-Sonochemistry*, **2**(1), S19-S25 (1995)**.**
- Contamine, F., F. Faid, A.M. Wilhelm, J. Berlan, and H. Delmas, "Chemical reactions under ultrasound: Discrimination of physical and chemical effects", *Chemical Engineering Science*, **49**, 5865-5872 (1994).
- Cramer, E., and W. Lauterborn, "On the dynamics and acoustic emission of spherical cavitation bubbles in sound field", *Acustica*, **49**, 226-238 (1981).
- Dähnke, S.W., and F.J. Keil, "Modeling of 3-D linear pressure fields in sonochemical reactors with homogeneous and inhomogeneous density distributions of cavitation bubbles", *Industrial and Engineering Chemistry Research*, **37** (3), 848-864 (1998).
- Dähnke, S.W., K.M. Swamy, and F.J. Keil, "A comparative study on the modeling of sound pressure field distributions in a sonoreactor with experimental investigation", *Ultrasonics-Sonochemistry***, 6** (4), 221-226 (1999).
- Donoho, D.L., "De-noising by soft thresholding", *IEEE Transactions on Information Theory*, **41**(3), 613-627 (1995).
- Ensminger, D., *Ultrasonics: Fundamentals, Technology, Applications*, Marcel Dekker Inc., New York (1988).
- Gilmore, F.R., *Hydrodynamic Laboratory Report*, California Institute of Technology, **26-4** (1954).
- Grossmann, S., S. Hilgenfeldt, M. Zomack, and D. Lohse, "Sound radiation of 3 MHz driven gas bubbles", *Journal of the Acoustical Society of America*, **102**, 1223-1227 (1997).
- Hilgenfeldt, S., D. Lohse, and M.P. Brenner, "Phase diagrams for sonoluminescing bubbles", *Physics of Fluids*, **8**(11), 2808-2826 (1996).
- Hilgenfeldt, S., D. Lohse, and M. Zomack, "Response of bubbles to diagnostic ultrasound: A unifying theoretical approach", *European Physics Journal*, **4**, 247-255 (1998).
- Ilyichev, V.I., V.L. Koretz, and N.P. Melnokov, "Spectral characteristics of acoustic cavitation", *Ultrasonics*, **27**, 357-361 (1989).
- Kirkwood, J.B., and H.A. Bethe, *Office of Science Research and Development Report 558*, USA (1942).
- Lauterborn, W., and U. Parlitz, "Methods of chaos physics and their application to acoustics", *Journal of the Acoustical Society of America*, **84**(6), 1975-1993 (1988).
- Lorczak, P.R., *Mathcad 8 Treasury: Volume II*, Mathsoft, Inc.: Cambridge, USA (1998).
- Martin, C.J., and A.N.R. Law, "The use of thermister probes to measure the energy distribution in an ultrasound field", *Ultrasonics*, **18**, 127-133 (1980).
- Martin, C.J., and A.N.R. Law, "The use of thermister probes for measurement of ultrasound intensity distribution", *Ultrasonics*, **21**, 85-90 (1983).
- Moholkar, V.S., S.P. Sable, and A.B. Pandit, "Mapping the cavitation intensity in an ultrasound bath using acoustic emission", *AIChE Journal*, **46**(4), 684-694 (2000).
- Press, W.H., S.A. Teukolsky, W.T. Vetterling, and B.P. Flannery, *Numerical Recipes*, Cambridge University Press, Cambridge (1992).
- Prosperetti, A., and K.W. Commander, "Linear pressure waves in bubbly liquids:

Comparison between theory and experiment", *Journal of the Acoustical Society of America*, **85** (2), 732-746 (1989).

- Ratoarinoro, C., A.M. Wilhelm, and H. Delmas, "Power measurement in sonochemistry", *Ultrasonics-Sonochemistry*, **2**(1), S43-S47 (1995).
- Romdhane, M., A. Gadri, F. Contamine, C. Gourdon, and G. Casamatta, "Experimental study of the ultrasound attenuation in chemical reactors", *Ultrasonics-Sonochemistry*, **4**(3), 235-243 (1997).
- Shah, Y.T., A.B. Pandit, and V.S. Moholkar, *Cavitation Reaction Engineering*, Plenum Press, New York (1999).
- Suslick, K.S., *Ultrasound: Its Chemical, Physical and Biological Effects,* VCH Publishers, New York (1988).
- Vlist, P. van der, M.M.C.G. Warmoeskerken, and S. Willemse, European Patent No. EP9401241 (1994).

APPENDIX A

COMPARISON OF DIFFERENT NON-STATIONARY SIGNAL ANALYSIS TECHNIQUES

In this appendix we briefly discuss and compare qualitatively and quantitatively (with help of an example) the two techniques, viz. Short Term Fourier Transform (STFT) and Wavelet Transform (WT) that are commonly used for the time-frequency analysis of the non-stationary signals.

A.1 Short term Fourier transform

For the analysis of the non-stationary signals the regular Fourier transformed in a two-dimensional time-frequency representation depending on time, which is called Short Term Fourier Transform (STFT). In the STFT the original signal $x(t)$ is seen through a window $g(t)$ of limited extent, centered at a certain time location, τ. The Fourier transform of the windowed signal, the STFT, is written as:

$$STFT(t,f) = \int x(t)\, g(t-\tau) \exp(-2i\pi ft)\, dt \qquad \text{(A.1)}$$

It is evident from the definition of STFT that it maps the signal in two-dimensional function in a time-frequency plane, and this analysis depends critically on the choice of window $g(t)$. The parameter "f" in equation A.1 is similar to the Fourier frequency, and it is the inverse of the length of the window $g(t)$. It can be inferred that, once a window is chosen for the STFT the time resolution (Δt) and the frequency resolution (Δf) is fixed over the entire time-frequency plane. It can also be inferred from above that, the time resolution of the signal can be manipulated at the cost of the frequency resolution and vice versa.

A.2 Wavelet transform

WT overcomes the resolution problem in the STFT. The basic difference between the STFT and WT is that, unlike STFT, where a window of fixed length is used, the WT uses shorter windows and higher frequencies and longer windows at low frequencies. Thus Δt and Δf in case of the WT vary in the time-frequency plane. Relation between Δf and f in the WT is given as:

$$\frac{\Delta f}{f} = \text{constant} \qquad \text{(A.2)}$$

When the above relation is satisfied, Δf and therefore Δt change with the center frequency of the analysis window. It can be perceived that the time resolution becomes arbitrarily good at high frequencies while the frequency resolution becomes arbitrarily good at low frequencies.

Mathematically the continuous wavelet transform (CWT) is defined as:

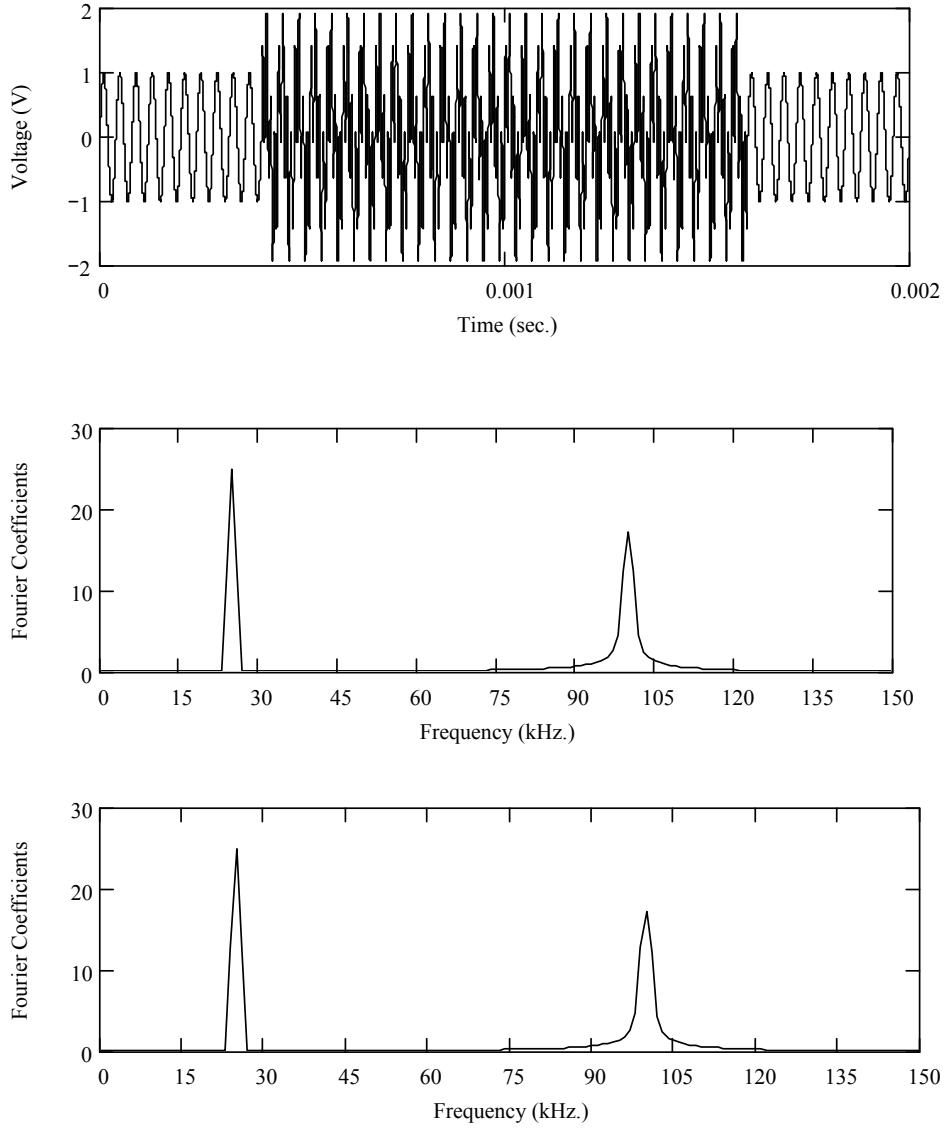

Figure 6: (A) Manually generated non-stationary signal. (B & C) Short Term Fourier Transform of manually generated signal (2 windows).

$$\mathrm{CWT}_x^{\psi}(\tau, s) = \Psi_x^{\psi}(\tau, s) = \frac{1}{\sqrt{|s|}} \int x(t)\, \psi^*\left(\frac{t-\tau}{s}\right) dt \qquad \text{(A.3)}$$

It can be inferred from the above equation, that the transformed signal is a function of two variables, s and τ, which are the scale and translation parameters respectively. ψ(t) is a transforming function termed as "*wavelet*", which is an oscillatory function of finite time length. The term τ is related to the time information, and it is related to the location of the transformation window as it is shifted through the signal. The parameter "scale" is analogous to the frequency in the Fourier transform. Larger scales refer to larger windows, and thus, represent lower frequencies, while the shorter scales refer to shorter windows, and thus, represent higher frequencies.

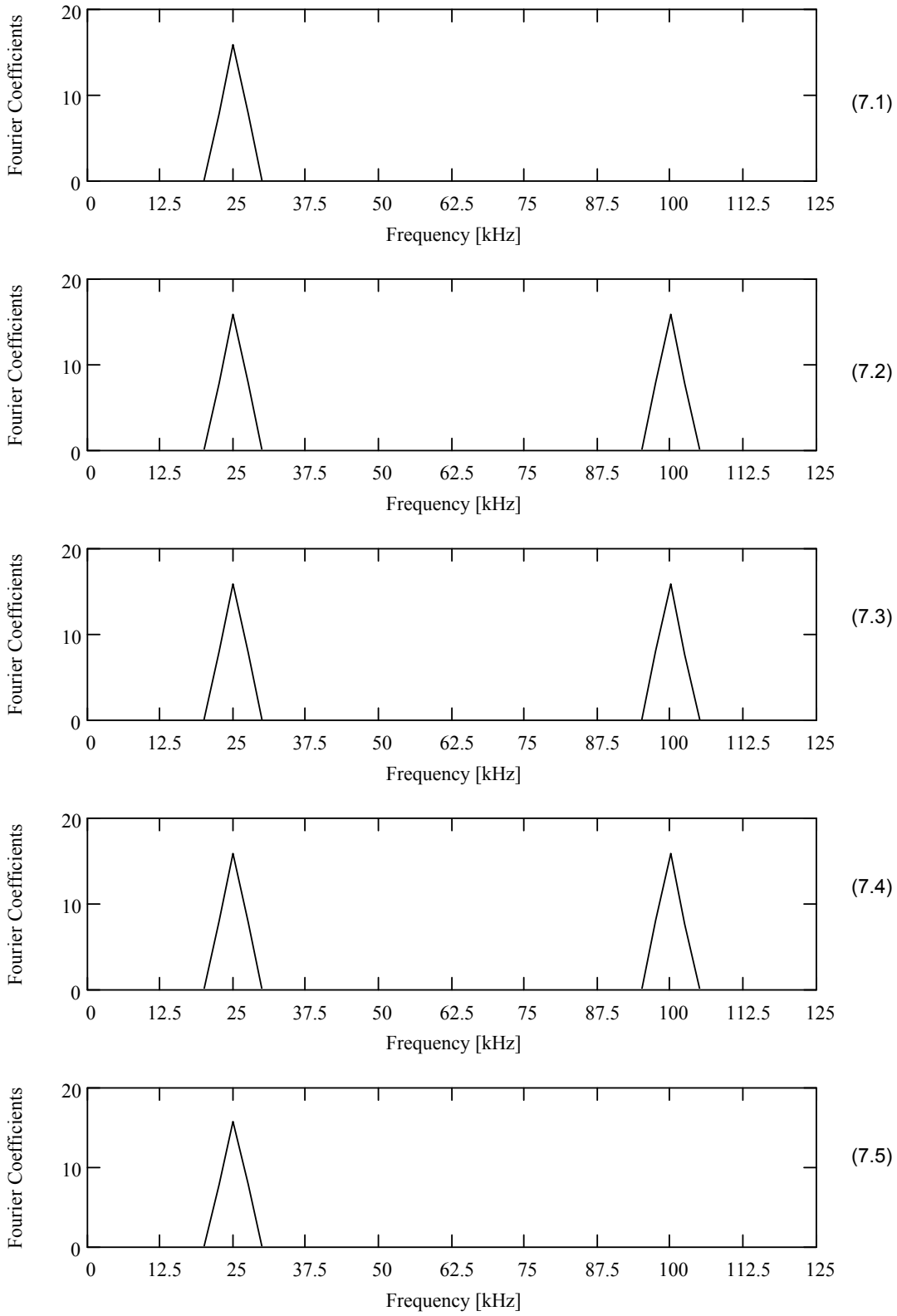

Figure 7: Short Term Fourier Transform of manually generated signal (shown in figure 6A) using 5 windows.

A.3 STFT vs. WT

In order to demonstrate the difference between STFT and WT, we present

herewith analysis of a manually generated signal with non-stationary components. The signal shown in figure 6A consists of a 25 kHz continuous wave (and we call this as the base frequency), with a high frequency disturbance (or noise with frequency 100 kHz.) superimposed on it for certain duration. The signal length is 2 msec and the sampling frequency is 10 MHz. In figure 6B and 6C the Fourier transform of the signal is shown through two windows. Both the windows in figure 6B and 6C show the peaks for base as well as noise frequency, and hence do not give a good time resolution of the signal. Next, splitting the signal in five windows (Figure 7) gives a better time resolution of the signal (i.e. it gives exactly time information of the occurrence of high frequency noise in the signal), nonetheless, a low frequency resolution outweighs this merit. On can easily realize that the frequency resolution is this case is reduced (i.e., the peaks corresponding to the base and noise frequency are less sharp than in figure 6B and 6C). Figure 8 shows the WT analysis of the same signal using Daubechies 4-coefficient wavelet. For brevity only two bands that contain the base and the noise frequency are shown instead of the complete WT decomposition. The merits of WT in terms of time and frequency

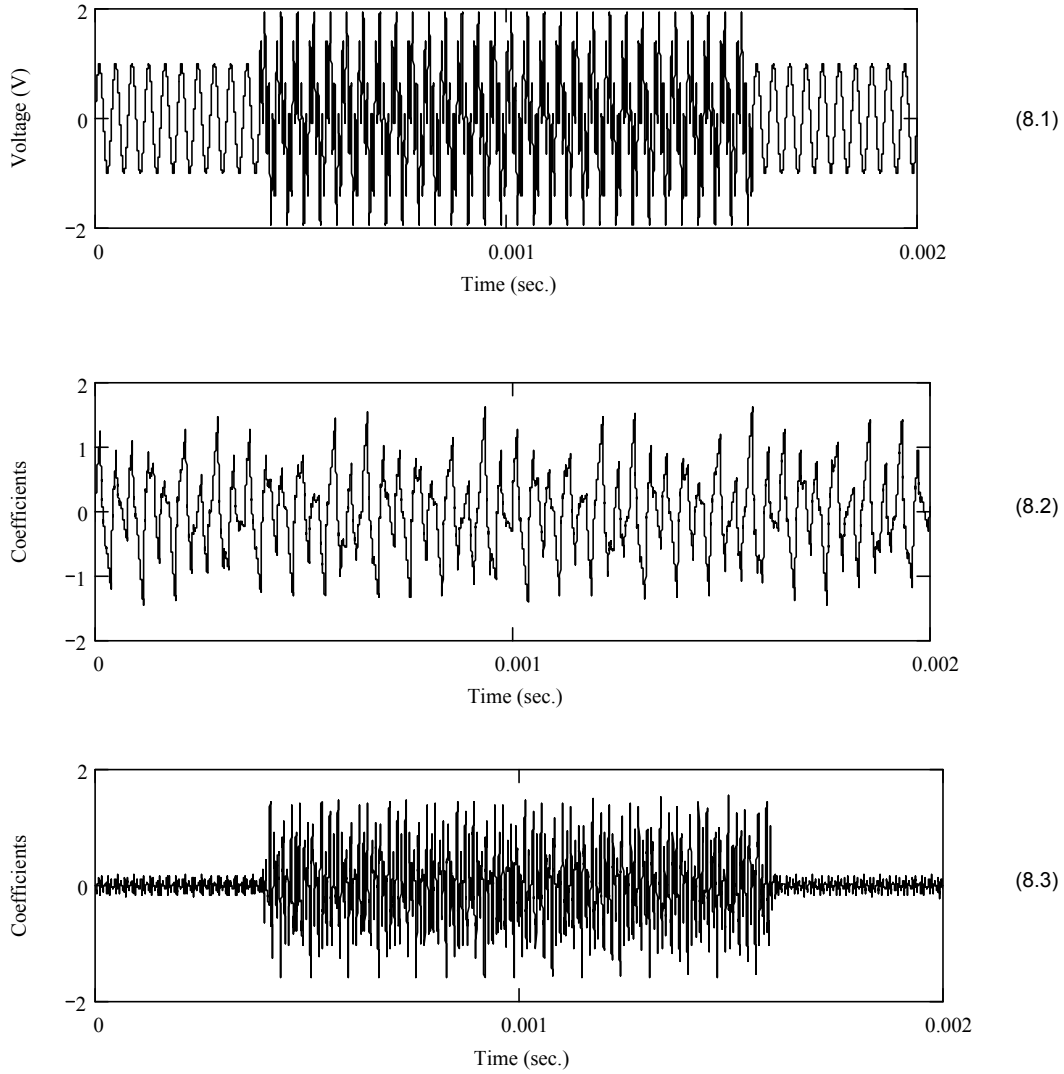

Figure 8: Wavelet transform analysis of the non-stationary signal. (8.1) Manually generated signal (same as shown in figure 6A); (8.2) WT of the signal (Low frequency band containing the base frequency); (8.3) WT of the signal (High frequency band containing the high frequency or noise).

resolution are evident from figure 8. In the low frequency band (figure 8.2) that contains the base frequency the energy (or intensity) is evenly distributed over entire time domain, while in case of high frequency band (figure 8.3) the energy is mainly concentrated at the center, where the noise occurs in the original signal under analysis. Thus, it can be concluded that the problem of simultaneous time and frequency resolution in STFT is overcome by the WT.

5

ENERGETICS OF AN ULTRASONIC PROCESSOR

5.1 Introduction

The use of ultrasound for various homogeneous and heterogeneous chemical processes, *sonochemistry*, is well known. One of the most recent applications of ultrasound is in the intensification of wet textile processes. The literature survey presented in chapter 1 indicates that the efficiencies of several wet textile processes, such as washing, rinsing, bleaching, mercerization etc., can be improved by application of ultrasound. Despite the encouraging results of these studies, to date, ultrasound based wet textile processes have remained in the laboratory with little industrial activity even on a pilot scale. The two major factors that have contributed to this effect are the lack of knowledge of the physical mechanism of the ultrasound enhanced wet textile processes and the drawbacks of the ultrasonic reactors mentioned in chapter 4.

In a sonic processor, the input electrical energy is transformed into cavitation energy, which is responsible for bringing about the desired sono-physical or sono-chemical change. This transformation occurs through various steps as shown in figure 1 (Shah *et al.*, 1999). First, the electrical energy is converted into mechanical energy in the form of shape oscillations of the piezoelectric transducer. This mechanical energy is then converted into acoustical energy, in the form of ultrasound waves, once the shape oscillations of the piezoelectric transducer are coupled to a medium such as water. The ultrasound energy is then transformed into cavitation energy through transient radial motion of the bubbles, driven by the ultrasound waves, during which high temperature and pressure pulses produced. These extremes of temperature and pressure produced during radial bubble motion are responsible for the sono-physical or sono-chemical effects. As a consequence, the overall energy efficiency of the ultrasonic processor is the product of the individual efficiencies of the discrete steps in the energy transformation chain described in figure 1. Therefore, simultaneous optimization of the individual steps in the energy transformation chain forms the basis of the optimization of an ultrasonic processor.

The aim of the present study is two-fold: first, the identification the various physical parameters that affect the efficiency of the energy transformation steps and, secondly, to establish the mechanism of independent and inter-dependent influence of these physical parameters on the energy transformation steps using basic theories of acoustics and bubble dynamics. Therefore, the present study addresses the problem of optimization of an ultrasonic processor in an *integrated* fashion. For this purpose, we have used the gas content of the system as a manipulation parameter. In this study, we deal with an air-water system, and, hence, hereafter the word liquid refers to water and the word gas refers to air. We demonstrate the effect of the variation in the free gas and dissolved gas in the medium on the energy transformation chain in the ultrasonic processor. The results of the experiments have been explained using a unified mathematical model developed on the basis of the equivalent circuit of a piezoelectric transducer. This mathematical model basically puts together the theory of the impedance tube, the theory of the acoustic wave propagation in the bubbly liquid, and the theory of rectified diffusion in the oscillating bubbles.

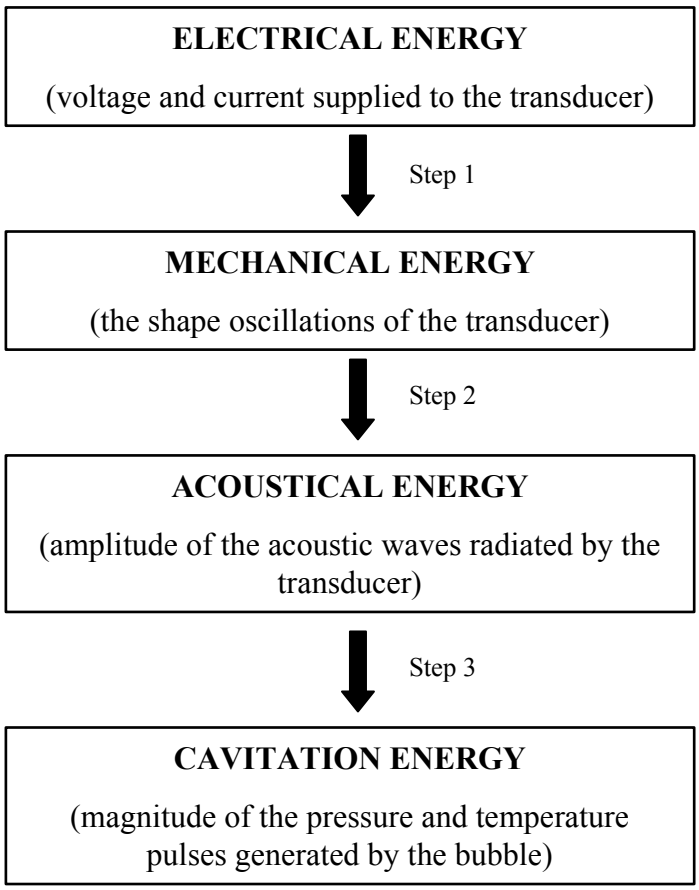

Figure 1: The energy transformation chain in an ultrasonic processor.

5.2 Previous work

Different perspectives of the ultrasonic processor optimization have been presented by many researchers using both experimental and theoretical investigations over the past several years. Martin and Ward (1992) have proposed a reactor design for sonochemical engineering, using the principles of both ultrasonics and chemical reaction engineering. Ratoarinoro *et al.* (1995) have used calorimetric techniques for the measurement of the power dissipation in ultrasonic reactors. Faid *et al.* (1998) have compared the axial and radial profiles of the solid-liquid mass transfer coefficients in three different types of ultrasonic processors, viz. a cup horn, a horn and a tube. The hydrodynamic behavior of an ultrasonic processor has been studied by Gondrexon *et al.* (1998) using residence time distribution measurements. A methodology for the optimization of the geometry of high frequency ultrasonic reactors for the degradation of organic compounds in aqueous solutions was presented by Renaudin *et al.* (1994). Horst *et al.* (1996) have reported the relationship between the consumption of the electrical power and its conversion, first into mechanical energy, and later, into cavitation energy in an ultrasonic processor using the Grignard reaction as the model process. Modeling of the acoustic pressure fields in sonic reactors of various shapes is an important aspect of their optimization, and several papers addressing this issue have appeared recently [for example Dahnke and Keil (1998, 1999), Laborde *et al.* (1998), Dahlem *et al.* (1999) and

Servant *et al.* (2000)]. Dahnke and Keil (1998, 1999) have used the model of Commander and Prosperetti (1989) for the linear acoustic wave propagation in bubbly liquids as a basis. Laborde *et al.* (1998) and Servant *et al.* (2000) have used the Aquilon CFD code for solving the model proposed by Caflisch *et al.* (1985) for the acoustic wave propagation in bubbly liquids. Dahlem *et al.* (1999) have used the SYSNOISE and FLUENT codes for simulating the acoustic streaming resulting from a radially vibrating horn. Application of a dual frequency ultrasound field for the enhancement of cavitation-assisted physical or chemical processes is a relatively new concept. Many papers have appeared that report the advantage of using a dual frequency ultrasound reactor for diverse wet textile processes as mentioned in the literature survey given in chapter 1. A theoretical model for the acoustic pressure field and the bubble dynamics in a dual frequency ultrasound processor has been proposed by Moholkar *et al.* (2000). More recently, Tsochatzidis *et al.* (2001) have reported the new method of using the phase Doppler technique for the determination of velocity, size distribution and concentration of cavitation bubbles. A more detailed review of the literature on the sonic reactors has been given by Keil and Swamy (1999), Thomson and Doraiswamy (1999), and Shah *et al.* (1999).

5.3 Experimental

5.3.1 Experimental system

Experiments were carried out in a cylindrical glass cell (Dimensions - ID: 60 mm; OD: 70 mm; Height: 80 mm). The cell had a 3 mm thick cork rubber lining on the inside wall that acts as an absorber for acoustic waves [reflection coefficient: 0.02, Ensminger (1988)]. This lining helped to achieve a unidirectional sound field in the cell by preventing reflections from the cell walls. The cell was mounted on a stainless steel bottom (thickness: 51 mm) that acted as a rigid reflector for the ultrasound waves [reflection coefficient: 0.99, Ensminger (1988)]. For the positioning of the hydrophone at a particular location between the ultrasound horn tip and the rigid reflector, the cell had two screw caps at a distance of 15 mm and 30 mm from the bottom. The ultrasound horn was mounted on the shaft of a laboratory jack and the cell was placed on the base. The base of the jack could be raised or lowered to adjust the distance between the rigid bottom of the cell and the ultrasound horn tip.

The ultrasound unit comprised of a custom built ultrasound horn with a central resonance frequency of 25 kHz, when vibrating in air. A sketch of the horn is shown in figure 2, along with its dimensions. The horn tip had a small circular groove in it. The horn also had the facility of cooling the piezoelectric element during operation in order to keep its temperature constant. The horn was driven by a signal generator (Hewlett-Packard Ltd., Model: 3324A) and a radio frequency amplifier (ENI Inc., Model 2100L). The amplifier had a maximum power output of 200W for an input impedance of 50Ω. The power consumption of the ultrasound horn was monitored by measuring the voltage and current supplied to it and the phase angle. For this purpose, a voltage probe (Tektronics Ltd., 6138A) and a current clamp (Farnell Inc., Model PR-20) were used.

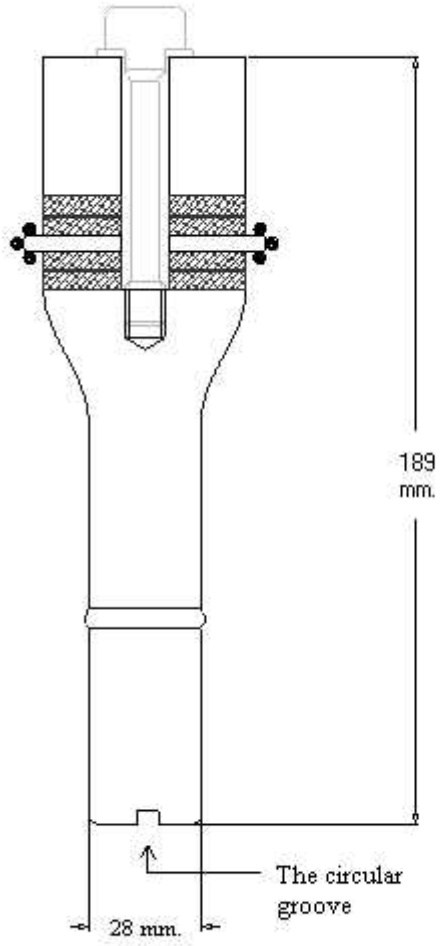

Figure 2: The design of the ultrasound transducer.

The measurements of voltage, current, and phase angle were carried out on a digital oscilloscope (Tektronics Ltd., Model 430A). For the measurements of the pressure signal, a small 4 mm hydrophone supplied by TNO-TPD (Delft, Netherlands) was used, along with a charge amplifier (Nexus Range, Type 2690) that converted the charge developed by the hydrophone into voltage. The output of the charge amplifier was monitored on the digital oscilloscope. The pressure signals measured on the oscilloscope were transferred to a computer via a GPIB card. The record length of the oscilloscope was set at 30000 points in 12 divisions with a time scale of 1 msec/div. Thus, the sampling frequency of the pressure signal was 2.5 MHz.

5.3.2 Experimental procedure

The experiments were performed in three sets, using water with different saturations of dissolved air as the medium. We used the dissolved oxygen content of the medium as a measure of the dissolved air concentration. The experiments were conducted at 20^{o}C. The saturation concentration of oxygen corresponding to this temperature is 9 ppm. In the first set, demineralised water saturated with dissolved air was used. In the second set, under-saturated demineralised water was used with the

dissolved oxygen content lowered to 2 ppm using the chemical degassing technique as described in chapter 4. In the third set, the same degassed water as in set 2 was used, but in this case the water was left standing undisturbed for about 30 minutes. This causes dissolution of almost all of the tiny air bubbles present in the liquid, since the liquid is highly under-saturated. In addition, the circular groove in the tip of the horn was filled with silicon rubber. This groove can entrap small amount of air as the horn tip is introduced in the liquid and, therefore, can provide nuclei for cavitation in liquid. After filling the groove with silicon rubber, this effect is eliminated. Therefore, in the third set, an attempt is made to de-nucleate the liquid by eliminating all the sources of cavitation nuclei. In each set, the cell was filled with 125 ml of the medium. The ultrasound horn was driven at a frequency of 25 kHz, with an input of $90mV_{rms}$ from the signal generator to the radio frequency amplifier. It must however be noted that the actual power absorbed by the ultrasound horn depends on the impedance of the medium in which the horn is oscillating. The distance between the tip of the horn and the rigid bottom was fixed at 6 cm, which is equal to the wavelength (λ) of the ultrasound of 25 kHz frequency. The hydrophone was placed at a distance of 3 cm from the bottom of the cell. This distance was decided on basis of the theory of standing waves described in chapter 2. Since the cell is driven below its cutoff frequency (approximately equal to 40 kHz) and, since the distance between the ultrasound horn tip and the bottom of the tube, which is a rigid reflector, is equal to the wavelength of the ultrasound, a standing wave field is generated in the cell as a result of the interference between the incident and the reflected wave. In a standing wave field, the resultant pressure amplitude is a function of both space and time. As described in chapter 2, in the case of an acoustic wave reflection from a rigid surface, the incident and reflected waves have a constructive interference at distances of $m\lambda/2$ and destructive interference at distances of $(2m+1)\lambda/4$ from the reflector (m being an integer). As such, in the standing wave field generated in the cell, the pressure maxima (or pressure antinode) occurs at a distance of 3 cm. ($= \lambda/2$) and the pressure minima (or pressure node, which is also called velocity antinode) occurs at distances of 1.5 cm ($= \lambda/4$) and 4.5 cm ($= 3\lambda/4$) from the bottom of the cell. The cavitation phenomenon is, therefore, prominent only at the position of pressure antinode, where the resultant pressure amplitude is doubled due to the constructive interference between the incident and reflected waves, as mentioned above. The cavitation phenomenon is absent at the position of pressure nodes for two reasons: first, the resultant acoustic pressure amplitude at these locations is negligibly small due to the destructive interference between the incident and reflected waves and, secondly, the cavitation nuclei or bubbles that exist at these locations migrate towards the pressure antinode, due to the Bjerknes forces exerted on them by the large pressure gradients at the pressure node. Since the principal aim of our experiments is to monitor the cavitation intensity in the cell produced under different conditions of the operating parameters, the hydrophone was placed at the pressure antinode in the standing wave field. The ultrasound horn was operated intermittently to avoid any significant rise in the temperature of the medium. Since the cavitation is a random phenomenon, 50 pressure signals were collected in each experiment. The peak-to-peak voltage (V_{p-p}) and peak-to-peak current (I_{p-p}) supplied to the ultrasound horn and the phase angle (ϕ) was noted

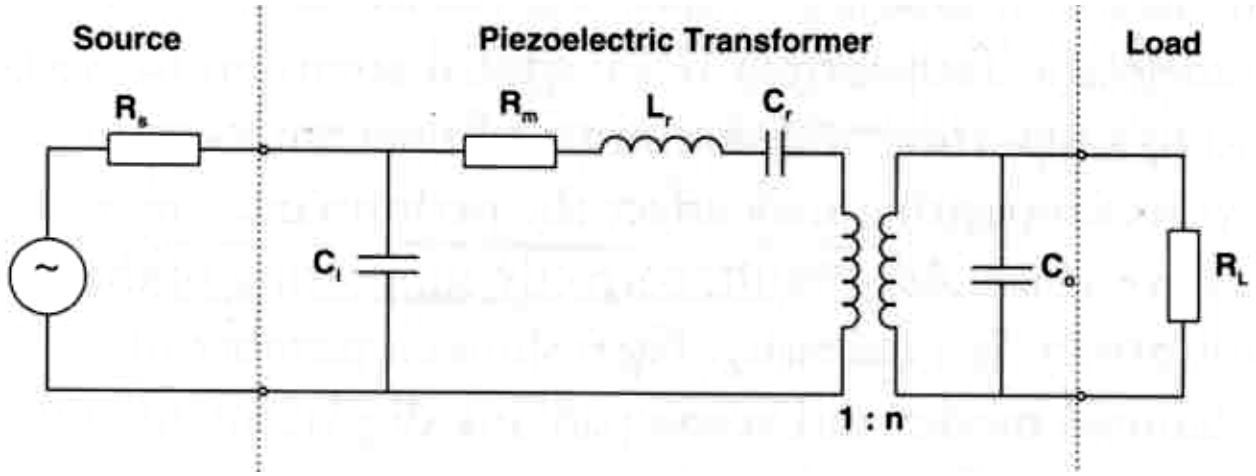

Figure 3: Equivalent circuit of a piezoelectric transducer.
[R_s is the source impedance or the internal impedance of the electrical power source].

every 30 sec. The FFT of the pressure signals measured with the hydrophone was obtained using the MathCad software (version 8.0). The power consumption of the ultrasound horn can be calculated using a simple formula described in chapter 3.

5.4 The physical model

Before proceeding to the development of the physical model, we discuss the equivalent circuit of a piezoelectric transducer. The electrical characteristics of the transducers are affected by the type of mechanical loading to which they are subjected. Since the influence of the mechanical load has characteristics of the electrical parameters of the transducer, it is useful for the design of a transducer that the mechanical loading parameters be represented by a circuit that also includes the electrical parameters of the transducers. Such a circuit is called *equivalent circuit* of a transducer, and is shown in figure 3. It can be seen that the converted mechanical impedance in the equivalent circuit has four components:

1. The inductance L_r due to the mass of the transducer.
2. The capacitance C_r due to the compliance of the transducer.
3. The resistance R_m due to the losses in the transducer (usually negligible).
4. The load resistance or radiation impedance (R_L), which is the product of the specific acoustic impedance of the medium in which the transducer vibrates (Z_R) and the area of the transducer.

Out of these, R_m, L_r, and C_r depend upon the material of construction and dimensions of the transducer and, hence, cannot be altered once the transducer is fabricated. However, the fourth component Z_R is subject to variation according to the conditions of the medium for ultrasound wave propagation. The physical significance of R_L can be described as the resistance to the oscillations of the piezoelectric transducer.

According to an analysis of the efficiency of the piezoelectric transducer, maximum power transfer between the electrical power source and the piezoelectric transducer should occur at resonance conditions (at which the frequency dependent component of the impedance or the *reactance* is zero), when the internal impedance of the electrical power source (R_s) matches the value ($R_m + R_L$), which is basically the load impedance (Ensminger, 1988). In most piezoelectric transducers, the value of R_m is quite small. R_m for the transducer used in the present study is 4Ω, while the internal impedance of the amplifier is 50Ω. It should however be noted that when $(R_m + R_L) > R_s$, the power transfer to the ultrasound horn drops.

For the development of the physical model, we take the specific acoustic impedance of the medium as the basis.

5.4.1 Theory of the impedance tube

Sound radiation within a fluid filled tube by a snugly fitting piston on one end and a rigid reflector on the other end is one of the most basic models in acoustics, which is used for the explanations of basic concepts. The experimental set-up used in this study resembles to some extent to this model: the circular glass cell with a rigid bottom corresponds to the impedance tube, and the ultrasound horn acting as the piston, although the diameters of horn and the cell are not same. The oscillatory motion of the piston driven by the external source, creates sound waves that travel in positive and negative x-direction in the tube (with x = 0 taken to be the mean position of piston face). We assume that the motion of the piston with velocity $V_o \cos(\omega t)$ creates a steady state acoustic field in the tube. The pressure and velocity in the standing wave field are functions of space and time as [Pierce (1989)]:

$$\frac{p}{\rho c} = \mathrm{Re}\left[e^{-i\omega t}\left(X\, e^{ikx} + Y\, e^{-ikx}\right)\right] \tag{1}$$

$$v = \mathrm{Re}\left[e^{-i\omega t}\left(X\, e^{ikx} - Y\, e^{-ikx}\right)\right] \tag{2}$$

The constants X and Y are determined by the boundary conditions at the two ends of the tube. These conditions are: At x = 0, $\hat{v} = V_o$ and at x = L, $\hat{p}/\hat{v} = Z$. Substituting the boundary conditions the values of X and Y are determined as:

$$X = V_o\left[1 + \frac{1}{V_o\left[\left(\frac{Z+\rho c}{Z-\rho c}\right)e^{-2ikL} - 1\right]}\right] \qquad Y = \frac{1}{\left[\left(\frac{Z+\rho c}{Z-\rho c}\right)e^{-2ikL} - 1\right]} \tag{3}$$

Resubstituting of X and Y in equations 1 and 2, and rearranging, we get the relation for amplitude of pressure in tube as function of x:

$$\hat{p} = \rho c V_o \left[\frac{Z \cos k(L - x) - i\rho c \sin k(L - x)}{\rho c \cos kL - iZ \sin kL} \right] \tag{4}$$

where $k = 2\pi/\lambda$ is the wave number. We can determine Z_R, the specific acoustic impedance at the face of the piston, by substituting $x = 0$ in equation 4. Expression for Z_R in the present study gets further simplified due to the fact that $Z = 4.5 \times 10^7$ kg/m^2-s (for stainless steel); $\rho c = 1.5 \times 10^6$ kg/m^2-s (for water) and, hence, $|Z/\rho c| >> 1$ as:

$$Z_R \equiv \left(\frac{\hat{p}}{V_o} \right)_{x=0} = -i\rho c \cot(kL) \tag{5}$$

It can be seen that Z_R is singular when $L = \lambda$ (i.e. the formation of the standing waves). Nonetheless, in reality for $L = \lambda$ the values of Z_R are very high but not singular, due to various losses (such as viscous losses) or the non-idealities in the medium.

In case the liquid in the tube contains dilute dispersions of the gas bubbles, Z_R can be determined by combining the theory of the impedance tube with the theory of the acoustic wave propagation in bubbly liquids that can be used to determine the velocity and the wavelength of sound in the bubbly mixture.

5.4.2 Acoustic wave propagation in bubbly liquids

Acoustic wave propagation in a two-phase medium has been a subject of both experimental and theoretical investigations over the past several decades with a large amount of published literature [for example Foldy (1945), Carstensen and Foldy (1947), Silberman (1952), Fox *et al.* (1955), Macpharson (1957), van Wijngaarden (1968, 1972), Caflisch *et al.* (1985)]. The most rigorous model for the linear acoustic pressure wave propagation in the bubbly liquids was given by Commandeer and Prosperetti (1989), which was a combination of the averaged equations for the bubbly mixtures given by Caflisch *et al.* (1985) and the nonlinear formulation for the dynamics of the bubble that includes viscous and thermal effects [Prosperetti *et al.* (1986)].

We give herewith only the main results of the analysis of Commander and Prosperetti (1989); for the complete derivation of the equations and their solutions the reader is referred to the original paper. The wave number k_m in the gas-liquid mixture is:

$$k_m^2 = \frac{\omega^2}{c^2} + 4\pi\omega^2 \int_0^\infty \frac{R_o \, f(R_o) \, dR_o}{\omega_o^2 - \omega^2 + 2ib\omega} \tag{6}$$

The complex sound speed in the mixture is:

$$c_m = \frac{\omega}{k_m} \tag{7}$$

c_m can be expressed, using equation 6, as:

$$\frac{c^2}{c_m^2} = 1 + 4\pi c^2 \int_0^\infty \frac{R_o\, f(R_o)\, dR_o}{\omega_o^2 - \omega^2 + 2ib\omega} \tag{9}$$

The general mathematical expression for a one-dimensional sound wave is:

$$P(x, t) = P_A \exp[i(\omega t - kx)] \tag{10}$$

In order to find the phase velocity and attenuation coefficient of the wave, we substitute $c/c_m = u - iv$ in this expression. Substitution and simplification gives:

$$\exp[i(\omega t - k_m x)] = \exp\left(-\frac{\omega v}{c} x\right) \exp\left[i\omega\left(t - \frac{u}{c} x\right)\right] \tag{11}$$

From this expression the phase velocity (V) and the attenuation coefficient (A) for the wave in gas-liquid mixture are deduced:

$$V = \frac{c}{u} \text{ and } A = \frac{\omega v}{c} \text{ [or in decibels} \approx 8.686 \left(\frac{\omega v}{c}\right)] \tag{12a and b}$$

Assuming that the number density of bubbles is n_b, and that all the bubbles in the gas-liquid mixture have uniform equilibrium radius, R_o we can simplify equation 9 as:

$$\frac{c^2}{c_m^2} = 1 + \frac{4\pi c^2 n_b R_o}{\omega_o^2 - \omega^2 + 2ib\omega} \tag{13}$$

For bubbles smaller than the resonant size for the ultrasound frequency (in other words for the case $\omega << \omega_o$), the natural oscillation frequency (ω_o) and the damping coefficient (b) are:

$$\omega_o^2 \approx \frac{P_o}{\rho R_o^2}\left(3\gamma - \frac{2\sigma}{P_o R_o}\right) \tag{14}$$

$$b = \frac{\gamma - 1}{10\gamma} \frac{P_o}{\rho D} + \frac{2\mu}{\rho R_o^2} \tag{15}$$

It can be seen that the V and A for the bubbly mixtures strongly depend on n_b (which can related to the bubble volume fraction β in the liquid) and R_o.

5.4.3 Cavitation nucleation and bubble dynamics

A discussion of cavitation nucleation is given in chapter 2, however we briefly reproduce it here for the convenience of the reader. For cavitation to occur, the medium must have pre-existing seed nuclei from which the bubbles can grow. The gas pockets

trapped in the crevices of the solid surface could be potential candidates for the cavitation nuclei. As written earlier, the ultrasound horn used in the experiments had a small circular groove at the tip. This groove may entrap a small amount of air, which can provide nuclei for cavitation. Once subjected to ultrasound, the bubbles can undergo either a stable and small amplitude nonlinear motion for several acoustic cycles called *stable cavitation* or may undergo an explosive growth followed by a transient collapse called as *transient cavitation*, which is a high-energy event. The minimum pressure amplitude required to generate transient cavitation is called transient cavitation threshold (P_T), which is a function of both the initial bubble radius and the frequency of the acoustic wave. A discussion about the transient cavitation threshold is given in chapter 2.

Experimentally, under normal conditions, the cavitation threshold P_T has a value around 1 bar, which we assume. This value would be typical for a bubble size distribution of 2-20 μm and frequency range of 20-100 kHz.

The radial motion of a bubble under the influence of ultrasound can be described by the bubble dynamics equation. For simulations, we have chosen the Gilmore equation (1952) based on Kirkwood-Bethe hypothesis (1942). This equation has been described in chapter 2, however we reproduce it briefly here:

The equation of the radial motion is:

$$R\left[1-\frac{U}{c}\right]\frac{d^2R}{dt^2}+\frac{3}{2}\left[1-\frac{U}{3c}\right]\left(\frac{dR}{dt}\right)^2=\left[1+\frac{U}{c}\right]H+\frac{U}{c}\left[1+\frac{U}{c}\right]\frac{dH}{dR} \tag{16}$$

H is the free enthalpy on the surface of the bubble:

$$H=\frac{n}{n-1}\frac{A^{1/n}}{\rho_o}\left\{\left[\left(P_o+\frac{2\sigma}{R_o}\right)\left(\frac{R_o}{R}\right)^{3\gamma}-\frac{2\sigma}{R}+B\right]^{\frac{n-1}{n}}-\left[P_\infty+B\right]^{\frac{n-1}{n}}\right\} \tag{17}$$

P_∞ is the pressure in the bulk liquid far from the bubble boundary that drives the bubble motion and can be expressed as:

$$P_\infty = P_o - P_A \sin(2\pi f t) \tag{18}$$

A, B and n are constants (For water A = 3001 atm., B = 3000 atm. and n = 7). In equation (16) c is the velocity of sound:

$$c=\left[c_o^2+(n-1)H\right]^{1/2} \tag{19}$$

where c_o is the velocity of sound at STP conditions. The amplitude of the acoustic waves radiated by the bubbles at a distance r >> R (far field) can be estimated from

$$P_s(r,t) = \frac{\rho}{4\pi r}\frac{d^2V_b}{dt^2} = \rho\frac{R}{r}\left[2\left(\frac{dR}{dt}\right)^2 + R\frac{d^2R}{dt^2}\right] \tag{20}$$

As mentioned in chapter 2, the magnitude of P_s is a measure for the cavitation intensity resulting out of the bubble motion. A representative value of r is taken as 10 mm. Based on the hypothesis of Hilgenfeldt *et al.* (1996), the bubble motion has been assumed to be isothermal by setting γ, the polytropic constant of the bubble contents, as 1.

5.4.4 Rectified diffusion

The transport of gas and vapor across the bubble wall during the radial motion of the bubble is an interesting and well-studied phenomenon in acoustic cavitation. As far as the vapor transport in the bubble is concerned, it is usually assumed that in a relatively cold liquid evaporation and condensation are much faster than the bubble wall velocity and, hence, the bubble interior is always saturated with water vapor. The transport of gas in and out of the bubble, however, has interesting features. As discussed earlier, a gas bubble in a liquid will dissolve in the absence of a sound field or any stabilization mechanisms. However, if the bubble undergoes radial motion under the influence of an acoustic wave, the situation is different. In this case, if the amplitude of the acoustic wave driving the bubble motion exceeds a certain threshold value, the bubble may grow due to a process of slow accumulation of gas inside it during oscillations. This process is termed rectified diffusion. The general mathematical formulation of the gas diffusion is given as follows:

Consider a gas bubble undergoing radial motion in a liquid with dissolved gas concentration C_o. The dissolved gas transport within a liquid in a spherically symmetric system is described by the diffusion equation:

$$\frac{DC}{Dt} \equiv \frac{\partial C}{\partial t} + v_r\frac{\partial C}{\partial r} = D_g\left[\frac{\partial^2 C}{\partial r^2} + \frac{2}{r}\frac{\partial C}{\partial r}\right] \tag{21}$$

In order to calculate the mass transfer of gas between the liquid and the oscillating bubble, one needs to solve equation 21 simultaneously with the bubble dynamics equation. The bubble dynamics equation and the diffusion equation are coupled through the term v_r, and the boundary condition at the bubble wall, which is a function of the gas pressure inside the bubble that varies during the radial motion of the bubble. For an oscillating bubble, the velocity at a distance r > R(t) is: $R^2(dR/dt)/r^2$. Substituting this into equation 21 we get the equation for the mass transport in the liquid:

$$r^2\frac{\partial C}{\partial t} + \left(R^2\frac{dR}{dt}\right)\frac{\partial C}{\partial r} = D_g\frac{\partial}{\partial r}\left(r^2\frac{\partial C}{\partial r}\right) \tag{22}$$

with boundary conditions:

$$C(R, t) = C_s P_i(R, t)/P_o$$

$$C(\infty, t) = C_o \tag{23}$$

Several researchers over the past few decades have given approximate solutions for the mass transport across the bubble wall during small amplitude radial oscillations by coupling the diffusion equation and bubble dynamics equation [for example Hsieh and Plesset (1961); Eller and Flynn (1965); Safar (1968); Crum (1984)].

More recently, a general and rigorous formulation of rectified diffusion has been given by Löfstedt *et al.* (1995) and Fyrillas and Szeri (1996) that can be applied to large amplitude non-linear motion of bubbles driven by acoustic waves with pressure amplitudes exceeding the transient cavitation threshold. In our physical model, we have used the formulation of Fyrillas and Szeri (1996) to assess the effect of the dissolved gas in the medium on the bubble growth or shrinkage during radial motion, which in turn influences the parameters Z_R, A and P_s. We briefly describe herewith the formulation of Fyrillas and Szeri (1996). For greater details the reader may refer to the original paper.

Fyrillas and Szeri (1996) have proposed the idea of treating the problem of rectified diffusion on the basis of "separation of time scales". The dissolved gas concentration in the liquid is split into two parts: first, the *oscillatory* part $C_{osc}(r, t)$ that changes on a fast time scale, T which is the period of the acoustic wave driving the bubble motion and, secondly, the *smooth* part $C_{smo}(r, t)$ that changes on a slow time scale $\bar{t}\,(=n\tau_D) >> T$. τ_D is called *diffusive* time scale and is defined as R_o^2/D_g. Thus, the total gas concentration in space and time is the sum of the smooth and the oscillatory parts:

$$C(r, t) = C_{osc}(r, t) + C_{smo}(r, t) \tag{24}$$

After solving the smooth and oscillatory parts of the diffusive problem using a singular perturbation analysis, Fyrillas and Szeri have shown that the contribution by the oscillatory part to the mass transport across bubble wall is negligible. However, the smooth part contributes to the change in the gas content of the bubble. The smooth profile $C_{smo}(r, \bar{t})$ is given by:

$$\overline{C}_{smo}(h) = C_o + \left[C_s \frac{\left\langle P_i(t) \right\rangle_{t,4}}{P_o} - C_o \right] \times \left\{ 1 - \frac{\int_0^h \frac{dh'}{\left\langle \left(3h' + R^3(t)\right)^{4/3} \right\rangle_{t,0}}}{\int_0^\infty \frac{dh'}{\left\langle \left(3h' + R^3(t)\right)^{4/3} \right\rangle_{t,0}}} \right\} \tag{25}$$

The growth or shrinkage of the bubble is indicated by a change in the mean radius of the bubble (R_o), which can be determined from:

$$\frac{dm_g}{d\bar{t}} = 4\pi R_o^2 D_g \left. \frac{\partial \overline{C}_{smo}}{\partial r} \right|_{r=R} = 4\pi \rho_g R_o^2 \frac{dR_o(\bar{t})}{d\bar{t}} \tag{26}$$

$$\left.\frac{\partial \overline{C}_{smo}}{\partial r}\right|_{r=R} = \frac{C_s}{R_o^2(\bar{t})} \frac{\left[\frac{C_o}{C_s} - \frac{\langle P_i(t)\rangle_{t,4}(\bar{t})}{P_o}\right]}{\int_0^\infty \frac{dh'}{\left\langle \left(3h' + R^3(t)\right)^{4/3} \right\rangle_{t,0}}} \tag{27}$$

Using equations 26 and 27 the rate of change in the mean radius of the bubble is:

$$\frac{d}{d\bar{t}} R_o(\bar{t}) = \frac{D\, C_s}{\rho_g\, R_o^2(\bar{t})} \frac{\left[\frac{C_o}{C_s} - \frac{\langle P_i(t)\rangle_{t,4}(\bar{t})}{P_o}\right]}{\int_0^\infty \frac{dh'}{\left\langle \left(3h' + R^3(t)\right)^{4/3} \right\rangle_{t,0}}} \tag{28}$$

The time averages (denoted by $\langle\ \rangle_{t,i}$) in equations 25, 27 and 28 are defined as:

$$\langle f(t)\rangle_{t,i} = \frac{\int_0^T f(t)\, R^i(t)\, dt}{\int_0^T R^i(t)\, dt} \tag{29}$$

The time average of P_i (internal pressure of the bubble) is calculated using the bubble dynamics equation. The space integral in the denominator of equation 28 can be taken ≈ $1/R_{max}$, as a saddle point approximation [Lohse and Hilgenfeldt (1997); Löfstedt *et al.* (1995)], where R_{max} is the maximum radius of the bubble during oscillations over one acoustic period. The initial conditions for the numerical solution of equations 16 - 19 along with equation 28 are: t = 0, R = R_o, dR/dt = 0, C(r, t = 0) = C_o. The values of C_s and D_g are taken as 0.022 kg/m^3 and 10^{-5} m^2 s^{-1} respectively. The values of other parameters used in the simulations are: ρ = 1000 kg m^{-3}, ρ_g = 1.2 kg m^{-3}, σ = 0.072 N/m, μ = 10 cP, γ = 1.4, c = 1500 m s^{-1}, f = 25 kHz, P_o = 101325 Pa, L = 6 cm. The value of P_A, in different sets of experiments, has been estimated using the simple formula for the acoustic intensity given in chapter 2, and assuming a transducer efficiency of about 40% [Shah *et al.* (1999)]. The pressure amplitude actually experienced by the bubbles (P_{Ae}) at the pressure antinode is less than the pressure amplitude at the tip of the horn, due to the attenuation of the ultrasound waves. The experimental techniques used in this study do not allow P_A from P_{Ae}. Therefore, we have used for the simulations of bubble dynamics in the different sets of experiments, values of P_A that are slightly less than those at the tip of the horn. Equations 16 - 19 and 28 are solved together using the Runge-Kutta fourth order method with adaptive step size control [Press *et al.* (1992)].

5.5 Results and discussion

As depicted in figure 1, the input electrical power to the ultrasonic processor undergoes various transformations before being finally dissipated in the system. The measurements of the cavitation intensity and the power consumption of the ultrasound horn give us quantitative tools to assess not only the individual efficiency of the steps in the energy transformation chain, but also help explore the mechanics and interrelations between these transformations. The power consumption of the horn represents the efficiency of step 1 in the energy transformation chain. The spectral characteristics of the pressure signals (or acoustic emissions, indicative of the cavitation intensity produced in the medium under different operating conditions) represent the efficiencies of steps 2 and 3 together in the energy transformation chain.

Three representative acoustic emission spectra (which are basically the FFT of the pressure signal measured with the hydrophone) in the first, second, and third set of experiments are shown in figures 4, 5 and 6 respectively (three acoustic emission spectra to show the reproducibility of the results). The power consumptions of the ultrasound horn in the three sets of experiments are depicted in figure 7. The acoustic emission spectra in the different sets of experiments reveal interesting features. In the acoustic emission spectra of the first set (with water saturated with dissolved gas as the medium), only the peak corresponding to the fundamental frequency is prominent, with a weak first harmonic (2f). A sharp rise in subharmonic (f/2), ultraharmonic (nf/2, where n = 3, 5, 7…etc.) and harmonic (nf, where n = 2, 3, 4, …etc.) emissions are seen in the acoustic emission spectra of the second set of experiments, in which under-saturated water was used as the medium. All the other components except the fundamental frequency disappear in the acoustic emission spectra of set 3, in which the circular groove in the tip of the horn was separated from the medium. The power consumption of the ultrasound horn shows a significant increase with increasing degree of degassing of water as indicated by power consumptions of first and second set of experiments, while it remain almost unaltered after the nucleating area in the tip of the horn is isolated from the bulk, as indicated by the power consumption values of set 2 and set 3.

The spectral characteristics of the acoustic emission (i.e. the frequency components present in the acoustic emission spectrum) help discern the kind of radial bubble motion (whether stable oscillatory or transient) from which the acoustic emission originates. Hence, the spectral characteristics of the acoustic emission can help in deducing the cavitation intensity (Moholkar *et al.*, (2000a); Frohly *et al.*, (2000)). An analysis of the acoustic emission is given in chapter 2. It is generally known that the acoustic emission spectrum consists of various frequencies related to the fundamental or driving frequency. These frequencies are either the subharmonic, the ultraharmonic or the harmonic of the fundamental frequency. The subharmonic component of the acoustic emission spectrum is of particular interest because it originates from high-energy transient bubble motion, and thus, is indicative of the cavitation intensity in the medium.

The explanations for the results of the three sets of the experiments follow from the numerical simulations of various physical phenomena, using representative values of the involved physical parameters. An important parameter in the numerical simulations is

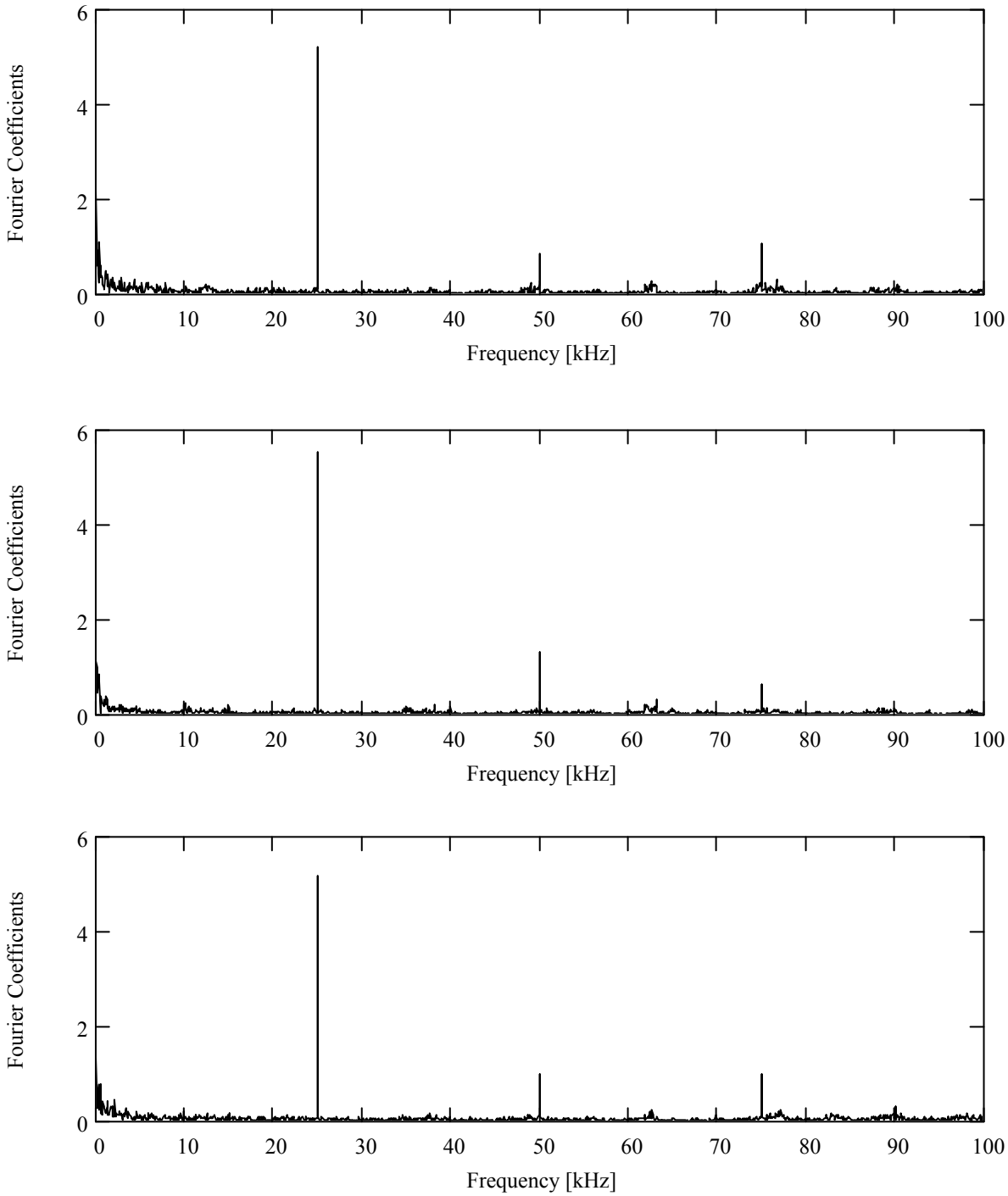

Figure 4: The acoustic emission spectra in experiment set 1.

the initial mean radius of the bubbles in the medium, which does not have a unique value. We assume that the bubble population in the medium is uniform in size with 10 μm as the mean radius prior to exposure to ultrasound. The simulations of Z_R and A are shown in figures 8A and 8B respectively. The simulations of the growth/shrinkage of the bubbles due to rectified diffusion for P_A above and below P_T, and for different saturations of the medium are shown in figure 9. Finally, the simulations of the radial motion of the

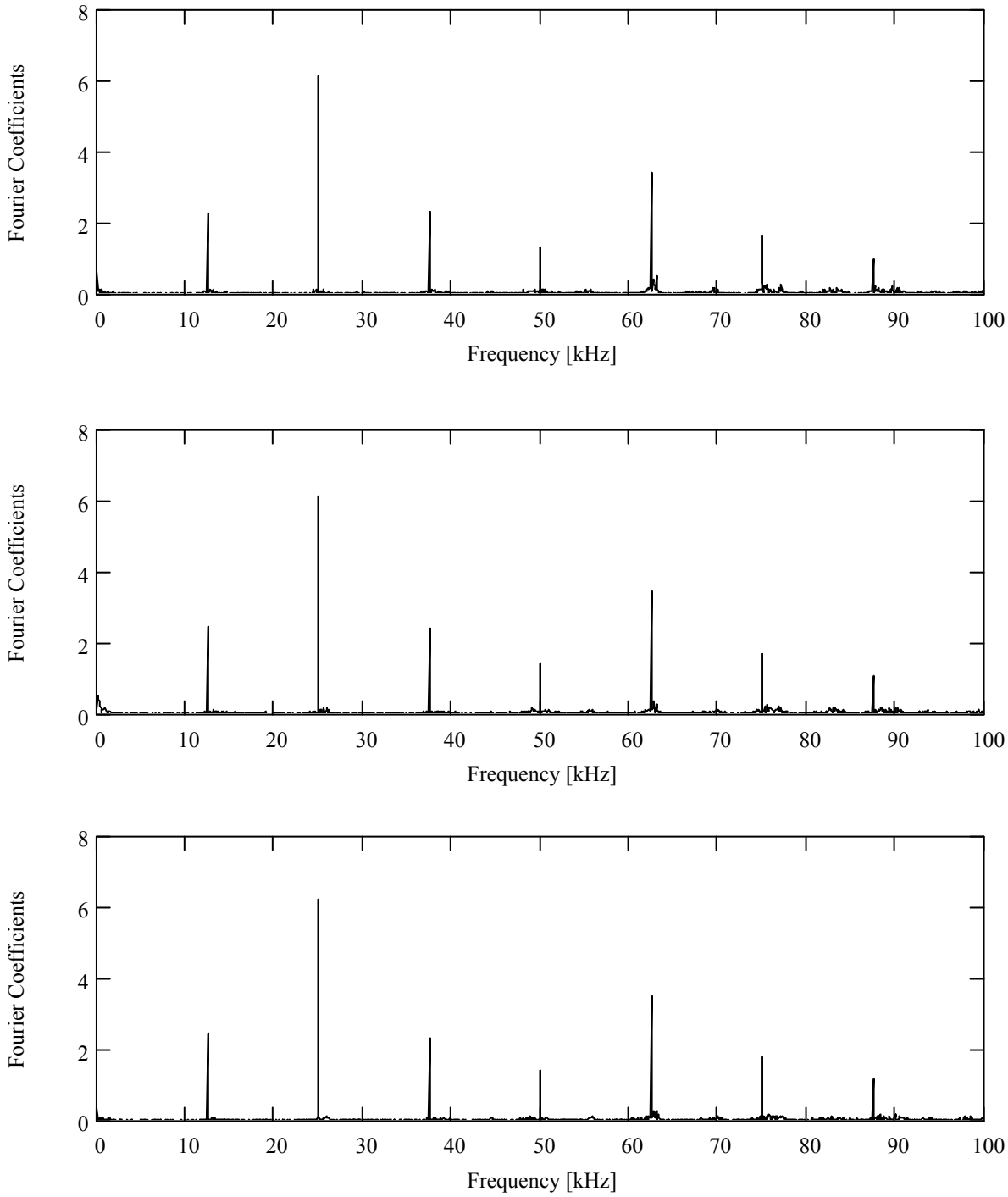

Figure 5: The acoustic emission spectra in experiment set 2.

bubbles of different initial radii for P_A above and below P_T are shown in figure 10 and 11 respectively. The parameters for the various simulations are given the figure caption.

The characteristic features of Z_R and A are evident from figures 8A and 8B, which depict the variation in Z_R and A with the bubble volume fraction in the liquid, and the mean radius of the bubble population. It can be inferred from figure 8, that Z_R is basically a strong function of the bubble volume fraction, and is little sensitive to the size distribution of the bubbles. On the contrary, A is a strong function of the size of the

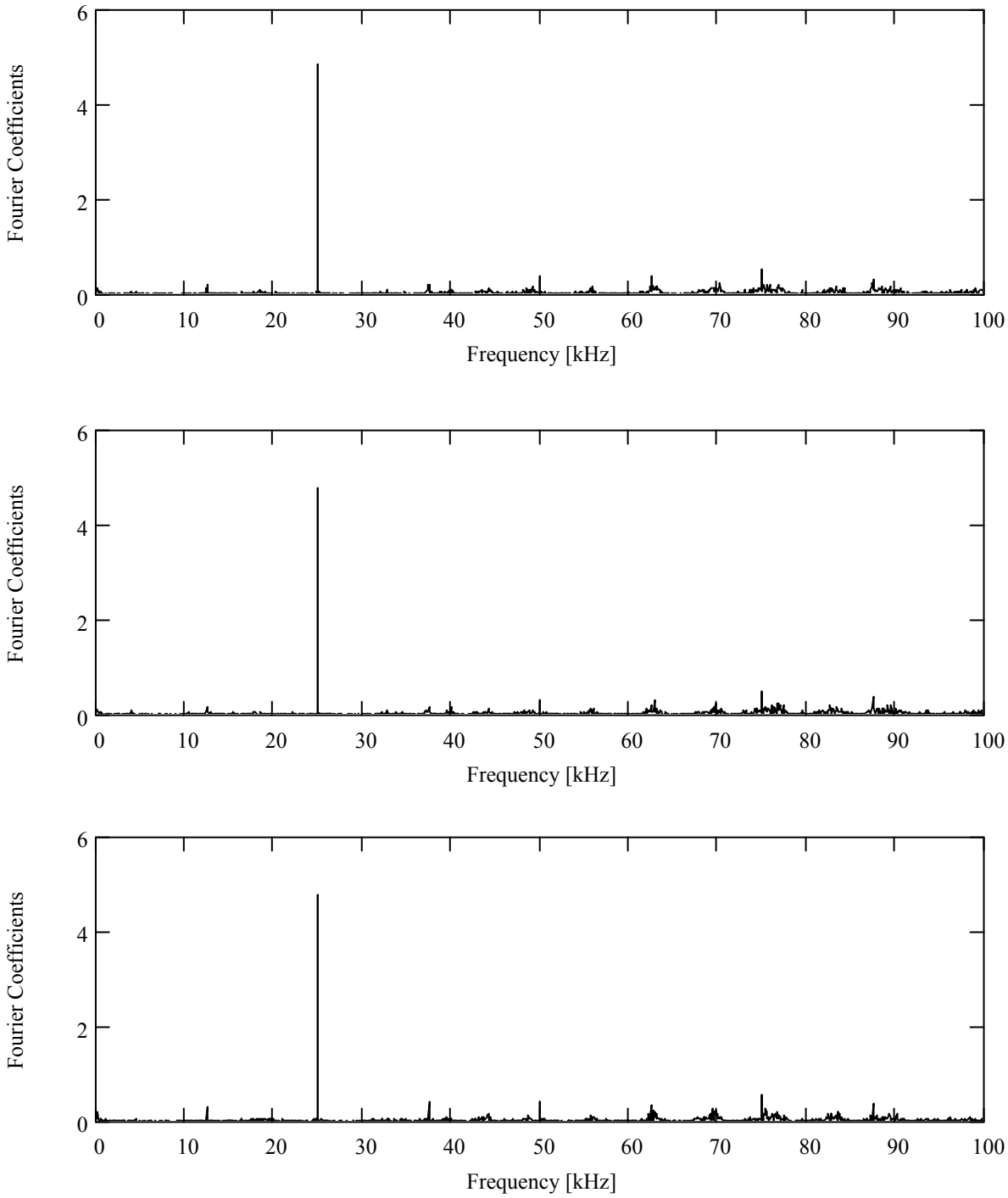

Figure 6: The acoustic emission spectra in experiment set 3.

bubbles. One can easily deduce, on the basis of the discussion on the equivalent circuit of the piezoelectric transducers given earlier that, since $R_m << R_s$, a lower bubble volume fraction in the medium would give a higher the value of Z_R, thus increasing the power consumption of the ultrasound horn. The bubble volume fraction in the medium changes continuously during the ultrasound irradiation, due to the growth and shrinkage of bubbles as a result of rectified diffusion. It can be inferred from figures 9A, that the bubbles oscillating in the nearly saturated medium ($C_o/C_s = 0.8$) grow in size, while

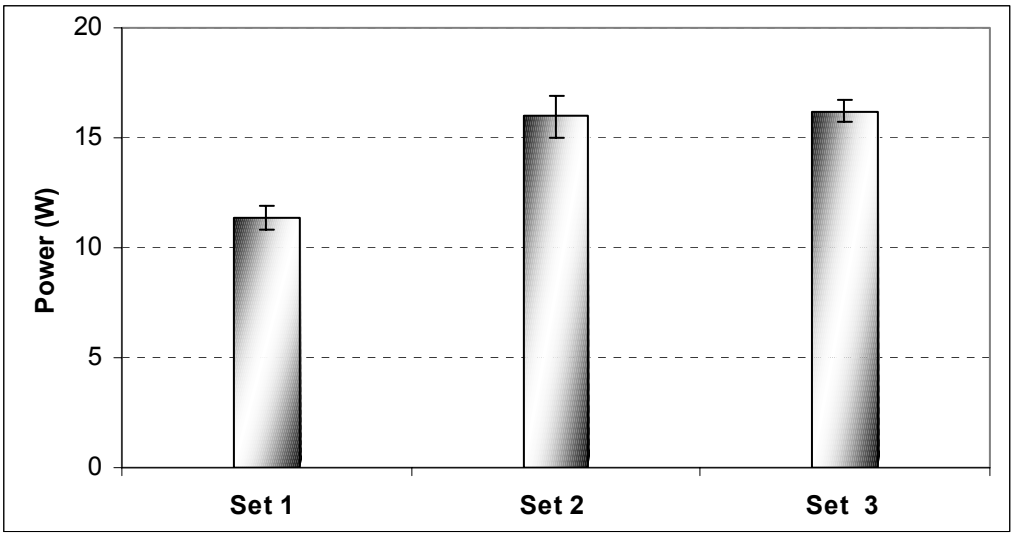

Figure 7: Power consumption of the ultrasound horn in different sets of experiments.

bubbles in the highly unsaturated medium ($C_o/C_s = 0.2$) shrink in size for the case of $P_A > P_T$. On the other hand, in the case of $P_A < P_T$, the bubbles shrink in size irrespective of the gas concentration in the medium as shown in figure 9B, although the rate of dissolution of the bubbles is a function of the saturation of the medium. At this point we must mention that although the percentage change in the mean bubble radius over 100 acoustic cycles is quite small, the growth or shrinkage of the bubble is significant for irradiation periods as short as 1 sec, which is equivalent to 25000 acoustic cycles for 25 kHz ultrasound. Finally, the numerical simulations of the radial motions of the bubbles of different mean radii driven by the acoustic wave with pressure amplitude above and below P_T are shown in figure 10 and 11 respectively. As mentioned earlier, we take a mean initial bubble radius of 10 μm as the basis for simulations. Figure 10 depicts the numerical simulations of the radial dynamics of bubbles of size 5, 10 and 15 μm. These sizes are selected taking into consideration the growth or shrinkage of a 10 μm bubble, when oscillating in media with different saturations of the dissolved gas. Figure 11 shows the radial dynamics of bubbles of initial sizes of 5, 7.5 and 10 μm. Again, these sizes are selected to represent the shrinkage of the bubble during oscillations. Figure 10 indicates that the cavitation intensity resulting from the radial bubble motion above the transient cavitation threshold has an optimum with the mean radius of the bubble. The magnitude of the sound pressure radiated by the bubbles driven by the ultrasound waves with pressure amplitudes greater than the transient cavitation threshold decreases after growth (from 10 μm to 15 μm) as well as shrinkage (from 10 μm to 5 μm) due to rectified diffusion. As far as the numerical simulations of the radial motion of the bubbles below transient cavitation threshold are concerned, the magnitude of the sound radiation and, hence, the cavitation intensity ever decreases with the shrinkage of the bubble.

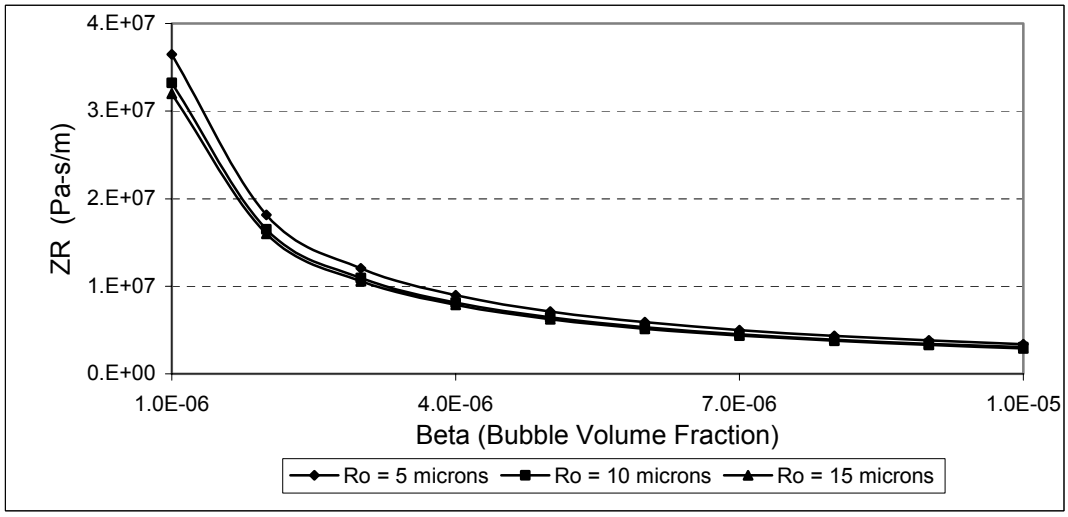

(A)

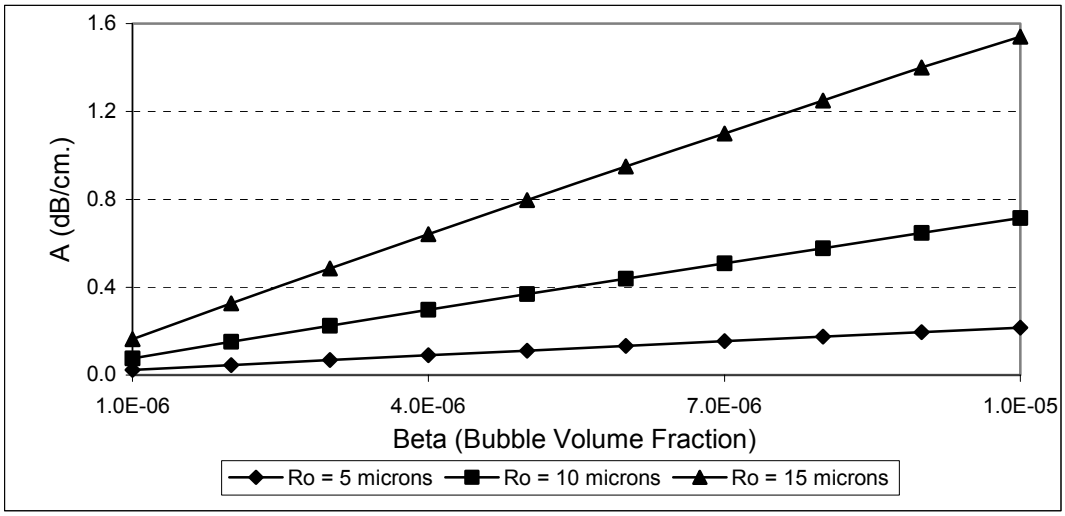

(B)

Figure 8: (8A) Variation in the specific acoustic impedance of the tube as a function of the bubble volume fraction and the mean radius of the bubbles. (8B) Variation in the attenuation coefficient of the tube as a function of the bubble volume fraction and the mean radius of the bubbles.

The results of the numerical simulations of various physical phenomena in an ultrasonic processor show that the cavitation intensity produced in the medium as a result of the radial bubble motion is a function of several parameters, which are strongly inter-dependent. These parameters are:

1. The number of bubbles (n_b).
2. The mean radius of the bubbles (R_o).
3. The bubble volume fraction of the liquid (β).
4. The attenuation coefficient for the ultrasound waves (A).
5. Specific acoustic impedance of the medium (Z_R).
6. The acoustic pressure amplitude (P_A).
7. The dissolved gas concentration in the liquid (C_o).

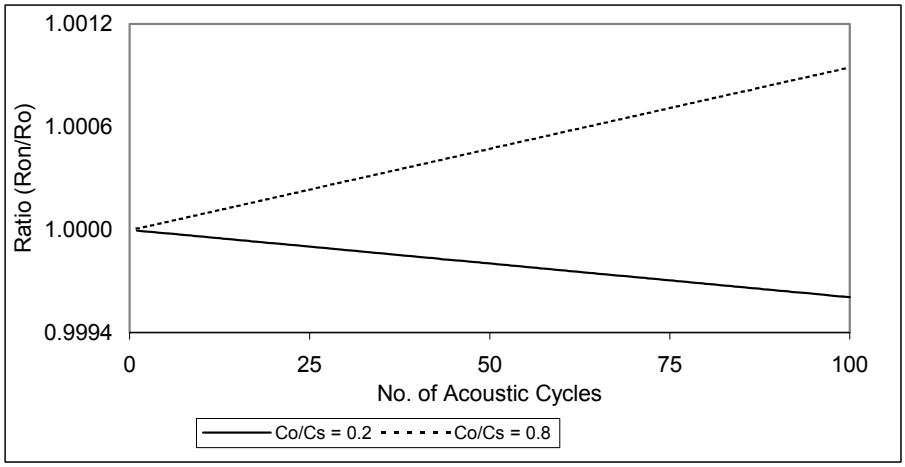

(A)

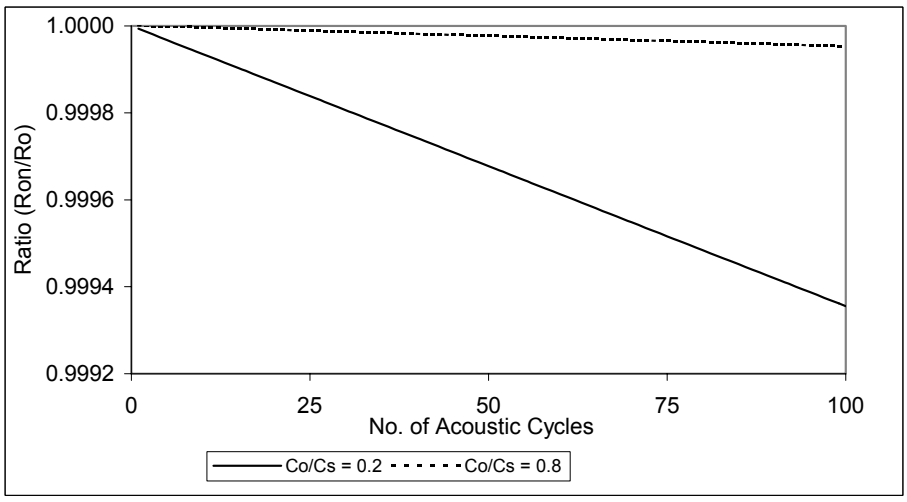

(B)

Figure 9: (9A) Growth and dissolution of the air bubbles due to rectified diffusion during radial motion driven by acoustic wave with $P_A > P_T$ in water with different saturations of dissolved air. Main parameters for simulations: R_o = 10 μm., P_A = 1.3 bar, f = 25 kHz. (9B) Dissolution of the air bubbles due to rectified diffusion during radial motion driven by acoustic wave with $P_A < P_T$ in water with different saturations of dissolved air. Main parameters for simulations: R_o = 10 μm., P_A = 0.8 bar, f = 25 kHz.

The inter-relations between these parameters, which can be deduced from the numerical simulations just presented, are shown in figure 12. The dotted arrows in figure 12 indicate an indirect or weak influence of a parameter over the other. For example, the dissolved gas concentration in the liquid changes with the growth or shrinkage of the bubble, due to rectified diffusion. As such, both n_b and R_o affect C_o. Nonetheless, for smaller values of β ($< 10^{-4}$ or so) the change in C_o is negligibly small and, hence, C_o practically remains constant. Similarly, the effect of n_b on cavitation intensity can also be neglected for smaller bubble populations because in this case the interaction between the adjacent bubbles is quite small, and the radial dynamics of a bubble is influenced mainly by the ultrasound.

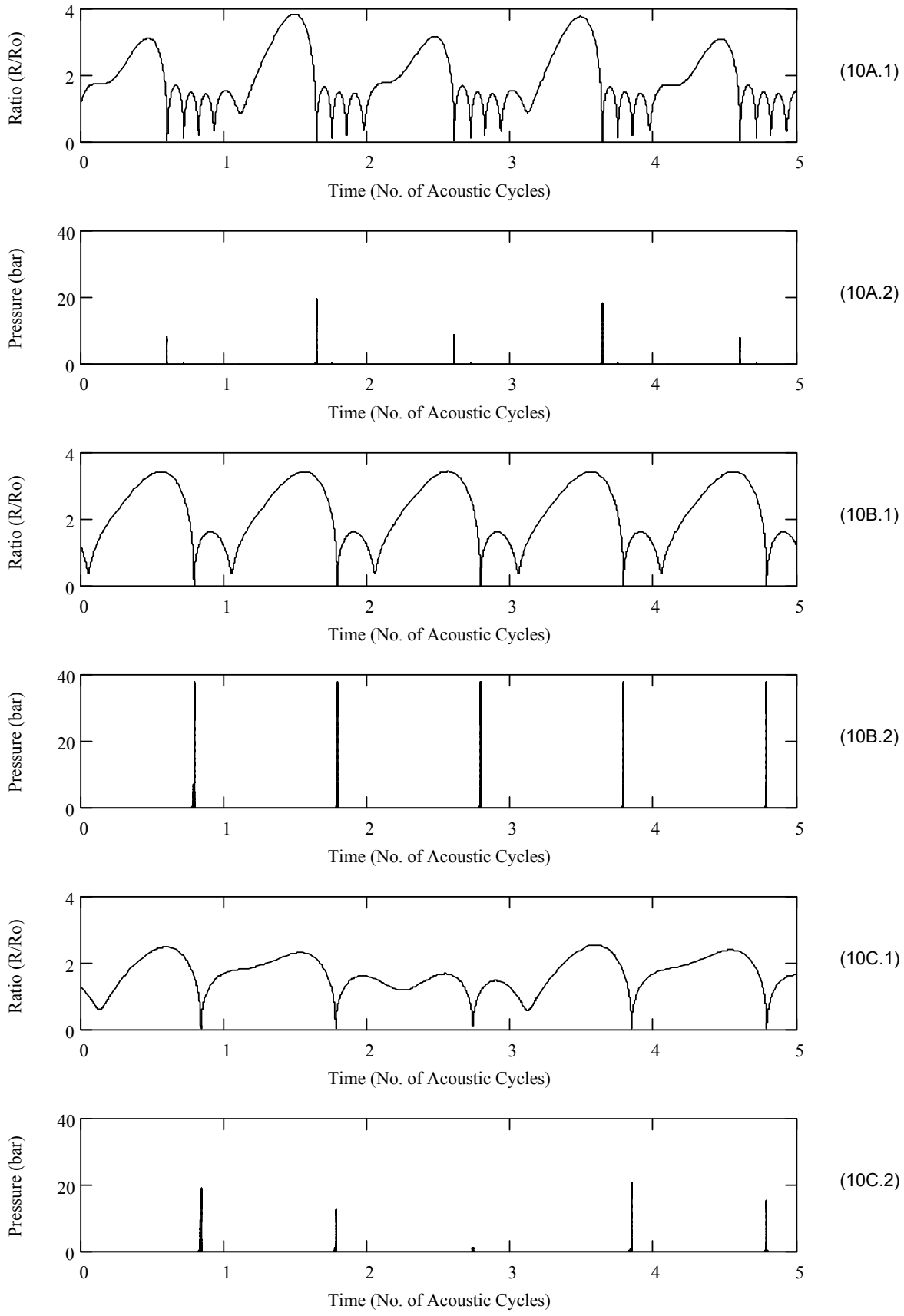

Figure 10: Simulations of the radial motion and sound emission from the bubble of different mean radii driven by acoustic wave with $P_A > P_T$. Parameters for simulations: **(A)** R_o = 5 μm, **(B)** R_o = 10 μm, **(C)** R_o = 15 μm. Other simulations parameters: P_A = 1.3 bar, f = 25 kHz.

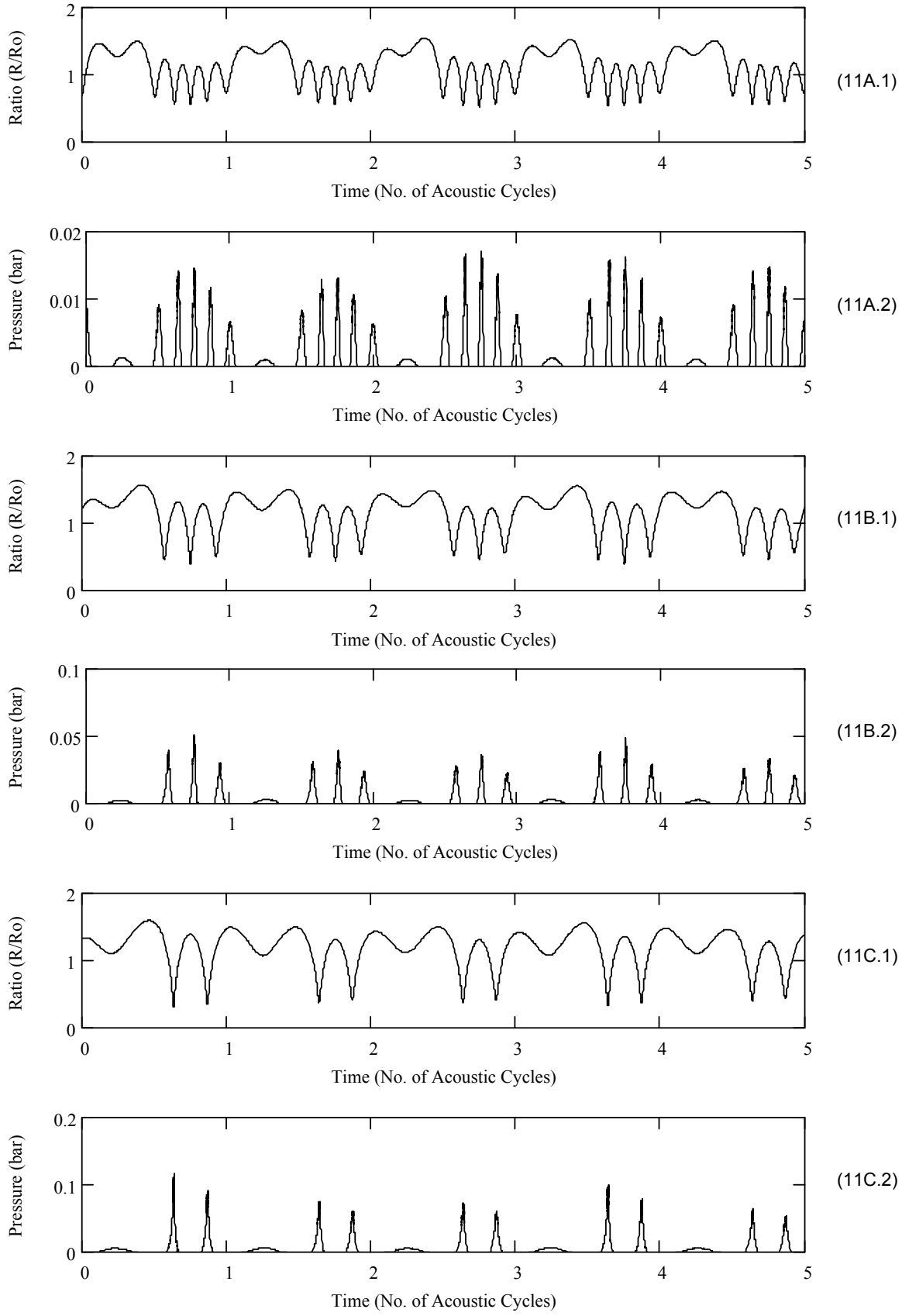

Figure 11: Simulations of the radial motion and sound emission from the bubble of different mean radii driven by acoustic wave with $P_A < P_T$. Parameters for simulations: (A) R_o = 5 μm, (B) R_o = 7.5 μm, (C) R_o = 10 μm Other simulations parameters: P_A = 0.8 bar, f = 25 kHz.

The results of the numerical simulations depicted in figures 8 to 11, along with figure 12 help to explain the experimental results presented in figures 4 to 7. In the first set of experiments, the lowest power consumption and no subharmonic emission were observed. It can be easily deduced that the low power consumption in set 1 is a consequence of the lower value of Z_R due to a higher value of β. This is obviously due to a large number of nuclei contributed by both the (non-degassed) medium, and air trapped in the tip of the horn. Presence of large bubble volume fraction in the medium reduces the speed of sound in it. Therefore, the wavelength is lesser than 6 cm. This causes *detuning* of the system, which results in reduction in power consumption. Low power consumption causes a reduction in the pressure amplitude of the acoustic waves generated by the horn, which gets further attenuated (and may even fall below the transient cavitation threshold) as it passes through the bubble clouds. As such, the acoustic pressure amplitude that a bubble, located away from the tip of the horn, experiences (P_{Ae}) is small in set 1. As mentioned earlier, the experimental techniques used in this study do not allow distinguishing between P_{Ae} and P_A. Nonetheless, one can easily perceive that in a gassy liquid P_{Ae} would be significantly smaller than P_A. Therefore, the bubbles in first set of experiments undergo either a large-amplitude non-linear motion and grow (if $P_{Ae} > P_T$) or slowly dissolve undergoing a stable oscillatory motion (if $P_{Ae} < P_T$) due to rectified diffusion as a result of the high dissolved gas concentration in the medium. In both the cases, the radial motion of the bubbles does not give rise to subharmonic emission, and the cavitation intensity produced by the bubbles is quite small.

The drastic change in the acoustic emission spectrum in the second set of experiments (where subharmonic as well as ultra-harmonics and harmonics are prominent), and the rise in the power consumption of the horn is a result of the degassing of the liquid. The principal effect of degassing the water is a significant rise in Z_R as a consequence of large reduction in n_b (since after degassing the medium, the nuclei for cavitation are contributed only by the air trapped in the groove in the tip of the horn) and, hence, a proportional reduction in β. This results in an increase in the power consumption of the horn with a proportional increment in P_A. A reduction in β also causes a rise in P_{Ae} due to the lesser attenuation by the bubble clouds. Due to these reasons, the bubbles in set 2 undergo a large-amplitude non-linear motion driven by the acoustic waves with a pressure amplitude greater than P_T that results in an intense subharmonic emission, as seen in figure 5. However, the combination of low C_o and high P_{Ae} would tend to dissolve the bubble during radial motion, due to the rectified diffusion as indicated by the simulations presented in figure 9. For this reason, theoretically, the cavitation intensity in set 2 is expected to decrease over a longer period of the ultrasound irradiation. But since the experiments in the present study were conducted only for a short duration, this effect has not been observed.

In the third set of the experiments, an interesting phenomenon was observed that all other frequency components in the acoustic emission spectrum except the fundamental (or ultrasound) frequency disappeared, while the power consumption of the ultrasound horn stayed the same as in the second set of experiments. The explanation for this effect is straightforward: after the degassing of the medium and the isolation of the

groove in the tip of the horn, there are no nuclei left for cavitation to occur. So β, in this case, is practically zero. This would theoretically mean that Z_R tends to infinity. But the non-linearity and the losses in the medium (such as viscous dissipation) make Z_R large yet finite. Therefore, although in this case P_A and P_{Ae} are same as in the second set of experiments, no subharmonic emission has been observed, thanks to the absence of cavitation due to lack of proper nuclei. Another interesting conclusion from the second and third set of experiments is that in the case of a degassed medium, where the value of β is very small (typically < 10^{-5}) Z_R is almost independent of β, which is evident from very similar power consumption values in the second and third set of experiments. The explanation for this can be given in terms of the sound velocity in water, since it appears in the expression for Z_R (equation 7). For β = 10^{-6}, c ≈1491 m/s, while that for pure (gas free) water, c ≈ 1500 m/s. Due to a minor change in the velocity of sound, Z_R is practically independent of β for degassed water.

5.6 Conclusion

The results of the experiments in this study show that the variation in the power consumption of the ultrasound horn and the subharmonic component in the acoustic emission spectrum are strong functions of the free and dissolved gas content of the medium. The combination of the experimental and theoretical results gives an overview of the influences of various physical parameters not only on the cavitation intensity (i.e., the final outcome of the energy input to an ultrasonic processor), but also provide an insight into the mechanism of various steps involved in the transformation of the electrical energy into the cavitation energy. The results of this study show that the influence of the different physical parameters on the conversion of electrical energy into cavitation energy is highly interwoven or inter-dependent, as shown in figure 12. Therefore, an "integrated" approach is inevitable for the optimization of the ultrasonic processors. A careful study of the energy conversion chain, as depicted in figure 1, and the inter-relations between the various physical phenomena, as described in figure 12, reveals that the two parameters that have critically important primary and secondary influence on the energy transformation chain and, hence, on the overall energy efficiency of the ultrasonic processor, are the free gas and the dissolved gas content of the medium. These two parameters are found to affect all the three steps in the energy transformation chain in different ways:

Step 1: Through the change in the specific acoustic impedance, which in turn affects the power consumption and the pressure amplitude of the acoustic waves generated by the horn.
Step 2: Via the change in the attenuation of the acoustic waves, due to bubble clouds, that affects the pressure amplitude of the ultrasound wave.
Step 3: Through the high temperature and pressure pulses resulting out of the radial motion of the bubble driven by ultrasound wave.

The major conclusion from the results of this study is that the set of process parameter values in the second set of experiments is the best possible combination for achieving the highest efficiency of complete energy transformation chain in the ultrasonic processor.

One of the major shortcomings of the ultrasound processors is the lack of precise knowledge of the mechanism of transformation of electrical energy into cavitation energy, the involved physical parameters, and the inter-relation between these parameters. The numerical and experimental results presented in this study not only attempt to fill this deficiency, but also propose an "*integrated*" method for ultrasound processor optimization, using the gas content of the system as a control parameter. We expect that this study will provide the basic mechanistic guidelines for the optimization of a large-scale ultrasonic processor for any physical or chemical application.

Notation

$\hat{p}$	-	complex pressure amplitude of the acoustic wave, Pa.
$\hat{v}$	-	complex velocity amplitude of the acoustic wave, m s^{-1}
A	-	attenuation coefficient of the bubble cloud, dB s^{-1}
b	-	damping constant, s^{-1}
c	-	velocity of sound in gas-free liquid, m s^{-1}
c_m	-	complex velocity of the sound in a gas-liquid mixture, m s^{-1}
C_o	-	dissolved gas concentration in the liquid, kg m^{-3}
c_o	-	the velocity of sound at the STP conditions, m s^{-1}
C_s	-	saturation gas concentration in the liquid, kg m^{-3}
D	-	thermal gas diffusivity, m^2 s^{-1}
D_g	-	diffusion coefficient of gas, m^2 s^{-1}
H	-	Enthalpy at the bubble surface, J kg^{-1}
k	-	wave number of the liquid, m^{-1}
k_m	-	complex wave number of the gas-liquid mixture, m^{-1}
L	-	length of the tube, m.
m_g	-	mass of gas in the bubble, kg.
n, m	-	integers >> 1.
n_b	-	number density of the bubbles, m^{-3}
p	-	pressure in the acoustic wave, Pa
P	-	pressure, Pa
P_∞	-	the pressure in the liquid away from the bubble surface, Pa.
P_A	-	pressure amplitude of the acoustic wave, Pa.
P_{Ae}	-	amplitude of the acoustic wave "experienced" by the bubble, Pa.
P_i	-	internal bubble pressure, Pa.
P_o	-	ambient pressure, Pa.
P_s	-	amplitude of the sound radiated by the bubble, Pa.
P_T	-	transient cavitation threshold, Pa
r	-	distance from the bubble center, m.

R - radius of the bubble, m.
R_{max} - maximum bubble radius during oscillation in one acoustic period, m.
R_{no} - the "new" mean bubble radius (after growth or shrinkage), m^{-1}.
R_o - initial or mean radius of the bubble, m.
R_L - the radiation impedance for the piezoeletric transducer, N-s m^{-1}
T - period of the acoustic wave driving bubble motion, s.
U - the bubble wall velocity (dR/dt), m s^{-1}
V - phase speed of sound in gas-liquid mixture, m s^{-1}
v - velocity in the acoustic wave, m s^{-1}
V_b - volume of the bubble, m^3
V_o - amplitude of the oscillatory velocity of the piston, m s^{-1}
Z - specific acoustic impedance of the rigid reflector, Pa-s m^{-1}
Z_R - specific acoustic impedance at the piston (or ultrasound horn) tip, Pa-s m^{-1}

Greek letters

β - bubble volume fraction in the liquid, dimensionless.
λ - wavelength of sound, m.
σ - surface tension of the liquid, N m.
ρ - density of the liquid, kg m^{-3}
ρ_o - density of the liquid in undisturbed state, kg m^{-3}
ρ_g - density of the gas, kg m^{-3}
ω - angular frequency of sound, s^{-1}
ω_o - natural oscillation frequency of the bubble, s^{-1}
γ - ratio of specific heats of gas, dimensionless
μ - viscosity of the liquid, kg m^{-1} s^{-1}
τ_D - diffusive time scale, s.

References

- Caflisch, R.E., M.J. Miksis, G.C. Papanicolaou, and L. Ting, "Effective equations for wave propagation in bubbly liquids", *Journal of Fluid Mechanics*, **153**, 259-273 (1985).
- Carstensen, E.L., and L.L. Foldy, "Propagation of sound through a liquid containing bubbles", *Journal of the Acoustical Society of America*, **19**, 481-501 (1947).
- Crum, L.A., "Rectified Diffusion", *Ultrasonics*, **22**, 215-223 (1984).
- Dahlem, O., J. Reisse, and V. Halloin, "A radially vibrating horn: A scaling-up possibility for sonochemical reactors", *Chemical Engineering Science*, **53**, 255-271 (1998).
- Dahnke, S.W., and F.J. Keil, "Modeling of linear pressure fields in sonochemical reactors considering an inhomogeneous density distribution of cavitation bubbles", *Chemical Engineering Science*, **54** (13-14), 2865-2872 (1999).
- Dähnke, S.W., and F.J. Keil, "Modeling of 3-D Linear Pressure Fields in

Sonochemical Reactors with Homogeneous and Inhomogeneous Density Distributions of Cavitation Bubbles," *Industrial and Engineering Chemistry Research*, **37** (3), 848-864 (1998).

- Eller, A.I., and H.G. Flynn, "Rectified diffusion through non-linear pulsations of cavitation bubbles," *Journal of the Acoustical Society of America*, **37**, 493-503 (1965).
- Ensminger, D., *Ultrasonics: Fundamentals, Technology, Applications*, Marcel Dekker Inc.: New York, p. 139-177 (1988).
- Faid, F., F. Contamine, A.M. Wilhelm, and H. Delmas, "Comparison of ultrasound effects in different reactors at 20 kHz.," *Ultrasonics-Sonochemistry*, **5**, 119-124 (1998).
- Foldy, L.L., "The multiple scattering of waves", *Physical Reviews*, **67**, 107-119 (1945).
- Fox, F.E., S.R. Curley, and G.S. Larson, "Phase velocity and absorption measurements in water containing air bubbles", *Journal of the Acoustical Society of America*, **27**, 534-547 (1955).
- Frohly, J., S. Labouret, C. Bruneel, I. Looten-Baquet, and R. Torguet, "Ultrasonic cavitation monitoring by acoustic noise power measurement", *Journal of the Acoustical Society of America*, **108** (5), 2012-2020 (2000).
- Fyrillas, M., and A.J. Szeri, "Dissolution or growth of soluble spherical oscillating gas bubbles", *Journal of Fluid Mechanics*, **277**, 381-407 (1994).
- Gilmore, F.R., *Hydrodynamic Laboratory Report*, California Institute of Technology, **26-4** (1952).
- Hilgenfeldt, S., D. Lohse, and M.P. Brenner, "Phase Diagrams for Sonoluminescing Bubbles," *Physics of Fluids*, **8**(11), 2808-2826 (1996).
- Horst, C., Y.S. Chen, U. Kunz, and U. Hoffmann, "Design, modeling, performance of a novel sonochemical reactor for heterogeneous reactions", *Chemical Engineering Science*, **51**, 1837-1846 (1996).
- Hsieh, D.Y., and M.S. Plesset, "Theory of rectified diffusion of mass into gas bubbles", *Journal of the Acoustical Society of America*, **33**, 206-215 (1961).
- Keil, F.J., and K.M. Swamy, "Reactors for sonochemical engineering – Present Status", *Reviews in Chemical Engineering.*, **15**(2), 85-155 (1999).
- Kirkwood, J.B., and H.A. Bethe, *Office of Science Research and Development Report*, **558**, USA (1942).
- Laborde, J.L., C. Bouyer, J.P. Caltagirone, and A. Gerard, "Acoustic cavitation field prediction at low and high frequency ultrasounds," *Ultrasonics*, **36**, 581-587 (1998).
- Löfstedt, R., K. Weninger, S.J. Putterman, and B.P. Barber, "Sonoluminescing bubbles and mass diffusion," *Physical Reviews E*, **51**, 4400-4410 (1995).
- Lohse, D., and S. Hilgenfeldt, "Inert gas accumulation in sonoluminescing bubbles", *Journal of Chemical Physics*, **107**, 6986-6997 (1997).
- Macpharson, J.D., "The effect of gas bubbles on sound propagation in water", *Proceedings of Physical Society of London Section B*, **70**, 85-92 (1957).
- Martin, P.D., and L.D. Ward, "Reactor design for sonochemical engineering," *Chemical Engineering Research and Design*, **70** (A3), 296-303 (1993).

- Moholkar, V.S., S. Rekveld, and M.M.C.G. Warmoeskerken, "Modeling of the acoustic pressure fields and the distribution of the cavitation phenomena in a dual frequency sonic processor", *Ultrasonics*, **38** (1-8), 666-670 (2000).
- Moholkar, V.S., S.P. Sable, and A.B. Pandit, "Mapping the cavitation intensity in an ultrasound bath using acoustic emission," *AIChE Journal*, **46**(4), 684-694 (2000a).
- Pierce, A.D., *Acoustics: An introduction to its physical principles and applications*, Acoustical Society of America, New York (1989).
- Press, W.H., S.A. Teukolsky, W.T. Vetterling, and B.P. Flannery, *Numerical Recipes*, Cambridge University Press, Cambridge (1992).
- Prospreretti, A., and K.W. Commander, "Linear pressure waves in bubbly liquids: Comparison between theory and experiment", *Journal of the Acoustical Society of America*, **85** (2), 732-746 (1989).
- Prosperetti, A., K.W. Commander, and L.A. Crum, "Nonlinear bubble dynamics", *Journal of the Acoustical Society of America*, **83**, 502-514 (1986).
- Ratoarinoro, C., A.M. Wilhelm, and H. Delmas, "Power Measurement in Sonochemistry," *Ultrasonics-Sonochemistry*, **2**(1), S43-S47 (1995).
- Renaudin, V., N. Gondrexon, P. Boldo, C. Petrier, A. Bernis, and Y. Gonthier, "Method for determining the chemically active zones in a high frequency ultrasonic reactor," *Ultrasonics Sonochemistry*, **1**, S81-S85 (1994).
- Safar, M.H., "Comments on papers concerning rectified diffusion of cavitation bubbles", *Journal of the Acoustical Society of America*, **43**, 1188-1189 (1968).
- Servant, G., J.P. Caltagirone, A. Gerard, J.L. Laborde, and A. Hita, "Numerical simulation of cavitation bubble dynamics induced by ultrasound waves in a high frequency reactor", *Ultrasonics Sonochemistry*, **7** (4), 217-227 (2000).
- Shah, Y.T., A.B. Pandit, and V.S. Moholkar, *Cavitation Reaction Engineering*, Plenum Press, New York (1999).
- Silberman, E., "Sound velocity and attenuation in bubble mixtures measured in standing wave tubes", *Journal of the Acoustical Society of America*, **27**, 534-546 (1955).
- Thompson, L.H., and L.K. Doraiswamy, "Sonochemistry: Science and Engineering", *Industrial and Engineering Chemistry Research*, **38**, 1215-1249 (1999).
- Tsochatzidis, N.A., P. Guiraud, A.M. Wilhelm, and H. Delmas, "Determination of velocity, size and concentration of ultrasonic cavitation bubbles by the phase-Doppler technique", *Chemical Engineering Science*, **56** (5) 1831-1840 (2001).
- van Wijngaarden, L., "On the equations of motion for mixtures of liquid and gas bubbles," *Journal of Fluid Mechanics*, **33**, 465-474 (1968).
- van Wijngaarden, L., "One-dimensional flow of liquids containing small gas bubbles," *Annual Reviews in Fluid Mechanics*, **4**, 369-396 (1972).

6

MECHANISM OF THE INTENSIFICATION OF WET TEXTILE PROCESSES WITH ULTRASOUND

6.1 Introduction

Ultrasound enhanced wet textile processing is a highly active area of research for more than six decades, as is evident from the literature study presented in chapter 1. Despite a large amount of literature published in this area, the exact physical mechanism of the intensification of these processes with ultrasound is not known yet. Several researchers have proposed different hypotheses for the observed process enhancement such as reduction in the boundary layer thickness between the textile and the bulk liquid; reduction in the size distribution of the dye particles that assists their faster diffusion; decrease in the dye aggregation; increased swelling of the fibers etc. Most of the results reported in the literature are system specific, which makes a general conclusion about the physical mechanism of the process rather difficult. Most of the studies have used commercial ultrasound equipment and, therefore, artifacts of the uncontrolled operational parameters of the equipment itself (such as variation in the power input, modulation of the ultrasound wave field etc.) cannot be separated from the principal conclusions of the study. In addition, very few studies try to form a link between the observed process enhancement and the "physical acoustics" related process parameters, such as the frequency and intensity of ultrasound, condition of the medium in which the process is carried out etc. These discrepancies make us conclude that most research in the ultrasonic wet textile processing is of a "black box" type, where the principal focus is on the results and not on the rationale.

In this chapter, we make an attempt to open this black box, and try to elucidate the exact physical mechanism of the ultrasonic enhancement of wet textile processing. Our approach is based on the idea of coupling the principles of wet textile processing with those of physical acoustics, i.e., ultrasound wave phenomena and bubble dynamics. For this study, we select a model wet textile process with a model fabric and monitor, whose transport across the fabric can help deduce the mechanism of the process. To begin with, we describe the different physical effects and mechanisms that exist in homogeneous and heterogeneous ultrasonic systems that could possibly contribute to the observed process enhancement and try to analyze their individual contribution. This distinction is achieved by manipulating certain process parameters that manifest their effect on the wet textile processes through their effect on the physical acoustics of the system, i.e., the ultrasound wave phenomena and the bubble dynamics. We make use of the results of the earlier chapters (viz. chapter 2 and 5) to select these process parameters. Another aim of this study is to throw light on the experimental factors that could be the source of the artifacts. This study is conducted in two kinds of ultrasonic equipments: (1) a commercial ultrasound bath; (2) specially built ultrasonic system comprising an ultrasound horn, a signal generator, and an amplifier.

6.2 Approach to the problem

The principal physical phenomena that occur in a homogeneous ultrasound field are:

1. The oscillatory motion of the fluid elements as a result of acoustic wave propagation.
2. Acoustic streaming, which is the circulatory current set up in the medium due to absorption of momentum of the acoustic wave by the medium.
3. Cavitation, which is the growth, oscillation and collapse of gas or vapor bubbles driven by the acoustic wave. For cavitation to occur, the medium is required to have nuclei – tiny gas pockets trapped in the crevices and motes of the walls of the processor that can get excited by ultrasound depending on the frequency and intensity of the acoustic wave. As stated in chapter 2, the radial motion of the bubbles is of two kinds – a small amplitude oscillatory motion for several acoustic cycles called *stable cavitation* and a large-amplitude motion comprising growth followed by violent collapse in one or two acoustic cycles called *transient cavitation*.
4. Near solid boundaries, an additional phenomenon can occur, which is termed "micro-streaming". This is an effect of the impedance of the acoustic wave on the object as a result of which an additional flow pattern is set up in the close vicinity of the surface due to the friction between the solid boundary and the oscillating fluid elements. In principle, the phenomenon of microstreaming is another manifestation of acoustic streaming.

In a system comprising liquid medium (water) with the textile, the phenomenon of cavitation can occur at three possible locations: (1) in the bulk liquid; (2) in the boundary layer between the textile and the bulk liquid; (3) inside the yarn of the textile (possibly due to the nucleation provided by tiny gas pockets trapped in the intra-yarn pores). Cavitation can contribute to the mass transfer enhancement in textiles and, hence, to the intensification of the textile treatment in several different ways:

- The oscillatory motion of the bubble creates a spherical velocity field that decays with the square of the distance from the bubble center. During instances of rapid bubble wall movement, where the bubble wall velocity can reach or exceed the speed of sound in the medium, this spherical velocity field can induce strong convection in the region in the close vicinity of the bubble.
- If the bubble is located in the close vicinity of a solid boundary, it can undergo deformation during transient collapse, which gives rise to a high-speed liquid jet directed towards or away from the boundary (depending on the characteristics of the boundary – whether rigid or free).

Since all these mechanisms are responsible for the creation of some kind of convection in the medium, these can contribute to the enhancement of the mass transfer in the textile material and, hence, to the intensification of the wet textile processes.

In order to make a distinction between the several possible mechanisms, which could possibly contribute to the enhancement of the mass transfer in the textiles, we divide the various physical phenomena described into two categories:

(1) Ultrasound wave or acoustics related phenomena, such as acoustic streaming and the oscillatory ultrasound velocity.

(2) Bubble dynamics or cavitation-related phenomena, such as the formation of a high-speed microjet.

General principles of ultrasound wave phenomena and bubble dynamics described in chapter 2, coupled with the energetics of the ultrasonic processor described in chapter 5 help us devise different experimental strategies that can help identify the separate contributions of acoustics and bubble dynamics to the enhancement of wet textile processing.

Standing waves: Placing the textile sample at different locations in the standing wave field (such as the pressure node and the pressure antinode) can help distinguish between the effects of acoustic and cavitation phenomena. At the pressure antinode cavitation phenomena will be dominant due to the large local pressure amplitude (which drives the transient bubble motion), and the ultrasound oscillatory velocity will be minimum, since the resultant movement of the fluid elements is zero. At pressure nodes (or velocity antinode), the reverse will be true: the ultrasonic oscillatory velocity will be dominant due to the large velocity amplitude, and cavitation will be practically absent due to the very small pressure amplitude. The circulatory acoustic streaming currents will, however, be present in the region between the pressure antinode and the pressure node. Since the velocity of these circulatory currents is quite small, of the order of few cm/s (Leighton, 1994), these are unlikely to contribute towards the intensification of the textile process as they cannot produce an intra-yarn flow that would enhance the rate of diffusion in the intra-yarn pores (which is the rate controlling step in the overall mass transfer in the textile materials as discussed in chapter 1). Nonetheless, these currents can help maintain the concentration of the monitor in the boundary layer between the bulk medium and the textile low, since the monitor diffusing out of the textile is carried into the bulk with the circulatory acoustic streaming currents.

Selective degassing of the medium and the textile: The results of chapter 5 indicate that the cavitation intensity in the medium passes through a maximum with the gas (in both free and dissolved form) content of the medium. Selective degassing of the medium and the fabric can demonstrate the role of cavitation in the intensification of the wet textile processes. In addition, the relative contribution of the cavitation occurring at different locations (in the bulk medium, in the boundary layer between the textile & the medium or inside the yarn) could also be estimated by this technique. The word “degassing” has different interpretations for the medium and the textile. For the medium, *degassing* essentially implies the reduction in the “dissolved” gas content. Of course, the free gas in the liquid will also decrease along with the dissolved gas. Nonetheless, free gas in the medium (in the form of micro-bubbles that can form nuclei for cavitation) is mainly contributed by the gas pockets trapped inside the crevices and motes of the wall of the processor and, hence, it is relatively independent of the dissolved gas content of the system. The word *degassing* for the textile essentially means *de-nucleating*. The tiny air pockets trapped in the intra-yarn pores of the textile can form nuclei for cavitation inside the yarn. Removal of these air pockets can suppress occurrence of cavitation inside yarn.

A more detailed discussion of these aspects and the technique for degassing of textiles is given subsequently.

***De-nucleation of the medium*:** The results of chapter 5 indicate that de-nucleation of the medium (which is careful removal all air pockets) causes the cavitation intensity in the medium drop to zero, even though the acoustic pressure amplitude is still larger than the transient cavitation threshold. [It should be specifically mentioned that the transient cavitation threshold for a medium is not well defined. This is due to the fact that transient cavitation threshold is a function of initial (or equilibrium) bubble size for a constant frequency. Due to a distribution in the initial bubble size, which also changes during ultrasound irradiation as a result of rectified diffusion, the transient cavitation threshold does *not* have a *unique* value. However, for 25 kHz frequency and a bubble size distribution of 2-20 microns, the approximate value of transient cavitation threshold is 0.9 bar. We have taken this value as transient cavitation threshold]. This technique is rather difficult to apply in large ultrasonic systems, due to the very large population of gas pockets trapped at different locations of the system. However, for smaller systems nearly complete de-nucleation can be realized. This approach can help clarify the contribution of cavitation phenomena in the medium to the intensification of the textile process. It needs to be specifically mentioned that in order to obtain a distinction between cavitation and acoustic related phenomena by de-nucleation, the acoustic pressure amplitude needs to be higher than the transient cavitation threshold.

Variation in the static pressure of the system: The results of the simulations of radial bubble motion presented in chapter 2 show that the transient motion of bubbles can be converted into a stable oscillatory kind, if the static pressure in the medium is raised keeping the acoustic pressure amplitude constant (and above the transient cavitation threshold). Thus, the cavitation intensity (and, hence, the contribution of cavitation to the process intensification) will decrease with rising static pressure. However, the acoustic related phenomena such as microstreaming, acoustic streaming and oscillatory ultrasound velocity are relatively unaffected by the variation in the static pressure. Thus, the experiments with the variation in the static pressure of the system can provide an important clue in distinguishing between the contributions of acoustic and cavitation.

Apart from these, two additional techniques that we use are:

- S.E.M. (Scanning Electron Microscope) analysis of the ultrasound treated and the original textile samples to explore any known symptoms of ultrasound (such as erosion due to the cavitation or change in the structure of the textile after ultrasound treatment).
- High-speed photography of the model wet textile process to see the patterns of the transport of the monitor from the textile.

6.3 Model wet textile process

As stated earlier, diffusion and convection in the intra-yarn and inter-yarn pores of the textile form one of the important mass transfer mechanisms in the textiles. So as to deduce the physical mechanism of the intensification of wet textile processes with ultrasound (which is basically the intensification of the mass transfer in the textile), a model wet textile process with a model fabric and a model diffusing substance that acts as a monitor for mass transfer needs to be selected. A proper study of the physical mechanism of the ultrasonic mass transfer enhancement will require that the model fabric and mass transfer monitor possess the following properties and characteristics:

- The monitor for the transport (in the form of a particle or a molecule) should be chemically inert. Cavitation is known to induce many chemical changes in the particles/molecules in the medium. In order to achieve unhindered transport of the monitor across the textile, the monitor should not undergo any chemical change during the transport.
- The monitor should not form any strong chemical or physical bond with the fibers of the textile that can hinder its transport across the fabric.
- The concentration per unit area of the monitor in the fabric should be constant, so that the samples used for different experiments should have the same initial concentration of the monitor diffusing out.
- The monitor should be completely reversible. A complete removal of the monitor from the textile should be possible and the original textile should be recovered after total extraction of the monitor.
- The original diffusion rate of the monitor should be slow enough to be "accelerated" by ultrasound. If the diffusion coefficient of the monitor is already very fast, then the acceleration due to ultrasound may not be discernible.
- The size of the monitor particles should be smaller than the intra-yarn pores of the textile, which will basically ensure the presence of the monitor in these pores. Another advantage of having a very small size of the monitor is the separation of the secondary effect of ultrasound that is hypothesized to be responsible for the intensification of the textile processes, viz. particle size reduction. Due to very small initial size, any further reduction in the size of the monitor will not occur and, hence, the above-mentioned secondary effect can be isolated.
- The fabric used in the model process should preferably be a plain weave with both inter-yarn and intra-yarn porosity that offers a simple geometry for the transport of the monitor.

In view of these requirements, we have selected EMPA 101 fabric (manufactured by ETH, Zurich) as the model fabric for the experiments with the model process being washing of EMPA 101 fabric using ultrasound treatment. The EMPA 101 fabric is a plain weave cotton fabric, 100 g/m^2, soiled with carbon soot and olive oil. The SEM images of this fabric are shown in figure 1 with three different magnifications (SEM machine: Jeol Inc., Model GSM 5800, Accelerating voltage: 5kV; Working distance: 10

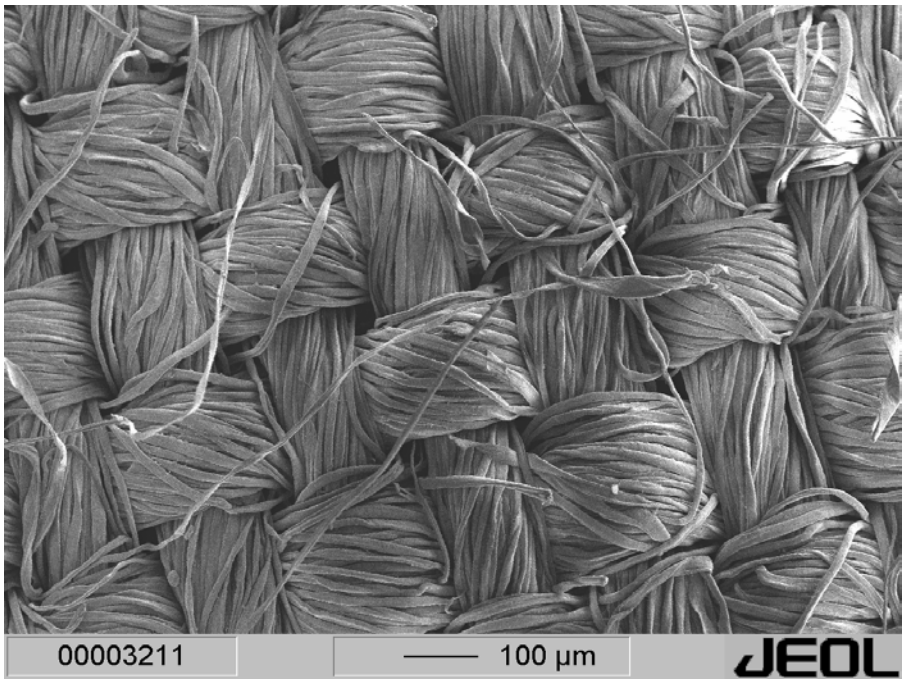

(A)

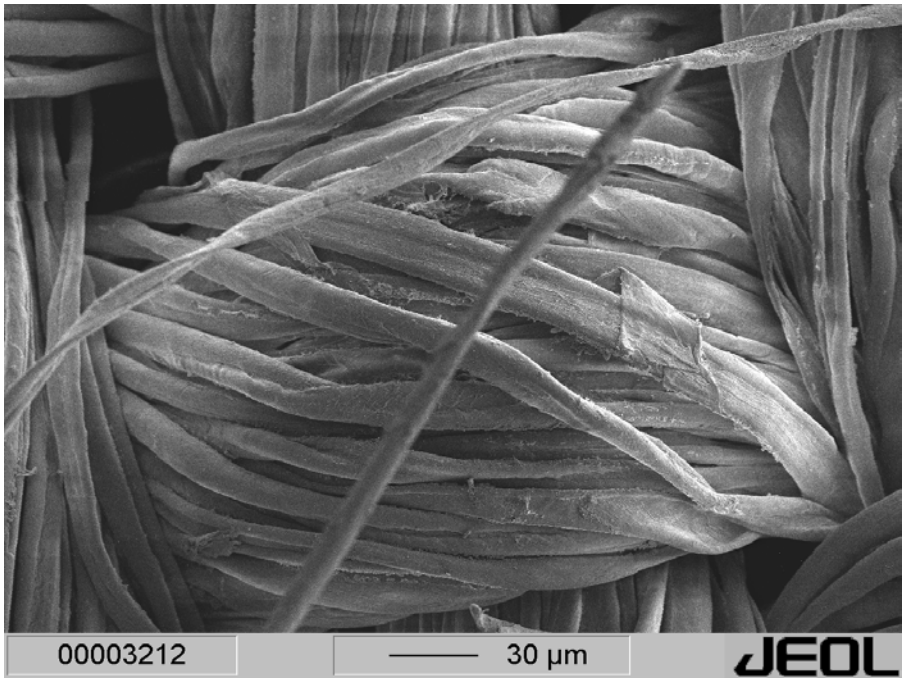

(B)

Figure 1: SEM images of the model EMPA 101 fabric. (A) Surface of the fabric (magnification: 100); (B) A single yarn (magnification: 400)

mm). Figure 1(A) shows an overview of the textile surface, figure 1(B) depicts a single yarn in the textile with a greater magnification while figure 1(C) shows a single fiber in this yarn. The layer of the soil (carbon soot and olive oil) on the surface of the fiber is clearly visible. A cross-section of the fabric (thickness: 7 µm.) was obtained by first soaking the textile in a monomer solution of epoxy resin while taking care to avoid

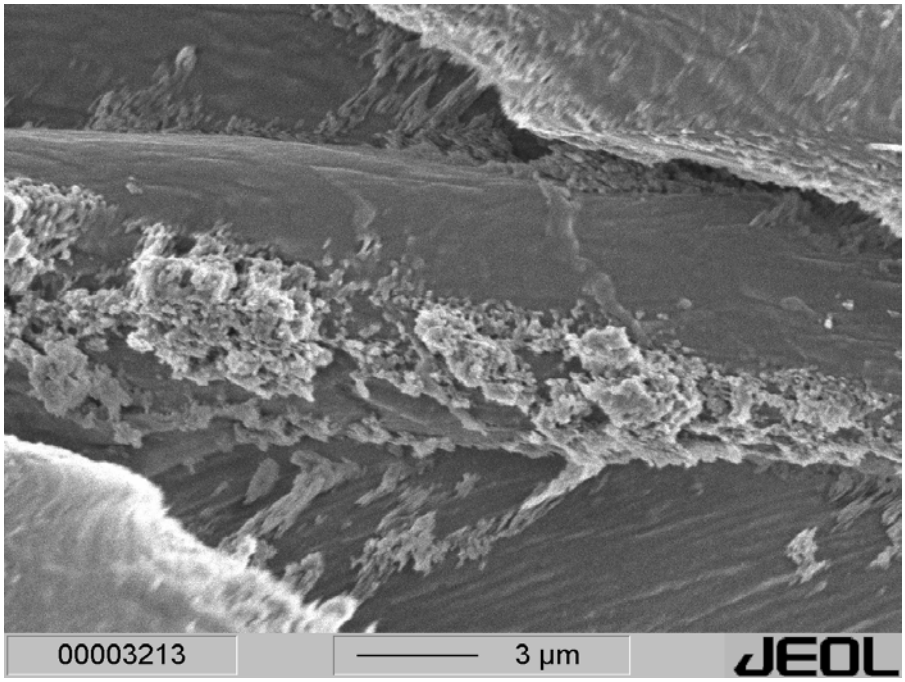

(C)

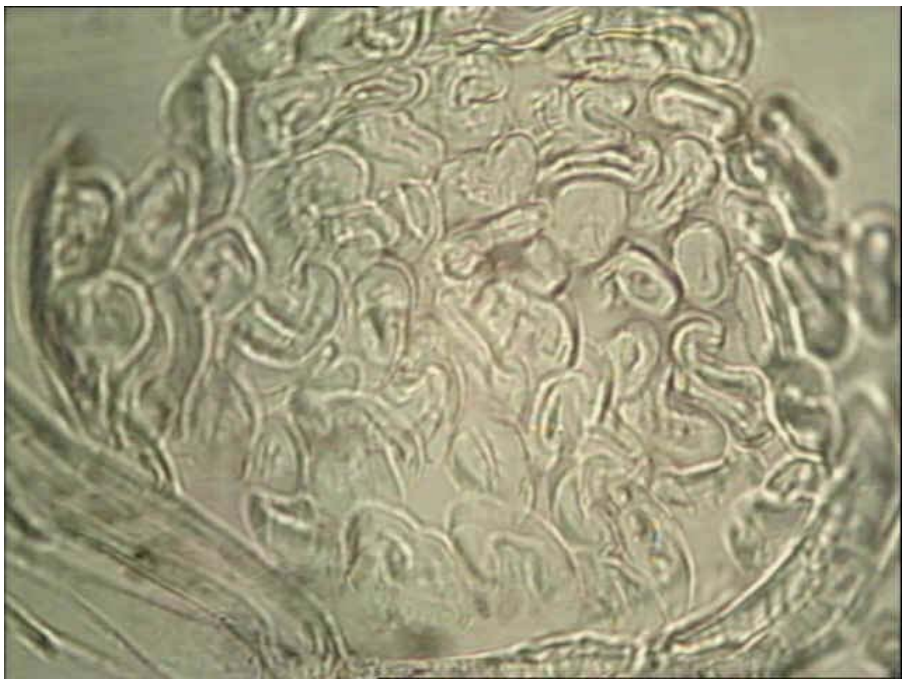

(D)

Figure 1 (*contd…*): SEM images of the model EMPA 101 fabric. (C) Fiber of the fabric: carbon soot on the surface of the fabric is clearly visible. (magnification: 5500); (D) Cross-section of a single yarn: some carbon particles are present inside the yarn (magnification: 500)

entrapment of air bubbles. It was then put in an oven where the monomer is converted into a cross-linked polymer with the textile entrapped in-between. Thus, in this procedure the textile was basically "freezed" in the resin matrix. Next, slices of the resin matrix were obtained with a super-cut machine (Reichert Jung Inc., Model 2050). Figure 1(D) shows the cross-section of the EMPA 101 fabric. The presence of the carbon particles

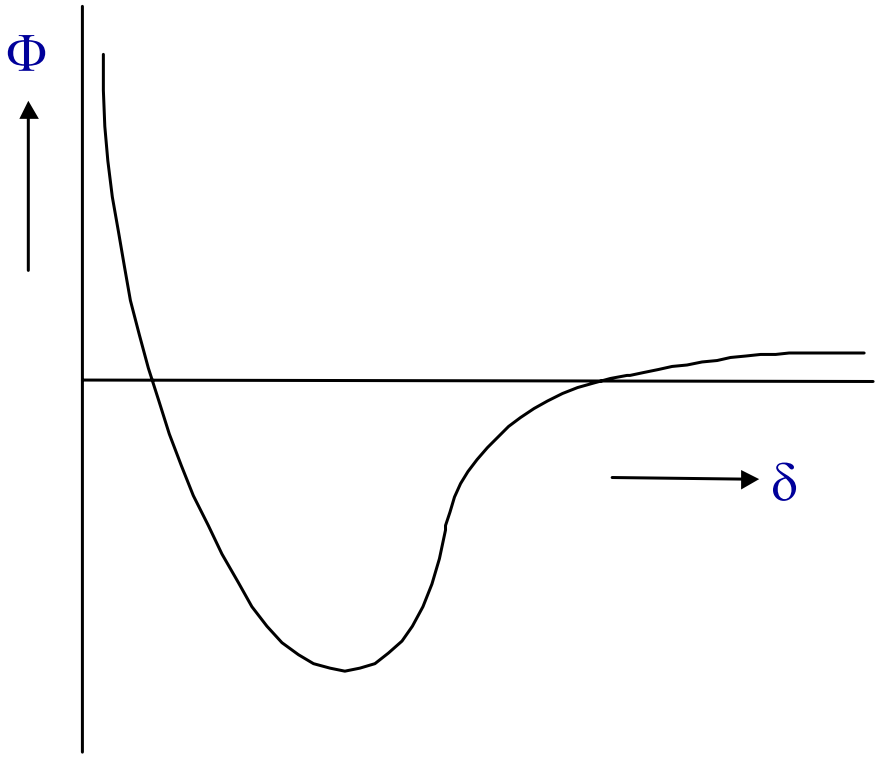

Figure 2: The potential energy (Φ) diagram for the removal of an adhering particle to the surface of the textile. It could be seen that the potential energy of the system shows a minimum with the distance from the textile (δ).

inside the yarn is clearly visible although the concentration of the carbon particles inside the textile is quite small. This indicates that the soil is unevenly distributed in the model fabric.

EMPA 101 fabric satisfies all of the requirements of the model fabric and monitor described above: the carbon particles are chemically neutral. In addition, they do not form any strong physical or chemical bond with the cotton fabric that can obstruct their transport. It could also be inferred from figure 1 that the size of the carbon particles is very small. As such, an exact determination of the size of the carbon particles is not possible. However, an approximate particle size that could be assumed for the purposes of calculations would be ~ 0.1 μm. or so (H. Koster, personal communication). The diffusion coefficient of these particles (as calculated from the Stokes-Einstein equation) is quite small ~ 10^{-12} m^2/s and, hence, the acceleration in their transport can easily be measured. The characteristics of the fabric such as the concentration of the carbon particles per unit area and volume of the textile are also closely reproducible.

Need for detergent in the model process: Although the EMPA 101 fabric meets most of the requirements for the model textile and model process, it possesses an inherent shortcoming: the carbon particles are not free to be transported by convection, but adhere to the fiber along with the oil. These particles therefore need to be loosened from the surface of the yarns and fibers before being transported in the bulk. This necessitates pretreatment of the textiles before the ultrasound treatment. In order to select a proper

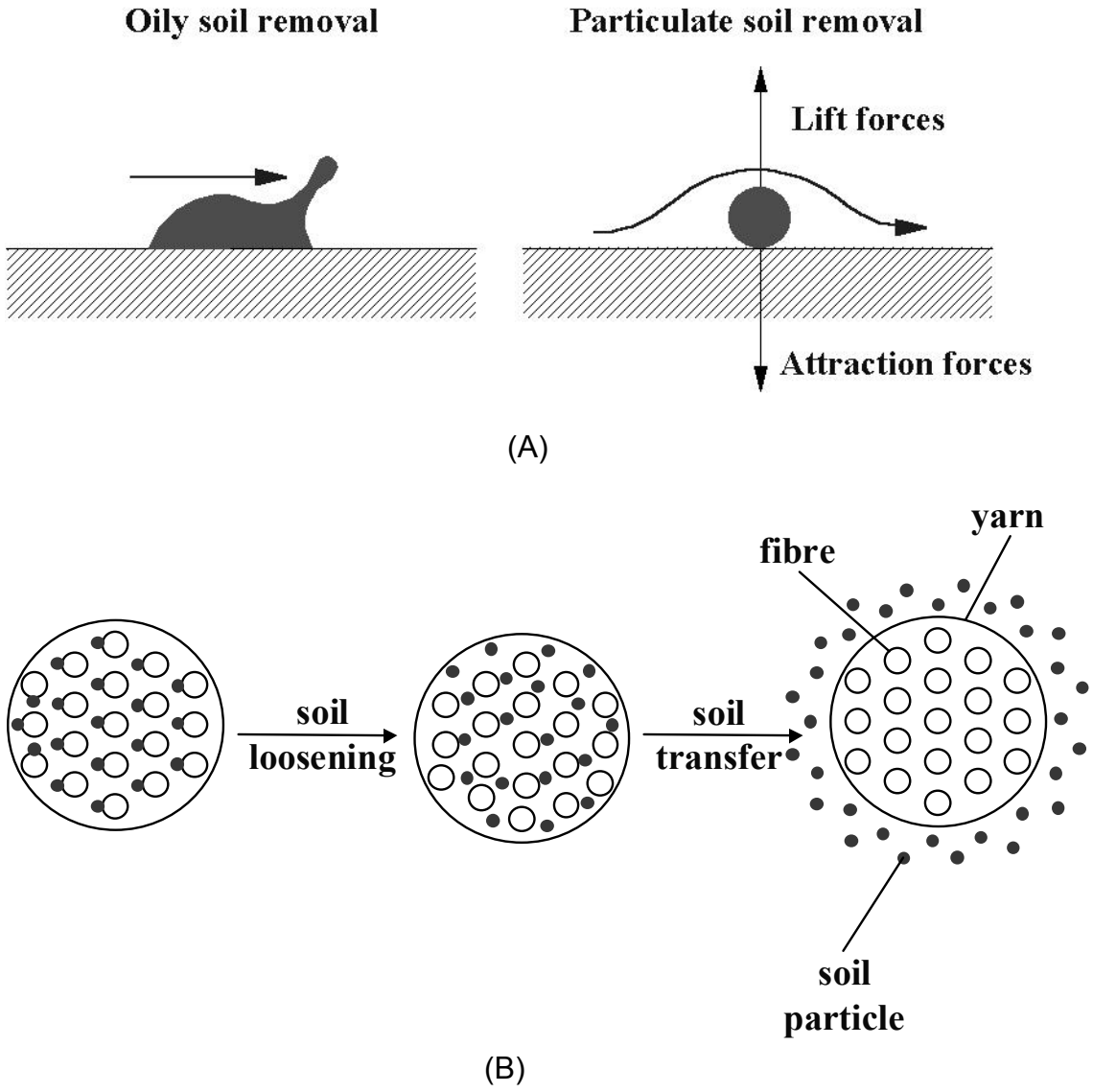

Figure 3: The detergency action in washing process. (A) The mechanism of loosening of oil and pigment soils from the surface of the textile. (B) The transport of loosened particle soil from the yarn to bulk due to convection.

pretreatment method, we make use of the theory of washing process (Jakobi and Lohr, 1987).

Different kinds of soils are broadly classified as oily/greasy soils, pigment soils and calcium containing soils. The soil on the EMPA 101 fabric is a combination of the oily/greasy (olive oil) and pigment (carbon soot) type of soils. Interfacial tension is the primary force resisting removal of oily soils, and this force needs to be minimized for the effectiveness of the washing process. An easy way of reducing the interfacial tension is to create adsorption layers comprised of ionic and non-ionic surfactants. For the pigment

soils, adhesion and displacement from the fabric surface are governed by the potential energy of the system, which passes through a minimum as a function of the distance of the particle from the fabric, as depicted in figure 2. This minimum is a measure of the potential barrier that must be overcome if the particle is to be removed from the fiber. When the particle is bound to the surface of the fiber, only a single common electrical double layer exists initially with no layer in the zone of contact between the particle and fiber. For the washing process to occur, new diffuse electrical double layers need to be created that lower the free energy of the system. These layers decrease the energy barrier for particle removal while increasing the energy barrier for particle deposition. An effective way of creating the diffuse electrical double layer and, hence, altering the fiber-pigment surface charges is to introduce a surfactant. Carbon black or soot acquires a negative charge in water. The negative charges of pigment and fibers are further increased by adsorption of an anionic surfactant. The corresponding mutual repulsion causes loosening of the carbon particles adhered to the fiber surface that assists their transport into the bulk due to convection. The process of the removal of pigment soil and particle soil is described in figure 3A, while the detergency action (soil loosening from the fiber surface and its transport to the bulk) is described in figure 3B.

In view of the above considerations, we have selected the anionic detergent sodium dodecyl benzene sulfonate for the pretreatment (surface wetting) of the EMPA 101 fabric before ultrasound treatment. We have used a solution of this detergent with concentration greater than the critical micelle concentration (CMC) for the wetting of the model fabric. It must be specifically mentioned that the extent to which the soil is loosened from the fabric surface due to detergent is a function of the time of soaking of the fabric. The longer the soaking time, the higher is the loosening of the soil from the fabric surface.

6.4 Experiments in commercial ultrasound bath

As an initial attempt towards establishing the physical mechanism of the ultrasonic enhancement of wet textile processes, experiments were carried out in a medium-scale (15-lit.) commercial ultrasound cleaning bath. Since most of the physical and chemical effects of ultrasound are attributed to (transient) cavitation, our first guess towards the physical mechanism of the ultrasonic wet textile treatments is transient cavitation. In order to assess the validity of this conjecture, we vary the position of the model textile in the standing wave field and selectively degas the fabric and the washing medium. A secondary aim of these experiments is to demonstrate the ultrasound-equipment related effects that can lead to artifacts, if ignored.

6.4.1 Experimental system

Experiments were carried out in a stainless steel ultrasound bath (Elma Inc., Model D-7700 Singen/Htw.; power 230 W). Figure 4 shows a schematic diagram of the experimental set-up. The dimensions of bath were: length: 30 cm.; width: 30cm.; height: 30 cm. The source of ultrasound was a detachable sonicator plate with dimensions:

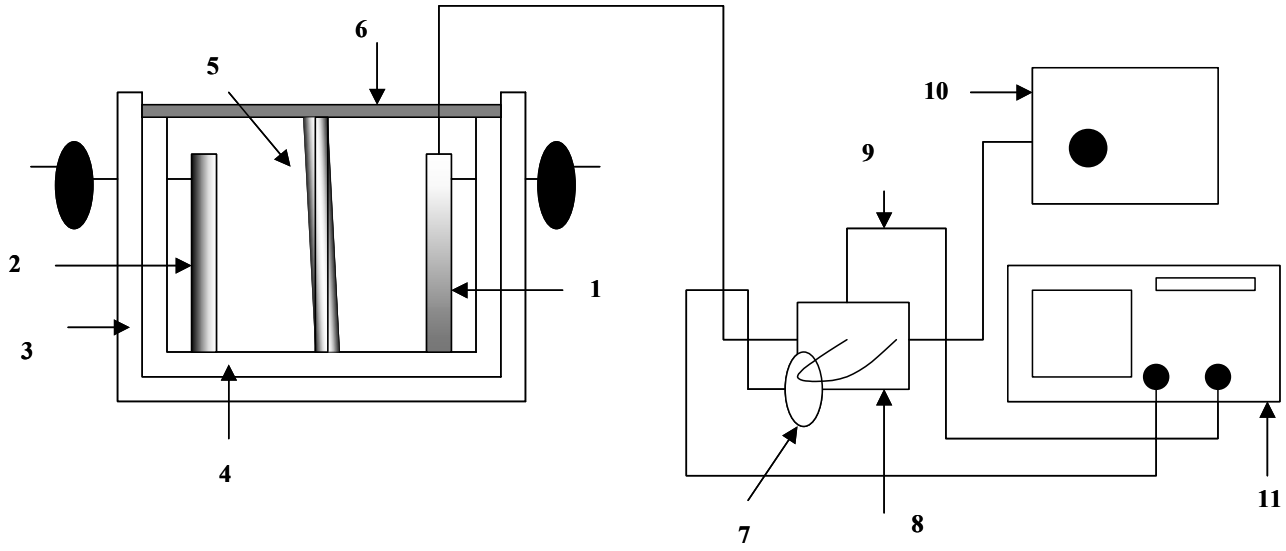

Figure 4: Experimental set-up for the washing experiments with commercial ultrasound bath. [Legends: 1 – Sonicator plate, 2 – Reflector, 3 – Thermal insulation of the bath, 4 – Absorbent rubber lining, 5 – Frame for the textile, 6 – Sliding bar, 7 – Current clamp, 8 – Voltage – current monitoring box, 9 – Voltage probe, 10 – Ultrasound amplifier, 11 – Digital oscilloscope].

breadth: 20 cm.; height: 20 cm. Thus, the sonicator plate had a surface area of 0.04 m^2. It had several transducers attached to it from inside. The ultrasound bath could adjust automatically the ultrasound frequency according to the variation in the resonance frequency of the transducers as a function of the system impedance. The frequency of the ultrasound waves generated by the sonicator plate during experiments was 30 kHz. The bath was lined from inside with 3 mm thick cork rubber. The cork rubber lining acts as an absorber for the ultrasound waves and, therefore, limits reflections from the walls, thus giving rise to an almost uni-directional sound field. A stainless steel frame (dimensions: height: 20 cm.; width: 20 cm.) was used to hold the model fabric during ultrasonic treatment. The bath had two parallel sliding bars at the top of the sonicator plate to fix the fabric frame in front of the sonicator plate. The sliding bars had grooves every 5 mm. that would assist fixing of the fabric frame at a particular distance from the sonicator plate. A 5-mm. thick stainless steel plate was used as a rigid reflector to create a standing wave field in the bath. The washing medium consisted of 1.75 g/l sodium dodecyl benzene sulphonate dissolved in demineralised water. For each set of experiments, the bath was filled with 13 liters of washing medium. The dissolved oxygen content of the medium was measured with an oxygen meter (Schott Handylab Inc., Model OX1). The voltage and current supplied to the sonicator plate were monitored on a 2-channel digital oscilloscope (Tektronics Ltd., Model 430A) using a voltage probe (Tektronics Ltd., Model 6138A) and a current clamp (Farnell Inc., Model PR 20).

6.4.2 Experimental procedure

Before conducting any physical or chemical process in an ultrasonic system, it is necessary to characterize the system to know its operational features. Characterization of the ultrasound bath was done in two parts: (1) an assessment of the power consumption

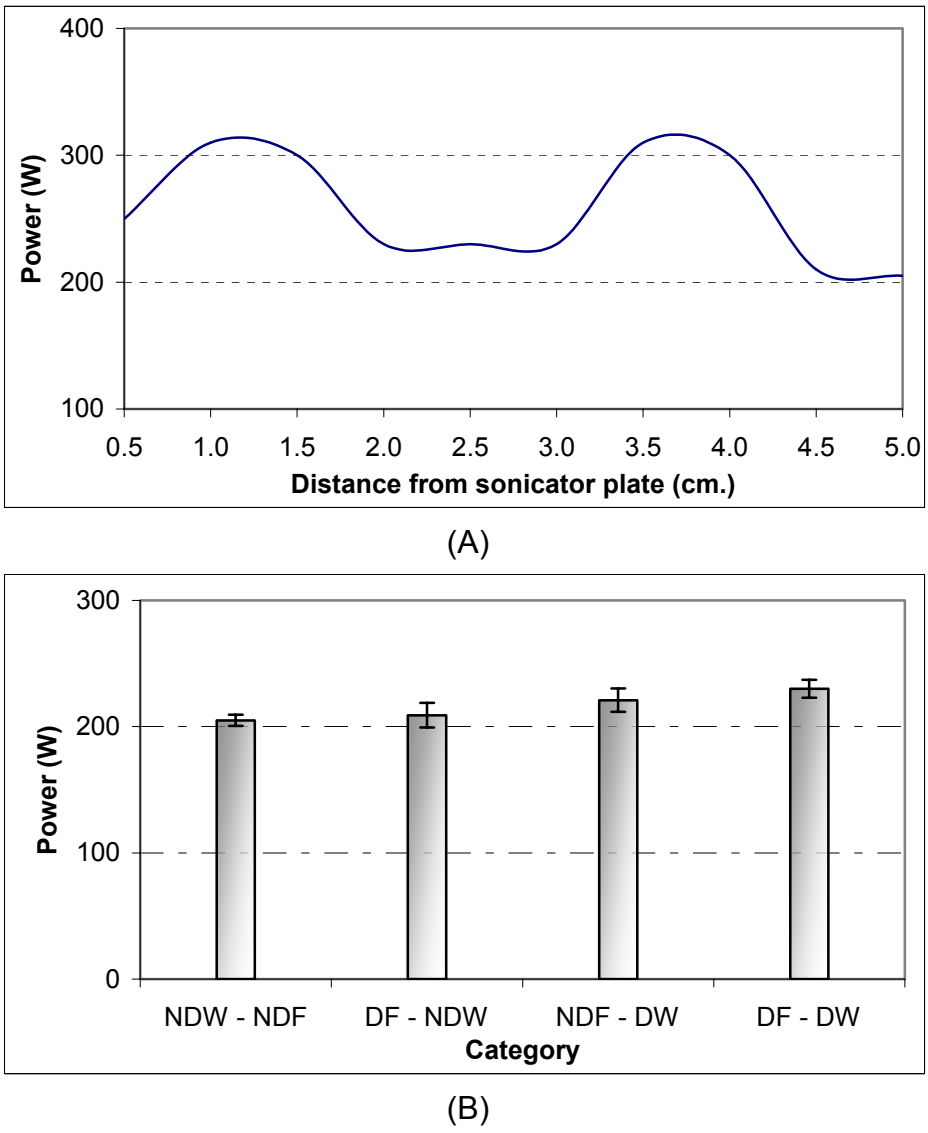

Figure 5: Power consumption of a commercial ultrasound bath. (A) Variation in the power consumption with the position of the fabric in the standing wave field. (B) Power consumption of the ultrasound bath in different categories of experiments.

for different processing conditions; (2) the mapping of the cavitation intensity in the bath at the location of the fabric.

***Power consumption of the bath*:** An important factor in the investigations in the physical and chemical effects of ultrasound is the energy input to the ultrasound equipment itself. A variation in this factor during different sets of experiments can give rise to artifacts that have roots in the variation of the energy dissipation pattern responsible for the physical or chemical effect. The electrical consumption of the ultrasound source can be a representative of the energy dissipation in the ultrasonic system. The electrical power consumption of the ultrasound source can be calculated from the measurement of the voltage, current supplied to the transducer, and the phase angle between them. The electrical power consumption of the bath was monitored as a function of the position of the model fabric in the standing wave field. The bath was filled with 13 liters of degassed

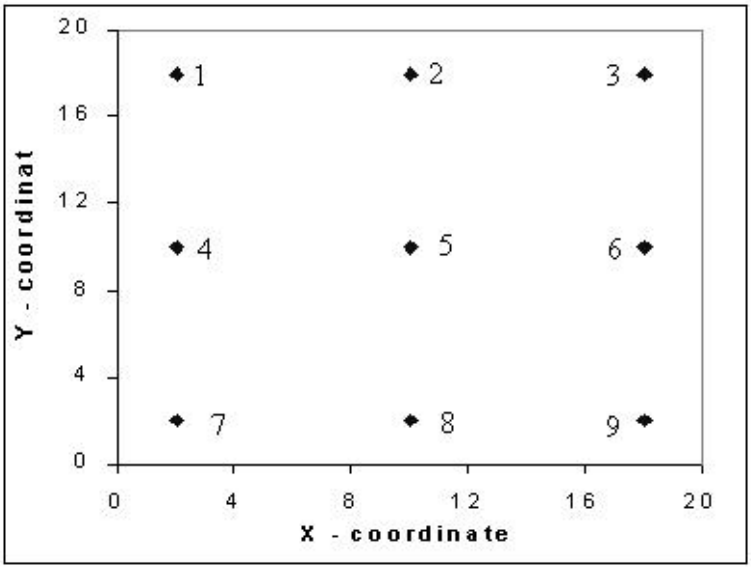

(A)

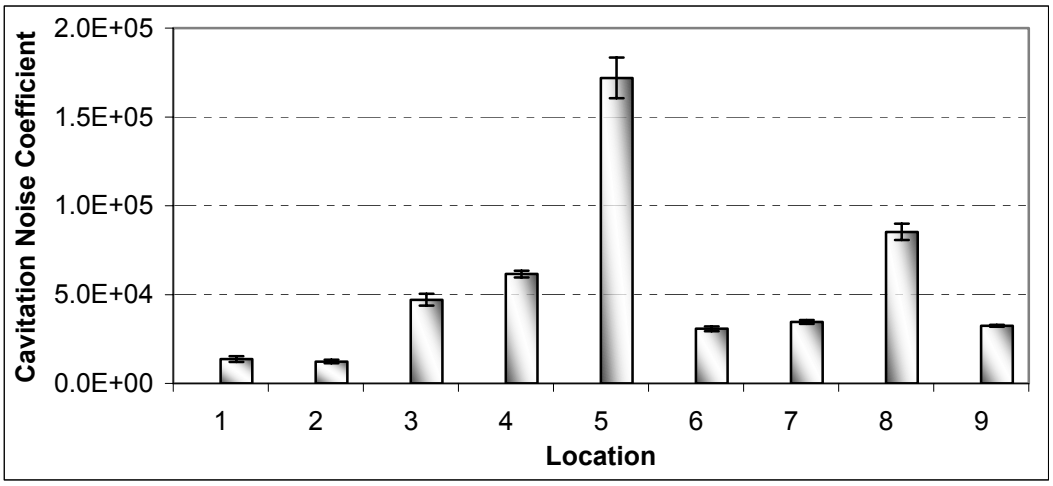

(B)

Figure 6: Characterization of the ultrasound bath. (A) Location of measurement of the cavitation intensity in the plane of washing experiments; (B) Cavitation noise coefficient distribution in the plane of washing experiments.

water (with a dissolved oxygen content lowered to 2 p.p.m.). A standing wave field was generated in the bath by placing a rigid reflector plate (made of stainless steel) in front of the sonicator plate at a distance of 5 cm, equal to the wavelength of 30 kHz ultrasound (denoted as λ). Next, the model fabric was placed in the frame and the frame was moved in the space between the sonicator plate and the reflector in steps of 5 mm. The power consumption of the ultrasound bath was monitored on a digital oscilloscope with the help of waveforms of the voltage and current consumed by the ultrasound transducers. The results of the measurements are shown in figure 5A. It can be seen that the power consumption of the ultrasound bath varies by as much as 50% with the textile positioned at the pressure node and the pressure antinode. The reason behind this variation is not

deducible due to the highly complex electrical construction of the signal generator and amplifier (which is not accessible to the user). Because of this large variation in the power consumption of the bath, the results of the experiments conducted at the pressure node and the pressure antinode cannot be compared.

Next, experiments were conducted to assess the variation in power consumption of the bath with selective degassing of the fabric and the washing medium for a fixed position of the model fabric in the standing wave field. Since these experiments were aimed at assessing the role of cavitation phenomena in the enhancement of the washing process, the position of the model textile was fixed at a distance of 2.5 cm from the sonicator plate (approximately a pressure antinode corresponding to $\lambda/2$, per discussion given in chapter 2). Figure 5B shows the power consumption of the bath for different processing conditions. It can be inferred from figure 5B that the power consumption remains more or less constant with a variation in the processing conditions. Thus, experiments with selective degassing of the textile and the washing medium conducted at one single location in the standing wave field can be compared with each other due to the constant power consumption of the bath.

Mapping the ultrasound field: As stated above, the location of the plane of the washing experiments was fixed at 2.5 cm. from the sonicator plate. The sonicator plate had several transducers attached to it from behind. These transducers did not produce a constant amplitude ultrasound wave but a modulated one with a modulation frequency of 100 Hz. The cavitation intensity at any particular location in the bath is a resultant of the interference between several ultrasound waves originating from different transducers. For this reason, mapping of the cavitation intensity in the plane of washing experiments was done using the method presented in chapter 4 (i.e. wavelet transform analysis of the acoustic emission). 9 measurement locations were chosen in the plane of experiments (numbered 1 to 9 in figure 6A). Prior to mapping of the ultrasound field, a standing wave field was generated in the bath by placing the rigid reflector plate in front of the sonicator plate. The bath was filled with 13 liters of degassed de-mineralized water with dissolved oxygen content lowered to 2 p.p.m. The bath was placed inside an x-y-z translation system, which was designed to hold the hydrophone at a particular position in the bath for the pressure signal measurement. The pressure signal measurements of duration 60 msec (averaging over 6 modulations) were carried out at each location with a small hydrophone (Brüel and Kæjer Ltd., Type 8103) connected to a charge amplifier (Nexus Amplifiers, Type 2690) with a sampling frequency of 1 MHz. To substantiate the reproducibility of the results, 10 pressure-signal measurements were obtained at each location. Wavelet transform analysis of the pressure signals was done with the program described in chapter 4. The cavitation noise coefficient (indicative of the local cavitation intensity) was defined as sum of the energy of levels 10, 12, 13 & 14 (which contain the sub-harmonic, ultra-harmonics and harmonics of the driving frequency, 30 kHz) in the wavelet transform of the pressure-signal. The spatial variation of the cavitation noise coefficient is shown in figure 6B. It can be inferred that the cavitation intensity is concentrated in the center of the plane of the washing experiments, while it decreases unevenly towards its sides. The explanation of this asymmetric reduction in the

cavitation intensity could be given along similar lines as in chapter 4, i.e., the difference in the electrical characteristics of the piezoelectric transducers and the irregular interference between the ultrasound waves generated by each of the transducers in the sonicator plate.

6.4.3 Techniques for degassing of water and fabric

Degassing of water was achieved using the chemical technique described in chapter 4. For degassing of the fabric, the method of pressurization was used. Since the model fabric has dual porosity – inter-yarn and intra-yarn porosity, removing all the air pockets trapped in these pores is quite difficult. Therefore, we use a simpler method based on the principles presented in chapter 2 and chapter 5 for degassing the fabrics. Instead of removing the air pockets from the textile, an attempt is made to dissolve these pockets locally using a high driving force for dissolution. This large driving force could be achieved by two means: first, soaking the fabric in water with lowered dissolved gas concentration and, secondly, increasing the saturation concentration of the gas in water by raising the static pressure of the system. With combination of these two techniques, even the tiniest (~ 5 μm or so) air pockets in the intra-yarn pores can be dissolved. Once dissolved, these air pockets cannot form nuclei for cavitation inside the textiles. Due to the large difference between the ultrasound wave period and the diffusion time scale of air (as explained in chapter 5), it is also not possible that these air pockets will diffuse out during the rarefaction half-period of the acoustic wave. For this reason, the required distinction between the cavitation in the bulk liquid in the close vicinity of the textile and the cavitation inside the textile can be achieved.

The model fabric pieces (height & width 20 cm.) were soaked in degassed water (with dissolved O_2 content lowered to 2 p.p.m.) in sealed plastic bags. The bags were then kept inside a pressure vessel with the pressure raised to 6.5 bars using compressed air for 12 hours. The plastic bag will avoid direct contact between water surrounding the textile and the compressed air. This procedure ensures a nearly complete dissolution of the air pockets, thus, essentially *de-nucleating* the textile.

6.4.4 Washing experiments

The experiments were divided into four different categories as follows:

- Non-degassed fabric and non-degassed washing medium (NDF-NDW).
- Degassed fabric and non-degassed washing medium (DF-NDW).
- Non-degassed fabric and degassed washing medium (NDF-DW).
- Degassed fabric and degassed washing medium (DF-DW).

In each of these categories, 5 experiments were performed with different pieces of the model fabric to assess the reproducibility of the results. The bath was filled in each set of experiments with 13 liters of the washing medium (1.75 g/l of sodium dodecyl benzene sulfonate). The fabric frame was fixed at a distance of 2.5 cm from the sonicator plate. The fabric was soaked for 5 minutes so as to wet its surface and loosen the soil

from it. As mentioned earlier, the soaking the fabric for a longer time will result in higher loosening the soil from the surface of the textile. Thus, the cleaning efficiency is also a function of the extent to which the soil is loosened from the surface of the textile. Since our prime interest in the present study is to assess the washing efficiency in terms of the soil transport from the textile, we have kept the soaking time of the fabric constant in all experiments. The dissolved oxygen content of the washing medium was ~ 10 p.p.m. (equal to saturation concentration at 20^{o}C) for the categories NDF-NDW and DF-NDW. In case of the categories with degassed washing medium (NDF-DW and DF-DW), the dissolved oxygen content of the medium was lowered to 2 p.p.m. using the chemical method described in chapter 4. The average temperature of the washing medium during experiments was $20(\pm 1)^{o}$C. The time of the ultrasonic treatment of the fabric was 3 min. After ultrasonic treatment the frame was removed from the ultrasound bath and was rinsed gently to remove the detergent solution over it. Later, the model fabric was removed from the frame and was dried in air.

6.4.5 Quantification of the washing efficiency

The conventional method of quantifying washing efficiency in textile research is to measure the change in the reflectance of the fabric and relate it to the soil removal through the Kubelka-Munk factor (denoted as K/S). This technique is quite useful for the quantification of the washing effect on textile samples of small size. However, the fabric samples used in the present study were of a large size. Thus, using the conventional methodology for the quantification of washing effect would not only be very cumbersome but would also introduce significant error if the fabric reflectance is measured by dividing the treated fabric sample into several smaller elements of smaller dimensions. Therefore, we have used a simpler method, which is derived from the conventional method described above for the quantification of the washing effect. This method is described as follows:

The ultrasound treated fabric was scanned using a digital scanner (Hewlett and Packard Inc., Model: ScanJet 6300C) to obtain a 8-bit gray scale bitmap image. The Grey scales of the bitmap image varied from 0 to 255; with 0 and 255 corresponding to the darkest and the whitest pixel respectively in the image. This image was then processed using Corel Photo-Paint software (version 8.0). Two main aspects of the image were analyzed:

- Average gray scale value of the pixels, which represents the overall washing efficiency on the entire fabric.
- The standard deviation in the gray scale value of the pixels in the fabric image that represents the uniformity or homogeneity of the washing effect over the entire fabric surface.

The washing efficiency (η) is defined on the basis of the percentage change in the gray scale as:

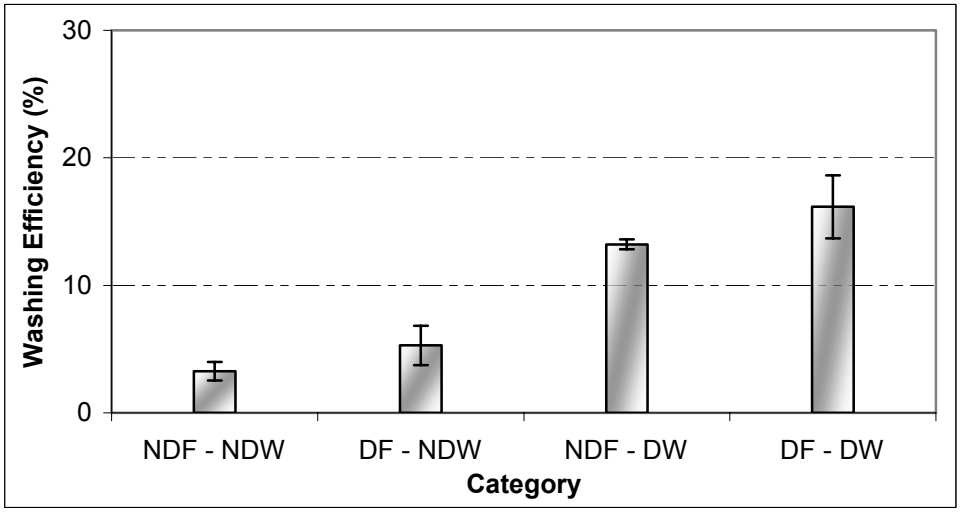

(A)

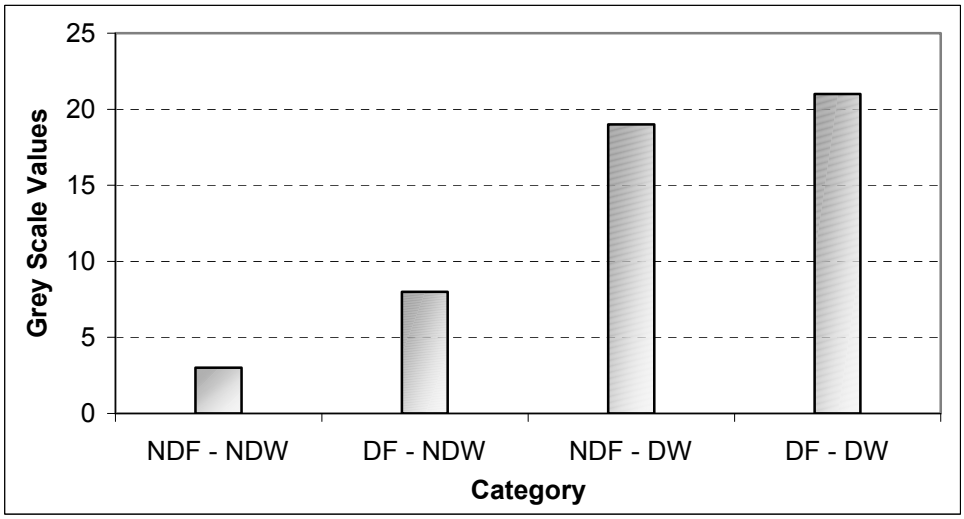

(B)

Figure 7: Results of the washing experiments in commercial ultrasound bath. (A) Trends in washing efficiency with different categories of experiments; (B) Average standard deviation in the gray scale of pixels in the images of samples in different categories of experiments.

$$\eta = \left(\frac{X - Y}{Y}\right) \times 100$$

X is the average gray scale value of the image of treated (or washed) model fabric and Y is the average gray scale value of the image of untreated model fabric.

6.4.6 Results and discussion

The trends in the washing efficiency with process parameters are shown in figure 7A, and the average standard deviation in the gray scale of the pixels in different sets of experiments is shown in figure 7B. Figure 8 shows the pictures of the ultrasound treated samples in different sets of experiments along with the gray scale-population distribution

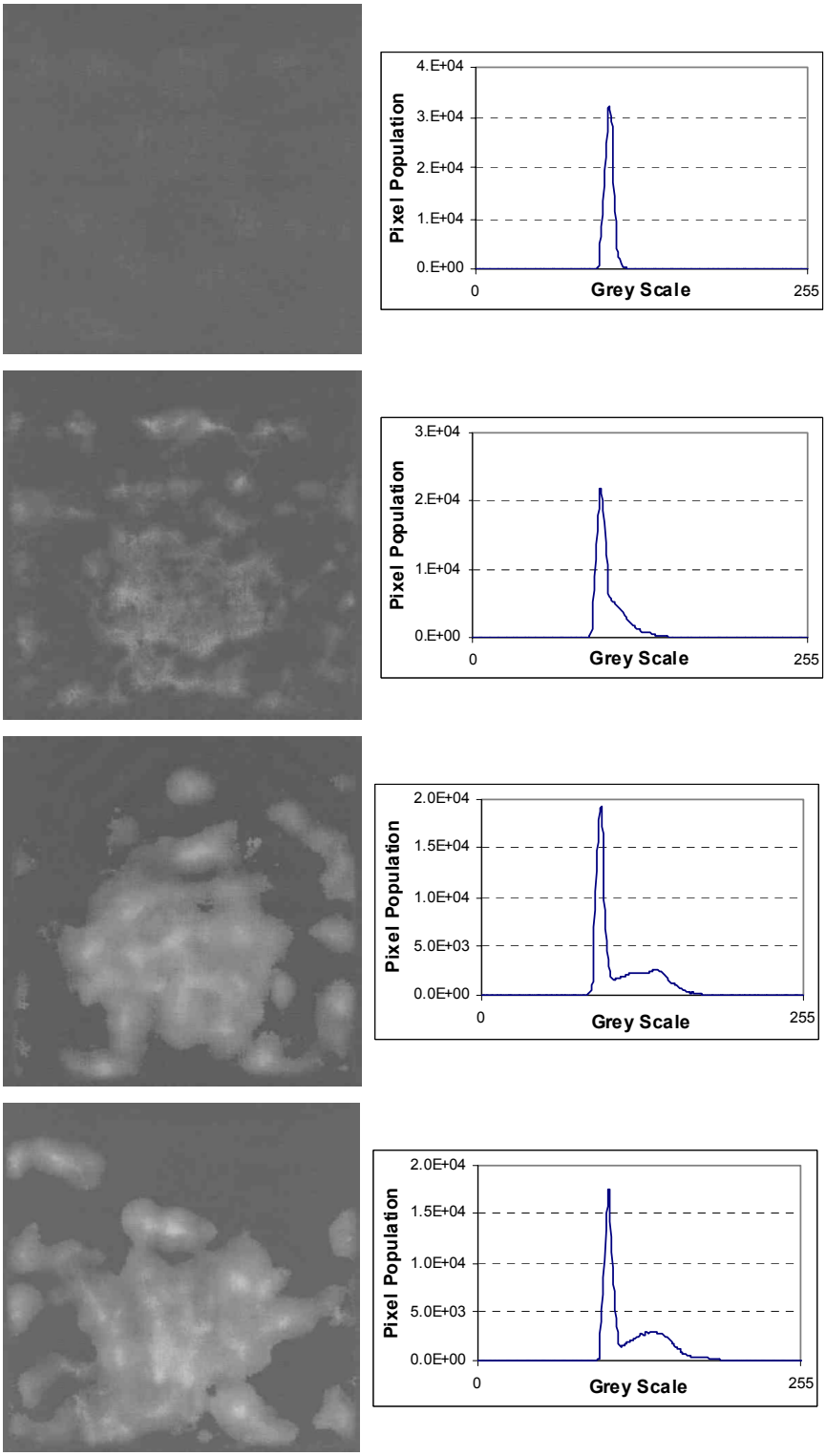

Figure 8: Pictures of treated EMPA 101 fabrics in ultrasound bath for different categories and the Grey scale population distribution of pixel in their images. (A) NDF-NDW; (B) DF-NDW; (C) NDF-DW and (D) DF-DW.

of the pixels. It can be inferred from figure 7A that a reduction in the dissolved gas content of the medium causes a sharp rise in the washing efficiency. Figure 7B reveals that the non-uniformity of the washing effect over the treated sample also rises with

degassing of the fabric and of the washing medium.

Interpretations of the results of the present study, on the basis of the results of chapter 5, help us resolve the physical mechanism of the ultrasonic washing process. It was demonstrated in chapter 5 that degassing of the washing medium causes an increment in the cavitation intensity in the medium. A marked rise in the washing efficiency with degassing of the washing medium indicates a significant role of cavitation phenomena in the washing process. A comparison of figures 6 and 8(C & D), which show complete image of the treated fabric, reveals an interesting result that the local variation in the washing efficiency over a single textile sample fairly corresponds to the variation in the cavitation noise coefficient (indicative of the cavitation intensity) in the plane of the washing experiments for the categories NDF-DW and DF-DW. This further supports the significant role of cavitation phenomena in the washing process. The rise in the standard deviation in the gray scale values of the pixels in the categories with degassed washing medium indicates more non-uniformity of the washing effect on the fabric surface. This result could be attributed to differences in cavitation intensity at different locations in the plane of washing.

As far as the question of the location of the cavitation phenomena responsible for the washing effect is concerned (whether in the bulk medium or inside the fabric itself), the present experiments do not provide a clear answer. A sharp rise in the washing efficiency with the degassing of the washing medium points towards a greater role of cavitation in the medium in the washing process; nonetheless, a small rise in the average washing efficiency with a large standard deviation after degassing of the fabric makes a firm conclusion about the location of cavitation rather difficult. Several experimental errors could also not be ruled out, such as a non-uniform degassing of the textile sample due to its large size, and the entrainment of air along with the fabric frame as it is introduced into the bath.

6.4.7 Conclusion

The present study provides useful clues in deducing the physical mechanism of the ultrasonic enhancement of the wet textile processes. Different combinations of the process conditions reveal that a variation in the gas content of the system (textile and washing medium) has a dramatic effect on the washing efficiency with ultrasound. This result points towards (transient) cavitation as the physical mechanism behind the ultrasonic enhancement of the washing process for the reasons explained in chapter 5. The conformity between the spatial variation of the cavitation intensity and the washing effect on the textile sample textile further corroborates the significant role of cavitation phenomena in the washing process. The question about the location of cavitation events, however, remains unanswered. Thus, this study necessitates more controlled experiments with smaller textile samples and a more precisely defined ultrasound field.

Another interesting aspect of this study is that it brings out the secondary effects that are responsible for production of artifacts during experiments of ultrasound assisted wet textile processing. These effects have their origin in variation of the power consumption of the system. So as to obtain accurate conclusions from the experiments

done with varying process conditions, it is of the utmost importance to have a constant-power ultrasound system that can provide a consistent basis for the comparison and the analysis of the results.

6.5 Experiments in the specially built ultrasonic system

The preliminary experiments towards establishing the physical mechanism of the ultrasonic enhancement of textile treatments indicated cavitation phenomena as the major contributor to the observed effects, although the question of the location of occurrence of the cavitation events remained unanswered. However, due to several experimental limitations, such as modulated ultrasound field, non-uniform cavitation intensity distribution, and large textile samples, a firm conclusion about the physical mechanism of the ultrasonic washing process could not be drawn. In addition, there were several secondary effects such as the presence of surfactant in the washing medium, which decreases the transient cavitation threshold. Due to the reduction in the cavitation threshold, the bubble population possibly rises, which may significantly disturb the standing wave field produced in the bath. In addition, the methods of variation in the static pressure of the system and the de-nucleation of the washing medium could not be applied due to the large size of the bath.

New experiments were performed using a much smaller apparatus, and with a special built ultrasonic system, which overcomes the demerits of the commercial ultrasound bath. Moreover, the new system was so designed as to use all the permutations and combinations of all the methods described earlier.

6.5.1 Experimental set-up

The experimental set-up is described (along with a schematic diagram) in detail in chapter 3. The only change made in this set-up for the present experiments was the removal of the hydrophone from the experimental cell. After the removal of the hydrophone, connections made for it in the experimental cell and the pressure-vessel were closed properly.

Characterization of the ultrasonic system: Since the ultrasonic system in the present experiments had precise electrical power regulation facility for different processing conditions, there was no need to assess the power consumption of the system, as done in the earlier study with the commercial ultrasound bath. However, the characterization of the sound field in the experimental cell needs to be done.

A standing wave field can be generated in the experimental cell by adjusting the distance between the stainless steel bottom (which acts as a rigid reflector) and the tip of the ultrasound horn equal to one wavelength (λ) of ultrasound. The basic principles of standing wave formation due to the acoustic wave reflection at a rigid surface, described in chapter 2, help us characterize the sound field in the experimental cell in the present work. According to the analysis of the pressure and velocity variation in the standing wave field given in chapter 2, the locations of pressure minimum (or velocity maximum)

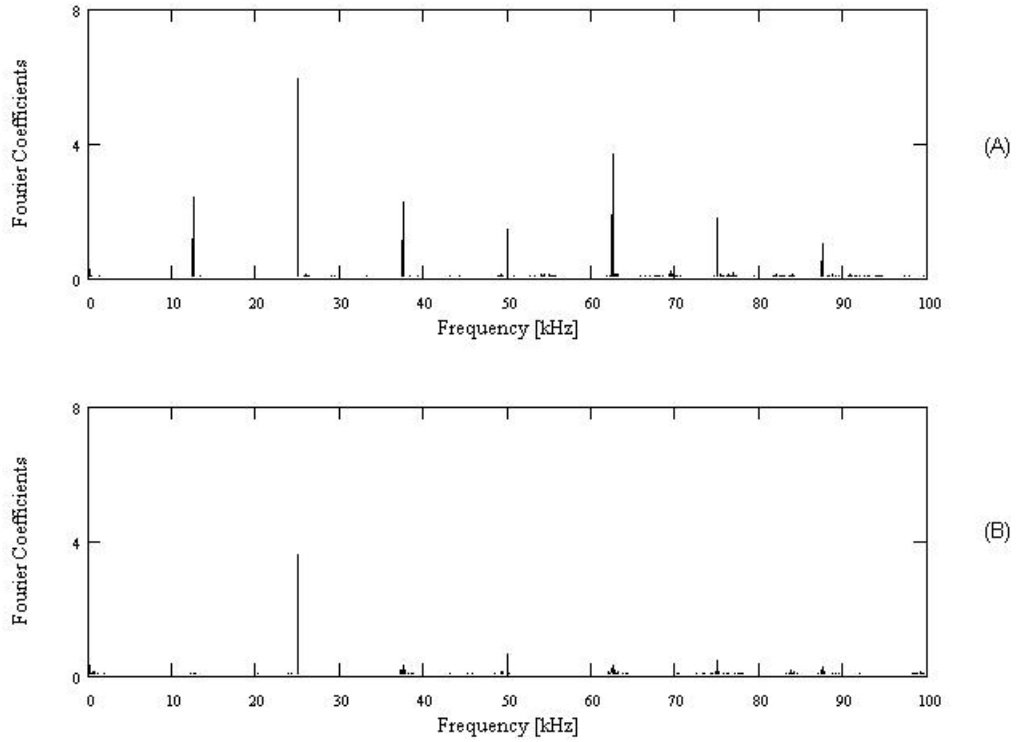

Figure 9: Characterization of the standing wave field generated in the experimental cell in specially built ultrasonic system. (A) Acoustic spectrum at pressure antinode (distance λ/2 from the rigid bottom). (B) Acoustic spectrum at pressure node (distance 3λ/4 from the rigid bottom).

occur at a distance of λ/4, 3λ/4, 5λ/4….etc while the locations of pressure maximum (or velocity minimum) occur at a distances of λ/2, λ, 3λ/2….etc. from the rigid surface for plane-wave reflection from it. In order to confirm this theoretical result, pressure measurements were done in the experimental cell using a very small (4 mm) (un-calibrated) hydrophone at two locations viz., at distances λ/4 & λ/2 from the rigid bottom of the cell with degassed water as the medium. The ultrasound horn was driven at 25 kHz with a power input of 20W. The distance between the tip of the horn and the rigid bottom of the experimental cell was adjusted to 6 cm (which is equal to wavelength of 25 kHz ultrasound in water). For a power input of 20W the ultrasound horn produced an acoustic wave with pressure amplitude ~ 1.3 bar (which is above the transient cavitation threshold for bubbles of sizes 5-10 μm at 25 kHz frequency according to the analysis of the transient cavitation threshold given in chapter 2). Since the ultrasound source in this system produces ultrasound waves with a constant pressure amplitude, the pressure signals measured at different locations in the cell can be analyzed using the conventional Fourier Transform as done by Moholkar *et al.* (2000). Figure 9 shows the FFT of the pressure signals (duration: 12 msec; sampling frequency: 2.5 MHz) obtained at distances λ/4 & λ/2 from the rigid reflector. The differences in the characteristics of the acoustic spectra shown in figure 9 are clear: the amplitude of the fundamental peak in the acoustic spectrum corresponding to the driving frequency (indicative of the acoustic pressure amplitude) at location λ/2 from the rigid reflector is much higher than the amplitude of the corresponding peak at location λ/4. In addition, the subharmonic peak (indicative of

transient cavitation) is quite prominent in the acoustic emission spectrum at location λ/2 while it is completely absent in the acoustic emission spectrum at location λ/4. Since the tiny hydrophone used in the present study was not calibrated, it is not possible to obtain the absolute values of the acoustic pressure amplitudes although their relative magnitudes at different locations can give approximate information about the locations of the pressure node and the pressure antinode. Interpretation of the above result is rather straightforward: At location of λ/2 from rigid bottom the incident and reflected waves add, and hence there is a pressure maximum, due to which the cavitation activity is also maximum. At location of λ/4 the incident and reflected waves have destructive interference, due to which the resultant acoustic pressure amplitude is minimum, and hence little cavitation activity is present. Another feature of the acoustic wave phenomena (mentioned earlier in chapter 3), which is clear from these results is that the resultant acoustic pressure amplitude at λ/4 is not zero, but has some positive residual value. A possible reason for this is that due to presence of small bubble fraction the wavelength of sound is not exactly 6 cm but somewhat less, which causes a shift in the position of pressure node. Thus the characterization of the acoustic wave field in the experimental cell approximately confirms the theoretical prediction of the location of the pressure node and the pressure antinode.

6.5.2 Washing experiments

The experiments were divided in four categories as done earlier:

- Non-degassed fabric and non-degassed washing medium (NDF-NDW).
- Degassed fabric and non-degassed washing medium (DF-NDW).
- Non-degassed fabric and degassed washing medium (NDF-DW).
- Degassed fabric and degassed washing medium (DF-DW).

Each of the above four categories of experiments were carried out at the pressure node and of the pressure antinode in the standing wave field. Thus, with the parameter of the different positions in the standing wave field, there were in total 8 sets of experiments. In addition, the static pressure of the experimental system was varied and the above-mentioned 8 sets of experiments were conducted at static pressures of 1 bar (atmospheric), 2 bar, 3 bar, and 5 bar. As far as the method of de-nucleation of the washing medium was concerned, it could not be applied to the sets with non-degassed washing medium (viz. NDF-NDW and DF-NDW) since de-nucleating gassy water is quite difficult. Therefore, experiments with de-nucleation of washing medium could be carried out only for the categories NDF-DW and DF-DW. Again, the experiments in these two categories were carried out at the pressure antinode and the pressure node.

In each set of the experiments 3 runs were conducted with different pieces of the model fabric (dia.: 60 mm) in order to assess the reproducibility of the results. The model fabric was soaked in the detergent solution (1.75 g/l of sodium dodecyl benzene sulfonate) for 5 minutes before ultrasonic treatment. The model fabric was then fixed between the glass rings of the experimental cell in a water bath (using either non-degassed or degassed water as the washing medium depending on the set) to avoid

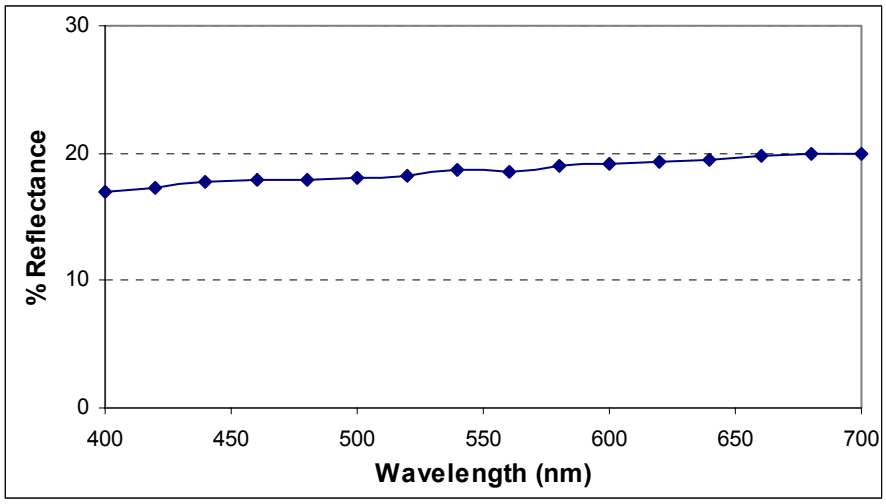

Figure 10: The reflectance of the EMPA 101 model fabric at different wavelengths measured using X-rite reflectometer.

entrapment of air beneath the fabric. Since the ultrasound effects are known to be directionally sensitive, a small identification mark was made on the side of the fabric facing the ultrasound horn, which would later assist in the separate quantification of the washing effect on the two sides of the fabric. In each experiment 250 ml water (degassed or non-degassed depending on the set) was used as the washing medium. It should be specifically mentioned that, unlike in earlier studies, there was no detergent present in the washing medium in the present experiments. The dissolved oxygen content of the washing medium was ~ 10 p.p.m. for the categories NDF-NDW and DF-NDW, while it was lowered to 2 p.p.m. for categories NDF-DW and DF-DW, using the chemical method described in chapter 4. The time of ultrasound treatment was 3 min with a power input of 20W to the ultrasound horn at 25 kHz frequency. The standing wave field was generated in the experimental cell by adjusting the distance between the ultrasound horn tip and the rigid bottom of the cell to one-wavelength of ultrasound. The small groove in the tip of the ultrasound horn (that can entrap some gas bubbles, as mentioned in chapter 5) was filled with silicon rubber to avoid random nucleation, due to irregular gas bubble entrapment in the groove of the horn. Instead, 10 μL solution of polystyrene latex particles suspension in water (particle size: 0.5 μm.; concentration: 2% wt.) was added to the washing medium for cavitation nucleation before the ultrasonic treatment. The tiny air pockets trapped in the polystyrene particle suspension can provide nuclei for cavitation in the washing medium (Holland and Apfel, 1990). This procedure ensures a uniform and consistent nucleation in the washing medium. For the experiments with de-nucleation of the washing medium, the experimental procedure was exactly the same except that the polystyrene suspension was not added to the washing medium. In addition, the water was left standing for about 20 minutes after degassing. This causes dissolution of most of the micro-bubbles in water, which could possibly form nuclei for cavitation. Thus, a nearly complete de-nucleation of the medium was achieved. After ultrasound treatment the model fabric was removed from the cell and was dried in air.

6.5.3 Quantification of the washing effect

Since the fabric samples used in the present study were of a small size, the conventional method of measuring the reflectance of the fabric for the quantification of the soil concentration in the fabric could be easily employed. An important parameter in the fabric reflectance measurement is the wavelength of the incident light, since the reflectance of the soil particles is a function of wavelength. For this reason, the reflectance measurements were carried out using an untreated piece of EMPA 101 fabric for a range of wavelengths of light (400 – 700 nm) using a reflectometer (X-Rite Inc., Model 968). The results of these measurements are shown in figure 10. It can be seen that the reflectance of the soil in the model fabric is almost insensitive to the wavelength of incident light. The reflectometer also had a facility of converting the reflectance measurement into L (lightness), a (color shift between green-red) & b (color shift between blue-yellow) values according to the CIELAB scales.

The washing efficiency was defined as follows:

$$\eta = \left[\frac{L_{treated} - L_{untreated}}{L_{untreated}} \right] \times 100$$

It should be pointed out that the lightness value of white cotton is ~ 87 (and not 100). As such, a washing efficiency (per definition above) of 85% would indicate complete removal of the soil from the fabric (or in other words total washing). The directional sensitivity of the washing effect was accounted for by first calculating the washing effect on one treated sample using the mean of L values on the front and the back side of the sample, and later, the overall washing efficiency in one set was calculated by averaging the L values of all 3 textile samples in that set calculated, as described above.

6.5.4 Results and discussion

The trends in the washing efficiency with different permutations and combinations of the process parameters are shown in figures 11 to 15. The coupling of the basic principles of the ultrasound wave phenomena and bubble dynamics, presented in chapter 2, and the energetics of the ultrasound processor, presented in chapter 5, to the results of the present study help us determine the mechanism of the ultrasonic washing process. The effects of the process parameters on the acoustics and cavitation related phenomena were described earlier. We divide the results of the experiments in three parts:

1. Experiments at atmospheric pressure (1 bar).
2. Experiments at raised static pressures (2, 3, and 5 bar).
3. Experiments with de-nucleation of the washing medium.

***Static pressure 1 bar*:** The results of the experiments with selective degassing of fabric and of the washing medium conducted at pressure antinode and pressure node are shown in figure 11 A and B respectively. The smallest washing efficiency at both pressure node

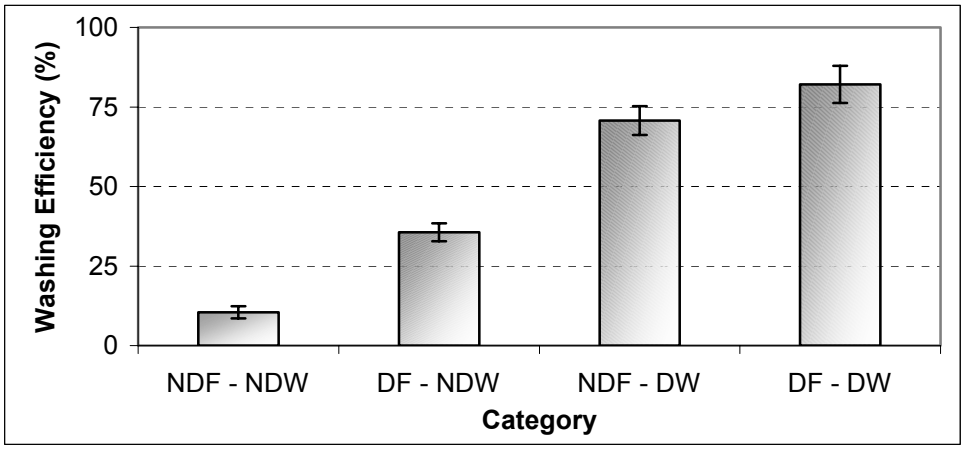

(A)

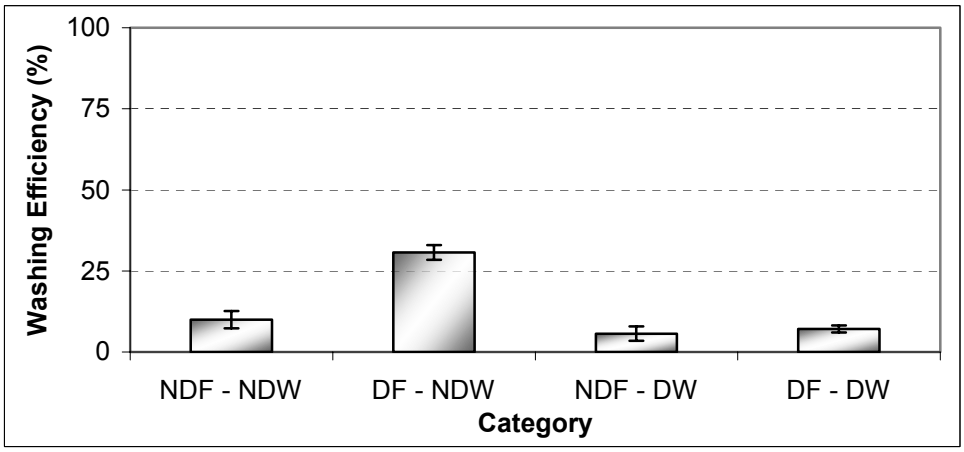

(B)

Figure 11: Trends in the washing efficiency in different categories of experiments conducted at static pressure 1 bar using specially built ultrasonic system. (A) Washing efficiencies at pressure antinode. (B) Washing efficiencies at pressure node.

and antinode is seen for the case NDF-NDW. This is obviously due to the large attenuation of the ultrasound waves in the gassy washing medium as a result of large bubble population and significant growth of the bubbles, due to the large dissolved gas concentration in the medium. As a result, the intensity of both cavitation and acoustics related phenomena in the medium are minimal. Degassing of the fabric alone does not cause a major change in the washing efficiency due to the fact that only a small fraction of the total cavitation nuclei in the medium are contributed by the fabric, due to large liquor ratio. Thus, phenomena of attenuation of the ultrasound wave and rectified diffusion do not change by degassing of the fabric. However, slightly higher washing efficiency for the category DF-NDW could be due to the fact that, since the fabrics were degassed by pressurization in water for 12 hours, the soil on the surface of the fabric could have been loosened to a larger extent (than the loosening by mere soaking in detergent solution) that could assist its easier transport away from the fabric. The

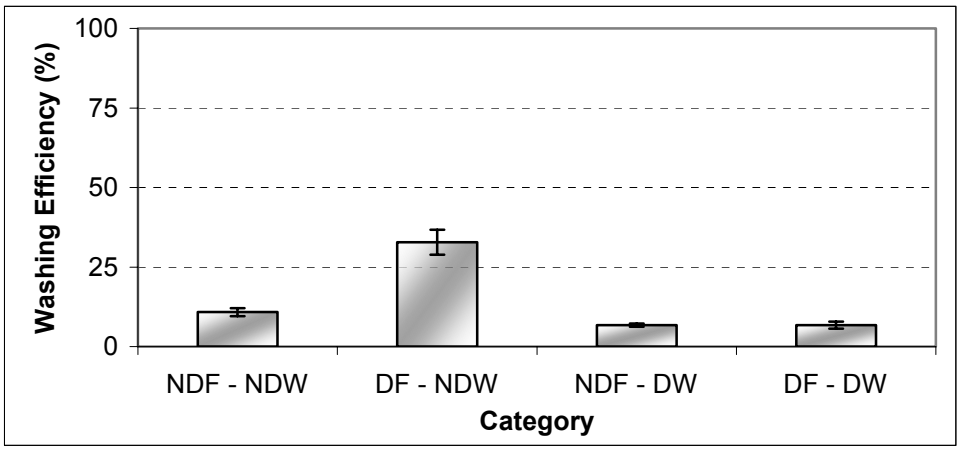

(A)

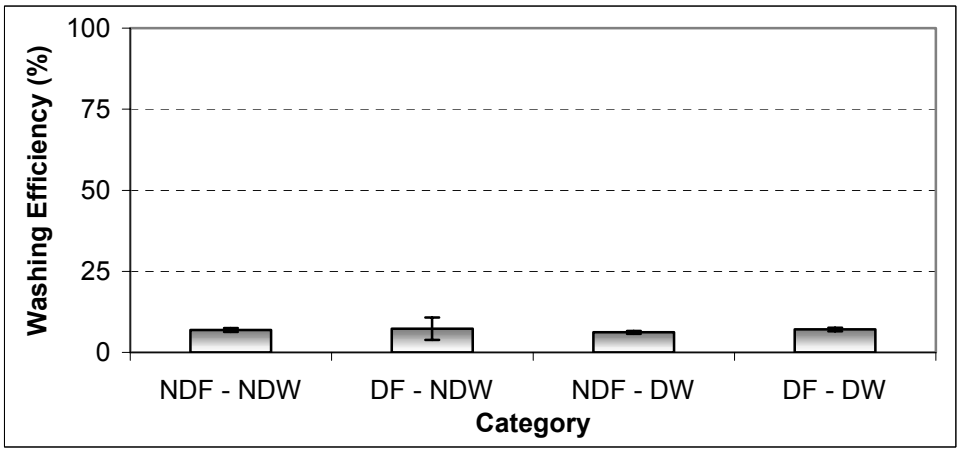

(B)

Figure 12: Trends in the washing efficiency in different categories of experiments conducted at 2 bar static pressure using specially built ultrasonic system. (A) Washing efficiencies at pressure antinode. (B) Washing efficiencies at pressure node.

washing efficiency shows a marked rise at the position of the pressure antinode for the category NDF-DW when the washing medium is degassed but not the fabric. When both fabric and washing medium were degassed, the washing efficiency at pressure antinode shows only a small rise over the washing efficiency in category NDF-DW. At the position of the pressure antinode cavitation related phenomena mainly contribute to the washing effect. Degassing of the medium raises the cavitation intensity in the medium, as explained in chapter 5. The rise in the washing efficiency at the pressure antinode with the degassing of the medium clearly points towards cavitation phenomena as the physical mechanism. Degassing of the fabric along with the medium makes no change to the cavitation intensity in the medium, which is reflected in no significant difference between the washing efficiencies of the categories NDF-DW and DF-DW. Although the average washing efficiency for the category DF-DW is slightly higher than the category NDF-DW, the error analysis reveals that the washing efficiencies in these categories are

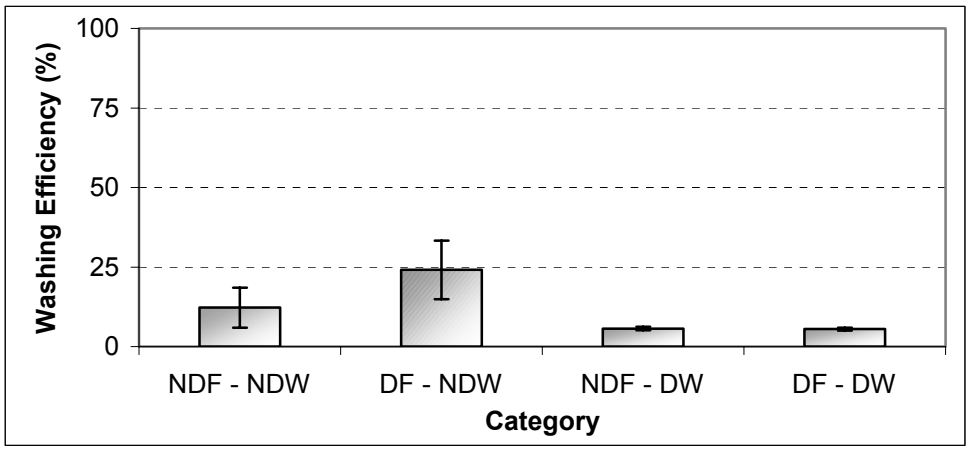

(A)

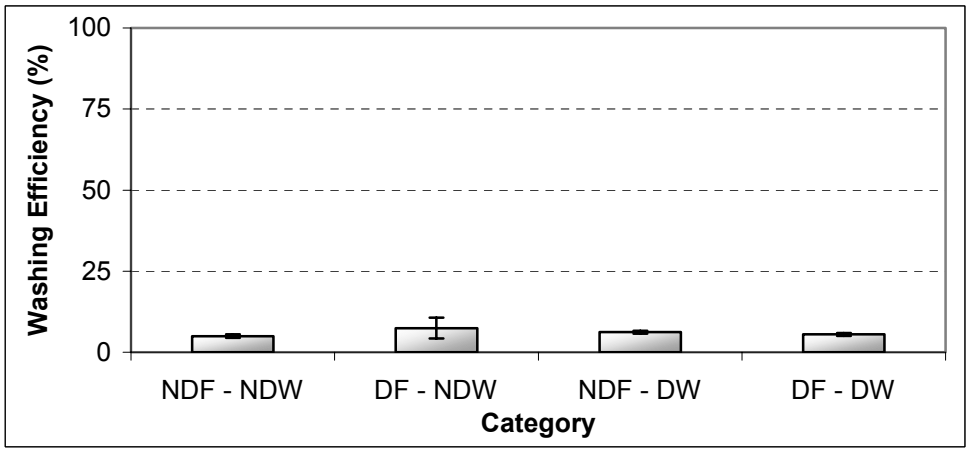

(B)

Figure 13: Trends in the washing efficiency in different categories of experiments conducted at 3 bar static pressure using specially built ultrasonic system. (A) Washing efficiencies at pressure antinode; (B) Washing efficiencies at pressure node.

quite closely overlapped. An explanation of this result can be given along similar lines as for the difference between the washing efficiencies for the categories NDF-NDW & DF-NDW: since a small fraction of the total number of cavitation nuclei are contributed by the fabric, the cavitation intensity at the pressure antinode does not change much with the degassing of the fabric. In addition, as mentioned earlier, the degassing technique of the fabric (that could result in more loosening of the soil from the fabric surface) can also be responsible for this difference. On the contrary, the washing efficiency at the pressure node is far smaller for the categories NDF-DW and DF-DW. At the position of pressure node (or velocity antinode) acoustics related phenomena (such as oscillatory ultrasound velocity) are dominant. Low washing efficiencies at the position of pressure node for the categories NDF-DW and DF-DW indicate a negligible role of acoustic phenomena in the washing process. Thus, the results of the washing experiments at atmospheric static pressure indicate that (transient) cavitation is the principal physical phenomenon behind

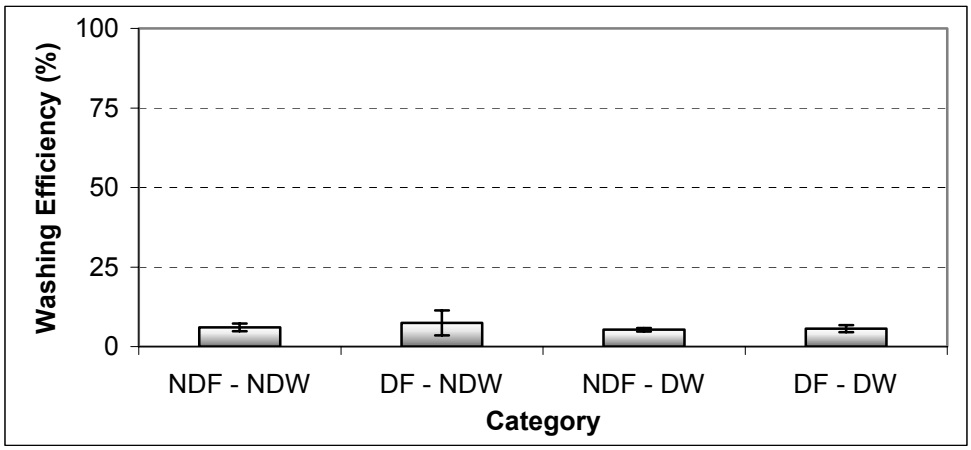

(A)

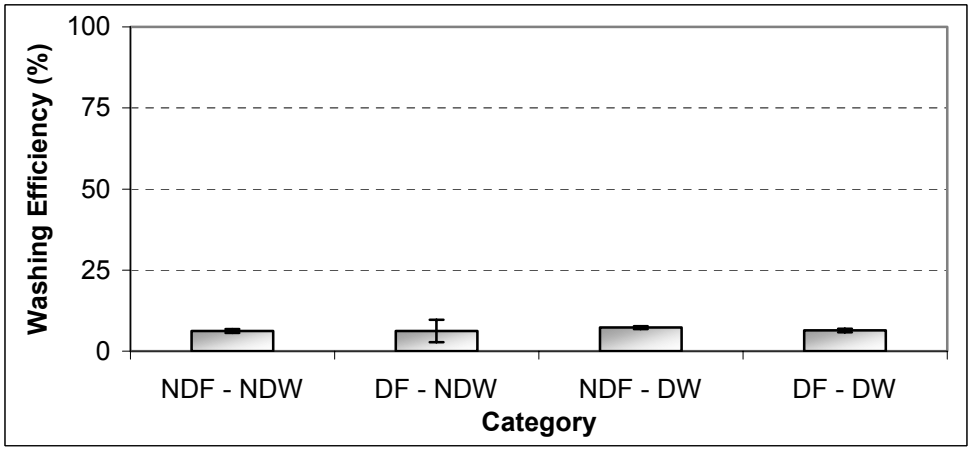

(B)

Figure 14: Trends in the washing efficiency in different categories of experiments conducted at 5 bar static pressure using specially built ultrasonic system. (A) Washing efficiencies at pressure antinode. (B) Washing efficiencies at pressure node.

the washing effect.

Raised static pressure: The results of the experiments with 1 bar over-pressure (i.e., total static pressure of 2 bar) shown in figure 12 reveal a sharp reduction in the washing efficiency, for the categories with degassed washing medium (NDF-DW & DF-DW) at the pressure antinode. At the pressure node the washing efficiencies for all four categories (which are already quite low for the atmospheric static pressure) do not seem to be affected much by the rise in the static pressure except for the category DF-NDW, for which the washing efficiency decreases with raised static pressure. An interesting observation is the higher washing efficiency for category DF-NDW at the pressure antinode. With rise in the static pressure to 3 bar the washing efficiency for all categories at both the pressure node and the pressure antinode drops further as depicted in figures 13A and B. The results of the experiments done at 5 bar static pressure are shown in figure 14A and B. It can be inferred from figure 14 that with static pressure raised to 5

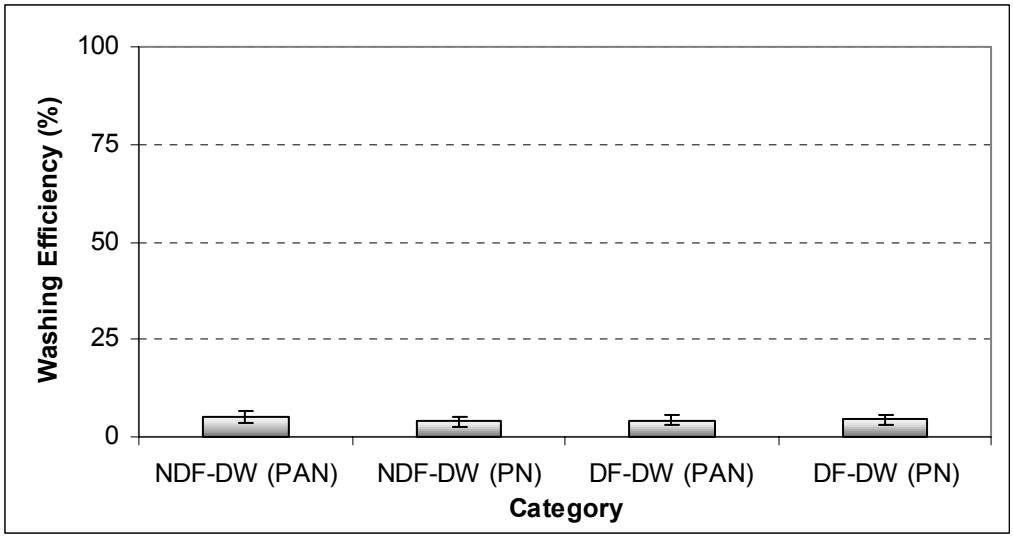

Figure 15: Trends in the washing efficiency in different categories with de-nucleation of the washing medium at 1 bar static pressure using specially built ultrasonic system.

bar the washing efficiency for all the categories at both the pressure antinode and the pressure node reduces practically to zero.

The results of the experiments at high static pressure help further confirm the physical mechanism of the ultrasonic washing process. As discussed in chapter 2 using numerical simulations, a rise in the static pressure of the system (with the acoustic pressure amplitude remaining constant) reduces the cavitation intensity in the medium due to the transition of the transient bubble motion to a stable oscillatory (NOTE: this statement is made under the assumption that the bubbles in the medium do not dissolve away immediately due to the rise in the static pressure). However, the acoustics related phenomena, such as acoustic streaming and oscillatory ultrasound velocity remain unaffected by a rise in static pressure. A drastic reduction in the washing efficiencies at the location of pressure antinode at higher static pressures confirms the principal role of the (transient) cavitation phenomena in the washing process. Very low washing efficiencies at the locations of pressure node support the conclusion of the experiments at atmospheric pressure that acoustic phenomena do not contribute to the washing effect. An interesting observation is the moderate washing efficiency observed for category DF-NDW at 2 bar and 3 bar static pressures. This could be an effect of the technique for the degassing of the fabric, as written earlier: higher loosening of the soil from the surface of the fabric, which results in its easier transport from the surface of the fabric.

De-nucleation of the washing medium: The results of the experiments done with de-nucleation of the washing medium are shown in figure 15. It can be inferred from these results that de-nucleation of the washing medium reduces the washing efficiency at both the pressure node and the pressure antinode practically to zero. The physical picture behind this is clear: with the absence of nuclei cavitation does not take place at the position of pressure antinode. Thus, the cavitation intensity at the pressure antinode drops to zero. However, acoustic related phenomena such as acoustic streaming remain

unaffected by the absence of nuclei. Thus, a sharp drop in the washing efficiency at the pressure antinode with the de-nucleation of the washing medium further confirms the role of the cavitation phenomena in the washing process. In addition, experiments with de-nucleation also provide a clear answer for the location of the occurrence of cavitation events responsible for the washing effect: it occurs in the medium close to the textile surface. No change in the washing efficiency at the location of pressure node after de-nucleation of the washing medium (as compared to the nucleated washing medium) supports the conclusion of the earlier experiments that the acoustic phenomena do not contribute to the washing process.

Therefore, the results of these experiments strongly suggest that transient cavitation in the medium in the close vicinity of the textile surface is the physical mechanism behind the washing process.

6.6 Microscopic analysis of ultrasound-treated fabrics

The collapse of cavitation bubbles near a solid surface results in the erosion of the surface. In fact the study of cavitation motivated by the erosion of blades of ship propellers. In the last few decades the subject of cavitation erosion has been widely studied from the fundamental point of view of underlying bubble dynamics to its application in the material testing. There are two possible causes of the physical damage to the solid boundary due to cavitation bubble collapse in its vicinity:

(1) The pressure pulse emitted into the surrounding liquid when a cavity or bubble collapses. The emitted spherical shock wave could have pressure amplitudes exceeding 1000 bar. For the case of an isolated bubble collapse in an infinite liquid, this shock wave is attenuated so rapidly that the solid surfaces only in the very close vicinity of the bubble (approximately within about the bubble radius at the start of the collapse) could suffer damage due to the shock wave. In the case of collapse of a bubble cluster, the damage can occur at much larger distances from the center of the cluster. This is because as the bubbles in each shell of the cluster collapse they trigger the collapse of a neighboring bubble in the inner shell (starting from the outermost shell), thus, passing their energy towards the center of the cluster. Therefore, the collapse at the center of the cluster is far more energetic than the collapse of a single bubble in an infinite fluid. As such, the shock wave generating out of such a *concerted* collapse can cause damage to much larger distances from the cluster center (Mørch, 1979; Hansson and Mørch, 1980; Hansson *et al*. 1982; Ellis, 1966).

(2) The second possible mechanism for cavitation erosion is the formation of high-speed liquid jets due to bubble involution that may traverse the bubble interior to penetrate the opposite bubble surface. A ring vortex would then emerge from the jet flow, and it may lead to the formation of a *bubble cavitation ring* from the toroidal shape enforced on the bubble by the jet. The torus itself can expand and collapse violently to form a ring-shaped cloud of smaller bubbles, which may then

grow, and collapse depending on their initial sizes (Benjamin and Ellis, 1966; Olson and Hammitt, 1969). The dynamics of the asymmetric collapse of the bubble (such as the velocity of the microjet resulting out of the collapse) mainly depends on the *standoff factor*, which is the ratio of the distance of the bubble center from the solid surface and the initial radius of the bubble at the beginning of the collapse (Naude and Ellis, 1961; Tomita and Shima, 1986). The jetting at the bubble collapse near a solid surface arises due to asymmetry of the flow caused by the surface. A transient pressure pulse generated by a shock wave can also cause the jetting as it passes over a bubble, the asymmetry of the flow in this case being introduced by the bubble surface itself. When a bubble cluster collapses near a solid surface, both of the above-mentioned effects are likely to be present due to the strong interaction between adjacent bubbles. The velocity of the jet is estimated to be of the order of one hundred meters per second, depending on the initial bubble size and standoff factor. The direction of the jet depends on the characteristics of the surface: for a rigid surface, the jet is directed towards the surface and for a free surface the jet is directed away from it (Plesset and Chapman, 1971; Blake *et al.*, 1986, 1987).

The conclusion of the washing experiments carried out with different permutations and combinations of processing conditions suggests that transient cavitation in the medium close to the textile surface is the physical mechanism of the washing process. In order to further verify this conclusion, the surfaces of the ultrasound treated textile samples were analyzed using SEM technique to see whether the well-known signature of cavitation near a surface (i.e. erosion) is present on the textile surface.

The SEM analysis was conducted on the ultrasound treated textile samples in the category NDF-DW with the textile placed at the pressure antinode. During the SEM analysis the textile samples were prepared by sputtering gold-palladium on both sides of the cleaned portion of the fabric since the fabric surface is not planar. The sample was placed support-free in the middle portion (where cleaning occurred) but fixed on the periphery in the SEM machine (Jeol Inc., Model GSM 5800, Accelerating voltage: 5kV; Working distance: 10 mm). In addition, to assess the extent of the depth of the washing effect in the fabric, cross-sections of the treated samples were made and analyzed under an optical microscope. Four pictures of the surface, a yarn and a fiber of the treated EMPA 101 fabric are shown in figures 16A, B, and C respectively. The magnifications used for different SEM images are given in the figure caption. The cross-section of a yarn of the ultrasound treated sample is shown in figure 16D.

Figures 16A through C clearly reveal erosion only on the surface of the treated sample (and not inside the yarn as indicated by the picture of the cross-section of the yarn), which gives further evidence of cavitation phenomena being responsible for washing process. A comparison of the SEM images of the untreated and treated model fabric shows complete removal of soil from the surface of the textile. A comparison of the cross-sections of the untreated and treated model fabric (figures 1D and 16D respectively) reveals an interesting result that the carbon soot particles present inside the

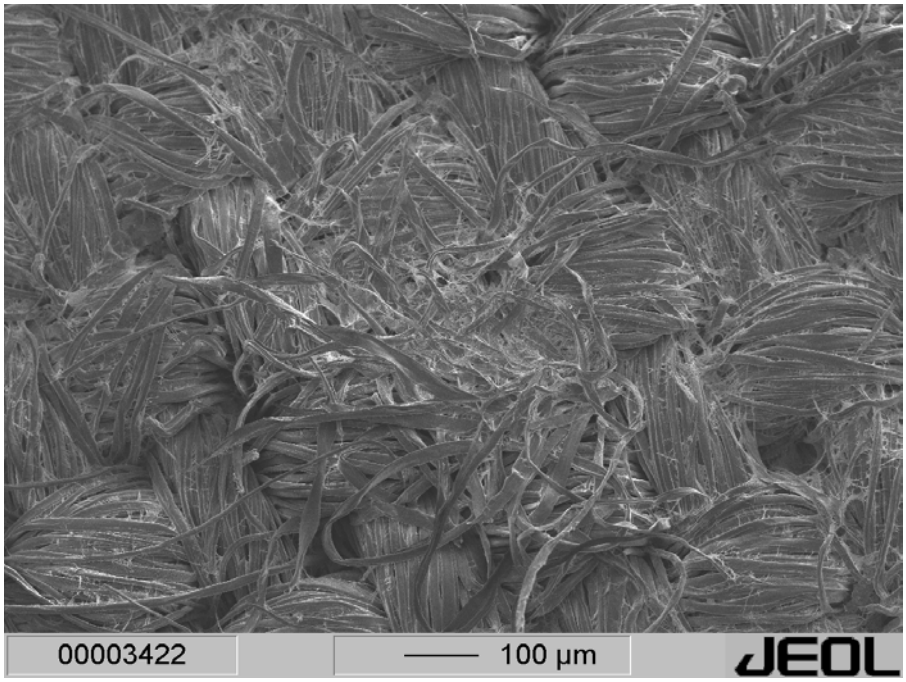

(A)

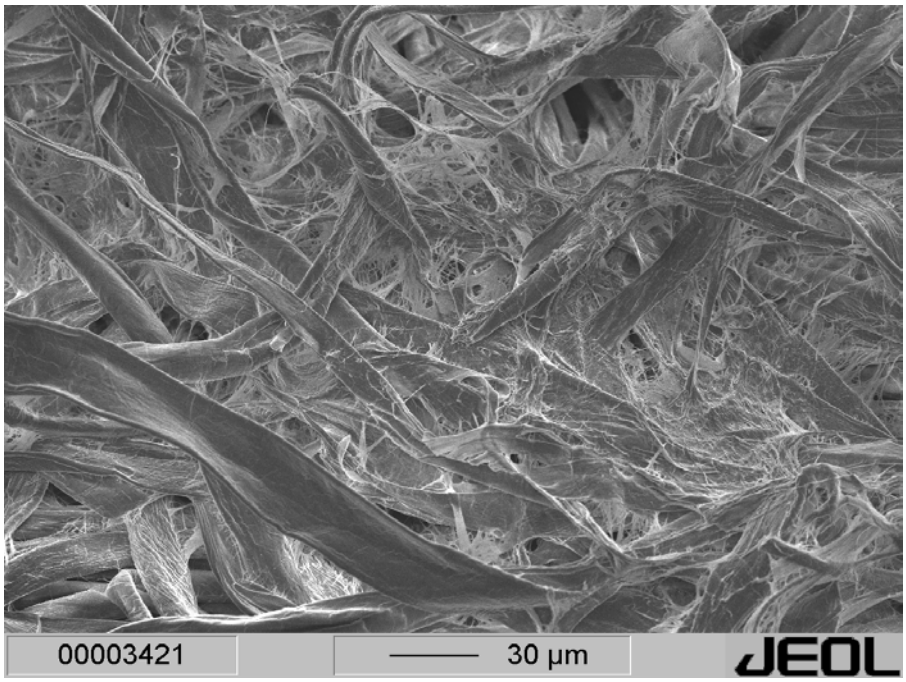

(B)

Figure 16: SEM images of ultrasound treated EMPA 101 fabric. (A) Surface of the fabric (magnification: 100). (B) A single yarn (magnification: 400)

yarn (or in the intra-yarn pores) have also been removed after ultrasonic treatment. A comparison over 15 samples of cross-sections (of treated and untreated model fabric) similar to those shown support this conclusion. This clearly indicates that the intense flow generated in the vicinity of the model fabric due to the transient cavitation is

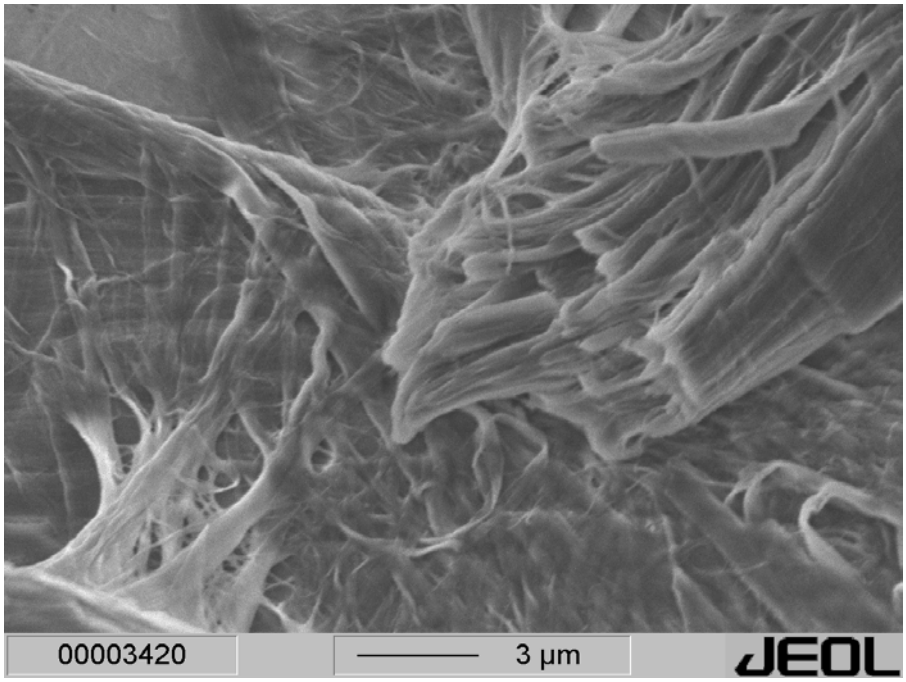

(C)

(D)

Figure 16 (*contd*…): SEM images of the model EMPA 101 fabric. (C) Fiber of the fabric: damage caused to the fiber is clearly visible. (magnification: 5500). (D) Cross-section of a single yarn: the carbon particles inside the yarn have been removed (magnification: 500).

capable of creating an intra-yarn convection, which removes the soil from the intra-yarn pores in a very small time. In addition, there is no erosion or damage visible inside the yarn. This supports the earlier conclusion that the cavitation phenomena responsible for the washing occurs outside the fabric (in the medium in the close vicinity of the fabric).

It should be pointed out that it is not clear from the SEM and cross-section analysis of the ultrasound treated sample as which of the above-mentioned mechanisms (shock wave or microjet) contributes the most to the damage of the fabric surface. However, such a study (to deduce the micro-mechanism of the damage of the textile surface) is beyond the scope of this thesis.

6.7 High-speed photographic studies

One of the very widely used tools in the fundamental research in bubble dynamics is high-speed photography. The speed of the photography can range from a few hundred to several million frames per second depending on the application. The video recording of the ultrasonic cleaning process at high speed could reveal interesting features of this phenomenon.

6.7.1 Experimental

The experimental set up (the experimental cell and the ultrasonic system) used in this study is same as in chapter 3. The model fabric used in this case was Vlisco cotton fabric (beached, 120 g m^{-2}, yarn cm^{-1}: warp – 46, weft - 38) dyed with BASF palanil pink disperse dye (conc: 20 g L^{-1}). The disperse dye does not form any chemical bond with the cotton fibers, and hence, is completely reversible. Thus, the transport of the disperse dye from the textile is of a physical nature. A high-speed camera (Kodak Imager CR 1000, frame rate: 2000 frames/sec.) was used for the imaging using a dark field illumination technique for observation of bubble motion. The photography was carried out in two parts:

1. Photography of the nucleation at the tip of the horn (2000 f/s).
2. Photography of the washing process for the category NDF-DW with fabric positioned at pressure antinode (250 f/s).

The conditions for the second part of the experiment were decided on the basis of the results of the earlier experiments (using EMPA 101 model fabric), that the washing efficiency was maximum at the pressure antinode for the category NDF-DW. In both experiments 250 ml demineralized water degassed to 2 p.p.m. of dissolved oxygen (using the chemical method described earlier) was used as the medium. The ultrasound horn was driven at 25 kHz with a power input of 20W, as in the earlier case of washing experiments with EMPA 101 fabric. The groove in the tip of the ultrasound horn was not filled, and thus, some air could be entrapped in it as the horn-tip is introduced in the washing medium. It must be specifically mentioned that in these experiments the polystyrene latex suspension was not added to the washing medium because of the alternative source of cavitation nuclei at the tip of the horn.

6.7.2 Results and discussion

Nucleation at horn tip*:* A selection from the series of consecutive frames sampled from

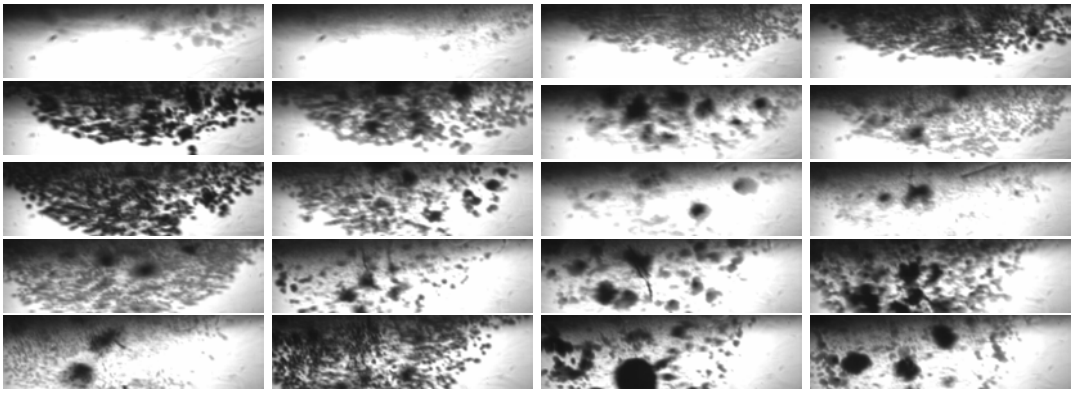

Figure 17: 20 frames (arranged sequentially left to right in consecutive rows) from a high-speed movie of bubble activity at the tip of the ultrasound horn. The upper edge of the frames is the tip of the horn. Frame size: 25 × 12.5 mm. Frame rate: 2000 f/s. Time interval between frames: 500 μsec.

the movie of the oscillations of the ultrasound horn tip is shown in figure 17, with information of other parameters given in the figure caption. The tip of the horn forms the upper edge of the photographic frames. As written earlier, the groove in the ultrasound horn tip may entrap a small amount of air, which can provide nuclei for cavitation. It can be seen that clouds of bubbles originate and grow at the tip of the horn due to the nucleation. Later, they get expelled in water periodically, probably due to Bjerknes forces at the tip of the horn. Thus, the results of high-speed photography confirm the hypothesis of the nucleation at the tip of the horn.

Ultrasonic washing process: Figure 18 shows a high-speed photographic record of the ultrasonic washing process. The *soiled* model fabric is seen at the center of each frame. As mentioned earlier, the frame rate of photography was 250 f/s so the interval between consecutive frames is 4 msec. Once the ultrasound is switched on, the bubble clouds generated at the tip of the horn get expelled into the bulk medium, as mentioned above. Once these clouds travel away from the horn tip, they arrive at the pressure node (or velocity antinode), which is located at a distance of $\lambda/4$ (which is 1.5 cm in present case) from the tip of the horn. As a result of large Bjerknes forces at the location of pressure node, these bubble clouds then travel towards the pressure antinode at which the fabric is located. As these bubble clouds travel towards the pressure antinode, they encounter larger and larger acoustic pressure amplitudes that drive their radial motion. Depending on their initial sizes, the individual bubbles in the bubble clouds then collapse under the influence of the large-amplitude acoustic waves.

In the second frame of the photographic record depicted in figure 18, two bubble clouds are clearly visible. It could be seen that the first cloud (which is the larger of the two) reaches the textile surface, while the second cloud collapses in bulk medium before reaching the textile surface. Dye release is observed to begin in frame 10 from the same location on the textile surface, where the first bubble cloud has reached. It must be noted that during the first 9 frames the ultrasound irradiation and, hence, the acoustics related phenomena, such as microstreaming and the ultrasound velocity (to a small extent) are present. However, no dye release from the textile is seen in the first 9 frames.

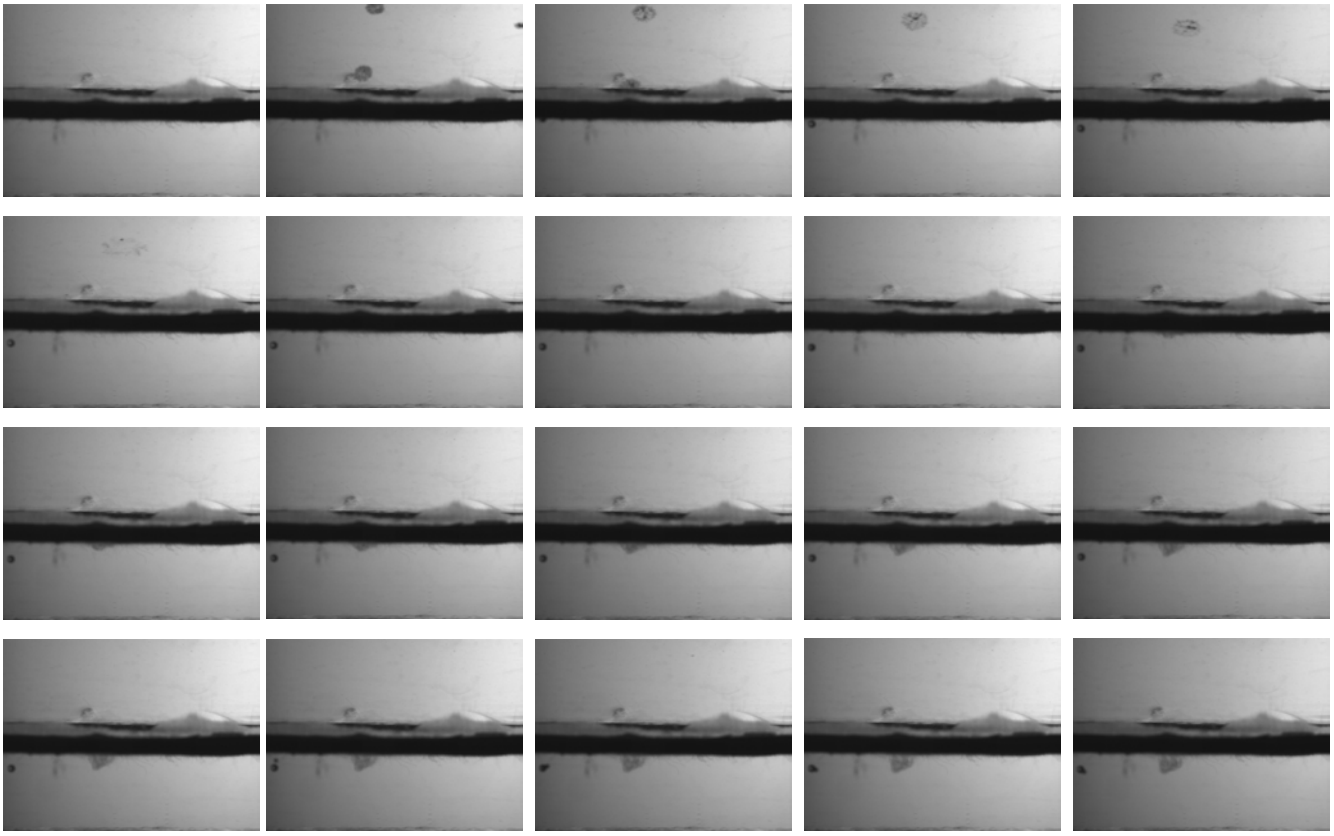

Figure 18: High-speed photographic records of the ultrasonic textile washing process. Frame rate: 250 f/s; Time interval between frames: 4 msec; Frame size: 25 × 25 mm. The frames are arranged sequentially in each row from left to right in consecutive rows. The textile is positioned at the center of the frame at the location of pressure antinode. The release of the dye from the textile is seen to commence after the bubble clusters collapse near the textile surface and not after the ultrasound irradiation is started.

Although the temporal and spatial resolution of the camera used in this study is not sufficient to resolve the final collapse phase of the first bubble cloud near the textile surface, it can be easily perceived from the picture series that the dye release commences with the collapse of the bubbles near the textile surface (and not under the action of the ultrasound itself). Thus, the high-speed photography record of washing process reveals that the cavitation activity near the textile surface is responsible for the dye release from the textile and, thus, corroborates the conclusions of the earlier experiments.

6.8 Overview

This chapter reports attempts to identify the physical mechanisms of the ultrasonic wet textile processes using washing of two model fabrics, viz. EMPA 101 fabric and cotton fabric dyed with disperse dye, as model processes. We have employed simple principles of acoustics and bubble dynamics for distinguishing between the various physical mechanisms present in an ultrasound field that could possibly contribute to the washing process. The experiments have been carried out in both commercial ultrasound equipment and a special built ultrasound system. The process parameters selected for the washing experiments, such as the gas content of the system, the static pressure, and the

position of the model fabric in the standing wave field manifest their effect on the washing process through their effect on the acoustics and the bubble dynamics in the system. In addition, the results of the experiments involving more advanced techniques, such as SEM analysis, image analysis of the cross-section of the ultrasound treated textile samples, and the high-speed photography corroborate the results of the experiments done with manipulation of the process parameters.

The conclusion of all the experiments and analyses presented in this chapter is that the transient cavitation in the medium (i.e. water) in the close vicinity of the textile surface is the physical mechanism of the ultrasonic wet textile processes.

References

- Benjamin, T.B., and A.T. Ellis, "The collapse of cavitation bubbles and the pressures thereby produced against solid boundaries", *Philosophical Transactions of the Royal Society*, **A260**, 221-240 (1966).
- Blake, J.R., B.B. Taib, and G. Doherty, "Transient cavities near boundaries. Part 2. Free surface", *Journal of Fluid Mechanics*, **181**, 197-212 (1987).
- Blake, J.R., B.B. Taib, and G. Doherty, "Transient cavities near boundaries. Part 1. Rigid boundary", *Journal of Fluid Mechanics*, **170**, 479-497 (1986).
- Ellis, A.T., *Proceedings of 6th Symposium on Naval Hydrodynamics*, Washington DC (1966) pp. 137-161.
- Hansson, I., and K.A. Morch, "The dynamics of cavity clusters in ultrasonic (vibratory) cavitation erosion", *Journal of Applied Physics*, **51**, 4651-4658 (1980).
- Hansson, I., V. Kendrinskii, and K.A. Morch, "On the dynamics of cavity clusters", *Journal of Physics D*, **15**, 1726-1734 (1982).
- Holland, C.K., and R.E. Apfel, "Thresholds for transient cavitation produced by pulsed ultrasound in a controlled nuclei environment", *Journal of the Acoustical Society of America*, **88**, 2059-2069 (1990).
- Jakobi, G., and A. Lohr, *Detergents and Textile Washing*, VCH Verlagsgesellschaft mbH, Weinheim (1987).
- Leighton, T.G., *The Acoustic Bubble*, Academic Press Inc., San Diego (1994).
- Moholkar, V.S., S.P. Sable, and A.B. Pandit, "Mapping the cavitation intensity in an ultrasound bath using acoustic emission", *A.I.Ch.E. Journal*, **46(4)**, 684-694 (2000).
- Morch, K.A. in *Erosion* (Preece, C.M. ed.), Academic Press, London (1979) pp. 309-353.
- Naude, C.F., and A.T. Ellis, "On the mechanism of cavitation damage by non-hemispherical cavities collapsing in contact with a solid boundary", *Journal of Basic Engineering* (*Transaction of ASME – D*), **83**, 648-656 (1961).
- Olson, H.G., and F.G. Hammitt, "High-speed photographic studies of ultrasonically induced cavitation", *Journal of the Acoustical Society of America*, **46**, 1272-1283 (1969).
- Plesset, M.S., and R.B. Chapman, "Collapse of an initially spherical vapor cavity

in the neighborhood of a solid boundary", *Journal of Fluid Mechanics*, **47**, 283-290 (1971).

- Tomita, Y., and A. Shima, "Mechanisms of impulsive pressure generation and damage pit formation by bubble collapse", *Journal of Fluid Mechanics*, **169**, 535-564 (1986).

7

MODELING AND OPTIMIZATION OF ULTRASONIC TEXTILE PROCESSES

7.1 Introduction

In the previous chapter, we deduced the physical mechanism of the ultrasonic enhancement of the wet textile processes. As mentioned in the previous chapters, the mass transfer in the inter and intra-yarn pores of the textile is one of the basic mechanisms of the wet textile processes. In order to assess the practical feasibility of the ultrasound assisted wet textile processing, it is necessary to quantify the mass transfer enhancement during ultrasonic textile treatments. The quantification of the mass transfer enhancement could be achieved by developing a mathematical model that combines the regular mass balance equations (with convection) with the convection velocity determined from the equations for radial bubble motion. However, due to complexity of the cavitation phenomena near the textile surface, formulation of a comprehensive mathematical model will be very difficult. Therefore, in this chapter, we make an attempt to quantify the mass transfer enhancement with a semi-empirical mathematical model.

Prevention of fabric erosion during ultrasonic treatment by producing the optimum cavitation intensity in the processor, is also an important issue for the practical application of ultrasonic textile processes. In addition, several inherent problems associated with the ultrasonic processors, such as erosion of the ultrasound source due to cavitation, non-uniform energy dissipation pattern and directional sensitivity of ultrasound effects also need to be addressed for the optimization of ultrasonic wet textile processes. In this chapter, an attempt is also made to propose possible solutions to these problems.

7.2 Quantification of mass transfer enhancement: Concept of convective diffusion coefficient

It was shown in chapter 6 that the occurrence of transient cavitation in the medium near the textile surface is the physical mechanism of the mass transfer enhancement in an ultrasonic washing process. High-energy transient bubble motion near the textile surface is responsible for the creation of strong convection in the close vicinity of the textile, which enhances the mass transfer in the textile. However, the micro-mechanism of this process is not clear. It is not known by which mechanism (formation of shock wave, formation of a high-velocity microjet or oscillatory spherical velocity field generated due to the radial motion of the bubble or a combination of all three possibilities) the convection responsible for the mass transfer enhancement is caused. A conventional approach to the modeling of the mass transfer enhancement due to convection, is to solve the mass balance equation after substitution of the fluid velocity determined from the bubble dynamics equation. But, due to the lack of knowledge of the exact velocity profile in the present case, such an approach is not possible. We, therefore, adopt an approximate method to estimate the mass transfer enhancement factor by an order of magnitude as described below:

The soil in the model fabric used in the present study (EMPA 101) is comprised of carbon particles and olive oil. The carbon particles are not soluble in the medium; however due to their very small size (~ 0.1 microns) they can be approximated as rigid

spheres diffusing in the continuum of the washing medium. Due to very small size, the buoyancy of the carbon particles is negligible. Therefore, the only force acting on these particles is the drag force due to the motion of the adjacent fluid elements. For this situation, the most common basis for the determination of the diffusion coefficient is the Stokes-Einstein equation:

$$D = \frac{\kappa T}{6\pi\mu d_p} \tag{1}$$

where κ is Boltzmann constant, μ is the viscosity of the medium, and d_p is the particle radius. Stokes-Einstein equation forms a useful tool for the determination of the diffusion coefficient of the carbon particles in the intra-yarn region (where negligible fluid flow occurs as described in chapter 1) in the conventional wet textile processes.

If the liquid, in which the particle is suspended, is moving due to convection currents set by density or pressure differences or due to external energy input from sources such as a mechanical stirrer, the diffusion coefficient of the particle is much higher than that predicted by the Stokes-Einstein equation. We designate this enhanced mobility of the particle due to the bulk fluid motion as *convective diffusion coefficient*. The convective diffusion coefficient is basically a synonym for the widely used term *eddy diffusion* in transport phenomena, which represents solute transfer due to turbulent fluid motion. However, due to lack of knowledge of the exact magnitude of the fluid velocity caused by the transient motion of the bubbles, which will help determine the Reynolds number for the fluid motion in the close vicinity of the textile and, hence, the flow regime, we have used the term *convective diffusion coefficient*.

7.2.1 Description of the fabric geometry

As mentioned earlier, a textile is comprised of yarns, which in turn are made of fibers. In order to propose a mathematical model for the diffusion process in the textile, it is necessary to assign a suitable geometry to the textile. For this purpose many possibilities exist. For example: 1. a porous plate (representing the textile as a whole); 2. a porous cylinder (representing a single yarn in the textile). In both of these cases a homogeneous porosity in the structure is assumed.

In order to make a proper choice for the textile geometry, one needs to take into account the relative sizes of the source of convection (i.e. the bubbles) and the structure through which the mass transfer occurs due to the convection (i.e. the textile). The typical diameter of a yarn is ~ 200 microns as is evident from the S.E.M. images of the EMPA 101 model fabric shown in figure 1 of chapter 6. The radius of bubbles that undergo transient motion near the textile surface (for 25 kHz frequency and acoustic pressure amplitudes 1.2 - 1.5 bar) oscillates between a few microns and perhaps 100 microns. An intense spherical velocity field is created in the close vicinity of the bubble during compression. During this phase, the porous structure, i.e. a single yarn in the textile, tends therefore to be larger than the dimensions of the source of convection, i.e. the bubble. This circumstance justifies considering the textile as a porous plate. However

while analyzing the effects of ultrasound treatment on large portion of the textile (or on a macroscopic scale) the dual porosity of the textile (viz. inter-yarn and intra-yarn porosity) needs to be taken into account.

7.2.2 Approach

As stated earlier, our approach to the problem of determining the mass transfer enhancement in ultrasonic wet textile processes is based on determining the convective diffusion coefficient for the soil removal in presence of ultrasonic irradiation. A ratio of the convective diffusion coefficient and the diffusion coefficient obtained from Stokes-Einstein equation gives the enhancement factor due to ultrasound. For the estimation of convective diffusion coefficient, we combine experimental and theoretical methods in three steps as follows:

1. Use an approximate method of cavitation nucleation near the fabric surface for the experimental determination of the rate of soil removal for different periods of ultrasound irradiation. The soil concentration in the fabric can be calculated from its reflectance using the Kubelka-Munk theory, which is discussed subsequently.
2. Solve the diffusion equation (Fick's second law) for a plane sheet to determine the concentration profiles of the diffusing substance for different time intervals, and obtain an expression for the total amount of diffusing substance transported across the plate per unit time.
3. Use experimentally measured values of soil removal from the model fabric for different time periods of ultrasonic treatments, and the theoretical expression for the soil removal (obtained in the previous step), find out the convective diffusion coefficient for soil under the effect of ultrasound irradiation.

7.3 Experimental

The basic experimental system (ultrasound horn, signal generator & amplifier, the experimental cell and other accessories) is described in detail in chapter 3. The only modification to this system was the addition of a timer switch between the signal amplifier output and ultrasound horn. This switch connects the amplifier output to the ultrasound horn only for a specified time period thus controlling the time of the ultrasonic textile treatment accurately. The timer switch used in these experiments offers time control in several different ranges: 0 – 1 sec (increment: 0.1 sec); 0 - 10 sec (increment: 1 sec); 0 - 1 min (increment: 0.1 min or 6 sec); 0 - 10 min. (increment: 1 min). The model fabric used in these experiments was EMPA 101 with demineralised water being the washing medium.

7.3.1 Source of cavitation nucleation

The cavitation nucleation in the medium is an important factor for any cavitation-aided physical or chemical process, because the physical or chemical effect depends, to a

significant extent, on the population and the size distribution of these nuclei. The time of ultrasound exposure is also an important factor in these processes. During the process, the initial nuclei population and their size distribution undergo changes due to fragmentation of the bubbles during radial motion and re-growth (and collapse) of the daughter bubbles. Therefore, for ultrasound processes of longer duration (as compared to the period of acoustic cycle) the effect of initial nuclei population and size distribution is likely to be smoothed out. However for a short ultrasound exposure, the initial nuclei population and size distribution is of crucial importance because these parameters are not likely to change much during the exposure. Thus, for experiments aimed at determining the kinetics of cavitation-aided physical or chemical processes, the source of cavitation nuclei (which determines the initial population and size distribution of the cavitation nuclei) is a parameter of paramount importance.

In case of bubble activity near a solid surface (in the present case the model fabric), the extent of convection produced by the bubble depends not only on the population and the size distribution of the cavitation nuclei but also on their distance from the fabric surface. Depending on the *standoff factor*, which is the ratio of the distance of the bubble center from the textile and the size of the bubble at beginning of collapse, the bubble may undergo different kinds of motions (Naude and Ellis, 1961; Tomita and Shima, 1986; Blake *et al.*, 1986; Philip and Lauterborn, 1998). For large standoff factors (> 3 or so), the bubble shape during the radial motion remains spherical without appreciable deformation and, thus, the velocity field produced around it is also spherically symmetric. For smaller standoff factors (typically between 1 – 1.5), the bubble undergoes deformation producing a high-velocity microjet directed towards the boundary, when the boundary is sufficiently rigid. In addition, the distribution of the cavitation nuclei over the surface of the textile is also an important factor because the dynamics of a single bubble is influenced significantly by the interaction with adjacent bubbles.

The nuclei close to the textile surface, before the start of ultrasound irradiation, can create the convection for soil removal almost immediately after ultrasound exposure. The nuclei initially away from the textile may not help in immediate removal of soil because of the rapid reduction in the intensity of velocity field away from the center of the bubble. However, during ultrasonic irradiation, circulatory flows are set up in the system due to absorption of the momentum of the acoustic waves by the liquid. Due to these flows, a bubble initially present away from the fabric can migrate towards the fabric surface (if it does not collapse before reaching the fabric), and create nucleation near textile that could assist the soil removal. However, in this case the rate of soil removal is determined by the time necessary for bubble migration and the intensity of convection created by the bubble. This obviously can lead to significant errors in the calculations of rate of soil removal, especially for smaller periods of ultrasound exposure. Due to above-mentioned complications, the choice of source of nuclei is of paramount importance in the accurate measurement of rate of soil removal and, hence, in the estimation of convective diffusion coefficient.

In our earlier experiments, we used a suspension of polystyrene latex particles to provide nuclei in the medium. The air pockets entrapped in this suspension can provide

nuclei for cavitation in the medium. However, these air pockets are distributed all over the medium (as a part of polystyrene particle suspension). Due to long time of ultrasound treatment (3 minutes), the above-mentioned effects due to irregularities of population, size distribution and location of nuclei were smoothened out and the overall washing effect for total time of treatment for consecutive experiments with same process parameters was more or less same. However, for the present study with very short periods of ultrasound exposure the nucleation by polystyrene latex suspension may not give good results. Instead, particles with surface crevices (that can entrap air pockets), placed on the fabric surface itself, can provide nucleation at desired location for production of instantaneous convection with ultrasound exposure without any time-lag effects arising out of factors just discussed.

Pumice stones, which are widely used for providing nuclei for boiling, can be used for the present purpose. Since these stones are commercially available in large sizes (> 3 mm or so), they may give rise to non-uniform nucleation. However, by reducing their sizes by grinding, restricting the size range after screening using sieves of certain mesh sizes, and adding an exact quantity of stones to the medium each time, this problem could be overcome to some extent. It must be noted that having uniform particle sizes may not be of much use as far as the uniformity of nucleation is concerned, because nuclei for cavitation are mainly contributed by the gas pockets trapped in surface crevices of the particles, and not by the particles themselves. In view of the above considerations, we have used pumice stones of size range of 200-400 microns as a source of nuclei in the present experiments. If added in large amounts, the pumice stones can cause changes to the power consumption of the system due to large bubble population in the system, which increases the compressibility of the medium, as explained in chapter 5. Therefore, we use a very small amount (20 mg) of pumice stones for the nucleation in each experiment. In order to assess the effect of presence of pumice stones on the power consumption of the ultrasound horn, experiments were conducted to measure the power consumption with and without the pumice stones in the medium. It was found that the power consumption of the ultrasound horn remained unchanged.

7.3.2 Experimental procedure

The results in chapter 6 revealed that the ultrasonic washing efficiency depends on the gas content of the fabric and the washing medium. A maximum washing efficiency is obtained with a degassed washing medium with the fabric positioned at a pressure antinode (which obviously means that maximum mass transfer enhancement is obtained at these conditions). Thus, we run the experiment with degassed water (and non-degassed fabric, although the effect of this latter feature is small) with the fabric positioned at a pressure antinode. In addition, in this case it is also easy to control the cavitation nuclei population since no nuclei are contributed by the medium and, hence, the number of nuclei in the system are directly proportional to amount of pumice stones added. Eight specific time intervals ranging from 0.1 sec to 2 sec were selected for ultrasound irradiation. For each interval 3 experiments were conducted with different pieces of the model fabric to assess reproducibility of results. In order to make pumice stones as the

sole source of nuclei, the circular groove in the tip of the horn was filled with silicon rubber to avoid entrapment of air in it. Power input to the ultrasound horn was 20W at 25 kHz frequency. At this power input, the ultrasound horn produces an acoustic wave with a pressure amplitude of ~ 1.3 bar. The rest of the experimental procedure is exactly the same as described in chapter 6 for the washing experiments in the specially built ultrasonic system. In order to assess the effect of the acoustic pressure amplitude on the convective diffusion coefficient, the set of experiments at 20 W power input was repeated at power input of 15 W, for which the ultrasound horn produces a wave with pressure amplitude of ~ 1.1 bar.

7.3.3 Data analysis

The quantification of the washing effect can be done by measuring the reflectance of the ultrasound treated sample. However, in order to determine the rate of soil removal we need to convert the reflectance measurements into soil concentrations. In addition, a linear relationship between soil concentrations and reflectance simplifies the calculations. This is done by plotting some function of the reflectance against concentration. For this purpose, Kubelka-Munk theory is often used, which is the simplest tool for the description of the optical properties of a turbid medium that absorbs and scatters light. In color science it is used to relate the concentration in an opaque layer by measuring the reflectance of a monochromatic light incident on the layer. A detailed analysis of Kubelka-Munk theory is available in several basic books on color science and optometry. The mathematical expression of Kubelka-Munk theory that relates the absorption coefficient (K), scattering coefficient (S), and the reflection coefficient of the layer (R_f) is:

$$\frac{K}{S} = \frac{(R_f - 1)^2}{2R_f} \tag{2}$$

K/S is also called as remission function denoted as $F(R_f)$. The Kubelka-Munk theory can also be applied to colored particles. For particles larger than the wavelength of light, the scattering coefficient is inversely proportional to the diameter:

$$S \sim \frac{1}{\sqrt{\bar{d}_p^2}} \text{ where } \sqrt{\bar{d}_p^2} = \sqrt{\frac{\sum_i n_i d_i^2}{\sum_i n_i}}. \tag{3}$$

If the distribution of particle diameters is very small, then one can approximate: $S \sim 1/d_p$. The Kubelka-Munk theory can be coupled with the Lambert-Beer law to convert the remission function into absolute concentration. In case of negligible scattering coefficient, the relationship between absorption coefficient K and concentration of soil C is:

$$K = \varepsilon C \ln(10) = \varepsilon_n C; \text{ where } \varepsilon_n = \varepsilon \ln(10). \tag{4}$$

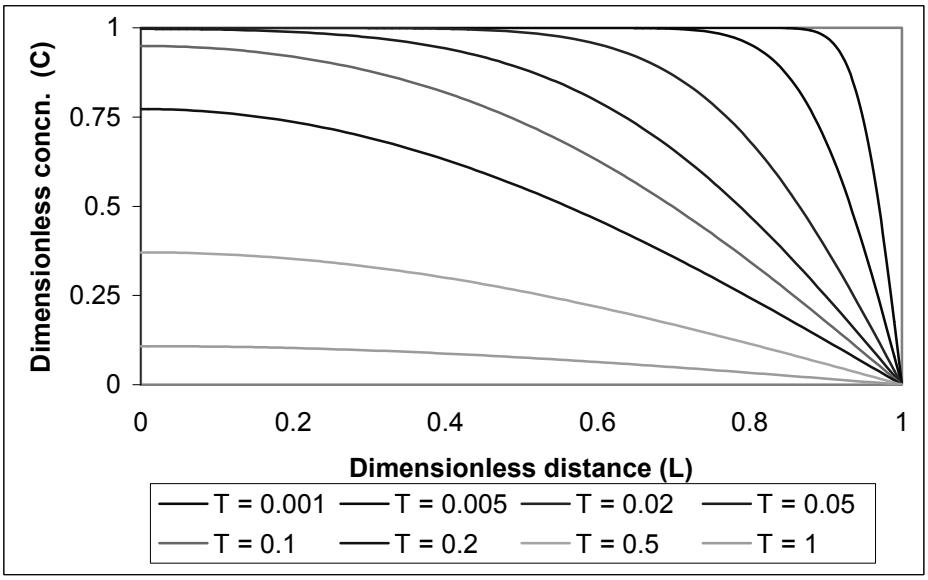

(A)

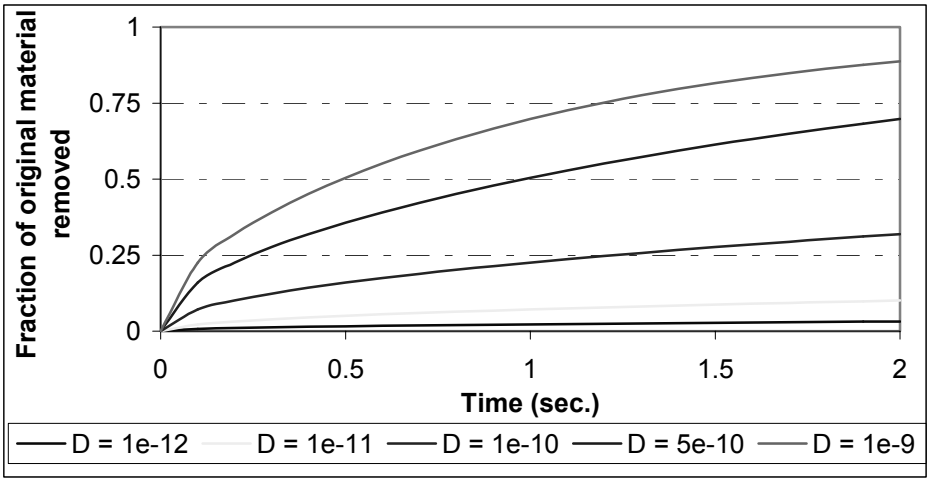

(B)

Figure 1: (A) Theoretically calculated concentration distribution curves [dimensionless concentration = $(C - C_1)/(C_o - C_1)$] in the porous sheet for various times with initially uniform concentration distribution (C_o = 1) and surface concentration (C_1 = 0). T is the dimensionless time: Dt/l^2. Other parameters for simulations: Diffusion coefficient (D) = 1×10^{-9} m^2 s^{-1}; Sheet thickness (l) = 100 microns. (B) Curves showing material transport through the porous sheet for different diffusivities. Values of D indicate the diffusion coefficient in m^2 s^{-1}. Other parameters: Original material amount: 1; Sheet thickness: 100 microns.

ε_n is the Naperian molar absorption coefficient, which is a constant. In Lambert- Beer law, the absorption coefficient is determined by using collimated light while Kubelka-Munk theory is applicable for diffused light. For this reason, a correction factor needs to be introduced in the equation relating the K and C. The corrected form of relationship is: $K = 2\varepsilon_n C$. This analysis makes two simplifying assumptions:

- The diameters of all carbon particles in the soil over textile are the same.
- The scattering coefficient of carbon particles is negligible.

In the present study it is not possible to independently determine ε_n since the

manufacturer of EMPA 101 model fabric does not supply the soil (carbon soot + olive oil) separately. Therefore, the soil concentrations need to be defined on a relative basis. The reflectance of untreated EMPA 101 textile is 16%, which corresponds to a K/S value of 2.205. Since the diameter of all particles is assumed to be same, the scattering coefficient is a constant and, hence, will be cancelled out in the calculations of relative soil concentrations. We assume that K = 2.205 corresponds to 100% soil concentration in fabric (or in other words no soil removal from the fabric). The reflectance of completely washed EMPA 101 fabric is ~ 70% which corresponds to K = 0.064. We assume that K = 0.064 corresponds to 0% soil concentration in fabric (or in other words complete removal of the soil from the fabric). The fraction of original soil removed from the fabric after ultrasound treatment for different time periods (M_t) is estimated by assuming a linear relation between K and M_t with: K = 2.205 at M_t = 0; K = 0.064 at M_t = 1, respectively.

7.4 The mathematical model

As discussed earlier, we approximate the geometry of the textile as a porous plate. 1-D unsteady state diffusion (in absence of velocity) in a porous plate is described by Fick's second law:

$$\frac{\partial C}{\partial t} = D\frac{\partial^2 C}{\partial x^2} \tag{5}$$

Let $-l < x < l$ denote the boundaries of the plate with thickness 2l. The solutions of equation 5 are listed by Carslaw and Jaeger (1959) for different boundary conditions.
For the conditions:

$C = C_1$, for $x = -l, l$
$C = C_0$, for $t = 0$

The concentration of the diffusing substance in the plate is (Crank, 1975):

$$\frac{C - C_1}{C_0 - C_1} = 1 - \frac{4}{\pi}\sum_{n=0}^{\infty}\frac{(-1)^n}{2n+1}\exp\left\{\frac{-D(2n+1)^2\pi^2 t}{4l^2}\right\}\cos\left[\frac{(2n+1)\pi x}{2l}\right] \tag{6}$$

The total amount of substance, which has left the plate after a time t (M_t), and the corresponding amount after infinite time (M_∞) are related by:

$$\frac{M_t}{M_\infty} = 1 - \sum_{n=0}^{\infty}\frac{8}{(2n+1)^2\pi^2}\exp\left\{\frac{-D(2n+1)^2\pi^2 t}{4l^2}\right\} \tag{7}$$

We show solutions of equations 6 and 7 for representative parameters (given in the figure

caption) in figure 1A and B respectively.

***Concentration profile for Fourier numbers > 0.1*:** It is convenient to introduce the Fourier number defined by

$$\mathrm{Fo} = \frac{\mathrm{Dt}}{\mathrm{l}^2} \tag{8}$$

For times such that Fo > 0.1, the concentration profile can be approximated by a more convenient expression. The detailed theoretical analysis of this (which is an extension of the penetration theory) can be found in several references such as Beek *et al.* (1999) and Warmoeskerken and Janssen (1997). We give herewith only the final result. The average concentration in the porous plate deduced from equation 6 is:

$$\frac{\mathrm{C}_1 - \langle \mathrm{C} \rangle}{\mathrm{C}_1 - \mathrm{C}_0} = \frac{8}{\pi^2} \exp\left(-\pi^2\ \mathrm{Fo}\right) \tag{9}$$

This means that plot of logarithm of the expression on LHS of equation 9 against Fourier number should yield a straight line with slope ~ –9.86.

7.4.1 Bubble motion near the fabric

It was shown in the previous chapter that the transient bubble motion near the textile surface gives rise to convection that enhances the mass transfer. However, the bubble motion near a solid boundary is a multi-faceted phenomenon, as discussed in the previous chapter. The kind of radial motion the bubble undergoes in the vicinity of the solid boundary, whether symmetric or asymmetric, depends on the physical characteristics of the boundary (such as elastic modulus) and also on the standoff factor.

Recently, Brujan *et al*. (2001, 2001a) have reported high-speed imaging studies of a vapor bubble dynamics near an elastic boundary. Brujan *et al*. (2001a) also report results for bubble motion as affected by the elastic modulus of the boundary. Brujan *et al*. (2001a) conclude that for boundaries with very low elastic modulus, the bubble motion is asymmetric (with formation of a jet) only for standoff factors smaller than 1. For cases where standoff factor ≥ 1, the bubble motion remains symmetric, as if occurring in an infinite fluid. Cotton fibers have a very low static elastic modulus (Morton and Hearle, 1997). It is likely that, at 25 kHz, the elastic modulus is still relatively small and, therefore, the cotton fabric acts as a soft boundary for a bubble oscillating in its vicinity. Thus, we present simulations of the bubble motion and the spherical velocity field generated around it using the Gilmore bubble dynamics equation presented in chapter 2:

$$\mathrm{R}\left[1 - \frac{\mathrm{U}}{\mathrm{c}}\right]\frac{\mathrm{d}^2\mathrm{R}}{\mathrm{dt}^2} + \frac{3}{2}\left[1 - \frac{\mathrm{U}}{3\,\mathrm{c}}\right]\left(\frac{\mathrm{dR}}{\mathrm{dt}}\right)^2 = \left[1 + \frac{\mathrm{U}}{\mathrm{c}}\right]\mathrm{H} + \frac{\mathrm{U}}{\mathrm{c}}\left[1 + \frac{\mathrm{U}}{\mathrm{c}}\right]\frac{\mathrm{dH}}{\mathrm{dR}} \tag{10}$$

H is the free enthalpy on the surface of the bubble:

$$H = \frac{n}{n-1}\frac{A^{1/n}}{\rho_o}\left\{\left[\left(P_o + \frac{2\sigma}{R_o}\right)\left(\frac{R_o}{R}\right)^{3\gamma} - \frac{2\sigma}{R} + B\right]^{\frac{n-1}{n}} - \left[P_\infty + B\right]^{\frac{n-1}{n}}\right\} \tag{11}$$

A, B and n are constants (For water A = 3001 atm., B = 3000 atm. and n = 7). P_∞, the pressure in the bulk liquid driving the bubble motion is:

$$P_\infty = P_o - P_A \sin(2\pi ft) \tag{12}$$

where P_o is the ambient pressure (in the present case the atmospheric pressure). P_A is the amplitude and f is the frequency of the ultrasound waves. The velocity in the bulk liquid at a distance r from the bubble center is:

$$u(r,t) = \frac{R^2}{r^2}\left(\frac{dR}{dt}\right) \tag{13}$$

7.4.2 Adoption of the diffusion model for the present study

While adopting the above models to explain the results of the present experiments, we need to take into consideration the possible discrepancies between the experimental and theoretical results, which could occur as a result of mismatches between the assumptions made in the model and the practical situation. One such mismatch is the geometrical difference between the model porous plate and the textile. As discussed earlier, the textile is modeled as a porous plate on the basis of the differences between sizes of an individual bubble and that of an individual yarn. However, during the experiments, we will be determining the rate of soil removal from the textile on a macroscopic scale. We will be quantifying the soil transfer rates by measurement of the reflectance of the textile. The reflectance is measured over a large area of the textile (and not for a single yarn). Therefore, this measurement technique will quantify the soil transfer not only in the intra-yarn pores but also in the inter-yarn pores. The reflectance of the fabric is a function of the average soil concentration in the textile. It was revealed by the S.E.M. image analysis of the surface and optical microscope pictures of the cross-section of the EMPA 101 model fabric that the soil is distributed unevenly over the textile surface. As a result of relatively much smaller intra-yarn pore volume than the inter-yarn pore volume, a large fraction of total soil concentration is present in the inter-yarn pores and on the surface of the textile and a much smaller fraction of the total soil is present in the intra-yarn pores. As discussed in chapter 1, due to geometrical constraints the intensity of the convection due to the radial bubble motion in the inter-yarn region is much higher than in the intra-yarn region. Thus, the soil removal process is expected to have two steps for which the rate of soil removal will differ: 1. rate for smaller time period of ultrasound irradiation during which only inter-

yarn soil is removed; 2. rate for longer time period of ultrasound irradiation during which both inter-yarn and intra-yarn soil is removed. It is obvious that in the first step of soil removal process the rate is expected to be higher than the second step, due to the presence of uneven fractions of the total soil in the inter-yarn and intra-yarn regions. This could give rise to a difference between the theoretical results predicted by the models (with assumption of constant diffusion coefficient with homogeneous porosity in the sheet) and the experimental results.

7.5 Results and discussion

The results of the experiments done with 20W and 15W power input to the ultrasound horn are shown in figures 2 and 3 respectively. It can be seen that the washing effect for both power inputs shows a gradual rise with time of ultrasound irradiation. However, for shorter ultrasound irradiation the rate of soil removal from the fabric is higher than for longer ultrasound treatments. This result may perhaps be interpreted from the discussion given in previous section. The soil distribution in the fabric is uneven; with larger fraction of the soil present in the inter-yarn pores and on the surface of the fabric. The results are consistent with the hypothesis that, for shorter ultrasound irradiation, only the soil on the fabric surface and in the intra-yarn pores is removed while for longer irradiation soil in the intra-yarn pores is also removed. However, since the intra-yarn soil forms only a small fraction of the total soil in the textile, the reflectance of the fabric does not rise significantly for longer ultrasound irradiation. A comparison of figures 2C and 3C reveals that larger power input (which means cavitation at larger pressure amplitude) results in faster and higher removal of soil from the fabric. Some experimental errors, however, need to be taken into account. In figure 3A, the reflectance of the fabric does not show a consistent rise with time of irradiation. Between 0.5 sec and 1 sec, it decreases slightly. We attribute this anomaly to the error in having exactly the same type of nucleation (size distribution and population of bubbles) produced near the textile surface in consecutive experiments. The dotted lines in figures 4 and 5 depict the measured fraction of the soil removed from the fabric as deduced from the reflectance measurements for acoustic irradiation at 20 and 15 W respectively. In these figures, the solid and dashed lines are graphs of the theoretical result of equation 6 for different values of the diffusion coefficient. It can be seen that a single value of the diffusion coefficient is inadequate to reproduce the data. To the extent that an "effective diffusion coefficient" can be defined, the data imply that it decreases with time. The initial portions of the curves are described reasonably well by equation 6 with $D = 2 \times 10^{-9}$ m^2 s^{-1} at 20 W and $D = 1 \times 10^{-9}$ m^2 s^{-1} at 15 W. Thus, the diffusion coefficient is found to increase with the acoustic pressure amplitude as expected. If the process can be described by a superposition of two different diffusive processes, characterized by different diffusion coefficients, at large times the solution will be dominated by the slower diffusive process and, therefore, one can estimate this smaller diffusion coefficients from the large-time behavior of the data. On the basis of this argument, one deduces from the data the values $D = 7.5 \times 10^{-10}$ m^2 s^{-1} at 20 W and 5×10^{-10} m^2 s^{-1} at 15 W. The shift between the two mass transfer rates occurs at approximately 0.4 sec

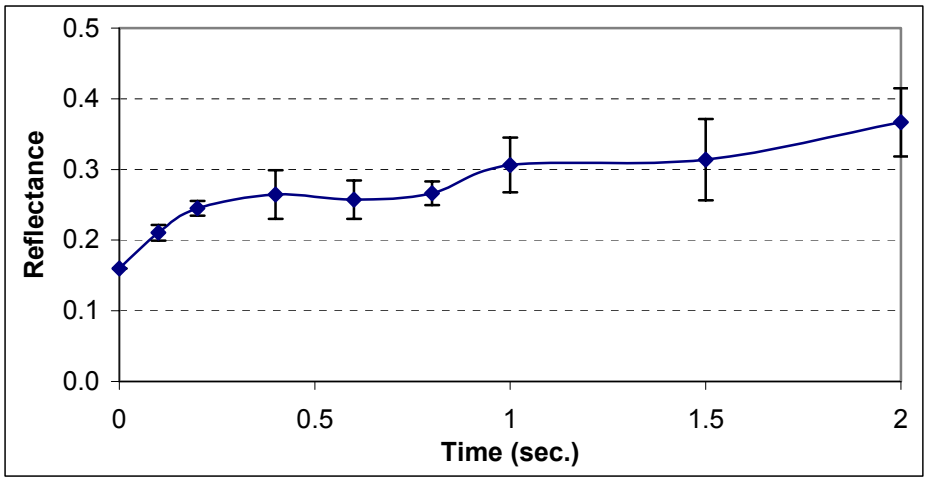

(A)

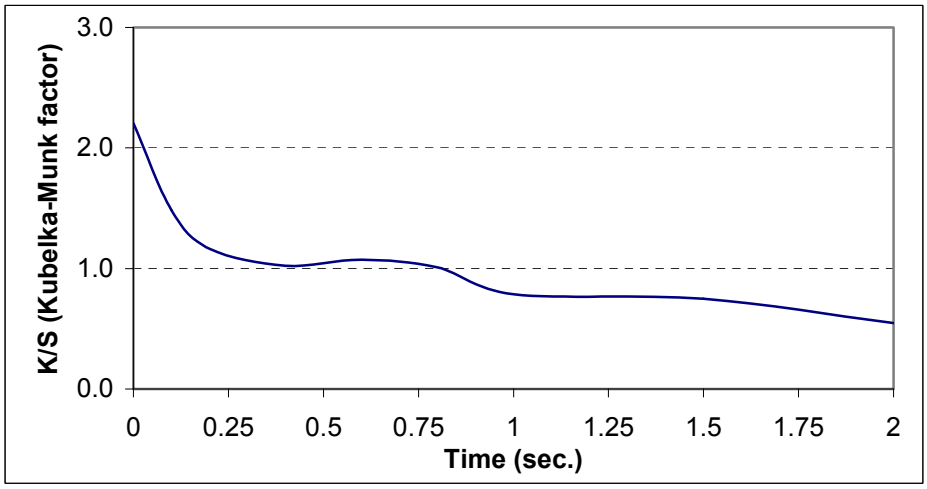

(B)

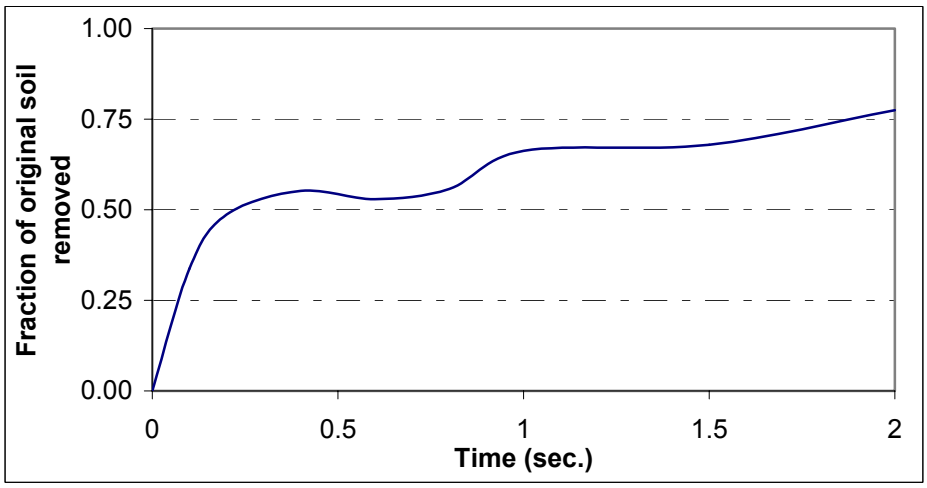

(C)

Figure 2: Experimental results for fabric treatment at 20W power input. (A) Reflectance of the fabrics treated for different time periods. (B) Kubelka-Munk factor for fabrics treated for different time periods (representative of the soil concentration in fabric). (C) Soil removal from the textile with time. [It should be noted that figures B and C represent analysis done using the average reflectance value of the treated sample; standard deviation is not taken into account].

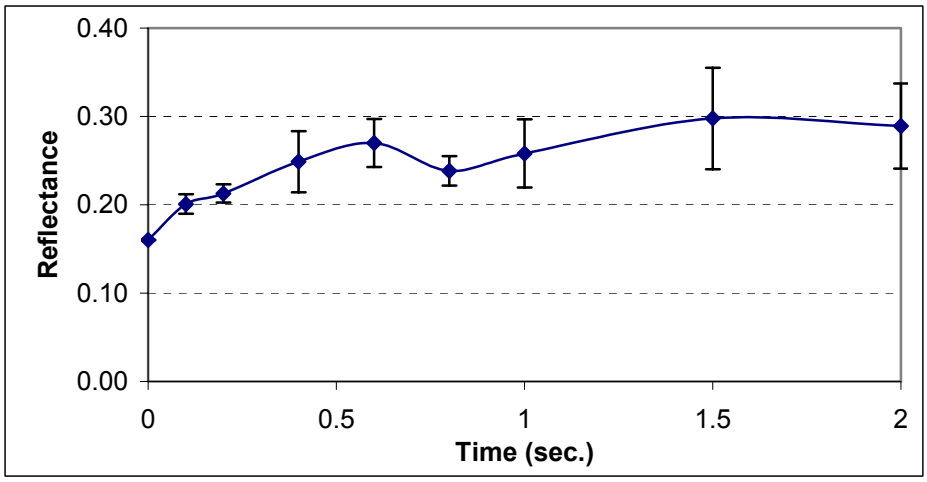

(A)

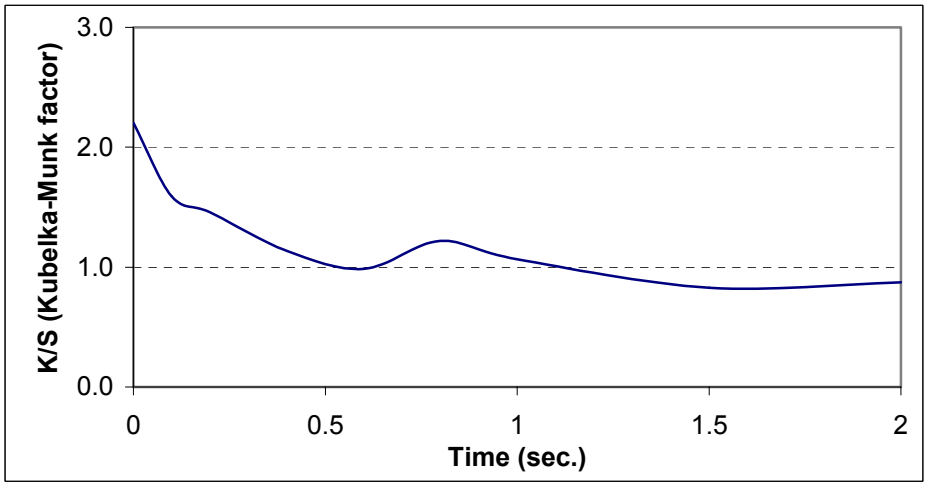

(B)

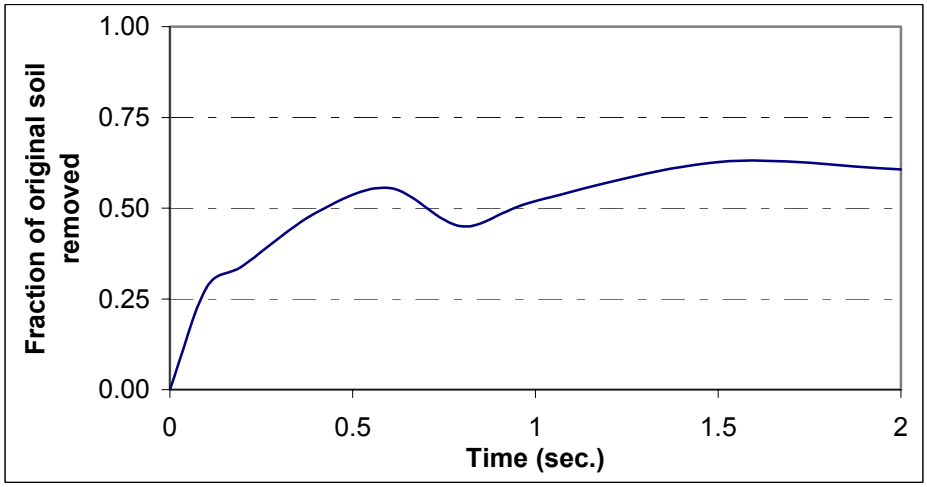

(C)

Figure 3: Experimental results for fabric treatment at 15W power input. (A) Reflectance of the fabrics treated for different time periods. (B) Kubelka-Munk factor for fabrics treated for different time periods (representative of the soil concentration in fabric). (C) Soil removal from the textile with time. [It should be noted that figures B and C represent analysis done using the average reflectance value of the treated sample; standard deviation is not taken into account].

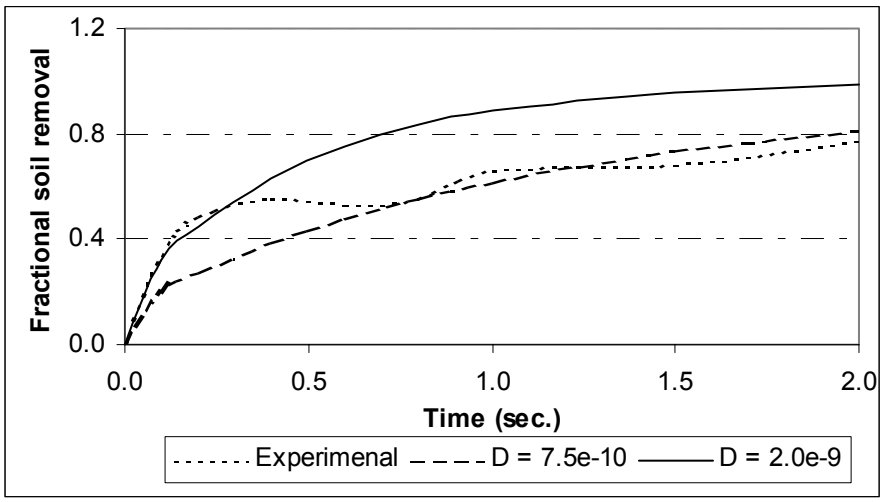

Figure 4: Features of mass transfer in fabric under ultrasonic treatment at 20W power. Comparison of the experimental soil removal rate with the theoretical soil removal for two different diffusion coefficients. (Values of D indicate diffusion coefficient in $m^2 s^{-1}$ for theoretical calculation of the soil removal curve).

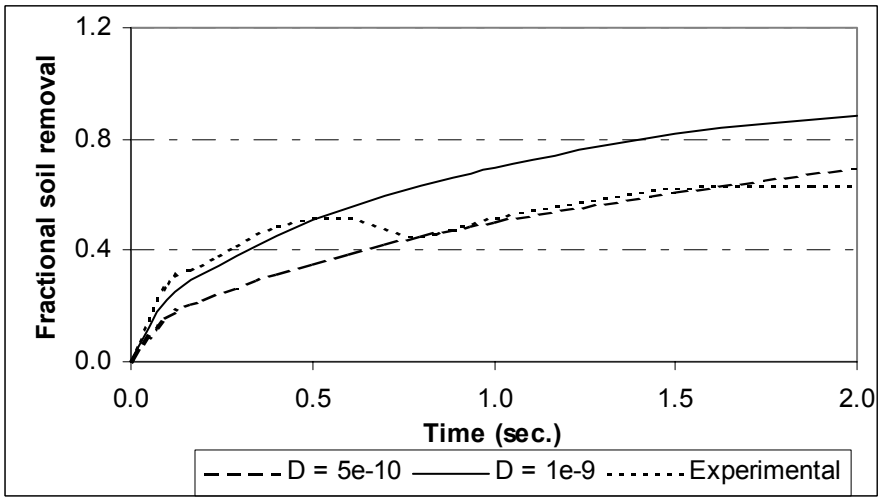

Figure 5: Features of mass transfer in fabric under ultrasonic treatment at 15W power. Comparison of the experimental soil removal rate with the theoretical soil removal for two different diffusion coefficients. (Values of D indicate diffusion coefficient in $m^2 s^{-1}$ for theoretical calculation of the soil removal curve).

(referring to figure 4), which corresponds to a Fourier number of ~ 0.03 as calculated with the smaller diffusion coefficient. A similar analysis for figure 5 (where the shift between mass transfer rates occurs at ~ 0.6 sec.) reveals that the Fourier number at which this shift occurs also is 0.03. Figure 6 shows plots of dimensionless average soil concentration in the fabric (with $C_1 = 0$) for $t > 0.5$ sec. for 20W and for $t > 0.6$ sec. for 15W power input. The value of convective diffusion coefficient the slopes of the plots (assuming fabric thickness of 100 microns) are: 5×10^{-10} m^2 s^{-1} for 20W and 3×10^{-10} m^2 s^{-1} for 15W. These values fairly match the values of convective diffusion coefficient

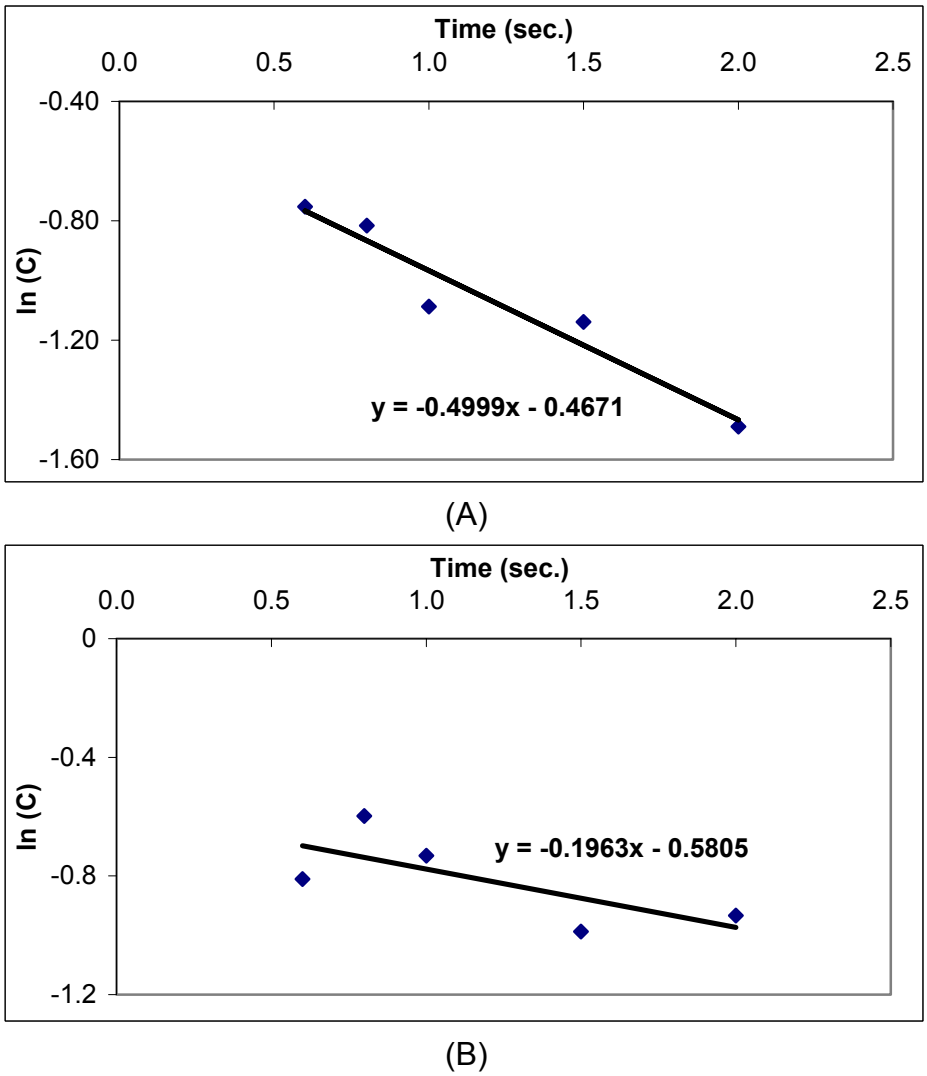

Figure 6: The logarithmic average concentration gradient (with linear approximation) for longer contact time. (A) Soil concentration for 20W power. (B) Soil concentration for 15W power. The slope of the line (= - $\pi^2 D/l^2$) indicates the convective diffusion coefficient.

given in figures 4 and 5 calculated from the series solution of diffusion equation (equation 8).

Mass transfer enhancement: As stated earlier, an approximate method of estimating the mass transfer enhancement is the ratio of convective diffusion coefficient and the diffusion coefficient in absence of convection using Stokes-Einstein equation (equation 1). Assuming that the carbon particles in the soil on model fabric are spherical, and have size ~ 0.1 microns, the diffusion coefficient is ~ 3×10^{-12} m^2 s^{-1}. This diffusion coefficient needs further correction for the porosity (ε) and tortuosity (α') of the fabric. The corrected diffusion coefficient is: (Rietema, 1976)

$$D_{\text{corrected}} = \frac{\varepsilon}{\alpha'^2} D_{\text{Stokes-Einstein}} \qquad (14)$$

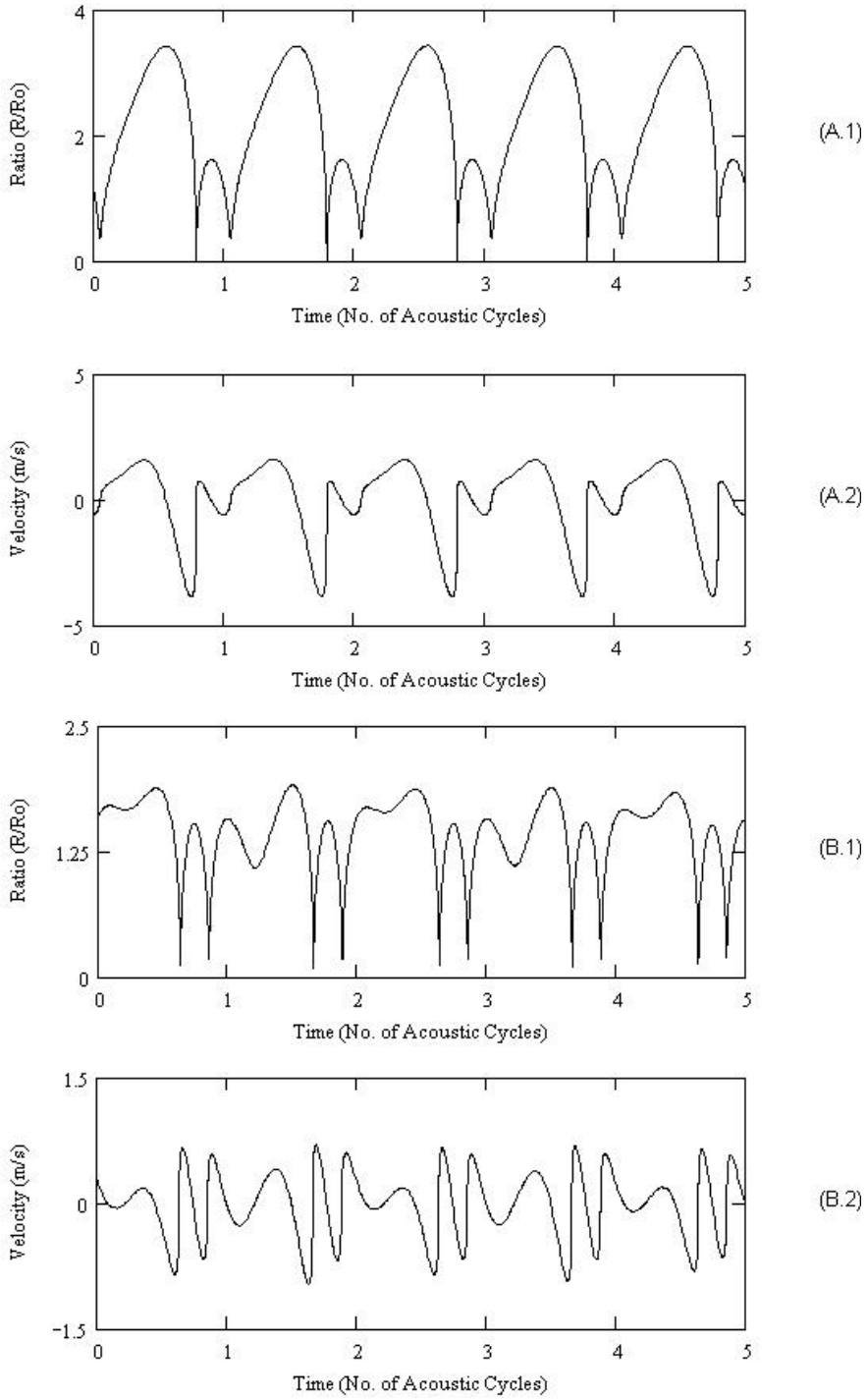

Figure 7: Radial dynamics and magnitude of spherical velocity field for oscillations of 10 μm. bubble near textile surface. The distance of bubble center from textile: 50 μm. Frequency: 25 kHz. (A) Acoustic pressure amplitude = 1.3 bar (for 20W power). (B) Acoustic pressure amplitude = 1.1 bar (for 15W power).

For typical values of $\varepsilon \sim 0.4$ and $\alpha' \sim 2$, the corrected diffusion coefficient is 3×10^{-13} m^2 s^{-1}. It could be inferred from the values of diffusion coefficient and convective diffusion coefficient that the order of magnitude range of the enhancement factor is in the range 1000 – 2000.

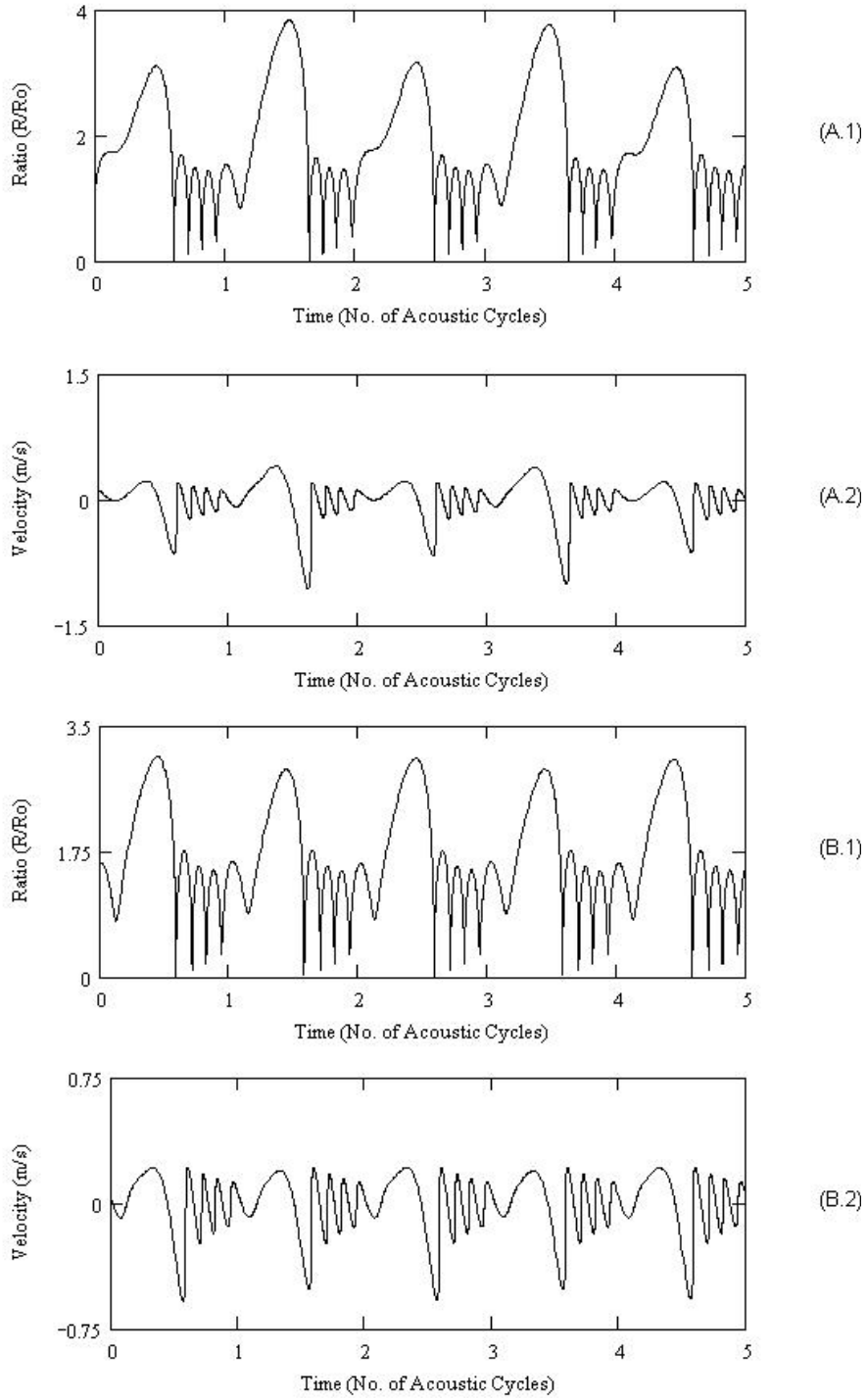

Figure 8: Radial dynamics and magnitude of spherical velocity field for oscillations of 5 μm. bubble near textile surface. The distance of bubble center from textile: 50 μm. Frequency: 25 kHz. (A) Acoustic pressure amplitude = 1.3 bar (for 20W power). (B) Acoustic pressure amplitude = 1.1 bar (for 15W power).

As mentioned earlier, a direct estimation of the convection velocities near the textile surface is not possible in the present experiments. However, simulations of the bubble dynamics equation can give us an order of magnitude estimate of the convection velocities. As is evident from the set of equations 13 – 16, the convection velocity near

the textile depends on initial bubble radius, the pressure amplitude and frequency of the acoustic wave driving bubble motion and the distance of the bubble center from the textile (or standoff factor). Figures 7 and 8 depict the radial dynamics and magnitude of the spherical velocity field created due to bubble motion for bubbles of two sizes, viz. 10 microns and 5 microns. The other parameters for the simulation are given in the figure caption. It can be seen that the bubble creates an oscillatory velocity field around it, with different magnitudes of the velocities in the two directions: towards and away from the bubble center. The (absolute) magnitude of the velocity field in any direction and, hence, the overall convection generated due to radial bubble motion increases with the acoustic pressure amplitude. The motion of the soil particle due to the convection created by the bubble motion is a function of the time-averaged velocity over several acoustic cycles. Since the purpose of the simulations presented here is to give an approximate estimate of the convection created by the radial bubble motion, we have not incorporated such complications in our analysis.

7.6 Prevention of fabric erosion during ultrasonic treatment

The S.E.M. image analysis of the ultrasound treated model fabric in the previous chapter showed erosion of the fabric surface, which is a well-known signature of the cavitation activity near a solid surface. Such erosion decreases the durability of the fabric after ultrasonic treatment. It is therefore desirable to conduct washing at acoustic pressure amplitudes just sufficient to cause the transient bubble motion (or in other words acoustic pressure amplitude slightly greater than the transient cavitation threshold), which could possibly reduce the fabric erosion during ultrasonic treatment.

To confirm that erosion is an increasing function of the acoustic intensity, S.E.M. analysis was carried out on fabric samples treated with acoustic waves of two different pressure amplitudes. As described in chapter 2, the transient cavitation threshold is a function of the initial bubble radius and the frequency of the acoustic wave driving the bubble motion. An approximate value of transient cavitation threshold for bubbles with initial size in the range 5 - 15 microns for 25 kHz frequency is ~ 1 bar. Using this value as a basis, the washing experiments with EMPA 101 model fabric were conducted at two acoustic pressure amplitudes, viz. 1.3 bar and 1.1 bar with a power input of 20W and 15W to the ultrasound horn. The experimental set up has been described in chapter 3. The experiments were conducted with non-degassed fabric and degassed washing medium with the fabric placed at pressure antinode. The time of the ultrasound treatment was 3 min. The rest of the procedure (such as soaking time, degassing technique etc.) is the same as described in chapter 6, for the experiments conducted using the special-built ultrasonic system.

The S.E.M. machine, used for the analysis, was from Jeol Inc. (Model GSM 5800). The sputtering of gold-palladium was done on both sides of the fabric due to non-planarity of the surface of the fabric. During S.E.M. analysis, the fabric was kept suspended in the central portion where cleaning occurred while the periphery fixed on the sample holder. Figures 10 and 11 show the S.E.M. images of the treated fabric

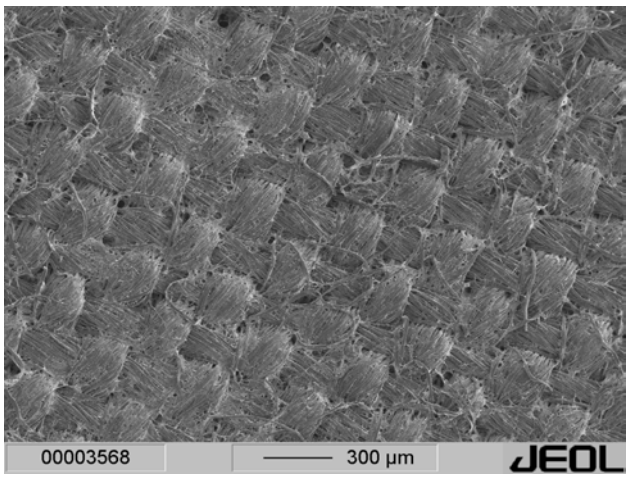

(A)

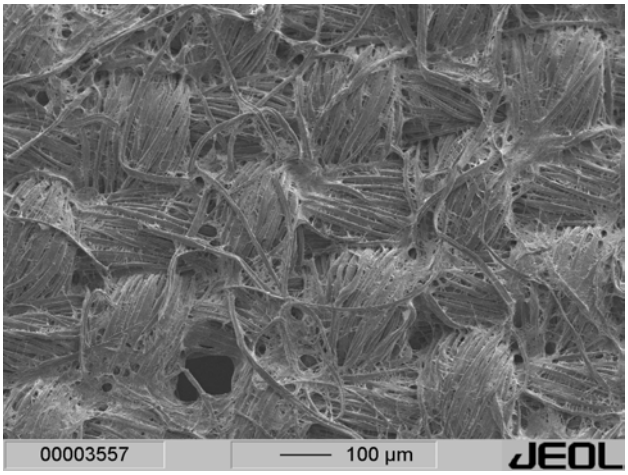

(B.1)

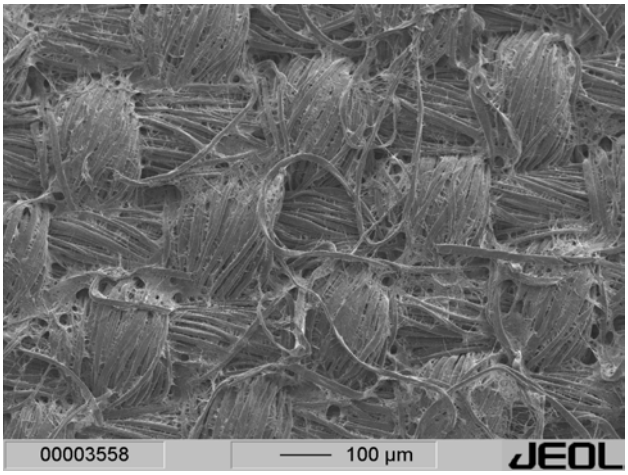

(B.2)

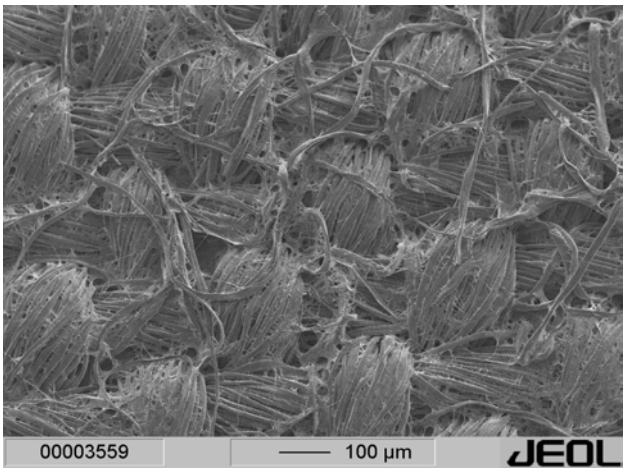

(B.3)

Figure 9: S.E.M. analysis of the fabrics treated at 20W power for the assessment of fabric erosion during ultrasonic treatment (accelerating voltage: 5kV): (A) Overview of the washed area (magnification: 45; working distance: 30 mm.). (B) Closer view of three sections of the washed area (magnification: 100; working distance: 9 mm.)

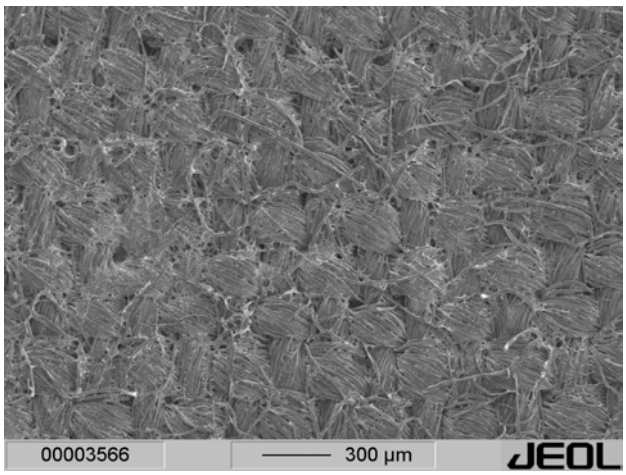

(A)

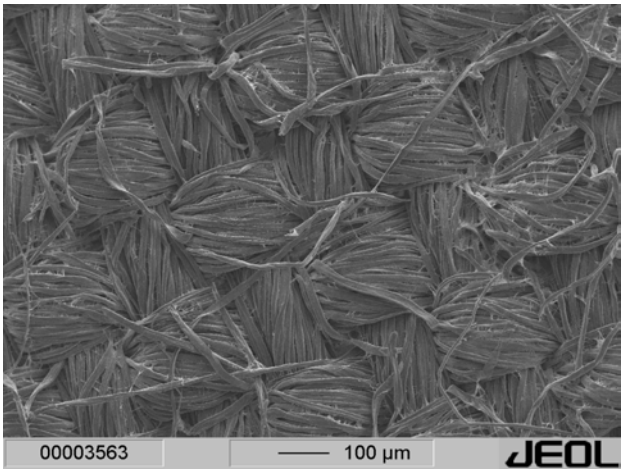

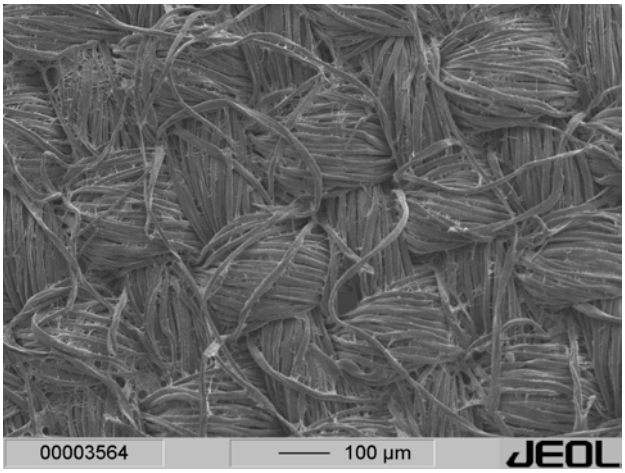

(B.1) (B.2)

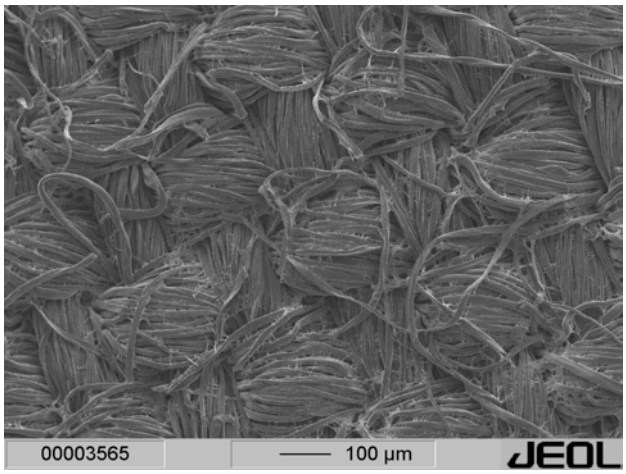

(B.3)

Figure 10: S.E.M. analysis of the fabrics treated at 15W power for the assessment of fabric erosion during ultrasonic treatment (accelerating voltage: 5kV): (A) Overview of the washed area (magnification: 45; working distance: 30 mm.). (B) Closer view of three sections of the washed area (magnification: 100; working distance: 9 mm.).

samples at 1.3 bar and 1.1 bar acoustic pressure amplitudes respectively. The parameters for obtaining the images (magnification, working distance and accelerating voltage) are given in the figure captions. Figures 9A and 10A, which show an overview of the cleaned area on the samples, do not reveal any notable difference in the fabric erosion. However, a closer look at the cleaned fabric surface with higher magnification (depicted in figures 9B and 10B) shows much less erosion on the surface of the sample treated with acoustic pressure amplitude of 1.1 bar than the sample treated with acoustic pressure amplitude of 1.3 bar. The difference between the figures 9 and 10 is even more evident after comparing them with the S.E.M. images of original EMPA 101 fabric shown in figure 1 of the previous chapter.

Thus, the above analysis confirms the proposition made at the beginning that reduction in the acoustic pressure amplitude (by reducing the power consumption of the ultrasound horn) could be a possible solution for reducing the fabric erosion during the ultrasound treatments.

7.7 Dual frequency ultrasound processor

The major shortcoming of ultrasound reactors, which has contributed mostly to their poor performance on an industrial scale operation, is that cavitation occurs only in the close vicinity of the surface of the sonicator and severely limits the volume of the active part of the reactor. Thus, the cavitation intensity differs widely in different parts of the reactors. Due to this variation, even a slight movement of the fabric during the ultrasonic treatment can cause a significant non-uniformity of the effect of ultrasound treatment such as the washing effect or the dye yield. Another shortcoming is the erosion of the sonicator itself due to cavitation in its vicinity. This necessitates replacement of the sonicator from time to time and increases the operational cost.

Recently, McCall *et al*. (1998) have reported better dye yields on cotton fabric using a dual frequency acoustic processor than a single frequency ultrasound horn. They also reported that the dye yield was independent of the position of the fabric in the acoustic field. Our aim in this work is two fold: First, to give an explanation to the results of McCall *et al*. (1998) with numerical simulations of the dual frequency acoustic field and the cavitation phenomena in it and, secondly, to provide a method to optimize the conditions of the dual frequency acoustic field for the production of uniform cavitation intensity in the reactor.

7.7.1 Mathematical model

The mathematical model for the dual frequency processor will be presented in two parts. First, the model for the acoustic pressure field is presented followed by the model for the bubble dynamics.

Modeling of the acoustic pressure field (Morse and Ingard, 1986): As explained in chapter 2, an ultrasound wave in a sonic processor is a simple harmonic wave, which after getting reflected at boundaries, such as the reactor wall, can give rise to a standing

wave. For a dual frequency acoustic field with waves of frequencies, f_1 and f_2 with a ratio f_2/f_1 as α, the pressure amplitude ratio P_{A1}/P_{A2} as β, and the phase difference ϕ, the total pressure in space and time in a one dimensional field is:

$$P(x, t) = 2\,P_{A1}\,[\cos(k\,x)\sin(\omega\,t) + \beta\cos(\alpha\,k\,x + \phi)\sin(\alpha\,\omega\,t)] \qquad (15)$$

where k is the wave number and ω is the angular frequency for the first wave. Next, we determine the average pressure amplitude in the bath, where the distance between the two sources of ultrasound is equal to the wavelength (λ_1) of the first acoustic wave with frequency f_1, by considering only the space dependent acoustic field. The average pressure $\bar{p}$ between the two sources is:

$$\bar{p} = \sqrt{\bar{p}^2} = \sqrt{\frac{k}{2\pi}\int_0^{2\pi/k} P_{A1}\left[\cos(k\,x) + \beta\,\cos(\alpha\,k\,x + \phi)\right]^2 dx}$$

$$= \sqrt{\frac{P_{A1}^2}{2\pi}\left[\pi + \frac{\beta}{4\alpha}^2\left(\sin(2\theta) + 2\theta - \sin(2\phi) - 2\phi\right) + \frac{2\,\beta\,\alpha}{(\alpha^2 - 1)}\left(\sin(\theta) - \sin(\phi)\right)\right]} \qquad (16)$$

where $\theta = 2\,\pi\,\alpha + \phi$.

The mean difference between the average pressure amplitude $\bar{p}$ and the local pressure amplitude P(x) in the region between the two ultrasound sources is a function of α, β and ϕ and is:

$$I(\alpha, \beta, \phi) = \int_0^{2\pi/k}\left[P(x) - \bar{p}\right]^2 dx \qquad (17)$$

$$= 2\,P_{A1}^2\left\{\frac{\pi}{k} + \frac{\beta^2}{4\,\alpha\,k}\left[\sin(2\theta) - \sin(2\phi) + 2\theta - 2\phi\right] + \frac{2\,\beta\,\alpha}{k\,(\alpha^2 - 1)}\left[\sin(\theta) - \sin(\phi)\right]\right\} -$$

$$\frac{2\,P_{A1}\,\beta\sin(\theta)}{\alpha\,k}\sqrt{\frac{1}{2\pi}\left[\pi + \frac{\beta}{4\alpha}^2\left(\sin(2\theta) + 2\theta - \sin(2\phi) - 2\phi\right) + \frac{2\,\beta\,\alpha}{(\alpha^2 - 1)}\left(\sin(\theta) - \sin(\phi)\right)\right]} \qquad (18)$$

The limit of the function $I(\alpha, \beta, \phi)$ for $\alpha = 1$ is:

$$\lim_{\alpha \to 1} I(\alpha, \beta, \phi) = P_{A1}\left[\begin{array}{l} 2\,P_{A1}\,\pi + P_{A1}\,\beta^2\sin(2\phi) + 2P_{A1}\,\beta^2\pi + 4\,P_{A1}\,\beta\,\pi\,\cos(\phi) + \\ \dfrac{\beta\sin(\phi)}{k}\sqrt{\dfrac{2\pi + \beta^2\sin(2\phi) + 2\beta^2\pi + 4\beta\,\pi\cos(\phi)}{\pi}} \end{array}\right] \qquad (19)$$

The variation of the function $I(\alpha, \beta, \phi)$ vs. α for different values of β and ϕ has

interesting features. A minimum of function I would imply a minimum average difference between P(x) and $\bar{p}$ over the space domain under consideration. We restrict the further analysis to only those sets of values of α, β and ϕ, for which the function I(α, β, ϕ) reaches a minimum, since the most uniform distribution of acoustic pressure amplitude can be obtained at these parameters. It should be noted that the local acoustic pressure amplitude could still fall to zero or below the transient cavitation threshold for these values. Therefore, we have set the following two conditions as *necessary and sufficient* for the selection of the set of values of α, β, ϕ as operating parameters.

1. I(α, β, ϕ) reaches a minimum; indicative of least mean difference between local acoustic pressure amplitude [P(x)], and the average acoustic pressure amplitude $\bar{p}$ for $0 \leq x \leq \lambda_1$.
2. The acoustic pressure amplitude should fall below the transient cavitation threshold in the close vicinity of the ultrasound sources (i.e., at $x = 0$ and $x = \lambda_1$), and should exceed the transient cavitation threshold everywhere else (i.e., $0 < x < \lambda_1$).

The objective behind condition 2 will be explained later.

Modeling of cavitation phenomena: The radial motion of the bubble can be described by the bubble dynamics equation. For the simulations we choose the Gilmore equation, which has been described earlier and in chapter 2. In our analysis, we substitute equation 15 for P_∞ in equation 11, which specifies the pressure as a function of space and time in the sound field, with the values of α, β, ϕ, P_{A1} and k determined by the algorithm described in preceding section. As stated in chapter 2, depending on the characteristics of the acoustic pressure field driving the bubble motion, the bubble undergoes either stable oscillatory motion for several acoustic cycles called *stable cavitation* or it may undergo an explosive growth followed by a transient collapse, called *transient cavitation,* which is a high energy event. The minimum acoustic pressure amplitude required to generate transient cavitation is the transient cavitation threshold, which is a function of the initial bubble radius as well as the frequency of the acoustic waves driving the bubble motion. For a typical bubble size distribution of 2-10 μm and frequency range of 20-100 kHz, the minimum value of transient cavitation threshold is found to be approximately 1 bar using the correlations given in chapter 2. On the basis of the energy mechanics of the radial bubble motion, Flynn (1964) has given an alternative definition of the transient cavitation as a bubble motion in which the compression phase is controlled by inertial forces. In order to achieve such a motion, Flynn (1964) has given the critical expansion ratio (R_{max}/R_o, R_{max} being the maximum radius reached during the expansion phase) in terms of the partial pressure of the gas in the bubble. Bubbles, which grow beyond this limit during the expansion phase, undergo transient collapse. The approximate value of the critical expansion ratio is 2.

7.7.2 Results of simulations

Simulations of the dual frequency acoustic field were carried out for operating conditions of P_{A1}, f_1 and β for different values of ϕ and a range of values of α to find the

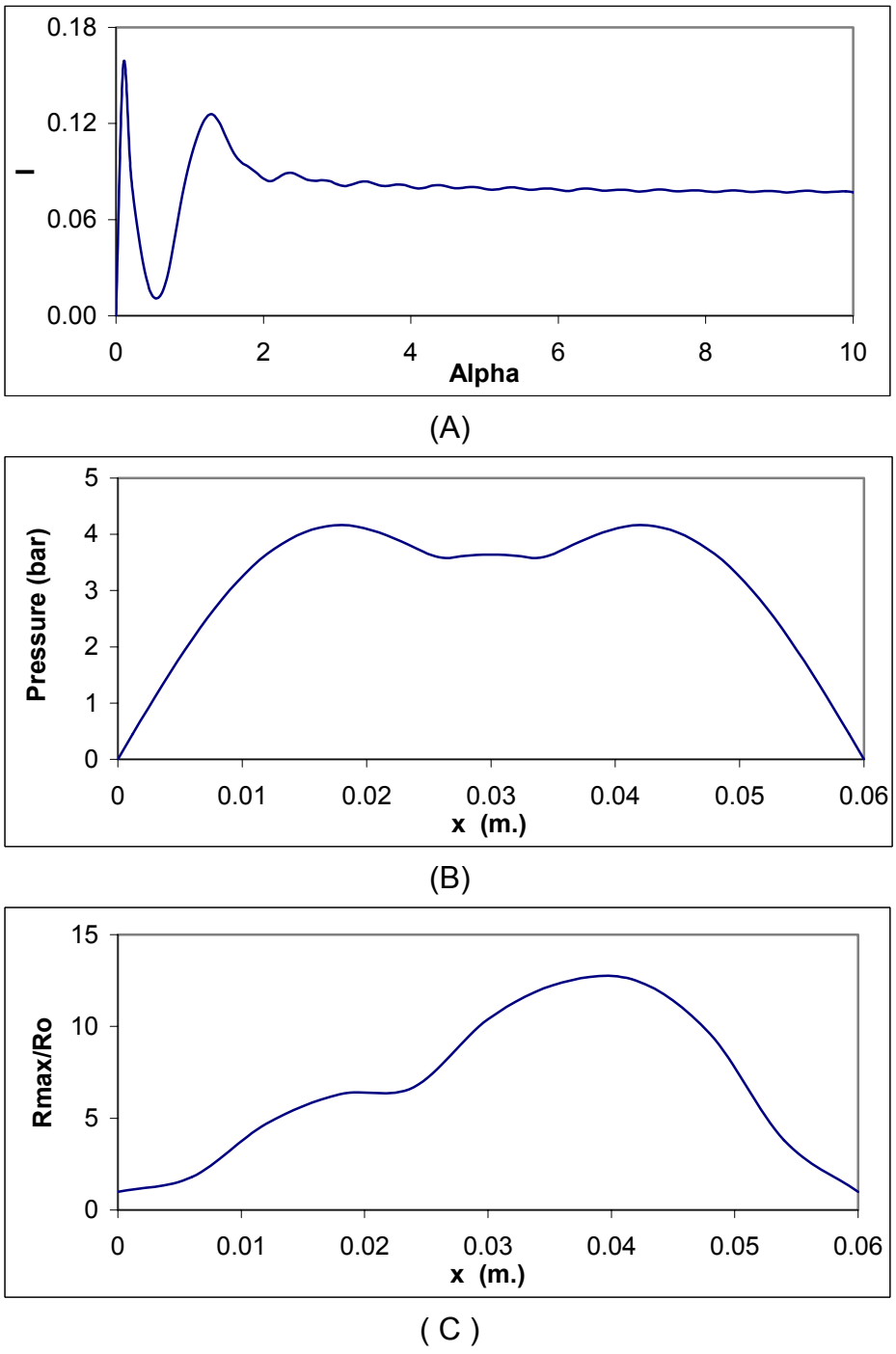

Figure 11: Results of simulations of the dual frequency ultrasonic processor with sub-harmonic coupling of frequencies. (A) Variation of function I vs. α. (B) Spatial variation of the pressure amplitude between the ultrasound sources. (C) Spatial variation of R_{max}/R_o ratio between the ultrasound sources. Parameters for simulation: α = 0.5, β = 1.4, ϕ = -π/2, P_{A1} = 0.65 atm., R_o = 5 μm., f_1 = 25 kHz.

sets of values of α, β and ϕ for which both the necessary and sufficient conditions, as outlined in preceding section, are satisfied. For brevity, only representative solutions have been depicted here. The results of the simulations reveal that the necessary and sufficient conditions described in preceding section are satisfied only if:

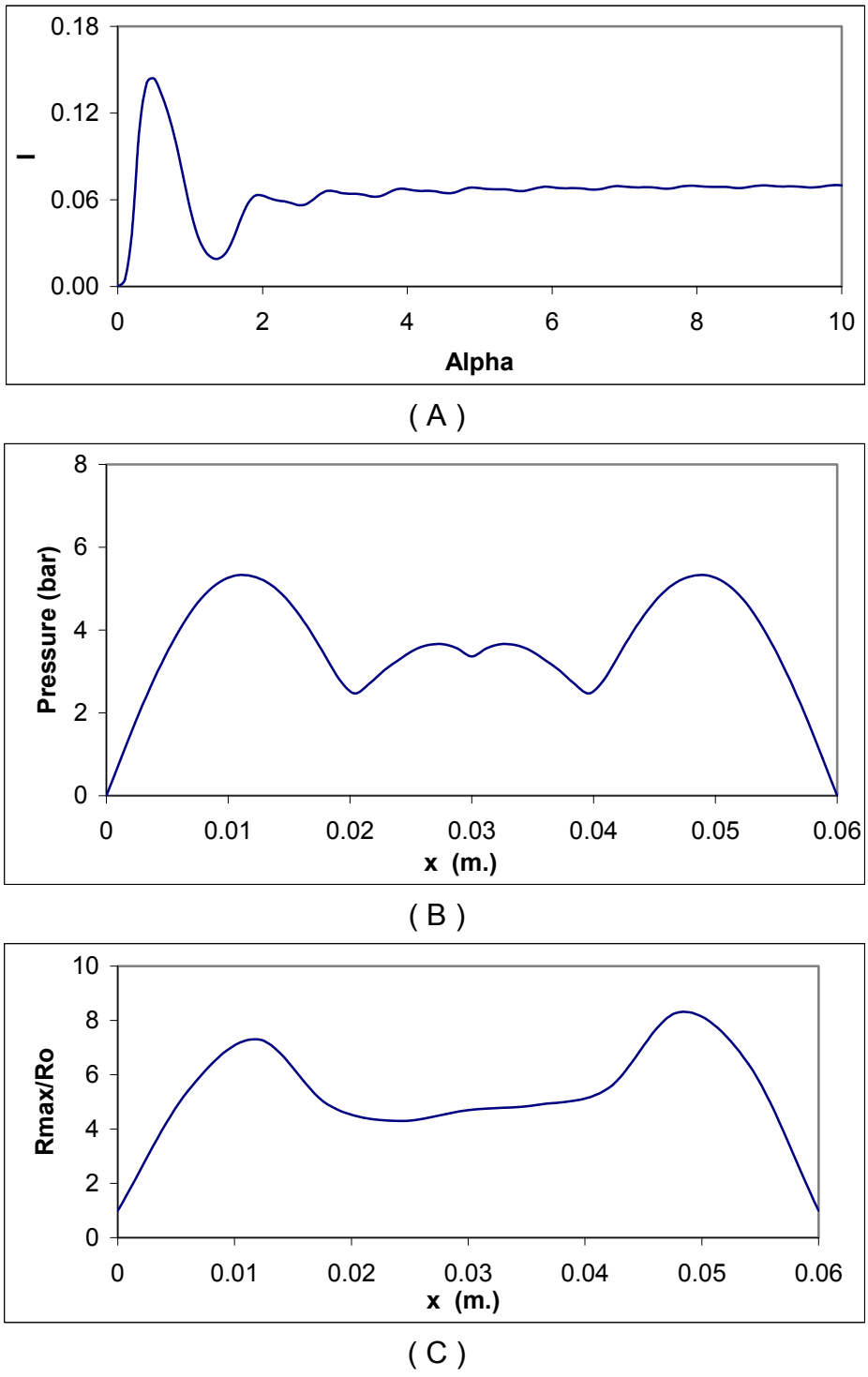

Figure 12: Results of simulations of the dual frequency ultrasonic processor with ultra-harmonic coupling of frequencies. (A) Variation of function I vs. α. (B) Spatial variation of the pressure amplitude between the ultrasound sources. (C) Spatial variation of R_{max}/R_o ratio between the ultrasound sources. Parameters for simulation: α = 1.5, β = 1.2, $\phi = \pi/2$, P_{A1} = 0.7 atm., R_o = 5 μm., f_1 = 25 kHz.

- The phase difference between the two acoustic waves is either $\pi/2$ or $-\pi/2$.
- The second or coupling frequency f_2 is either the first subharmonic (α = 0.5), ultraharmonic (α = 1.5, 2.5, 3.5,…..) of the first or main frequency f_1.

Figure 11 shows the results of the simulations for the case when the coupling frequency is a subharmonic of the main frequency ($\alpha = 0.5$). Other parameters for the simulations are given in the figure caption. Figure 12 shows similar results for the case when f_2 is an ultra-harmonic of f_1 ($\alpha = 1.5$). Other parameters for the simulations are given in the figure captions. It should be noted that although in figures 12(B) and 13(B) the pressure amplitude falls to zero at $x = 0$ and λ_1, in practice it does have a small, finite magnitude. Figures 11(C) and 12(C) reveal that there is no bubble growth in the vicinity of the ultrasound sources and that transient cavitation events occur in the center between the ultrasound sources, i.e., the pressure amplitude is above 1 bar and the bubble grows beyond the critical ratio given in the preceding section. Therefore, the occurrence of the transient cavitation is restricted in the central region between the two ultrasound sources, and not near the sources. Thus, the effect of the ultrasound treatment on the fabric will be independent of the position of the fabric in the central region between the two ultrasound sources. This reduces the undesired result of non-uniformity of the process effects (such as dye yield or washing efficiency) over the textiles due to movement of the fabric between the ultrasound sources. The operational problem of erosion of the sonicator surface can also be avoided using the dual frequency technique described above, since bubbles do not grow above the transient cavitation threshold in the close vicinity of the sonicator surface. In addition, acoustic pressure amplitudes exceeding the transient cavitation threshold can be obtained even with an individual ultrasound source operating at low power, with individual acoustic pressure amplitude below the transient cavitation threshold. This enhances the mechanical stability of the system.

7.8 Overview

This chapter describes an approximate theoretical model for a quantitative estimate of the mass transfer enhancement in the ultrasonic textile treatments. Suitable optimization strategies for the ultrasonic wet textile process for large-scale application are also described.

In absence of precise quantification of the convection created due to transient bubble motion near the textile surface, we defined a *convective diffusion coefficient*, which is representative of the mass transfer enhancement due to ultrasound. The geometry of the textile was modeled as a porous plate. The experimental results were correlated to the theoretical values of soil removal with time using solutions of the diffusion equation. The soil removal from the textile showed two distinct regimes with two different convective diffusion coefficients. This result was explained in terms of the non-uniform initial distribution of soil in the textile and the dual porosity of the textile; inter-yarn and intra-yarn porosity. Textile treatments at higher acoustic pressure amplitudes were found to give higher diffusion coefficients. The order of magnitude of the mass transfer enhancement, which was defined as the ratio of convective diffusion coefficient to molecular diffusion coefficient, is in the range 1000 - 2000.

The second aspect of the optimization of the ultrasonic wet textile process is the prevention of the erosion of the textile surface during treatment. S.E.M. analyses of the

surfaces of two textile samples, treated at different acoustic pressure amplitudes (with different power input), revealed that a reduction in the acoustic pressure amplitude (while maintaining its value above the transient cavitation threshold) could be a possible way of reducing the textile erosion during ultrasonic treatment. However, the earlier analysis of the mass transfer enhancement showed that the above-mentioned advantage is offset by longer time of treatment due to the low mass transfer rates at lower acoustic pressure amplitudes.

Thirdly, a simple model was presented to explain the better performance of a dual frequency acoustic processor, which has been employed by many researchers successfully for the intensification of wet textile treatments. Simulations were carried out to describe the effect of a dual frequency ultrasound field on the spatial distribution of the cavitation events in the ultrasonic processor. It was evident from the simulation results that the bubble growth and, hence, the mode of cavitation at different locations in the ultrasonic processor can be controlled by the application of a dual frequency field, and the manipulation of the characteristic parameters of such a field. It means that the major disadvantages of the sonic reactors, such as directional sensitivity of the cavitation events and erosion of the ultrasound source, can be overcome by the application of a dual frequency field. This is an interesting result and it opens up new opportunities for the design and optimization of the sonic reactors for diverse physical or chemical processes.

Notation

A, B - constants in the equation of state of water, Pa.
C - concentration of the diffusing substance, kg m^{-3} or mol m^{-3}.
c - velocity of sound, m s^{-1}.
D - diffusion coefficient, m^2 s^{-1}.
d_p - diameter of the diffusing particle, m.
$\bar{d}_p$ - average particle diameter, m.
f, f_1, f_2 - frequencies of the acoustic wave, Hz.
H - free enthalpy on the bubble surface, J kg^{-1}.
K - absorption coefficient, m^{-1}.
k - wave number of the acoustic wave, m.
l - half-thickness of the porous sheet, m.
M_∞ - mass of diffusing material transported in infinite time, kg or kmol.
M_t - mass of diffusing material transported in time t, kg or kmol.
n - constant in equation of state for water, dimensionless.
P - pressure, Pa.
P_∞ - pressure in the bulk liquid, driving the bubble motion, m s^{-1}.
$P(x)$ - local acoustic pressure amplitude, Pa.
P_A, P_{A1}, P_{A2} - pressure amplitude of the acoustic wave, Pa.
P_o - static pressure in the medium, Pa.
R - radius of the bubble, m.
R_f - reflectance of the textile, dimensionless.

R_o - initial bubble radius, m.
S - scattering coefficient, m^{-1}.
T - temperature, ^oK.
t - time, s.
U - bubble wall velocity, m s^{-1}.
u - magnitude of the spherical velocity field around the bubble, m s^{-1}.
x - distance coordinate, m.

Greek letters

α - ratio of frequencies of two acoustic waves, dimensionless.
α' - tortuosity factor due to porosity of fabric, dimensionless.
β - ratio of pressure amplitudes of two acoustic waves, dimensionless.
ε - porosity, dimensionless.
ϕ - phase difference between the acoustic waves, rad.
γ - polytropic constant of the bubble contents, dimensionless.
κ - Boltzmann constant, J $^oK^{-1}$.
λ_1 - wavelength of first acoustic wave, m.
μ - viscosity of the liquid, Pa s^{-1}.
ρ - density of the liquid, kg m^{-3}.
ρ_o - density of the liquid in undisturbed state, kg m^{-3}.
σ - surface tension, N m^{-1}.
ω - angular frequency, rad s^{-1}.

References

- Beek, W.J., K.M.K. Muttzall, and J.W. van Beek, *Transport phenomena*, John Wiley & Sons Ltd., Chichester (1999).
- Blake, J.R., B.B. Taib, and G. Doherty, "Transient cavities near boundaries. Part 1. Rigid boundary", *Journal of Fluid Mechanics*, **170**, 479-497 (1986).
- Brujan, E.-A., K. Nahen, P. Schmidt, and A. Vogel, "Dynamics of laser-induced cavitation bubbles near an elastic boundary", *Journal of Fluid Mechanics*, **433**, 251-281 (2001).
- Brujan, E.-A., K. Nahen, P. Schmidt, and A. Vogel, "Dynamics of laser-induced cavitation bubbles near elastic boundaries: influence of elastic modulus", *Journal of Fluid Mechanics*, **433**, 283-314 (2001a).
- Carslaw, H.S., and J.C. Jaeger, *Conduction of heat in solids*, Clarendon Press, Oxford (1959).
- Crank, J., *The mathematics of diffusion*, Clarendon Press, Oxford (1975).
- Flynn, H.G., "Physics of Acoustic Cavitation in Liquids," *Physical Acoustics*, Vol. IB, W. P. Mason, ed., Academic Press, New York (1964).
- Janssen, L.P.B.M., and M.M.C.G. Warmoeskerken, *Transport phenomena data companion*, Delft University Press, Delft (1997).
- McCall, R.E., E.R. Lee, G.N. Mock, and P.L. Grady, "Improving dye yields of vats

on cotton fabric using ultrasound", *AATCC International Conference & Exhibition 1998 - Book of Papers*, 188-194 (1998).

- Morse, P.M., and K.U. Ingard, *Theoretical acoustics*, Princeton University Press, Princeton (1986).
- Morton W.E., and J.W.S. Hearle, *Physical Properties of Textile Fibers*, The Textile Institute, Manchester (1997).
- Naude, C.F., and A.T. Ellis, "On the mechanism of cavitation damage by non-hemispherical cavities collapsing in contact with a solid boundary", *Journal of Basic Engineering* (*Transaction of ASME – D*), **83**, 648-656 (1961).
- Phillip, A., and W. Lauterborn, "Cavitation erosion by single laser produced bubbles", *Journal of Fluid Mechanics*, **361**, 75-116 (1998).
- Rietema, K., *Fysische Transport en Overdrachtsverschijnselen*, Het Spectrum, Utrecht (1976).
- Tomita, Y., and A. Shima, "Mechanisms of impulsive pressure generation and damage pit formation by bubble collapse", *Journal of Fluid Mechanics*, **169**, 535-564 (1986).

ACKNOWLEDGMENT

The completion of this Ph.D. thesis brings an end to the student phase of my life (although I am not sure, because it is said that a man remains a student in his entire life!). It has been a very long journey, often patience-testing, full of ups & downs, joys & griefs and successes & failures. But, at last, it is ending with a happy note, thanks to the blessings of God, the almighty and most merciful.

I feel short of words to express my gratitude towards my thesis advisors, Prof. Marijn Warmoeskerken and Prof. Andrea Prosperetti. Although the subject of textile research was completely new to me, Marijn familiarized me to it very quickly. Apart from supervising my thesis work, Marijn gave me an *industrial perspective* of academic research. What I learned from Marijn in past four years is an asset for my post-Ph.D. personal as well as professional life. I was indeed fortunate to have Prof. Prosperetti as my co-advisor. Being an outstanding scientist as well as an outstanding teacher, he explained to me the most difficult topics in physical acoustics in a very lucid way, which helped me apply them easily for process engineering purposes.

I am grateful to my colleagues Vincent Nierstrasz, Herman Lenting, and Sander Rekveld for their advice and assistance during research. I received valuable help from Henk Gooijer in this project. I was able to draw many ideas from Henk's experience in the field of ultrasound assisted wet textile processing and flow resistance of textile materials, and several discussions that I had with him. Many thanks to you, Henk! I express my sincere gratitude towards our group secretary, Bartie for her motherly love and care. I am grateful to Jeroen Dunnewijk for important suggestions during this project based on his experience in Stork R&D, and his help in the tedious and tiresome job of proof reading and grammar correction of the thesis! Additionally, I am thankful to the fellow Ph.D. students in the group, Monica and Pramod, for their help and cooperation during my work, and to my (only!) M.Sc. student Michiel Huitema, for his help in the early stages of this project.

I would especially like to acknowledge my gratitude to Prof. A.B. Pandit, under whose guidance I started my graduate career in 1993, as a research assistant. I thank him for the basic lessons in cavitation and bubble dynamics that I received from him, and for the encouragement and support during my work with him as well as during my education abroad.

This project, which was of completely interdisciplinary nature, spanned areas of chemical engineering, physics, mathematics, electrical engineering and textile chemistry. Therefore, I got an opportunity to interact with scientists and experts from fields other than chemical engineering. I deem myself very lucky in that I have privilege to thank the following people for their invaluable help, which played important role in successful completion of this thesis: Detlef Lohse, Lawrence Crum, Sascha Hilgenfeldt, Ronald Holweg, Frits van Beckum, John Blake, Ruud van Domme, M. Bos, Claus-Dieter Ohl, Rene Breeuwer, Giles Keen, Pete van der Vlist, and Mike Bailey. I also thank my thesis examination committee members Hans Kuipers, Paul Kiekens, JanWillem Gerritsen and

Andre de Haan.

I am indebted to the members of the WTT (*Werkgroep Textieltechnologie*) for their interest in my research and for the help they offered this project in various ways. Especially, I thank Henri Aal, Anton Tijhuis, Pieter Zuuring, Harry van de Ven, Jan van Driel, and Karel Vrieling. In addition, I am thankful to the staff of TNO-Textiel for their help: Anton Luiken, Aike Wypken, Anton Kaasjager, and Dan Ravensberger.

During this project I was very lucky to have got assistance from a wonderful team of technicians. The experimental work would not have been possible without help of our enthusiastic technician, Benno Knaken. The contribution that Benno did to this project was more than a mere technician. His creative ideas in designing experimental set-up were of critical help in achieving the goal of the experiments. Furthermore, I thank Bert Kamp, Murat Ucer, Herman Koster, Ruud van der Blink, Joop Snoeyenbos, Jan van Veen and Dick Witteveen. I also express my gratitude towards Mark Hulshof, Bert Vos and the staff of the SGA for their kind cooperation. The help of CT-library staff in the literature survey is gratefully acknowledged.

I thank my assistants during promotie function Vinit Chilekar and Charudatta Patil for their help. Thanks are also due to my laboratory colleagues, viz. Alice, Tatjana, Ulrika, Anita, Karel, Jeroen and Xander for their company. Moreover, I thank all the members of the contemporary UT-Indian community for all the help and cooperation I received from them.

I am grateful to Helen, Jose, and "Mr. Raf" for accommodating me as a family member. I wholeheartedly thank Renuka & Shubharaj Buwa, Shital & Anand Savkar, Shrinivas Kulkarni, Allwyn Tellis, and Ayaz Rabbani for their friendship and care over years.

Above all, my largest debt of thanks is owed to my parents. It was their love, care, support, sacrifice and encouragement that made me what I am today! *Matrudeo Bhav, Pitrudeo Bhav!!*

ABOUT THE AUTHOR

Vijay S. Moholkar was born on September 1, 1972 in Mumbai (India). He completed his primary education in Nutan Marathi Vidyalay, and secondary education in Haribhai Deokaran High School at Solapur (Maharashtra, India). After completing higher secondary education at D.A.V. Dayanand College (again at Solapur) in 1989, he joined University Department of Chemical Technology (abbreviated as UDCT), University of Mumbai for undergraduate degree (Bachelor of Chemical Engineering or B. Chem. Engng.). After getting the bachelor's degree in August 1993, he worked as a Research Assistant (August 1993 – June 1994) in the group of Professor A. B. Pandit on a project on the design and scale-up of cavitation reactors for chemical processing. In August 1994 he joined the Master of Chemical Engineering (or M. Chem. Engng.) program at University Department of Chemical Technology, under the supervision of Professor Pandit. During his masters studies he was also appointed as *Singhanee* Associate Lecturer in Chemical Engineering by UDCT. As an Associate Lecturer, Vijay was mainly involved in the supervision of undergraduate practical courses. After completing the M. Chem. Engng. program in April 1996, Vijay was appointed as Lecturer in Chemical Engineering in UDCT by University of Mumbai. In August 1997 he joined University of Illinois at Urbana Champaign for Ph.D., but soon shifted to University of Twente in July 1998. Vijay's Ph.D. project, supervised by Professor M.M.C.G. Warmoeskerken and Professor A. Prosperetti, involved both fundamental and applied research on ultrasonic wet textile treatments. Vijay has also worked as a scientific consultant to Electric Power Research Institute, Palo Alto (USA), while he was a Lecturer at UDCT. So far he has published 10 research papers and has made several presentations of his work in international conferences in Europe, India, and USA. He has also coauthored, along with Professor A.B. Pandit and Professor Y.T. Shah of Clemson University (USA), a book titled *Cavitation Reaction Engineering* published by Plenum Press/Kluwer Academic.